

Investigation into the Machining of Biomedical Grade Polymers, Considering Cryogenic Pre-Cooling

BARRY ALDWELL BA BAI PGDIP MIEI

DEPARTMENT OF MECHANICAL AND MANUFACTURING ENGINEERING
TRINITY COLLEGE DUBLIN

A thesis submitted to the University of Dublin in partial
fulfilment of the requirements for the degree of

DOCTOR IN PHILOSOPHY

SEPTEMBER 2015

Supervisor:

DR. GARRET E. O'DONNELL

Declaration

I declare that this thesis has not been submitted as an exercise for a degree at this or any other university and it is entirely my own work.

I agree to deposit this thesis in the University's open access institutional repository or allow the library to do so on my behalf, subject to Irish Copyright Legislation and Trinity College Library conditions of use and acknowledgement.

Barry Aldwell BA BAI PgDip MIEI

September 2015

Summary

Polymers have found widespread use as engineering materials, due to their low density, ease of processing, and corrosion resistance. While traditional polymer processing techniques are capable of making a wide range of part geometries, there are some applications where polymers do not deliver the required dimensional accuracy or surface finish, requiring a machining operation to be carried out as a finishing step. One example of this is in Ultra High Molecular Weight Polyethylene (UHMWPE) inserts in orthopaedic implants, where the polymer component is functionally replacing the cartilage of the joint. In order to minimise wear it is necessary to have as smooth of a finish as possible. For the biomechanics of the joint replacement to match the original joint the part must mate perfectly with the opposing part. These parts are machined in order to achieve the required finish and dimensional accuracy. There is a significant gap in the literature on the topic of UHMWPE machining, thus requiring operators to use trial and error to choose tooling and machining parameters. These decisions are often made with little understanding of the machining characteristics of the material, leading to delays in production and waste of raw material used in trial machining operations.

This work experimentally investigates the machining of UHMWPE. The viscoelastic properties of the material as a function of temperature, the location of the material in the stock, and strain rate are first established. Machining tests are carried out to acquire experimental data on the effect of changes to the raw material, in the form of antioxidant additives and crosslinking, on the machinability of UHMWPE. Other parameters varied include tool rake angle and cutting edge radius, along with cutting speed and depth of cut in orthogonal machining experiments. This is followed by a study on the effect of workpiece pre-cooling to cryogenic temperatures on machining, in light of the earlier findings on the effect of temperature on the viscoelastic properties of the material. Finally, a study is carried out on the occurrence of material relaxation after unloading in machining, both as a result of workpiece clamping forces, and as a result of machining forces.

During machining operations the cutting forces and tool temperature were recorded, along with high speed video of the cutting zone. Chips were collected from each cutting operation. In addition, the surface roughness of the machined surface was measured,

with select surfaces being analysed using a Scanning Electron Microscope (SEM). The quantitative data was then analysed using statistical analysis software to evaluate which of the workpiece, tooling, and machining parameters were causing variation in the responses.

It was found that the addition of antioxidant or crosslinking of the material did not fundamentally change the machinability of the material. The major factor determining the quality of the machined surface was the ratio of the cutting edge radius to the depth of cut, along with the rake angle of the tool. Machining with positive rake angles and depths of cut greater than the cutting edge radius led to smooth machined surfaces with low surface roughness.

In the study of workpiece cooling to cryogenic temperatures, higher cutting forces and temperature generation were observed, but with an improvement in surface roughness. The choice of tooling and machining parameters remained important in order to achieve a good surface finish. It was identified that certain chip formation mechanisms caused pitting or ridges on the machined surface perpendicular to the direction of the cut.

It was observed that stress relaxation will occur after removal of a static force, with a timescale of 200 to 2000 minutes required before reaching a steady state. Machining with positive rake angles, sharp tools and a range of depths of cut did not cause a detectable level of stress relaxation.

From the work carried out it can be concluded that in order to achieve low surface roughness and a smooth finish in UHMWPE, it is necessary to machine using a tool with a positive rake angle, and with a cutting edge radius greater than the depth of cut. In cases where an even finer finish is desired, consideration should be given to cryogenic cooling of the workpiece, potentially using an in-process cooling system. Finally, care should be taken when clamping UHMWPE to avoid undue force, which could cause stress relaxation after unloading.

Acknowledgements

The 1492 days that I have spent working on my PhD would have been far more difficult without the support of my parents, Rita and John, my brother Conor, and my girlfriend Jennifer. They have each helped me in ways that they probably aren't even aware of, and I will be forever grateful.

Throughout my work I have relied upon my supervisor, Dr. Garret O'Donnell, for his guidance and insight, without which this work would have been impossible. Thanks are also due to Eamonn Mullins for his advice on all matters statistics. Funding for this work was provided by the Irish Research Council and DePuy Synthes. I would like to thank Dr. Ray Hanley, Jimmy O'Mahony and Mark O'Donovan from DePuy Synthes (Ireland) for their assistance over the years, and for hosting me on my visits to the plant in Ringaskiddy, to watch how the professionals do it! On the TCD side I also have to thank Mick Reilly, JJ Ryan, Gordon O'Brien and the rest of the technical staff in the Department of Mechanical & Manufacturing Engineering for their work and assistance, particularly with experimental work.

My time as a postgraduate student wouldn't have been the same without my fellow postgrads. In no particular order I'd like to thank Rory Stoney, Eoin O'Driscoll, Kate Smith, Paul Ervine, Darren McDonnell, Kevin Kerrigan, Stuart Murphy, Robin Mooney, Aoife Nic Chraith, Emma Brazel, and Jeff Morgan. Thanks must also be extended to Sarah Nangle for her assistance with proofreading.

Finally, I have to thank the officers, NCOs and Gunners of 1 Gun Bty, 62 Field Artillery Regiment, with whom I served for 9 years. In particular I must thank my fellow NCOs and AGDCs for their support and comradeship, which continues long after the official stand down of the Regiment.

Contents

| | |
|---|-----------|
| Contents | i |
| List of Figures | v |
| List of Tables | ix |
| Nomenclature | xi |
| 1 Introduction | 1 |
| 1.1 Polymers as engineering materials | 1 |
| 1.2 Research objectives | 4 |
| 1.3 Thesis overview | 5 |
| 2 Literature review | 7 |
| 2.1 Introduction to polymer materials | 7 |
| 2.1.1 Applications of polymers | 8 |
| 2.1.2 Polymer properties | 8 |
| 2.1.3 Polyethylene | 15 |
| 2.1.4 Manufacture of polymers | 19 |
| 2.1.5 Traditional polymer processing | 19 |
| 2.2 Polymers for biomedical applications | 21 |
| 2.2.1 Applications in total joint replacement | 21 |
| 2.3 Machining of polymers | 23 |
| 2.3.1 Viscoelastic behaviour | 24 |
| 2.3.2 Cutting forces | 29 |
| 2.3.3 Heat generation | 30 |
| 2.3.4 Surface quality | 30 |
| 2.3.5 Tool selection | 31 |
| 2.3.6 Past work on the machining of polyethylene | 32 |
| 2.4 Process monitoring in the machining of polymers | 35 |
| 2.5 Statistical analysis of experimental data | 36 |
| 2.5.1 Design of experiments | 36 |
| 2.5.2 Analysis of Variance | 36 |
| 2.5.3 Chi-square analysis | 37 |
| 2.5.4 Multiple linear regression | 37 |
| 2.6 Summary | 39 |

| | | |
|----------|---|-----------|
| 3 | Experimental setup | 41 |
| 3.1 | Experimental methodology | 41 |
| 3.2 | Material analysis | 42 |
| 3.3 | Workpiece design | 44 |
| 3.4 | Force measurement | 45 |
| 3.5 | Temperature measurement | 46 |
| 3.6 | Surface roughness measurement | 47 |
| 3.7 | Chip formation analysis | 48 |
| 3.8 | Surface integrity analysis | 49 |
| 3.9 | Design of experiments | 50 |
| 3.9.1 | Design of experiments applied to orthogonal cutting investigations | 50 |
| 3.9.2 | Design of experiments applied to cryogenic cutting investigations | 51 |
| 3.9.3 | Design of experiments applied to workpiece relaxation investigations | 51 |
| 3.10 | Data processing | 54 |
| 4 | Material analysis | 55 |
| 4.1 | Shore hardness testing | 56 |
| 4.2 | Fourier Transform Infrared Spectroscopy | 57 |
| 4.3 | Dynamic Mechanical Analysis | 59 |
| 4.3.1 | Varying material | 59 |
| 4.3.2 | Varying frequency of loading | 62 |
| 4.4 | Differential Scanning Calorimetry | 65 |
| 4.5 | Discussion | 67 |
| 5 | Fundamental investigation into orthogonal cutting of UHMWPE | 69 |
| 5.1 | Background and methodology for characterisation of orthogonal cutting of UHMWPE | 69 |
| 5.2 | Machining forces | 71 |
| 5.2.1 | Cutting force | 71 |
| 5.2.2 | Thrust force | 73 |
| 5.3 | Tool temperature | 75 |
| 5.4 | Surface roughness | 78 |
| 5.5 | Chip formation | 80 |
| 5.5.1 | Chip examination | 80 |
| 5.5.2 | Chip thickness | 81 |
| 5.5.3 | Video of chip formation | 83 |
| 5.5.4 | Analysis of chip formation mechanisms | 85 |
| 5.6 | Analysis of machined surface | 86 |
| 5.6.1 | Varying tool sharpness | 86 |
| 5.6.2 | Varying tool rake angle | 87 |
| 5.7 | Discussion | 88 |
| 6 | Cryogenic cooling of UHMWPE for machining operations | 91 |
| 6.1 | Background and methodology for characterisation of cryogenic cooling of UHMWPE for machining operations | 91 |
| 6.2 | Machining forces | 92 |
| 6.2.1 | Cutting force | 92 |

| | | |
|----------|---|------------|
| 6.2.2 | Thrust force | 94 |
| 6.3 | Tool temperature | 96 |
| 6.4 | Machined surface analysis | 98 |
| 6.4.1 | Microscopy | 98 |
| 6.4.2 | Chip thickness | 101 |
| 6.4.3 | Surface roughness | 103 |
| 6.4.4 | Quantification of surface profile variation | 106 |
| 6.4.5 | Analysis of chip type, deformation and crack-type chip formation | 112 |
| 6.4.6 | Determination of chip formation mechanism | 114 |
| 6.5 | Discussion | 117 |
| 7 | Viscoelastic relaxation of UHMWPE following machining operations | 119 |
| 7.1 | Background and methodology for characterisation of viscoelastic relaxation of UHMWPE following machining operations | 119 |
| 7.1.1 | Static loading methodology | 119 |
| 7.1.2 | Machining operations methodology | 121 |
| 7.2 | Relaxation of test samples after static loading | 122 |
| 7.2.1 | Constant stress | 122 |
| 7.2.2 | Constant strain | 128 |
| 7.3 | Relaxation of test samples after machining operations | 135 |
| 7.3.1 | Machining forces | 135 |
| 7.3.2 | Change in dimensions | 136 |
| 7.4 | Discussion | 138 |
| 8 | Conclusions and further work | 139 |
| 8.1 | Conclusions | 139 |
| 8.1.1 | Fundamental investigation into machining of UHMWPE | 139 |
| 8.1.2 | Cryogenic pre-cooling of UHMWPE for machining operations | 140 |
| 8.1.3 | Viscoelastic stress relaxation in machining | 141 |
| 8.1.4 | Contribution to knowledge | 143 |
| 8.1.5 | Concluding remarks | 143 |
| 8.2 | Further work | 144 |
| | References | 147 |
| | Appendix A DSC Report | 165 |
| | Appendix B Tensile testing | 179 |
| | Appendix C Statistical analysis of tool temperature in machining | 181 |
| C.1 | Results corresponding to chapter 5 | 181 |
| C.2 | Results corresponding to chapter 6 | 185 |
| | Appendix D ANOVA tables for chapter 5 | 191 |
| | Appendix E ANOVA tables for chapter 6 | 197 |
| | Appendix F ANOVA tables for chapter 7 | 203 |

List of Figures

| | | |
|------|---|----|
| 1.1 | Plastics demand in the EU, by sector | 1 |
| 1.2 | Plastics demand in the EU, by polymer type | 2 |
| 1.3 | Flowchart showing makeup of chapters | 6 |
| 2.1 | Typical stiffness curve for polymers, with machinability regions | 10 |
| 2.2 | Effect of temperature and strain-rate on stress-strain response of PMMA | 11 |
| 2.3 | Effect of strain rate on tensile strain to failure in HDPE | 12 |
| 2.4 | Hysteresis as a function of temperature and imposed strain in UHMWPE | 13 |
| 2.5 | Models for viscoelastic behaviour | 13 |
| 2.6 | Chemical structures of ethylene and polyethylene | 15 |
| 2.7 | Effect of increasing molecular weight on mechanical properties | 17 |
| 2.8 | Stress - strain relation as a function of strain rates for UHMWPE | 18 |
| 2.9 | Typical total joint replacement solutions | 21 |
| 2.10 | Graph of effect of ratio of edge radius to depth of cut on effective rake angle in cutting | 26 |
| 2.11 | 3D visualisation of effect of ratio of edge radius to depth of cut and nominal rake angle on effective rake angle | 26 |
| 2.12 | Cutting arrangement for increasing tool edge radius r | 27 |
| 2.13 | Force components in orthogonal machining | 30 |
| 2.14 | Heat sources and heat distribution in the cutting process | 31 |
| 2.15 | Fishbone diagram with the parameters that affect surface roughness | 32 |
| 3.1 | Experimental methodology | 41 |
| 3.2 | Workpiece design | 44 |
| 3.3 | Sample force data | 45 |
| 3.4 | Sample temperature data | 46 |
| 3.5 | Profilometer and spindle setup | 47 |
| 3.6 | Toolholder with force sensor and camera mounted | 48 |
| 3.7 | Experimental setup | 48 |
| 3.8 | Data acquisition flowchart | 54 |
| 4.1 | Locations of samples machined from raw bar/rod stock for material analysis | 55 |
| 4.2 | FTIR results for UHMWPE | 57 |
| 4.3 | FTIR results for AOX | 57 |
| 4.4 | FTIR results for XLK | 58 |
| 4.5 | Storage modulus for all samples | 59 |

| | | |
|------|---|-----|
| 4.6 | Loss modulus for all samples | 60 |
| 4.7 | Tan Delta for all samples | 61 |
| 4.8 | Storage modulus for varying strain rate | 62 |
| 4.9 | Loss modulus for varying strain rate | 63 |
| 4.10 | Tan Delta for varying strain rate | 64 |
| 4.11 | DSC results for all samples | 65 |
| | | |
| 5.1 | Toolholder and data acquisition system | 69 |
| 5.2 | Main effects plot for cutting force | 71 |
| 5.3 | Interactions plot for cutting force | 72 |
| 5.4 | Main effects plot for thrust force | 73 |
| 5.5 | Interactions plot for thrust force | 74 |
| 5.6 | Graph showing effect of tool sharpness on tool temperature | 75 |
| 5.7 | Main effects plot for temperature | 76 |
| 5.8 | Main effects plot for temperature, excluding highly worn tools | 77 |
| 5.9 | Main effects plot for surface roughness | 78 |
| 5.10 | Interactions plot for surface roughness | 79 |
| 5.11 | Sample of chips collected after machining operations | 80 |
| 5.12 | Main effects plot for chip thickness | 81 |
| 5.13 | Interactions plot for chip thickness | 82 |
| 5.14 | High speed camera images showing effect of varying tool sharpness at low depth of cut | 83 |
| 5.15 | High speed camera images showing effect of varying tool rake angle | 84 |
| 5.16 | SEM images showing effect of varying tool sharpness | 86 |
| 5.17 | SEM images showing effect of varying tool rake angle | 87 |
| | | |
| 6.1 | Main effects plot for cutting force | 92 |
| 6.2 | Interactions plot for cutting force | 93 |
| 6.3 | Main effects plot for thrust force | 94 |
| 6.4 | Interactions plot for thrust force | 95 |
| 6.5 | Main effects plot for peak temperature | 96 |
| 6.6 | Difference in tool temperature data for machining of cryogenically pre-cooled workpieces | 97 |
| 6.7 | Sectioned view of workpiece, showing material flow at low depths of cut due to rubbing | 98 |
| 6.8 | Optical microscope images of machined surface | 99 |
| 6.9 | Scanning electron microscope images of machined surface | 99 |
| 6.10 | Surface profile of machined surfaces | 100 |
| 6.11 | Main effects plot for chip thickness | 101 |
| 6.12 | Interactions plot for chip thickness | 102 |
| 6.13 | Main effects plot for surface roughness | 103 |
| 6.14 | Interactions plot for surface roughness | 104 |
| 6.15 | Boxplot of mean values of R_a as a function of effective rake angle | 105 |
| 6.16 | Boxplot of RMS as a function of chip type and observation of crack-type chip formation in profilometer output | 106 |
| 6.17 | Boxplot of RMS as a function of rake angle, sharpness and temperature | 108 |

| | | |
|------|--|-----|
| 6.18 | Boxplot of RMS as a function of effective rake angle | 109 |
| 6.19 | Surface topography and profilometer data, for outlier point | 110 |
| 6.20 | Example of surface profile where discontinuous chip was formed without evident cracking | 114 |
| 7.1 | Scatterplot of thickness as a function of time | 122 |
| 7.2 | Scatterplot of thickness as a function of $\log_{10}(\text{time})$ | 123 |
| 7.3 | Effects of including indicator variables on slopes and intercepts of regression models | 124 |
| 7.4 | Temperature at core of UHMWPE sample after removal from liquid nitrogen, while warming in air | 127 |
| 7.5 | Strain as a function of time for constant strain loading | 128 |
| 7.6 | Stress as a function of time for constant strain loading | 129 |
| 7.7 | Stress as a function of strain for constant strain loading | 130 |
| 7.8 | Scatterplot of thickness as a function of $\log_{10}(\text{time})$ | 131 |
| 7.9 | Scatterplot of thickness as a function of $\log_{10}(\text{time})$, with outliers removed | 132 |
| 7.10 | Machining forces recorded during cutting operations | 135 |
| 7.11 | Change in diameter of machined samples as a function of time | 136 |
| B.1 | Tensile testing results for varying sample temperature and strain rate | 180 |
| C.1 | Main effects plot for temperature | 182 |
| C.2 | Interactions plot for temperature | 182 |
| C.3 | Main effects plot for temperature, excluding highly worn tools | 183 |
| C.4 | Interactions plot for temperature, excluding highly worn tools | 185 |
| C.5 | Main effects plot for peak temperature | 187 |
| C.6 | Interactions plot for peak temperature | 189 |
| F.1 | Residuals plot for samples with constant stress applied for 100 seconds | 205 |
| F.2 | Residuals plot for samples with constant strain applied for 100 seconds | 207 |
| F.3 | Residuals plot for samples with constant strain applied for 100 seconds, with outliers removed | 209 |
| F.4 | Residuals plot for diameter of machined samples | 209 |

List of Tables

| | | |
|------|---|-----|
| 2.1 | Comparison of the properties of polymers and other materials | 9 |
| 2.2 | Main absorptions of polyethylene in the IR region, and their assignment | 14 |
| 2.3 | Typical properties of UHMWPE | 17 |
| 2.4 | Variation in properties of UHMWPE after 6 years of aging | 19 |
| 2.5 | Factors affecting cutting action in plastics | 24 |
| 2.6 | Types of chip formed in polymer machining | 28 |
| 2.7 | Critical rake angle as a function of cutting speed and depth of cut for polyethylene | 33 |
| 3.1 | Properties of extruded GUR 1020 | 42 |
| 3.2 | Types of material analysis used | 43 |
| 3.3 | Factors used in design of experiments for chapter 5 | 50 |
| 3.4 | Sharpness levels | 50 |
| 3.5 | Effective rake angles for depths of cut and tool sharpness levels used | 50 |
| 3.6 | Factors used in design of experiments for chapter 6 | 51 |
| 3.7 | Factors used in design of experiments for section 7.2.1 | 52 |
| 3.8 | Factors used in design of experiments for section 7.2.2 | 52 |
| 3.9 | Factors used in design of experiments for section 7.3 | 52 |
| 3.10 | Nominal final diameters used to maintain constant machining times | 53 |
| 4.1 | Shore hardness values for each material | 56 |
| 5.1 | Factors used in design of experiments for fundamental investigation into orthogonal cutting of UHMWPE | 70 |
| 6.1 | Factors used in design of experiments | 91 |
| 6.2 | Chip types and associated RMS values for profilometer data | 107 |
| 6.3 | Summary of ANOVA tables for RMS | 110 |
| 6.4 | P values for Chi-square analysis of variation between factors | 112 |
| 6.5 | Chi-square table for rake angle and deformation | 112 |
| 6.6 | Chip formation mechanisms identified from experimental data | 115 |
| 7.1 | Factors used in design of experiments for constant stress loading | 120 |
| 7.2 | Factors used in design of experiments for constant strain loading | 120 |
| 7.3 | Factors used in design of experiments for machining operations | 121 |
| 7.4 | Regression model information for constant stress loading | 125 |
| 7.5 | Slope coefficients and P values for constant stress loading | 125 |
| 7.6 | Intercept coefficients and P values for constant stress loading | 126 |

| | | |
|------|---|-----|
| 7.7 | Decrease in stress due to viscoelastic stress relaxation under constant strain | 129 |
| 7.8 | Regression model information for constant strain loading | 132 |
| 7.9 | Slope coefficients and P values for constant strain loading | 133 |
| 7.10 | Intercept coefficients and P values for constant strain loading | 134 |
| 7.11 | Regression model information for machining operations | 136 |
| 7.12 | Coefficients and P values for machining operations | 137 |
| A.1 | Sample numbers for material analysis | 165 |
| C.1 | ANOVA table for temperature | 184 |
| C.2 | ANOVA table for temperature, excluding highly worn tools | 186 |
| C.3 | ANOVA table for peak temperature | 188 |
| D.1 | Factors used in design of experiments for chapter 5 | 191 |
| D.2 | ANOVA table for cutting force | 192 |
| D.3 | ANOVA table for thrust force | 193 |
| D.4 | ANOVA table for surface roughness | 194 |
| D.5 | ANOVA table for chip thickness | 195 |
| E.1 | Factors used in design of experiments for chapter 6 | 197 |
| E.2 | ANOVA table for cutting force | 198 |
| E.3 | ANOVA table for thrust force | 199 |
| E.4 | ANOVA table for cut chip thickness | 200 |
| E.5 | ANOVA table for surface roughness | 201 |
| E.6 | ANOVA table for RMS of profilometer output | 202 |
| F.1 | Factors used in design of experiments for constant stress loading | 203 |
| F.2 | Factors used in design of experiments for constant strain loading | 203 |
| F.3 | Factors used in design of experiments for machining operations | 203 |
| F.4 | ANOVA table for samples with constant stress applied for 100 seconds | 204 |
| F.5 | ANOVA table for samples with constant strain applied for 100 seconds | 206 |
| F.6 | ANOVA table for samples with constant strain applied for 100 seconds, with outliers removed | 208 |
| F.7 | ANOVA table for diameter of machined samples | 208 |

Nomenclature

Acronyms

| | |
|--------|--|
| AOX | UHMWPE which has antioxidant additives included during manufacture |
| CFRP | Carbon Fiber Reinforced Polymer |
| CNC | Computer Numerical Control |
| DAQ | Data Acquisition |
| DMA | Dynamic Mechanical Analysis |
| DSC | Differential Scanning Calorimetry |
| FTIR | Fourier Transform InfraRed spectroscopy |
| HDPE | High Density Polyethylene |
| LDPE | Low Density Polyethylene |
| LLDPE | Linear Low Density Polyethylene |
| NI | National Instruments |
| PE | Polyethylene |
| PET | Polyethylene terephthalate, sometimes written as poly(ethylene terephthalate) to clarify that it is not a type of polyethylene |
| PMMA | Poly(methyl methacrylate), otherwise known as Plexiglas [®] or Perspex [®] |
| PP | Polypropylene |
| PS | Polystyrene |
| PUR | Polyurethane |
| PVC | Polyvinyl Chloride |
| RMS | Root Mean Square |
| SEM | Scanning Electron Microscope |
| UHMWPE | Ultra High Molecular Weight Polyethylene |
| ULMWPE | Ultra Low Molecular Weight Polyethylene |
| UTS | Ultimate Tensile Strength |
| XLK | UHMWPE which has been crosslinked, often through irradiation |

Machining terms

| | |
|----------|--|
| α | Rake angle |
| θ | Angle of the resultant of cutting force and thrust force |
| CS | Cutting speed |
| DOC | Depth of cut |
| F_c | Cutting force in orthogonal cutting |
| F_r | Resultant of cutting force and thrust force |
| F_t | Thrust force in orthogonal cutting |
| h_t | Minimum cutting thickness/minimum depth of cut |
| r | Cutting edge radius |

Statistical terms

| | |
|-------|--|
| ANOVA | Analysis of Variance |
| DF | Degrees of Freedom |
| DOE | Design of Experiments |
| F | F statistic |
| MSE | Mean Square Error |
| P | P value, typically corresponding to a T or F statistic |
| SS | Sum of Squares |
| T | T statistic |

Units

| | |
|-------------|---|
| $^{\circ}C$ | Degree Celsius |
| g | Gram |
| J | Joule |
| K | Degree Kelvin |
| m | Meter |
| min | Minute |
| mol | Mole |
| N | Newton |
| Pa | Pascal |
| R_a | Surface roughness parameter for arithmetic average of absolute values of deviation of surface from mean line |
| R_z | Surface roughness parameter for average distance between highest peak and lowest valley in each sampling length |
| rev | Revolution |
| T_g | Glass transition temperature |
| T_m | Melting temperature |
| W | Watt |

Chapter 1

Introduction

1.1 Polymers as engineering materials

Polymers have found widespread applications as engineering materials, with total EU demand for polymers reaching 46.3 million tonnes in 2013 [1]. Figure 1.1 shows EU demand for polymers by sector. It can be seen that the biggest consumer of polymer products is the packaging sector, accounting for nearly 40% of demand, ahead of building and construction, which is the source of 20.3% of demand. The large size of the “other applications” sector speaks to the versatility of polymers, and the wide range of applications across which they are used.

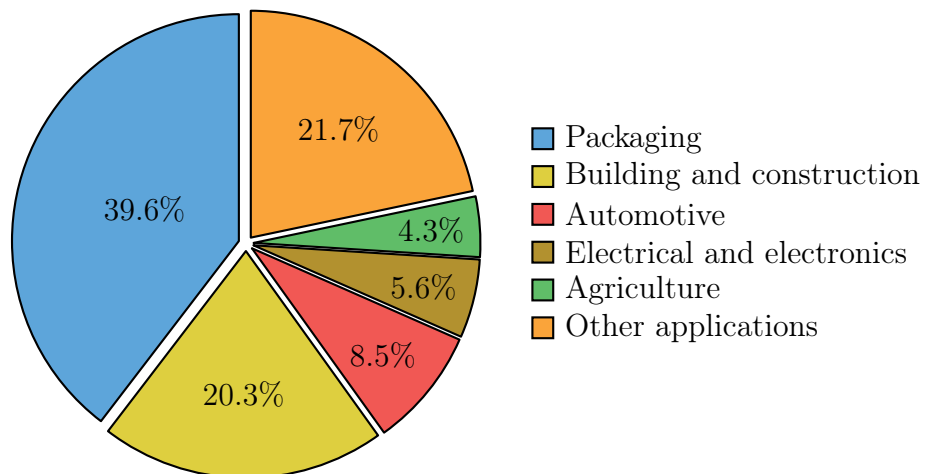


Figure 1.1: Plastics demand in the EU, by sector. Data from 2013. The “other applications” group includes sectors such as consumer and household appliances, furniture, sport, and health and safety. Adapted from [1].

This demand for polymers is met and exceeded by the EU plastics production industry, which produced 57 million tonnes of polymer products in 2013. The surplus above the level of demand resulted in a positive trade balance of €18 billion [1]. Europe

INTRODUCTION

is the second largest producer of polymers, behind China, with world production in 2013 of 299 million tonnes. Demand for polymers is likely to continue to grow, with emerging nations such as China, India and Vietnam expected to see their demand for polymers grow at a rate three times that of Europe and North America [2].

Eurostat [3] figures for the EU rubber and plastics products manufacturing sector in 2013 show that the sector is a major employer and economic force within the EU, with over 66 thousand enterprises employing over 16 million people. The industry has a gross turnover of €327 billion, with total value added of approximately €80 million. The plastics industry is also a major factor in innovation, contributing over 4% of patents submitted in the EU from 2003 to 2012 [4].

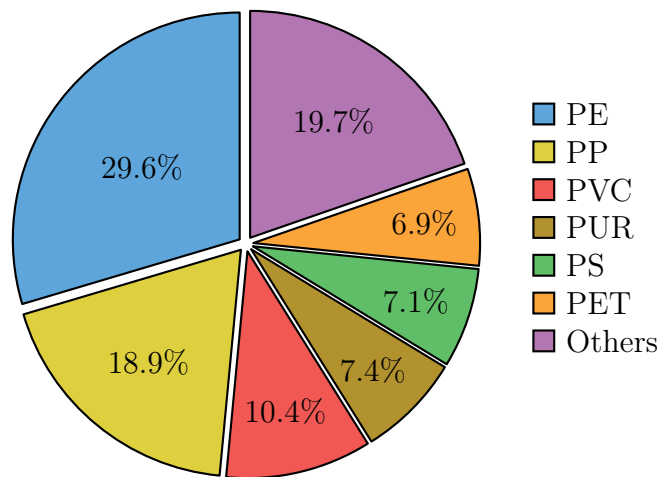


Figure 1.2: Plastics demand in the EU, by polymer type. Data from 2013. Adapted from [1].

Figure 1.2 shows EU demand for polymers broken down by polymer type. The choice of which polymer to use when designing a component depends upon the properties required, the manufacturing operations to be used, and the final application of the polymer. In many applications polymers provide improved performance and reliability when compared to alternative materials, often combined with lighter weight and increased corrosion resistance.

It can be seen in figure Figure 1.2 that polyethylene accounts for nearly 30% of the demand for plastics within the EU. The versatility of polyethylene sees it in use for applications from plastic bags to conveyor belt guides and chopping boards. One sector where polyethylene has found a niche application is in orthopaedic implants, where a variety of polyethylene is used for bearing surfaces [5]. This variety is known as Ultra High Molecular Weight Polyethylene (UHMWPE), and it is used in orthopaedic implants due to having high resistance to mechanical wear, without causing wear of the opposing material [6, 7]. This wear resistance is a result of the high molecular

1.1. POLYMERS AS ENGINEERING MATERIALS

weight of the material, which increases fracture toughness [8], which can be increased further through additives and radiation crosslinking of the material [9]. UHMWPE finds use in a wide variety of orthopaedic implants, including those used for hip, knee and shoulder replacements, with approximately one million UHMWPE components implanted worldwide per year [10].

For these applications it is necessary to create implants which functionally mimic the original joint, often requiring complex freeform geometry on the finished part, to replicate the joint being replaced. As the material is to be a wear surface, it is also necessary to have a smooth surface finish. While many methods have been developed to manufacture components from polymers using moulding and forming processes, many of these do not deliver the required surface finish or dimensional accuracy, or are incapable of achieving complex freeform geometries, which necessitate further finishing operations. Alternatively, it may be desirable to manufacture small production runs of parts, either for customisation purposes, lean manufacturing, or prototyping of a design. Traditional polymer processing methods such as injection moulding, vacuum forming, or extrusion are unsuitable for small production runs due to the high cost of tooling, with machining providing a more economical approach.

The use of material removal operations such as turning, milling and drilling as a finishing operation for polymers has not seen much research interest, with many publications assuming that common metal cutting and woodworking tooling, and their associated cutting parameters, are applicable to the machining of polymers. This often leads to poor surface finish and a lack of dimensional accuracy, resulting in part rejection, inefficiency and increased cost.

1.2 Research objectives

The goal of the present research is to characterise the machining of Ultra High Molecular Weight Polyethylene (UHMWPE), a biomedical grade polymer commonly used in total joint replacement applications. This will be achieved by:

- Implementing a process monitoring and data acquisition system to monitor the cutting forces, cutting temperatures and chip formation mechanism during machining of biomedical grade polymers for a variety of cutting, tooling and workpiece parameters.
- Characterising the chemical, mechanical and thermal properties of the materials under study within the operating parameters typically found while machining.
- Making use of appropriate statistical analysis techniques to analyse the data collected.

This approach will be used to answer four research questions, which are as follows:

1. What are the machining and tooling factors influencing machining forces, tool temperature, chip formation mechanisms, and surface quality?
2. Do modifications of the material, such as the addition of an anti-oxidant chemical or crosslinking of the polymer chains, cause any fundamental change in the machinability of the material?
3. What effect does the use of cryogenic cooling of the workpiece prior to machining have on the machinability of the material and surface quality of the machined surface?
4. What implications does viscoelastic stress relaxation have for machining of UHMWPE?

1.3 Thesis overview

This thesis is divided into eight chapters, including this introductory chapter.

- Chapter 2 provides an introduction to polymer materials, their use in biomedical applications, and the state of the art in the machining of polymers. The statistical analysis techniques and process monitoring systems to be used in later chapters are also discussed.
- Chapter 3 describes the experimental methodology applied within this work, including the types of analysis carried out, the process monitoring system used, and the design of experiments for the following chapters.
- Chapter 4 details the testing of material properties carried out on the types of UHMWPE used for machining tests in subsequent chapters. The results of this testing informs the later analysis of experimental data.
- Chapter 5 is a study on the orthogonal cutting of three blends of UHMWPE, when varying machining and tooling parameters. This provides a baseline on the room temperature machining of UHMWPE.
- Chapter 6 expands upon the results shown in the preceding chapter by extending the analysis to include cryogenically pre-cooled workpieces, highlighting the influence of material temperature on the machinability of UHMWPE.
- Chapter 7 presents results on the viscoelastic stress relaxation of UHMWPE, both under controlled loading conditions and after machining operations.
- Chapter 8 presents the main conclusions of the work carried out, outlining the contributions to knowledge contained within this thesis, and provides some future directions for work in the field.

The major types of analysis used within chapters 4 to 7 are shown in figure 1.3.

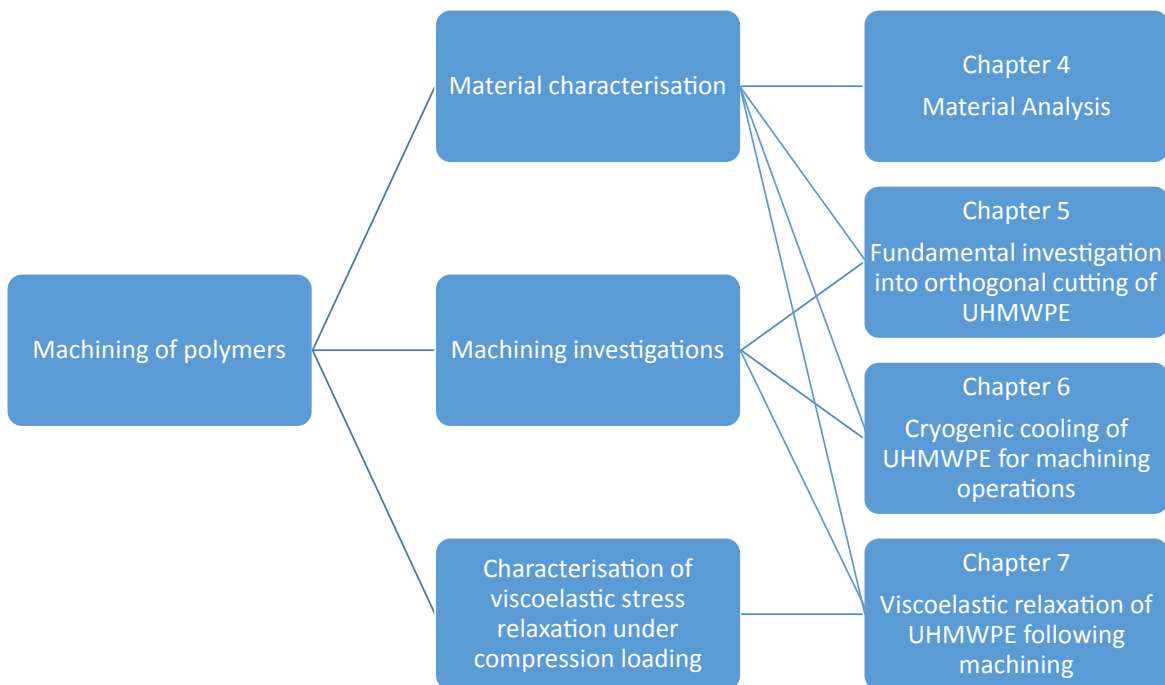


Figure 1.3: Flowchart showing makeup of chapters.

Chapter 2

Literature review

2.1 Introduction to polymer materials

Polymers are materials which consist of large molecules of repeating units¹. Any material with this structure is considered a polymer, which includes a wide variety of natural and synthetic materials. Examples of naturally occurring polymers include wool, silk, amber, rubber, and DNA. These materials have been in common use for centuries, but it was not until the 19th century that attempts to create a synthetic polymer were successful, with the synthesis of Parkesine² [11]. Since then there has been an explosion in polymer technology, with a wide variety of synthetic polymers being manufactured and used for a vast array of applications. For engineering applications polymers can broadly be grouped into two varieties: [12]

1. Thermoplastic materials.
2. Thermosetting materials.

Thermoplastic materials will soften and flow when heated, while thermosetting materials typically undergo a crosslinking process which binds the polymer chains together, preventing flow at high temperature [12]. As a result these materials do not soften or flow when heated. This crosslinking process may be caused by the heating of the material, by the addition of a catalyst (as in two part epoxies), or by irradiation or chemical treatment of a polymer which is normally a thermoplastic [13]. Heating of thermosetting materials after the crosslinking process has occurred will not soften the material and cause it to flow. Excessive heating will lead to breakdown of the polymer rather than any softening or melting.

¹These units are named “mers”, from the Greek word *meros*, meaning part. Chains of multiple mers are thus referred to as poly-mers.

²Named after its inventor, Alexander Parkes. While not widely adopted, it led to the development of Celluloid, a key element in photography and motion pictures.

2.1.1 Applications of polymers

Polymers have found many application areas, often due to their unique properties and ease of manufacture. Some applications are as lightweight or easy to manufacture replacements for parts previously manufactured from wood or metal. Examples of this include car interior trim, some parts of firearms, household piping, and applications as simple as paperclips. In 1975 polymers contributed 6% of the mass of an automobile, whereas in 2005 this had risen to 13% [14].

An injection moulded paperclip, for example, can be produced in large batches using a single step from raw material to finished part, using a machine which can be used for multiple other applications. In comparison, a traditional metal paperclip requires multiple drawing and annealing operations to obtain wire of the correct size, followed by three bending steps per clip, performed using a specialised machine with limited alternative applications.

Global demand for polymers is high, and continues to rise, from 196 million tonnes in 2005, to 270 million tonnes in 2010, with projected demand of over 360 million tonnes in 2015 [15]. Polymers can be found in many applications where other materials would be unable to provide the required performance. An example of this is the use of CFRP³ as light weight structural components in high performance automotive and aerospace applications, and the use of polystyrene as an energy absorbing material in bicycle helmets and packaging.

One area where polymers have had a large impact has been the biomedical sector [12]. Many polymers can be made to provide high levels of biocompatibility, which reduces the chance of rejection by the immune system. Examples of this can be seen in the cosmetic surgery industry, where prostheses such as breast implants must be made to have a long lifespan inside the human body, while meeting criteria for aesthetics. A growing application area for biomedical grade polymers is the creation of custom orthopaedic implants for individuals, based upon their personal needs. An example of this is orbital wall defect treatment, where a custom implant is created for the patient using a CT scan of their skull [16]. Materials with a low coefficient of friction and high wear resistance also find uses as structural components in total joint replacement [6], as a replacement for a load bearing cartilage surface.

2.1.2 Polymer properties

Just as different metals have a variety of properties, different polymers can exhibit very different behaviour to applied thermal or mechanical loads. Many of these properties

³Carbon Fibre Reinforced Polymer, a type of composite material

are a function of the exact molecular makeup of the material, the level of crystallinity and crosslinking, the temperature of the material, the strain rate of applied loads, and even on parameters such as the strain history of the material, or the geometry of the polymer melt during polymerisation [17]. A comparison of the properties of some typical polymers and other materials is shown in table 2.1. It can be seen that polymers typically have far lower modulus of elasticity and ultimate stress, higher percentage elongation to fracture, and lower thermal conductivity than metals.

Table 2.1: Comparison of the properties of polymers and other materials. Adapted from [18].

| Material | Modulus of elasticity | Poisson's ratio | Ultimate stress | % elongation to fracture | Thermal conductivity |
|----------------------|------------------------------|------------------------|------------------------|---------------------------------|-----------------------------|
| | <i>GPa</i> | | <i>MPa</i> | | <i>W/mK</i> |
| Polyethylene | 0.7 - 1.4 | 0.4 | 7 - 28 | 15 - 300 | 0.4 |
| Nylon | 2.1 - 3.4 | 0.4 | 40 - 80 | 20 - 100 | 0.3 |
| Elastomers | 0.0007 - 0.004 | 0.47 - 0.5 | 7 - 20 | 100 - 800 | 0.13 - 0.16 |
| Aluminium | 70 - 79 | 0.33 | 100 - 550 | 1 - 45 | 177 - 237 |
| Steel, high strength | 190 - 210 | 0.27 - 0.3 | 550 - 1200 | 5 - 25 | 33 - 60 |

2.1.2.1 Viscoelastic behaviour

One of the key properties of polymers, which must be understood in order to allow any analysis, is the viscoelastic nature of the response of the material to applied loads [19]. This viscoelasticity is best described as a response which has both elastic/instantaneous and viscous/transient elements, with the elastic component proportional to the strain and the viscous component proportional to the strain rate.

The exact nature of the response depends on many factors, including [17, 19–27]:

1. The magnitude of the applied load
2. The temperature of the material
3. The strain rate or frequency of oscillation of the applied load
4. The strain history of the material
5. The crystallinity of the material
6. The level of crosslinking in the material
7. Any orientation of the polymer chains in the material or other anisotropy

8. Any aging or degradation of the material

One of the features of viscoelasticity is that the changes in the nature of the response to applied load due to time and temperature are similar, and can often be compared, using a principle known as time-temperature superposition [28]. It is possible to think of the behaviour of the material at high temperatures as being equivalent to that at room temperature over a longer time period or lower strain rate. It is worthy of note that this equivalence does not hold across the entire temperature range, as polymers have what is known as a glass transition temperature (T_g) [29]. The change in material stiffness at the glass transition temperature is shown in figure 2.1.

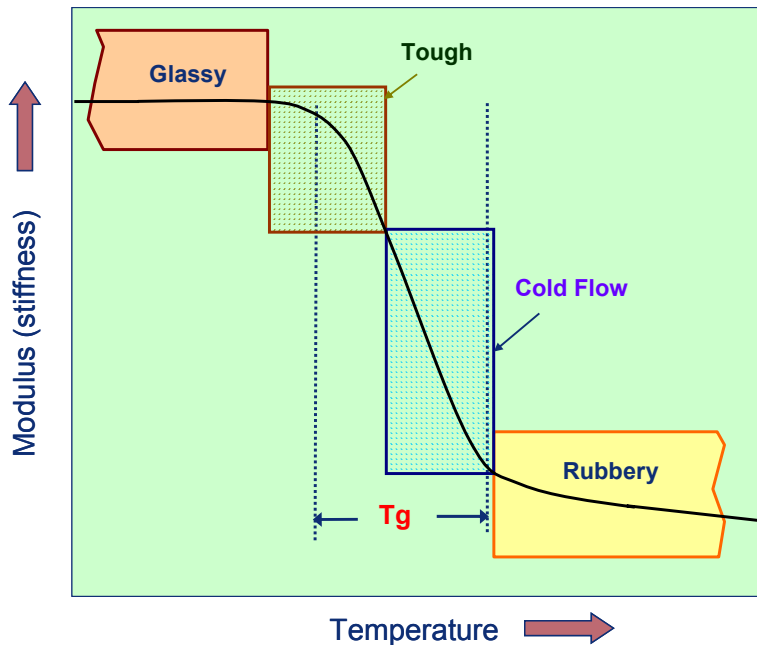


Figure 2.1: Typical stiffness curve for polymers, with machinability regions [30].

Below the glass transition temperature the material will react in a stiff, elastic manner, behaving as a glassy solid. Above the glass transition temperature the material will react in a rubbery, viscous manner, as the local mobility of the polymer chains increases. This is illustrated in figure 2.2, which shows stress-strain response of PMMA at a variety of temperatures and strain rates, and in figure 2.3, which shows HDPE samples after tensile testing across a range of strain rates. Amorphous polymers have a steep reduction in modulus at T_g , while semicrystalline polymers have a more gradual change, as the melting point of the crystals will be above T_g . Thus the crystallinity of the polymer will influence the nature of the change of the mechanical properties at the glass transition temperature, in addition to directly changing the mechanical properties [12,31].

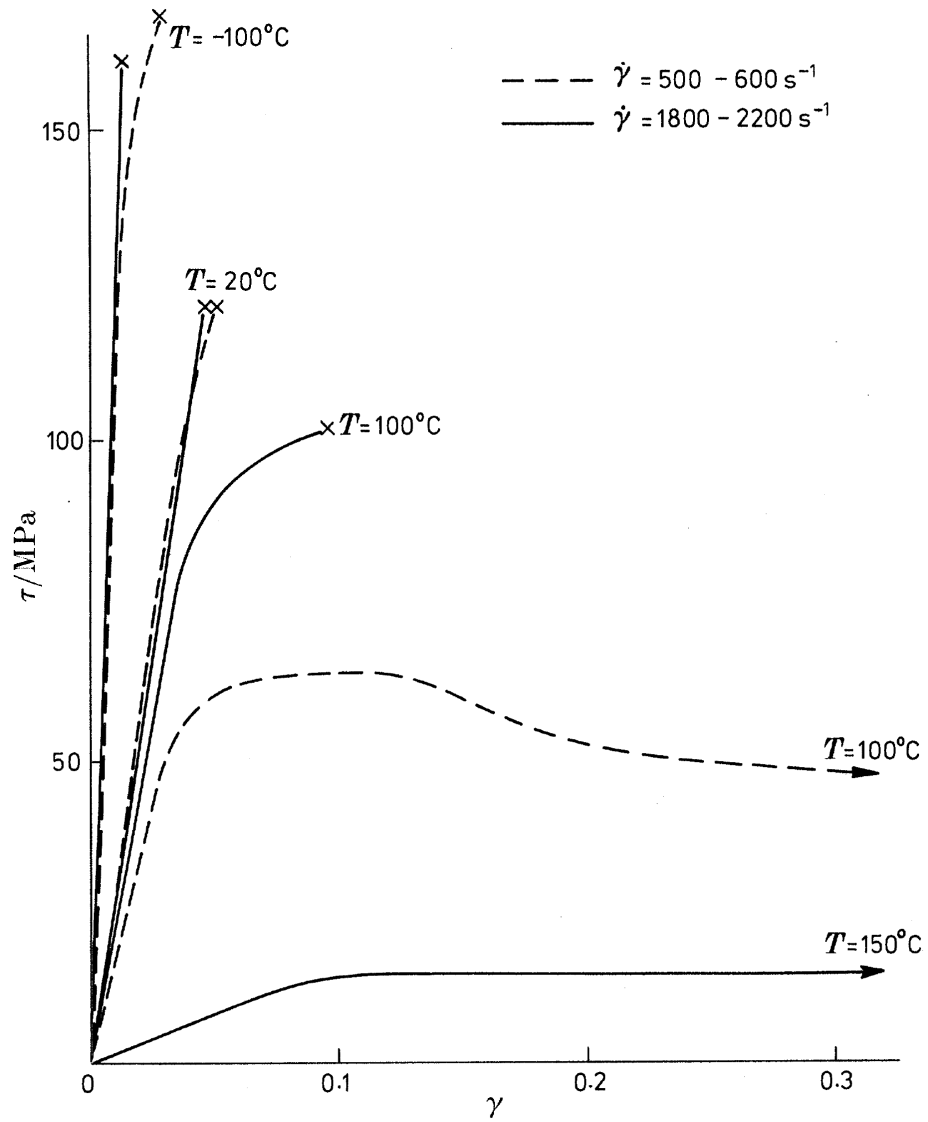


Figure 2.2: Effect of temperature and strain rate on stress-strain response of PMMA, with nominal T_g of 120°C . Crosses denote fracture [32].

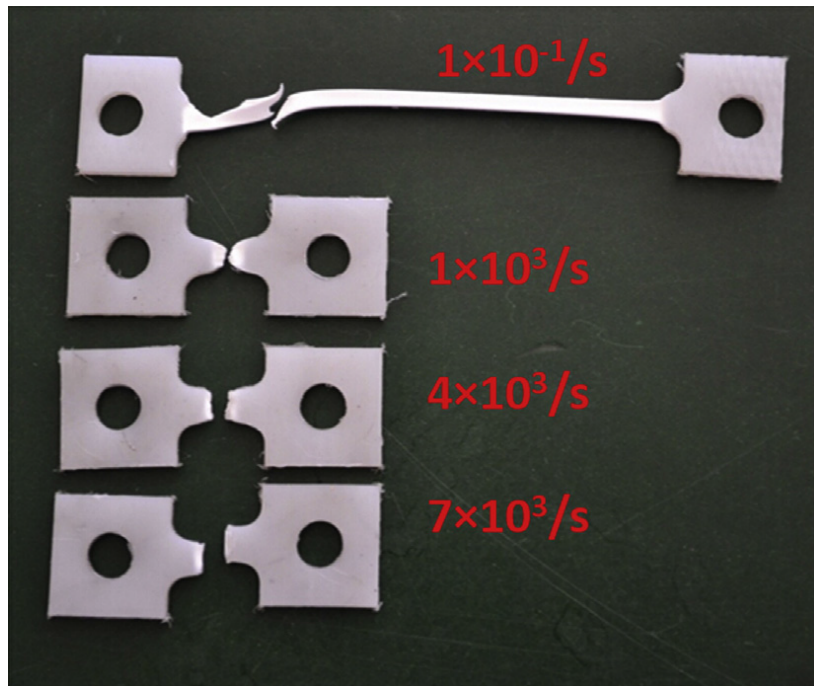


Figure 2.3: Effect of strain rate on tensile strain to failure in HDPE [33].

Any isotropy in the material can also have a large effect on the properties of a polymer, with extreme cases of isotropy causing an order of magnitude difference in the tensile yield stress of the material parallel and perpendicular to the direction of the isotropy [19]. This is caused by the orientation of polymer chains allowing easier movement in one direction. The effects of viscoelasticity are easily demonstrated through a creep test conducted on a sample which has been heated to above the glass transition temperature of the polymer. Under constant applied stress the material will continue to strain over time. If the load is removed before failure the material will display recovery toward the original, undeformed shape. Similarly, applying a constant strain to the material will lead to stress relaxation, and gradual recovery after the removal of the load. This behaviour also leads to large hysteresis effects in cyclic loading conditions [34, 35], as shown in figure 2.4.

There are many models which attempt to accurately represent viscoelasticity. Many of these models make use of combinations of spring and damper systems, as shown in figure 2.5. By using these elements it is possible to conduct relatively simple analysis using well established techniques for control system analysis. The simplest models used are the Maxwell model, as shown in figure 2.5a, and the Kelvin or Voigt model, as shown in figure 2.5b. Both of these models are simple combinations of a spring and viscous damper in series and parallel respectively. While these models each show some promise in their representation of viscoelasticity [36], neither captures both creep/relaxation

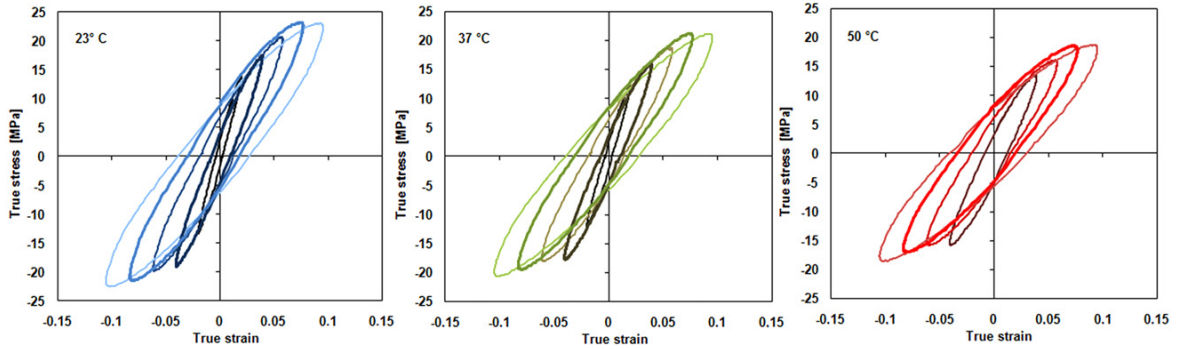


Figure 2.4: Hysteresis as a function of temperature and imposed strain in UHMWPE [34]. Colours indicate varying temperature, while shades within each colour show behaviour after increasing number of cycles.

and recovery accurately. By combining the models in series, as shown in figure 2.5c, a closer representation of these three features can be achieved [29, 37]. An alternative approach is to combine the Maxwell and Voigt models in parallel, forming what is known as the Standard Linear Solid model, as shown in figure 2.5d. This model displays correct general behaviour, but is insufficient for numerical modelling.

By adding further spring-damper systems in parallel with the Standard Linear Solid model it is possible to improve the accuracy of the model, forming what is known as the Generalised Maxwell model. This approach of having a large number of elements combined in series and parallel leads to the concept of representing the viscoelastic response of a material to applied load as a series of exponential terms, known as a Prony series [38, 39], whereby the constants for a model are generated from experimental data, with the accuracy of the model increasing with the number of terms used in the series [20, 40].

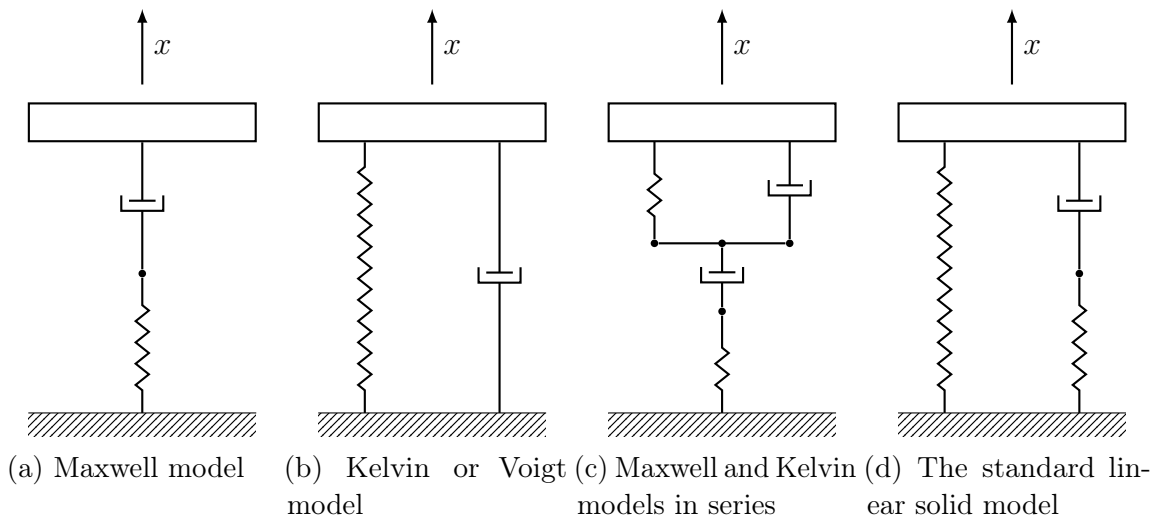


Figure 2.5: Models for viscoelastic behaviour

2.1.2.2 Quantification of viscoelasticity

Experimental data for the viscoelastic behaviour of polymers is typically collected through Dynamic Mechanical Analysis (DMA) [41, 42], where a test sample is subjected to cyclic loads over a range of frequencies and/or temperatures, to evaluate the nature of the response. As the load is cyclic it is possible to break it down into an elastic component which is in phase with the applied load, and a viscous component which is 90° out of phase with the applied load [43]. These components are referred to as the storage modulus and loss modulus, respectively. Using this data it is possible to evaluate which component dominates across the frequencies/temperatures used. This method is most commonly used to evaluate the glass transition temperature of viscoelastic materials, by monitoring for the change from elastic-dominated to viscous-dominated behaviour.

Alternatively, Differential Scanning Calorimetry can be used to measure the glass transition temperature from the variation in heat capacity at thermal transitions during heating [44], though Greco and Maffezzoli [45] have shown that for polyethylene this method is sensitive to the heating rate used, while Göschel and Ulrich [46] have successfully used this technique to identify changes in mechanical properties due to radiation-induced crosslinking.

Where concerns exist about variations in the chemical or molecular structure of a material it is appropriate to use Fourier Transform Infrared Spectroscopy to compare and analyse polymer samples [47]. This method measures the absorbance of a sample to light across a range of wavelengths, which varies depending on the chemical makeup and molecular structure of the material. Gulmine *et al.* [48] studied the effects of scanning parameters and sample type on FTIR results in polyethylene, finding that it was possible to distinguish between HDPE, LDPE and LLDPE from FTIR data. The main absorptions of polyethylene and their chemical assignments are shown in table 2.2.

Table 2.2: Main absorptions of polyethylene in the IR region, and their assignment [48].

| Wavenumber cm^{-1} | Assignment | Intensity |
|----------------------|------------------------------|-----------|
| 2919 | CH_2 asymmetric stretching | Strong |
| 2851 | CH_2 symmetric stretching | Strong |
| 1473 and 1463 | Bending deformation | Strong |
| 1377 | CH_3 symmetric stretching | Weak |
| 1366 and 1351 | Wagging deformation | Medium |
| 1306 | Twisting deformation | Weak |
| 1176 | Wagging deformation | Very weak |
| 731 - 720 | Rocking deformation | Medium |

2.1.3 Polyethylene

Polyethylene is one of the most widely used polymers, having been discovered accidentally in 1931 due to an oxygen leak into a high pressure experiment involving ethylene, leaving a waxy solid residue [49]. It is chemically one of the simplest polymers available. Ethylene consists of two carbon and four hydrogen atoms, giving it a chemical formula of C_2H_4 , as shown in figure 2.6a. When polyethylene is formed the double bond between the carbon atoms is opened out and used to create a long chain of repeating units, as shown in figure 2.6b. The chemical formula for polyethylene is $-(C_2H_4)_n-$, where n is the degree of polymerisation, or the number of repeat units in an individual polymer chain. This degree of polymerisation is an important factor in determining the mechanical properties of the finished part [6].

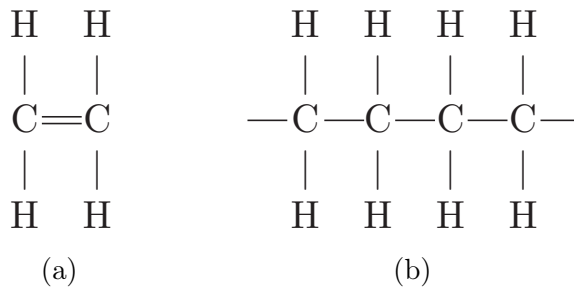


Figure 2.6: Chemical structure of a) ethylene and b) polyethylene.

Polyethylene powder is formed from ethylene gas, then compressed and baked in proprietary conditions to form solid bars. The properties of polyethylene depend on the density and molecular weight of the material, the crystallinity and level of crosslinking in the material, and in some cases on any additives which may have been used in the manufacture of the material. Typical additives included in the powder before consolidation are calcium stearate [50], used to ease processing, and antioxidants such as vitamin E [6, 51] and α -tocopherol [13, 52, 53], though many other additives are available for a variety of purposes [54].

As mentioned earlier, the length of the polymer chains is an important factor in the mechanical properties of the bulk material. The average length of these chains is measured through the molecular weight of the material, in g/mol . Since it is known that a single ethylene molecule has a molecular mass of $28.052 g/mol$ ⁴, the average chain length can easily be inferred. It is often also important to study the distribution of molecular weight throughout the material to ensure homogeneity. The variation in properties are shown in table 2.3 and figure 2.7.

⁴4 hydrogen and 2 carbon atoms, with atomic weights of 1.008 and 12.01 g/mol respectively

Factors involved in the characterisation of polyethylene include:

- Molecular weight
- Density
- Level of branching
- Level of crosslinking

For most industrial purposes polyethylene is separated into 2 grades: high density (HDPE) and low density (LDPE) [12]. HDPE has greater stiffness and is more suitable for structural applications such as blow-moulded bottles, fuel tanks, extruded pipes and waste containers⁵, while LDPE is more suited for packaging applications, such as plastic bags and shrink wrap.

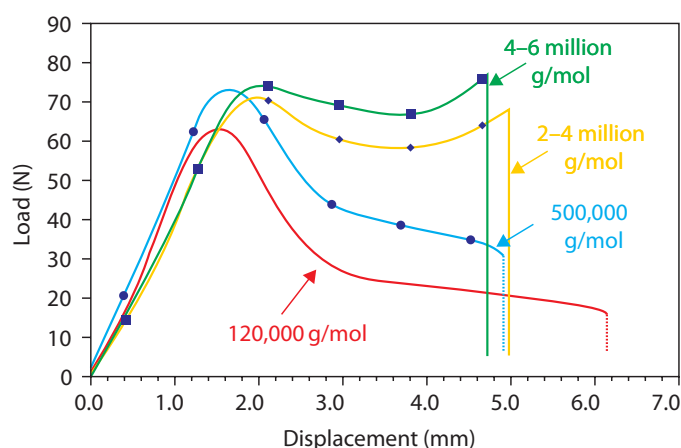
For more specialist applications there is a need for a version of polyethylene with material properties exceeding that of HDPE. This is achieved by increasing the molecular weight of the material by a factor of 20 or more, thus forming a material known as Ultra High Molecular Weight Polyethylene (UHMWPE). A comparison of the typical properties of HDPE and UHMWPE is shown in table 2.3, while the effect of increasing molecular weight on mechanical properties is illustrated in figure 2.7, and the effect of strain rate on compressive stress-strain behaviour is shown in figure 2.8. However, this increase in chain length prevents traditional melt processing of the material, as upon heating the material will decompose before the viscosity drops sufficiently to allow processing [54]. UHMWPE is generally processed in powder form due to this limitation, though it is possible to create melt-processable UHMWPE through blending with Ultra Low Molecular Weight Polyethylene (ULMWPE) [55].

UHMWPE displays improved mechanical properties compared to HDPE [57], and is also more resistant to wear, which is important in biomedical applications [7, 56, 58–60]. This wear resistance can be further improved through the use of irradiation or chemical treatment to crosslink the material [9, 13, 52, 61–63]. This process may also alter the mechanical properties of the material [64, 65], and cause the formation of free radicals [50, 62], and thus oxidation [7, 66] and associated degradation of mechanical properties [67, 68]. In extreme cases this degradation can cause failure of the part [69, 70]. Annealing and remelting procedures can help to reduce the level of oxidation [31]. Advances in crosslinking processes are being developed with the aim of eliminating this free radical formation, thus preventing oxidation of the material [71], while providing improvements in wear rates over plain UHMWPE [5].

⁵More commonly known as “wheelie bins”

Table 2.3: Typical properties of UHMWPE. Mechanical properties measured at 23 °C [56].

| Property | Unit | UHMWPE | HDPE |
|--|----------------------|----------------------|---------------|
| Molecular weight | 10^6 g/mol | 2 - 6 | 0.05 - 0.25 |
| Melting temperature | $^{\circ}\text{C}$ | 125 - 138 | 130 - 137 |
| Poisson's ratio | | 0.46 | 0.4 |
| Specific gravity | | 0.932 - 0.945 | 0.952 - 0.965 |
| Tensile modulus of elasticity | GPa | 0.8 - 1.6 | 0.4 - 4 |
| Tensile yield strength | MPa | 21 - 28 | 26 - 33 |
| Tensile ultimate elongation | % | 350 - 525 | 10 - 1200 |
| Impact strength, Izod, 3.175mm thick specimen | J/m | > 1070 (no break) | 21 - 214 |
| Degree of crystallinity | % | 39 - 75 | 60 - 80 |

Figure 2.7: Effect of increasing molecular weight on mechanical properties of UHMWPE. Data is from small punch tests performed at room temperature at a rate of 0.5 mm/min [6], using punch with hemispherical head to penetrate 0.5 mm thick samples [72].

Viscoelasticity in polyethylene has been studied by Drozdov and Yuan [73, 74], who observed stress relaxation, creep, and nonlinear stress - strain behaviour in tensile tests of LDPE. Similar research using compressive loads has been carried out by Lee and Pienkowski, who have found that compressive creep under static loading is a significant factor for UHMWPE [75]. It should be noted that creep under dynamic loading such as that seen in total joint replacements is smaller in magnitude [76] than under static loading, and that this creep reduces wear in service [77].

The viscoelastic behaviour of UHMWPE under compressive loading has been studied by Brown *et al.* [78], who carried out DSC to characterise the thermal behaviour of the material, along with DMA tests over a large range of strain rates and temperatures on HDPE, UHMWPE, and crosslinked polyethylene. In this work it was observed that

a large number of authors have attempted to evaluate a glass transition temperature for polyethylene, with estimates ranging from -69°C to 10°C . The work concludes that HDPE has a glass transition temperature of 3°C , while T_g for UHMWPE and crosslinked polyethylene was unable to be determined. This is in contrast to the work of Beake, who with other authors [79] reported a T_g for LDPE of -126.8°C , and whose work has reported a T_g for UHMWPE of $\sim -122^{\circ}\text{C}$ [80], evaluated from nanoindentation creep of samples. Kutz [6], in his book on the use of UHMWPE as a biomaterial, reported a T_g of -120°C , though the method by which this was evaluated is unclear. Göschel and Ulrich [46] carried out DMA tests on UHMWPE with varying levels of crosslinking, finding that the glass transition temperature of the material in all cases was between -118° and -121°C .

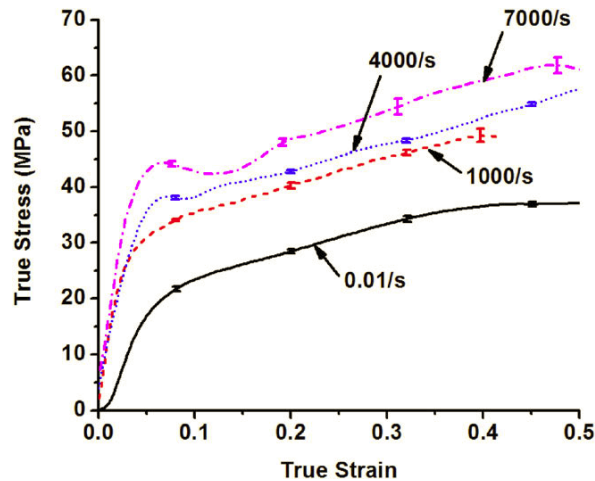


Figure 2.8: Stress - strain relations as a function of strain rates for UHMWPE [81].

It should be noted that in addition to the effects already discussed, the properties of polyethylene change as the material ages [44, 82], and, in the case of biomedical applications, post implantation [83, 84]. The effects of 6 years of aging at elevated temperature and humidity are shown in table 2.4. Many specialised testing procedures exist to evaluate changes in the properties of materials used in biomedical implants [72], as degradation in the material properties can occur following implantation, due to factors such as wear [83], changes in fatigue mechanisms at body temperature [85], and oxidation due to cycling loading and wear [86, 87]. These changes could potentially compromise the wear resistance of the material [88]. Hasenkamp *et al.* [89] have conducted research on the integration of strain sensors into UHMWPE components in total knee replacement orthopaedic implants in order to monitor the component for material degradation, though there are significant regulatory obstacles to human implantation of such a device.

Table 2.4: Variation in properties of UHMWPE after 6 years of aging at $25 \pm 3^\circ\text{C}$ and $80 \pm 5\%$ humidity for 6 years in air [44].

| Property | Unit | Nonaged specimen | Aged specimen |
|---------------------|------------------|------------------|-----------------|
| Young's modulus | <i>MPa</i> | 1136 ± 30 | 790 ± 12 |
| Yield stress | <i>MPa</i> | 20.4 ± 0.25 | 18.2 ± 0.33 |
| Fracture stress | <i>MPa</i> | 25 ± 0.3 | 20.1 ± 0.4 |
| Fracture strain | | 1157 ± 40 | 880 ± 30 |
| Crystallinity | % | 55 | 67 |
| Melting temperature | $^\circ\text{C}$ | 132.84 | 136.3 |
| Lamellar thickness | <i>nm</i> | 23.5 | 32.6 |

In addition to biomedical applications, UHMWPE is also used to manufacture Dyneema[®], a competitor to Kevlar[®] [90–92].

2.1.4 Manufacture of polymers

Polymers are typically formed from a base powder or gas [6], using elevated temperature and/or pressure, and sometimes with the addition of a catalyst⁶. The growth of the polymer chains is influenced by many factors, such that it can be considered quasi-random, and may or may not occur in an ordered fashion. When the structure is disordered the resulting bulk material is amorphous, whereas when areas of ordered structure occur the bulk is considered semi-crystalline [11]. The amount of the material which shows an ordered structure is referred to as the crystallinity of the polymer. This, along with the mean molecular weight and the molecular weight distribution, are of interest in the study of the physical properties of the polymer. It is worthy of note that some polymers will never align in a crystalline manner, and will remain completely amorphous, while the crystallinity of other polymers will depend on the molecular weight.

2.1.5 Traditional polymer processing

One of the great advantages of polymers is their ease of processing compared to metals. Often it is possible to manufacture a finished part directly from a base powder material in one operation [6]. The typically large % elongation to fracture for polymers allows the easy manufacture of thin walled products such as drinks bottles and refuse sacks, while the flow properties of thermoplastics at high temperatures facilitates flow based techniques such as injection moulding.

⁶Often in commercial products the exact consolidation process for a polymer is proprietary

LITERATURE REVIEW

Extrusion is an example of a continuous process where raw material in powder form is used to produce a finished part of constant cross section [12]. Extrusion of polymers differs from extrusion of metals in that it typically uses a screw extruder to mix the raw material into a form suitable for extrusion. Extrusion can also be used to coat another product through a process known as “extrusion covering”. An example of everyday use of this process is adding a layer of plastic to a metal wire in order to provide electrical insulation.

Polymers can also be processed through moulding, forging and casting, in a similar manner to metals. Moulding operations performed at elevated temperature are known as thermoforming operations. Injection moulding of polymers is similar in concept to die casting of metals, but is capable of producing a much larger range of parts due to the flow properties of polymers. Often injection moulding operations are performed using a reciprocating screw extruder machine [93], which allows direct production from raw materials, and produces a more homogeneous polymer melt, thus increasing the quality of the finished products.

A processing operation unique to polymers is blow moulding, where an extruder is used to produce a hollow tube of material called the parison, which is then placed inside a mould and inflated. The increased pressure causes the material to expand to fill the mould. After cooling the mould is opened and the part ejected, followed by another parison being produced, and the process repeated. This process is used to produce plastic drinks bottles, which can be identified by the presence of weld marks on the bottle, where the halves of the mould meet.

2.2 Polymers for biomedical applications

As noted in section 2.1.1, polymers find many applications in the biomedical industry. The focus of this work is on polymers for total joint replacement applications.

2.2.1 Applications in total joint replacement

Some examples of total joint replacement technology are shown in figure 2.9. Of note is that all examples shown include key components manufactured by machining of polymers.

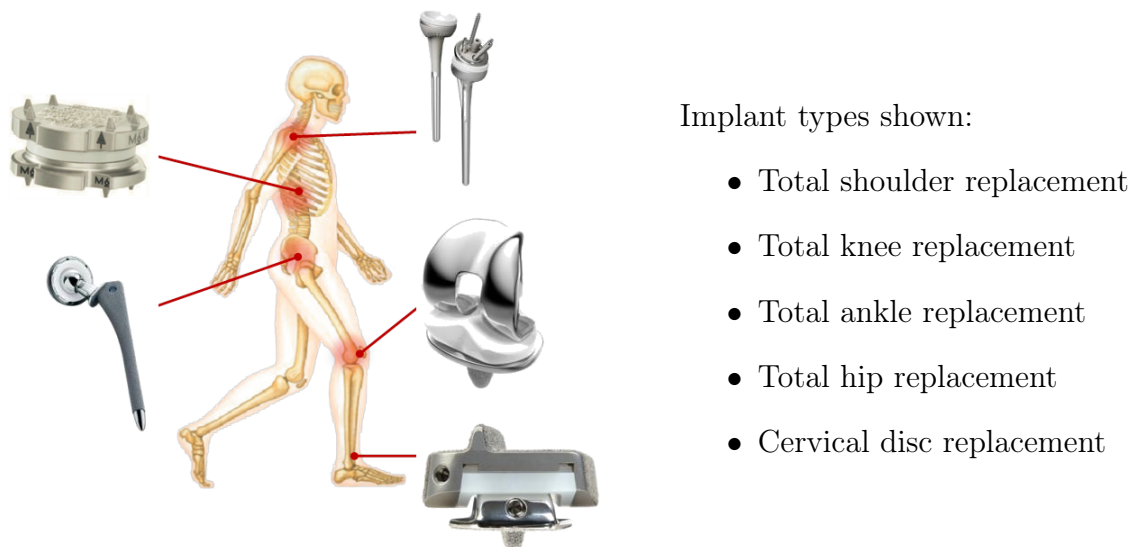


Figure 2.9: Typical total joint replacement solutions. All images copyright DePuy.

In total joint replacements the use of polymer as a bearing surface in conjunction with metal components is popular [9,12]. In the case of a hip replacement the acetabular cup is manufactured from polymer, while in a knee replacement the condyle surfaces of the tibia are replaced by a polymer insert [50]. In these applications high dimensional accuracy is required, as in vivo the joint replacement will be subject to boundary lubrication [6], which typically requires the mating surfaces to have a gap of $< 0.5 \mu m$ [94], which would require high levels of conformity between bearing surfaces.

Polymers also find use in other areas, such as replacement patellas, and in ankle, shoulder and spinal disc replacement surgery. In these applications the component is subject not only to the standard biomedical rigours of operating in the hostile environment of the human body, but also to mechanical loads, and the inherent issues of creep, fatigue and wear. Of importance in these applications is the surface finish of the bearing surface, as a smooth finish will minimize the wear rate observed [95]. In manufacturing drawings and academic studies the average surface roughness value,

LITERATURE REVIEW

R_a , is typically used [96], though the presence of any high points on the surface is also relevant, as these will detach easily under load and become large wear particles [97, 98]. Other surface roughness parameters such as the peak-to-peak height, R_z , should also be considered as part of any analysis of surface quality.

2.3 Machining of polymers

The machining of polymers has been a topic of interest for as long as polymers have been used as an engineering material. While traditional polymer processing is sufficient for many applications, there remain areas where machining is necessary, possibly due to low production quantities, complex geometry, or surface finish or dimensional requirements. Despite the fundamental differences between polymers and metals [99], it was not until the 1960s that scientific investigations into the chip formation mechanisms which occur in polymer machining began, with the works of Kobayashi, Rao *et al.* and Kazanskii. Kobayashi [100, 101] wrote what is considered to be the most comprehensive work on machining of polymers, establishing the factors affecting the machining of polymers, as shown in table 2.5, and identifying six chip formation mechanisms encountered during machining operations, as shown in table 2.6. His work also identified the significance of workpiece deformation during machining, and proposed the concept of a critical rake angle, in addition to providing guidelines and advice on a variety of machining operations for ten thermoplastics, including polyethylene, and two thermosets. Kobayashi also noted in his work on the machining of PVC that cutting forces increase when the edge radius of the cutting tool increases, and that when the edge radius approaches the depth of cut that the tool tends to deform the material rather than cut it. The work of Rao *et al.* [102] occurred contemporaneously with that of Kobayashi, and concentrated on different materials, showing the sensitivity of chip formation mechanisms to tool geometry and feed rates when cutting Delrin[®]. Kazanskii [103] identified five chip formation mechanisms as opposed to Kobayashi's six, merging two related but distinct mechanisms from the nomenclature of Kobayashi, but with the other mechanisms corresponding well. He also identified the need for specialised machine tools for polymers, and the need for research into the machinability of polymers.

Work since has acknowledged that polymers are difficult to machine well [104], with Shih *et al.* [18] investigating the effect of fixture design and milling tool geometry on the machining of elastomers, finding that the design of the flutes of milling cutters can cause the workpiece to be pulled out or pushed in to the workpiece fixturing, and that cooling of the workpiece can improve stiffness and thus machinability. Rubenstein and Storie [105] noted the effect of workpiece deformation ahead of the cutting edge on analysis using the Merchant shear plane theory, while also observing the transition from brittle to ductile cutting when machining perspex. As noted by Carr and Feger [106] in their work on single point diamond milling, by Quadrini [41] in his work on drilling, and by Song *et al.* [96] in their work on milling, achieving a smooth surface finish can require care, along with understanding of the viscoelastic nature of the polymer. In

Table 2.5: Factors affecting cutting action in plastics. Adapted from Kobayashi [101].

| Factor | Has major effect on |
|-----------------------------|---|
| <i>Tool design</i> | |
| Rake angle | Chip formation |
| Relief angle | Tool wear |
| Point radius | Roughness of cut surface |
| Tool material | Tool wear |
| <i>Machining conditions</i> | |
| Depth of cut | Chip formation and roughness of cut surface |
| Cutting speed | |
| Feeding speed | |
| Ambient work temperature | Heat generated and gumming and burning |
| Cooling system | |

biomedical applications a smooth surface finish with few high points is often key to minimizing the wear rate in vivo, thus prolonging the useful life of the part.

Care must also be taken to ensure that the machining operation is not fundamentally altering the crystallinity of the polymer, as has been shown to occur in sample preparation by microtome in the work of Costa *et al.* [107]. Fundamental work into the fracture mechanics behind polymer machining has been conducted by Wyeth, both working independently [108] and in conjunction with Atkins [109], with a mixed-mode fracture model appearing to explain the transition from shearing to cracking/spalling ahead of the tool tip with increasing depth of cut in PMMA, with similar results observed in polyurethane foam by Malak and Anderson [110].

Handbooks for machinists typically only feature machining parameters for specific common polymer types [111], while handbooks produced by plastics manufacturers tend to give broad ranges for cutting parameters and tool geometry, and general advice on troubleshooting of common machining issues [112]. Publications specific to plastics often provide more detailed information, but only for the most commonly used polymers, with no guidance for when tools should be resharpened or how to achieve high levels of surface quality [54].

2.3.1 Viscoelastic behaviour

As noted in section 2.1.2.1, the viscoelastic nature of polymers complicates analysis of the reaction of the material to applied loads. This is particularly true when it comes to machining [113]. While computer models exist for UHMWPE implants in service conditions [114], and for crack propagation under simplified conditions [109, 115], there is no such model for machining. Any FEA models for machining of polymers tend to

use simplified material behaviour, such as assuming hyperelasticity [116].

It is known that viscous deformation of the workpiece is a factor in polymer machining [117]. The high dependency of the material response on strain rate and temperature [118] means that proper selection of cutting conditions is essential to achieve good surface finish and dimensional accuracy [106].

Due to the relatively large workpiece deformation encountered [101], the edge radius of the cutting tool is a factor which is of increased importance. This effect has been investigated in metal cutting, and it has been found that when the edge radius approaches the depth of cut the effective rake angle presented to the workpiece becomes negative [119], and the material will tend to deform under the cutting edge [120]. The factor of importance thus becomes the ratio of the edge radius, r , and the depth of cut, DOC , as shown in equation 2.1.

$$\frac{r}{DOC_{\text{Nominal}}} \quad (2.1)$$

This leads to the concept of a minimum cutting thickness or minimum depth of cut [121] for a given edge radius, below which the material will be plowed, or compressed, rather than cut [122]. This is often referred to as the size effect, and is illustrated in figure 2.12. A similar effect can be achieved with an extremely negative rake angle [123], even with a low edge radius. Conversely, situations where the edge radius approaches the depth of cut have been shown to cause a situation where the rake angle experienced by the workpiece is less than the nominal rake angle of the tool. The limiting value of $\frac{r}{DOC}$ is shown in equation 2.2 [124], with the equation for the effective rake angle shown in equation 2.3 [125, 126]. The effect of edge radius and nominal rake angle on the effective rake angle in cutting is shown in figure 2.10, with a three dimensional plot shown in figure 2.11.

$$h_t = r(1 + \sin \alpha_{\text{Nominal}}) \quad (2.2)$$

$$\alpha_{\text{Effective}} = \begin{cases} \sin^{-1}\left(\frac{DOC}{r} - 1\right) & \text{for } DOC \geq h_t \\ \alpha_{\text{Nominal}} & \text{for } DOC < h_t \end{cases} \quad (2.3)$$

While it would be expected that tool wear in polymer machining would be low due to the lower modulus of elasticity compared to metals, the low thermal conductivity of the material causes tool heating, which leads to tool wear [106, 130]. Tool wear can also occur as a result of tribo-chemical and tribo-electrical mechanisms [131].

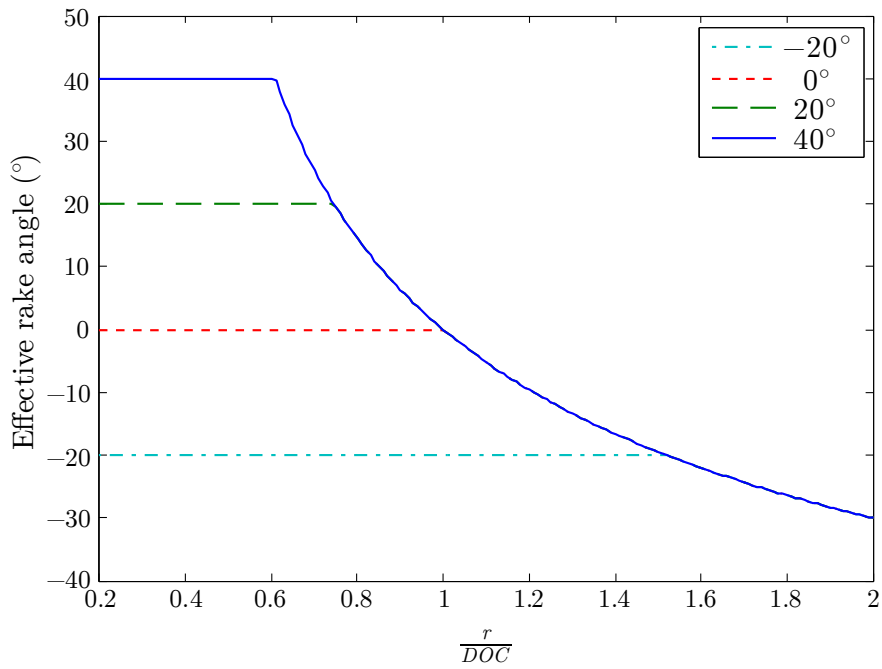


Figure 2.10: Graph of effect of ratio of edge radius to depth of cut on effective rake angle in cutting, for a range of common rake angles. Adapted from [127, 128].

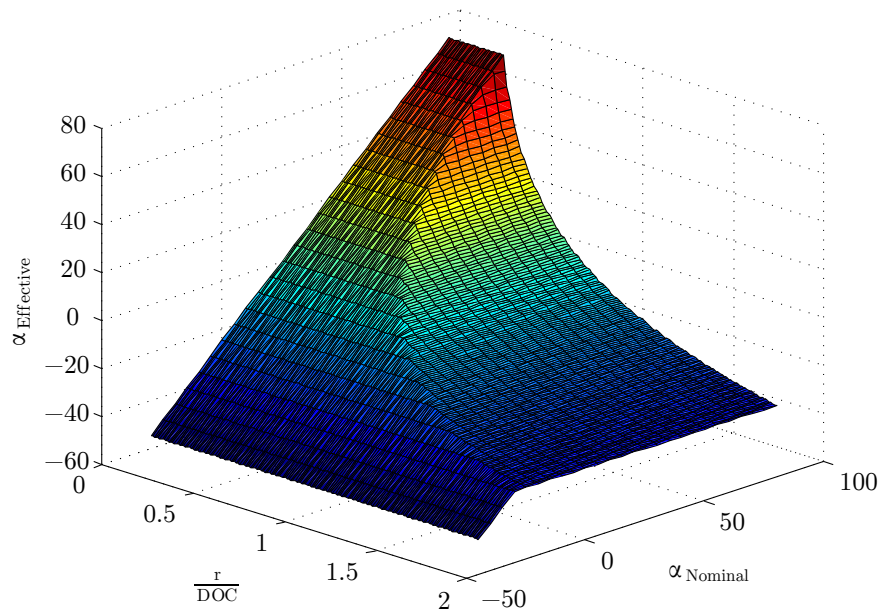
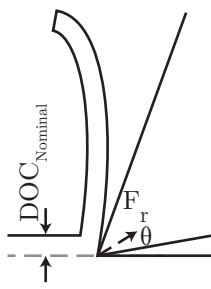
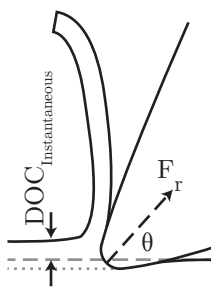


Figure 2.11: 3D visualisation of effect of ratio of edge radius to depth of cut and nominal rake angle on effective rake angle in cutting. Adapted from [127, 128].



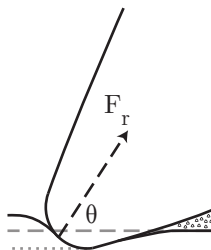
(a) Sharp tool

- $\frac{r}{DOC} \approx 0$
- Little workpiece deformation
- No difference between nominal and actual depth of cut
- Continuous chip
- Low cutting forces
- Small contact area



(b) Worn tool

- $\frac{r}{DOC} < 1$
- Some workpiece deformation
- Some difference between nominal and actual depth of cut
- Continuous chip
- Higher cutting forces
- Increased contact area



(c) Highly worn tool

- $\frac{r}{DOC} > 1$
- Large workpiece deformation
- Large difference between nominal and actual depth of cut
- Discontinuous chip - potentially spalling
- High contact forces
- Large contact area on clearance face - little contact on rake face

Figure 2.12: Cutting arrangement for increasing tool edge radius r . Adapted from [122, 129].

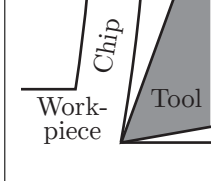
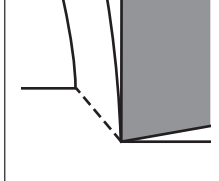
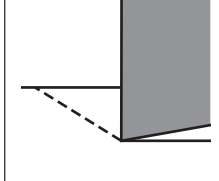
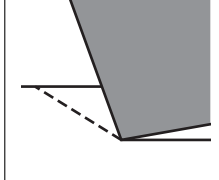
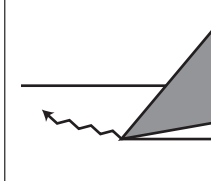
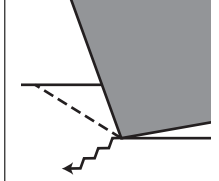
2.3.1.1 Chip formation

The types of chip formed in polymer machining are shown in table 2.6 [101]. These chip formation mechanisms are distinct from those which apply in metal machining, and thus it is not valid to assume that machining parameters which are considered optimum for metal cutting can also be assumed to be optimum for polymers. In particular the lack

LITERATURE REVIEW

of a shear plane in certain chip formation types means that many of the metal cutting theories are not applicable. It has been shown that the chip formation mechanism can change due to a relatively small change in machining conditions [101,105,109], meaning that the chip formation mechanism must be quantified and understood for any analysis of machining to be undertaken.

Table 2.6: Types of chip formed in polymer machining. Dashed lines show shear planes, while zigzag lines show crack formation. Adapted from Kobayashi [101]

| Type of chip | Cause | Chip formation |
|--|---|---|
| Continuous - Flow* | Produced by high elastic deformation |  |
| Continuous - Shear | Shear plane generated upwards from the point of the cutting tool, shearing occurs along this plane. Continuous because of small shear intervals |  |
| Discontinuous - Simple shear | Shear plane generated upwards from the point of the cutting tool, shearing occurs along this plane. Larger shear intervals, therefore discontinuous chips |  |
| Discontinuous - Complex | Chips are produced by complex stress resulting from the action of a large compressive stress operating in combination with a shear stress |  |
| Discontinuous - Crack | Chip formed by a type of brittle fracture. Cracking around the point of tool |  |
| Discontinuous - Complex (shear with crack) | Crack occurs at a downward angle from the cutting point as well as separation of material along usual shear plane. When the crack grows, a new shear plane forms from the tip of the crack to the free surface and the plastic deformation zone is enlarged |  |

2.3.1.2 Cryogenic machining

One method of avoiding the problems associated with viscoelastic behaviour is to machine with the workpiece kept at or below the glass transition temperature, maintaining it in a glassy solid state with a mostly elastic response to applied loads. This typically alters the chip formation mechanism to allow more favourable cutting and improved surface finish [30, 132], though cooling does not always provide an improvement [133]. Depending on the glass transition temperature of the polymer in question, this can be achieved simply by machining in a water bath, while in others it is necessary to use cryogenic machining⁷ [134], typically using liquid nitrogen. It is often necessary to implement a control system for cooling to ensure that the material is kept in the optimum temperature range for machining [135], and to compensate for the thermal contraction of the workpiece [136]. The work of Crabtree *et al.* [137] and Dhokia *et al.* [138] has demonstrated the ability of cryogenic machining to allow for the machining of materials which are typically difficult to machine at room temperature, such as neoprene and other elastomers, though care is required to maintain workpiece temperature to avoid poor cut surface quality [139, 140]. Work by Brunette *et al.* [141] has shown higher drilling forces when using cryogenic cooling with recycled plastics, along with complex behaviour because of the alloy nature of the recycled polymer, resulting in a dependence of the chip formation mechanism on the feed rate used, which may be a disadvantage when attempting to obtain high surface quality.

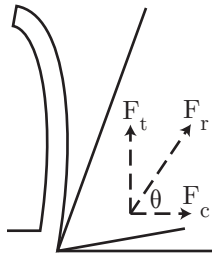
2.3.2 Cutting forces

The cutting forces experienced in polymers are typically lower than metals [101], and dependent on the chip formation mechanism [109] and tool material [142]. Shear angle relationships for cutting force prediction have been developed [101, 102], but are highly specific to a particular polymer [143].

For analysis purposes orthogonal cutting provides a simple approach. Typically forces are divided into components as shown in figure 2.13. F_c is the cutting force, parallel to the axis of the cut, and F_t is the thrust force, normal to the surface of the workpiece. These can also be analysed as the resultant F_r and angle θ .

The magnitude of F_t is of interest, as large forces normal to the surface are likely to deform the material, possibly leading to relaxation over time, which can cause problems with dimensional accuracy. Thus it is desirable to minimise the thrust force. The dependency of the magnitude of the cutting forces on the rake angle leads to the concept of a critical rake angle [101, 144], which is the rake angle for a particular cutting

⁷Machining at a temperature less than 120 K [104]



- F_c : Cutting force
- F_t : Thrust force
- F_r : Resultant of F_c and F_t
- θ : Angle between F_c and F_r

Figure 2.13: Force components in orthogonal machining.

conditions where $F_t = \theta = 0$ and $F_c = F_r$, so there is no thrust force deforming the material.

2.3.3 Heat generation

The sources of heat generation are shown in figure 2.14a. Zone A represents heat generation from workpiece deformation [145], while zones B and C represent heat generation from chip - tool and tool - workpiece contact respectively. The distribution of this heat is shown in figure 2.14b. The exact nature of this heat distribution will depend upon the contact areas between the chip, tool and workpiece and upon the chip formation mechanism, but due to the low thermal conductivity of polymers [113] it is anticipated that a large fraction will enter the tool, and that the proper application of coolant to the cutting zone during machining will greatly reduce the cutting temperatures [146, 147]. Bahadur *et al.* carried out research in the 1970s into the sliding friction of polymers, finding that it was sensitive to normal load, contact pressure, sliding velocity and temperature [148, 149]. Wang *et al.* have recently shown that wear mechanisms and coefficients of friction may change when transitioning from dry sliding to seawater lubrication [150]. A metal cutting model adapted for polymers by Gubbels shows expected temperature rise during polymer machining to be in the order of tens of degrees, with the original model being modified to take into account storage of energy through deformation [151].

2.3.4 Surface quality

The factors which effect surface roughness are shown in figure 2.15. The creation of a good surface finish ($R_a < 0.1 \mu m$ [95]) in polymer machining is reliant upon achieving favourable cutting conditions and chip formation [106, 117], which for some polymers can only be achieved using cryogenic machining [132]. Past work has focussed on the effect of machining parameters [152], tool geometry and material properties on the surface roughness of the machined surface, and on prediction using techniques such as

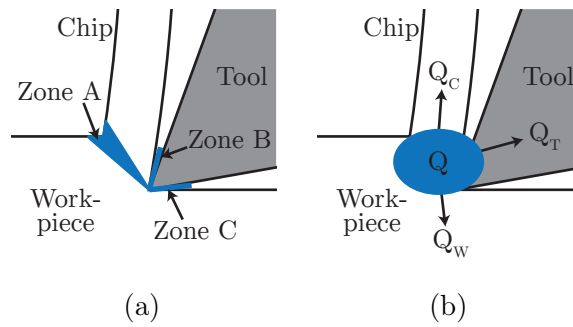


Figure 2.14: Heat sources and heat distribution in the cutting process. Adapted from [141].

neural networks [153, 154] and genetic algorithms [155]. The achievement of as uniform a surface as possible is crucial in minimising wear in the case of unlubricated metal on polymer sliding, as is typically found in total joint replacements [6]. This is due to the harder metal tending to deform the softer polymer, with any surface asperities causing large contact pressures [156]. In a study on wear in UHMWPE components in total joint replacement application, Benson *et al.* [98] used kinematic simulators for machined and direct compression moulded UHMWPE, finding that moulded inserts show less wear than machined samples, most likely as a result of the machined sample having far higher initial surface roughness ($R_a = 0.0698 \mu\text{m}$ for moulded, $R_a = 2.4818 \mu\text{m}$ for machined), thus showing the importance of surface quality in total joint replacement applications.

2.3.5 Tool selection

It has been shown thus far that the chip formation, cutting forces, heat generation and surface roughness of finished parts are all directly or indirectly influenced by tool geometry. Despite this, the effect of tool geometry in polymer machining has largely been ignored since the work of Kobayashi and his development of the concept of a critical rake angle. Many works since then have simply used commercially available metal cutting or woodworking tooling [113, 141, 158], with parameters such as tool sharpness only being addressed in very broad terms [107, 159]. This is despite the knowledge that tool geometry has a large effect on the part quality in finishing operations in metal cutting [160], with cutting force, thrust force and temperature being extremely sensitive to tool edge radius [161].

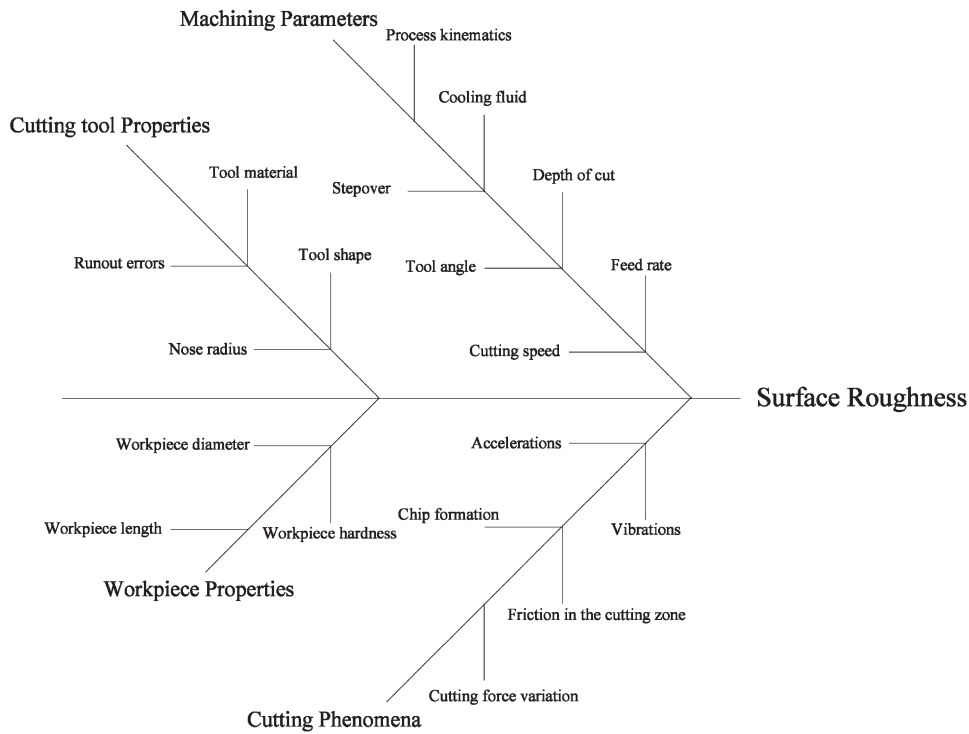


Figure 2.15: Fishbone diagram with the parameters that affect surface roughness [157].

2.3.6 Past work on the machining of polyethylene

As previously detailed, Kobayashi [101] provided machining data for a variety of polymers, including polyethylene. He noted that polyethylene has good machinability, but that the effects of generated heat and workpiece deformation must be considered while machining it. His work concentrated on machining using sharp tools only, with only continuous chips observed. These consisted of the continuous - flow* type at low cutting speeds and continuous - shear type at high cutting speeds. In his analysis of cutting forces, he found F_c to be proportional to depth of cut, and inversely proportional to rake angle, while the relationship between F_t and depth of cut was dependent on rake angle, with positive rakes having an inversely proportional relationship with depth of cut, negative rakes having a proportional relationship with depth of cut, and a rake angle of 0° causing there to be no variation in thrust force due to depth of cut. The critical rake angle values proposed by Kobayashi for a variety of cutting speeds and depths of cut are shown in table 2.7. The critical rake angle decreases with increasing depth of cut and increasing cutting speed, but this relationship is nonlinear, and thus must be established experimentally. Kobayashi emphasised the importance of machining using tooling with the critical rake angle for the machining parameters chosen when machining polyethylene, to avoid thrust forces which would cause the material to “spring back”, and lead to dimensional inaccuracy.

Table 2.7: Critical rake angle as a function of cutting speed and depth of cut for polyethylene [101].

| | | Depth of cut (<i>mm</i>) | | |
|--------------------------------|-----|----------------------------|-----|------|
| | | 0.05 | 0.1 | 0.15 |
| Cutting speed (<i>m/min</i>) | 0.8 | 41° | 30° | 24° |
| | 50 | 35° | 25° | 20° |
| | 100 | 26° | 16° | 13° |
| | 200 | 18° | 9° | 8° |
| | 400 | 10° | 4° | 3° |

Yong-hwan [162] studied oblique cutting of HDPE, finding that continuous chips were usually formed when using positive rake angles, with negative rake angles on occasion producing discontinuous chips. His work also included analysis of chips and machined surfaces, observing some material flow and smearing effects under unfavourable machining conditions. Salles and Gonçalves [152] also carried out oblique cutting experiments, but on UHMWPE, investigating the effect of feed rate and cutting speed on surface roughness, along with inspecting chips and machined surfaces using an optical camera. Increases in feed rate were found to cause increases in R_a , with cutting speed not having any clear effect on surface roughness. However, as the depth of cut is not varied or even specified this data can not be considered representative of all machining conditions.

Song *et al.* [96] conducted a study on the effects of machining parameters on the coefficient of friction and wear factor of milled UHMWPE under dry reciprocating sliding, finding that depth of cut and cutting speed did not appear to influence the coefficient of friction. In addition, the wear factor varied depending on the combination of cutting speed and feed rate, with wear factor decreasing with increasing cutting speed if feed rate was kept constant, but increasing with increasing cutting speed if the ratio of cutting speed to depth of cut was kept constant. Surface roughness results showed that varying the depth of cut led to the discovery of an optimum depth of cut, above or below which both the surface roughness and wear factor increased. The authors concluded that plastic deformation and ploughing were the main wear mechanisms for machined UHMWPE surfaces.

Drilling of polyethylene has seen some interest, with Brunette *et al.* [141] conducting experiments on the drilling of recycled plastic consisting of approximately 80% polyethylene, across a range of workpiece temperatures, and finding that tangential and thrust forces increased with increasing feed rate, while spindle speed did not have a clear effect on either force. Workpiece temperature showed unusual behaviour, which

the authors attributed to an interaction between the differing thermal properties of the constituent plastics, and the formation of a built up edge on the tool at certain temperatures. Altan and Altan [163] used multiple regression analysis to investigate burr formation in drilling of UHMWPE using HSS drill bits with and without coatings, but their regression model had a P value of $P = 0.0769$, with the model showing feed rate having $P = 0.0465$ and tool type having $P = 0.0739$. The 90% level of statistical significance was used by the authors, rather than the more generally accepted 95% level. Campos Rubio *et al.* [164] conducted similar drilling experiments in UHMWPE, POM, and PTFE, using a full factorial design of experiments to analyse the effects of feed rate, spindle speed, and drill point angle on circularity error, surface roughness and thrust force in drilling. They found that UHMWPE showed higher circularity error and surface roughness than the other materials studied, but similar levels of thrust force, with a particularly poor surface finish being observed when drilling at low feed rate and spindle speed.

Costa *et al.* [107] studied the effect of microtomy on the material properties of UHMWPE, using microtome knives of two differing sharpnesses. It was found that low cutting depths caused substantial permanent deformation of the sample in the form of shrinkage in direction of cutting. The use of a blunt knife was found to cause post-cut crystallisation of the sample upon ageing in ambient conditions. It was also observed that the blunt knife left a smeared surface when compared to that produced by the sharp knife. In non-traditional machining, Caiazzo *et al.* [165] used a CO₂ laser beam to cut sheets of polyethylene of varying thicknesses, finding that it cut well at relatively low power levels and provided surface roughness values of $R_a \approx 1 \mu m$, but with large variations in kerf width and low quality of cut edges.

As can be seen, the machining of polyethylene is an area which has received relatively little research interest, with no information available on the effects of tool wear, or the magnitude of the deformation of workpieces after machining using a rake angle other than the critical rake angle. There is also little information available on cryogenic machining of polyethylene, with the only work published being on the topic of recycled polymers in the form of a mixture of a variety of different types of polymer [141], which makes it difficult to use the data presented for a single polymer.

2.4 Process monitoring in the machining of polymers

In order to analyse machining operations it is necessary to implement a process monitoring system. Typical “close to process” measurable phenomena in machining include: [166]

- Force
- Torque
- Strain
- Vibration
- Temperature
- Acoustic emission

In addition, as noted in sections 2.3.1.1 and 2.3.2, it is necessary to monitor the chip formation mechanism in order to characterise the machining process. Post-process monitoring would include the measurement of dimensional accuracy and surface roughness. In the machining of polymers there has been relatively little attention paid to in-process sensors other than force and temperature [167].

The measurement of cutting temperature in the machining of polymers is a challenge, with large temperature gradients in the tool likely [168] due to the low thermal conductivity of the material, and dynamic thermocouple techniques unsuitable due to most polymers being electrical insulators. This leaves embedded thermocouples and pyrometry as the most viable techniques for temperature measurement, with both having significant issues. Even the smallest thermocouples display issues with thermal inertia and distance from the cutting edge which make them suitable only for steady state cutting operations [169], while pyrometry relies on accurate values of emissivity being known [170], and a clear line of sight from the pyrometer to the area being measured. One possible area of future development is in the use of embedded thin film thermocouples [171], though these are only suitable for coated tools.

2.5 Statistical analysis of experimental data

The need to use a statistical approach for analysis of large amounts of data has been recognised since the early 20th century [172]. By use of appropriate statistical tests and methods it is possible to both simplify analysis and improve the certainty of conclusions, and to easily compare data sets. In this work a statistical approach to experimental design was taken, with analysis of variance (ANOVA) used to assist with and support the making of conclusions from the data available. Chi-square analysis and multiple linear regression are also used where appropriate.

2.5.1 Design of experiments

Design of experiments is concerned with the organisation of the conduct of experiments in order to minimise undetected variation [173]. The independent variables are referred to as factors, with the values that the factors are set to known as levels. The dependent variable(s) under study are known as responses. By looking at the average value of the response at each level for every factor it is possible to construct a main effects plot, which consists of a graph for each factor showing the variation in the response at each level. An extension of this is an interaction plot, which displays the variation of the response due to two factors by the use of multiple curves per graph.

One factor which must be taken into account when designing an experiment is the balance between the number of experiments to be undertaken and the number of factors to be used [174]. In the case of a full factorial experiment, every possible combination of levels across all factors is used. In the case of there being 3 factors, each with 2 levels, the total number of experiments will be $2^3 = 8$. When the number of factors and levels grows the total number of experiments required for a full factorial experiment quickly becomes infeasible, which leads to the concept of a fractional factorial experiment, where some combinations are omitted, typically by assuming that certain high-order⁸ interactions are insignificant compared to the main effects. Care must be taken with these experimental designs, however, as if this assumption proves incorrect it is impossible to distinguish the effect of the interaction from one of the main effects, a state known as aliasing [173].

2.5.2 Analysis of Variance

Analysis of variance is used to analyse the statistical significance of the data means shown in main effects and interactions plots. This is achieved by creating a regression

⁸Involving the majority of the factors

model of the response as a function of the factors, and separating the variation down to that which is due to the factors and the chance variation which is unexplained by the factors. In order to assess the statistical significance of a factor the variation due to that factor is compared to the unexplained variation using an F test. If the variation due to that factor is large enough to reject the null hypothesis⁹ then the factor is judged to be significant [174].

2.5.3 Chi-square analysis

Chi-square analysis is used for analysis of categorical data, generally in the form of a table of counts of occurrences of two factors. The null hypothesis for the test is that the data are evenly distributed through the table, and thus the two factors are unrelated. Expected values for the data being evenly distributed are calculated using the row and column totals, as shown in the following equation:

$$E_{ij} = \frac{\text{Row Total} \times \text{Column total}}{\text{Overall total}} \quad (2.4)$$

The overall contribution of each cell, with observed value O_{ij} and expected value E_{ij} to the deviation from being evenly distributed is calculated as:

$$\chi_{ij}^2 = \frac{(O_{ij} - E_{ij})^2}{E_{ij}} \quad (2.5)$$

The contributions of each cell are summed up to give the χ^2 (Chi-square) statistic for the table.

$$\chi^2 = \sum \frac{(O_{ij} - E_{ij})^2}{E_{ij}} \quad (2.6)$$

This total is then used to calculate if the deviation of the table from an even distribution is statistically significant, using critical values from the χ^2 distribution for the required level of statistical significance. It should be noted, however, that this analysis is typically only valid for expected counts of not less than five in each cell [173].

2.5.4 Multiple linear regression

Multiple linear regression is used to fit a linear equation to allow prediction or analysis of a continuous variable, referred to as the response, as a function of other variables, known as predictors. Predictors may be continuous or categorical, with categorical predictors often included as letters to prevent them from being inadvertently used as

⁹In this case the null hypothesis is that the long run variation due to the factor is small enough to be explained by the chance variation, typically with a certainty of $\alpha = 0.05$

continuous predictors in error. Special cases of categorical variables known as indicator variables, which are binary variables which correspond to some difference in the data set, can be used to assess the statistical significance of this difference. For example, a single linear regression would yield an equation of the form:

$$y = m \times x + c \quad (2.7)$$

With y being the response, x being a continuous predictor, m being the slope of the line and c being the intercept. If one element of the data is suspected to have a different intercept but the same slope, this could be incorporated into the model using an indicator variable i :

$$y = m \times x + c + d \times i \quad (2.8)$$

The regression model will fit a value to the coefficient d which will correspond to the change in slope for the data points where the indicator variable i is equal to 1. For data where the indicator variable is 0 the intercept will be c , while for data where the indicator variable is 1 the intercept will be $c + d$. As detailed earlier, an ANOVA accompanying the regression model will include T and F tests of the statistical significance of the value of d , with the null hypothesis being that it is zero, and that there is no difference in intercepts. In the case where it is suspected that there is a difference in slope the following model would be used:

$$y = m \times x + c + d \times i \times x \quad (2.9)$$

By multiplying the indicator variable by the predictor the coefficient d will now capture changes in slope due to the data where the indicator variable is 1. For cases where the indicator variable is 0 the slope will be m , while for cases where the indicator variable is 1 the slope will be $m + d$, with the same tests of statistical significance possible as noted above. Regression models often include multiple indicator variables, interacting with both slope and intercept. In cases where a predictor has a finite number of discrete values it is often desirable to represent this as a number of indicator variables, as this allows any non-linear effects to be easily captured using multiple linear regression.

2.6 Summary

The importance of polymers as an engineering material is clear from growing global demand for their production, with close to 30% of EU annual polymer demand being for blends of polyethylene [1]. With the wide variety of uses found for polymer products, traditional machining operations are becoming more common in the production of polymer components, with a resulting need for knowledge on machining and tooling parameters for commonly used engineering polymers. This would allow for selection of appropriate tooling, speeds and feeds to achieve the desired surface quality and dimensional accuracy, with consideration taken for the viscoelastic properties of the material. In the case of polyethylene this is particularly evident, due to the scarcity of publications on the topic.

Several works in the past have suggested that the machining of polymers is fundamentally similar to the machining of metals or wood, and can be modelled using similar shear plane assumptions [101, 102, 143]. This is despite the differences in the physical properties of the materials, and the chip formation mechanisms which occur. There exists a gap within the literature for fundamental knowledge of the machinability of common polymers. This would take the form of experimental work assessing the effect of tooling, workpiece and material parameters on machining, in light of the viscoelastic material properties of the workpiece. This would require implementation of an in-process measurement chain, followed by the extraction of relevant features from the data collected, and use of appropriate statistical analysis on the extracted features to analyse the effect of the parameters varied.

LITERATURE REVIEW

Chapter 3

Experimental setup

3.1 Experimental methodology

The experimental methodology used is shown in figure 3.1. This methodology is used to analyse the machining of polymers, by quantifying the viscoelastic properties of the material pre-process, observing and recording the machining behaviour of the material in-process, and analysing the resulting machined surface post-process. Pre-process analysis consists of chemical, mechanical and thermal tests on material samples, in the form of Fourier Transform Infrared Spectroscopy, Dynamic Mechanical Analysis and Differential Scanning Calorimetry respectively. The aim of these tests is to establish if any variation exists within or between the polymers being tested. In-process analysis takes the form of process monitoring of force, temperature and chip formation during machining, while post-process analysis concentrates on evaluating the resulting chip and machined surface. The machined surface is evaluated by measuring the surface roughness, and by using a Scanning Electron Microscope to obtain high magnification images of the surface.

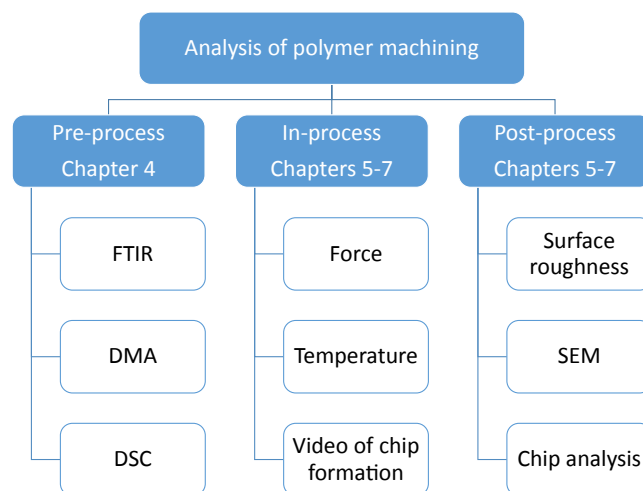


Figure 3.1: Experimental methodology, showing 3 phases of quantification.

3.2 Material analysis

Three types of Ultra High Molecular Weight Polyethylene (UHMWPE) were studied:

1. Plain GUR 1020 (UHMWPE)
2. GUR 1020 with antioxidant material added (AOX)
3. Crosslinked GUR 1020 (XLK) ¹

These varieties were chosen due to their common use in the manufacture of orthopaedic implants. Plain UHMWPE has been a popular material for these applications [7], with antioxidants typically included to prevent material degradation in vivo [175], while crosslinking is used to increase wear resistance [51]. Typical properties for extruded GUR 1020 are given in table 3.1. Of interest is the effect of antioxidant and crosslinking on the machinability of the material. While it is known that crosslinking improves the wear characteristics of UHMWPE, it can also degrade the mechanical properties [176], depending on the process used to crosslink the material. In contrast, the addition of typical antioxidants to UHMWPE has been shown to have little to no effect on static mechanical properties, but may act as a plasticiser [6], which may alter the chip formation mechanism in machining. The AOX and XLK materials were manufactured from the same source of consolidated UHMWPE powder as used for the plain UHMWPE.

Table 3.1: Properties of extruded GUR 1020. Values are means \pm standard deviation [6].

| Property | Units | Value |
|-----------------------|--------------|----------------|
| Density | kg/m^3 | 935 ± 1 |
| Tensile yield | MPa | 22.3 ± 0.5 |
| UTS | MPa | 53.7 ± 4.4 |
| Elongation to failure | % | 452 ± 19 |

In order to assess the effect of the antioxidant additive and crosslinking on the properties of UHMWPE it was decided to use three analysis techniques, as detailed in table 3.2.

FTIR was carried out using a Perkin Elmer Spectrum One NTS with Attenuated Total Reflection (ATR) Sampling Accessory, with software correction. The instrument was cleaned down and calibrated with no sample in the ATR holder before each reading. The amplitudes of the plots produced were calibrated using wavenumber 1368, which corresponds to a carbon-hydrogen bond [47]. DMA was carried out in a Pyris Diamond

¹Crosslinked through a 50 kGy radiation dose, followed by melting and annealing

Table 3.2: Types of material analysis used to characterise viscoelastic behaviour of UHMWPE.

| Acronym | Name | Property quantified |
|----------------|---|------------------------------------|
| FTIR | Fourier Transform Infrared Spectroscopy | Chemical composition |
| DMA | Dynamic Mechanical Analysis | Viscoelastic mechanical properties |
| DSC | Differential Scanning Calorimetry | Thermal properties |

DMA using liquid nitrogen cooling, in tension, at a frequency of 1 Hz . Differential Scanning Calorimetry was carried out using a TA 2010 differential scanning calorimeter, with further detail on the experimental setup and calibration provided in appendix A.

3.3 Workpiece design

Orthogonal cutting tests were performed without the use of coolant². The workpiece dimensions before machining tests were carried out are shown in figure 3.2a. Each workpiece contained five discs of width 2.2 mm , with a gap of 2.2 mm between each disc. This allowed for orthogonal cutting operations to be carried out, using single edge cutting tools of width greater than the discs. The cutting operations were carried out using an Okuma LT15-M, using high speed steel tooling. The constant surface speed feature of the machine was used to provide a constant cutting velocity. The lathe was programmed to carry out machining operations at a range of combinations of cutting speed and depth of cut, with the depth of cut being the feed of the tool into the workpiece disc, in $\text{mm}/\text{revolution}$. The levels used for these parameters are detailed in section 3.9. It was found that chip buildup on the tool caused the corruption of force data. In order to avoid this a slot was milled in the discs perpendicular to the direction of the cut, as shown in figure 3.2b. This slot prevented a single continuous chip from forming by causing a new cut to begin at the point where the tool passed the slot in the disc.

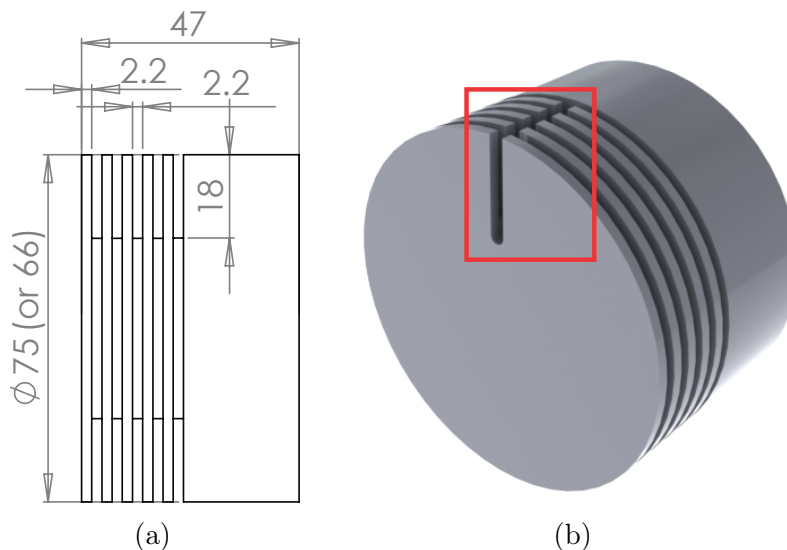
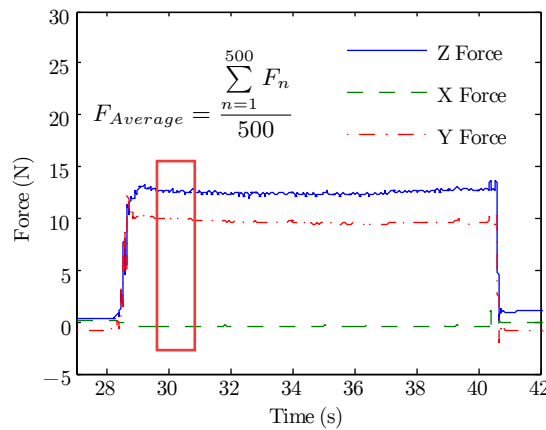


Figure 3.2: Workpiece design, showing a) Dimensions (mm) and b) Slot cut in discs.

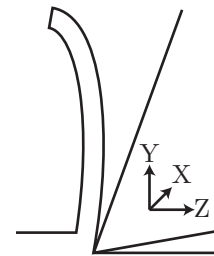
²While in a production environment coolant would be used in order to allow more aggressive machining parameters to be used, this work includes only short duration cuts of 10 seconds or less, with a concentration on the overall trends observable for each response being measured. The use of coolant would cause lower tool temperatures than those observed in air, and likely lower cutting force due to the lubrication effect of the coolant.

3.4 Force measurement

Force was measured using a Kistler type 9602 force sensor mounted in a custom toolholder. Sample force data is shown in figure 3.3a, with the direction of the axes shown in figure 3.3b. It can be seen from figure 3.3b that the Z force corresponds to the cutting force, while the Y force corresponds to the thrust force. In order to compensate for any errors or misalignment during the mounting of the force sensor, the resultant of the X and Y forces was used as the thrust force.



(a) Sample force data



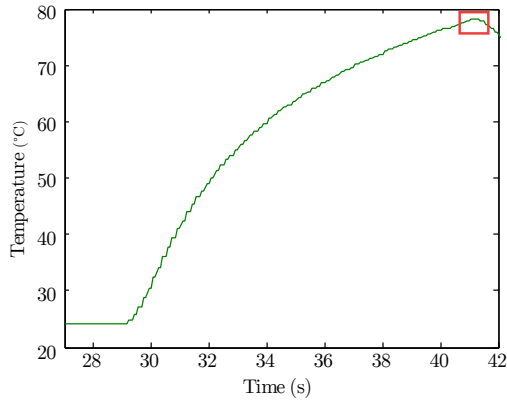
(b) Force components

Figure 3.3: Sample force data, and relationship with cutting forces. Cutting parameters were 0° rake angle, sharp tool, 155 m/min cutting speed, $0.06\text{ mm/revolution}$ depth of cut, material XLK.

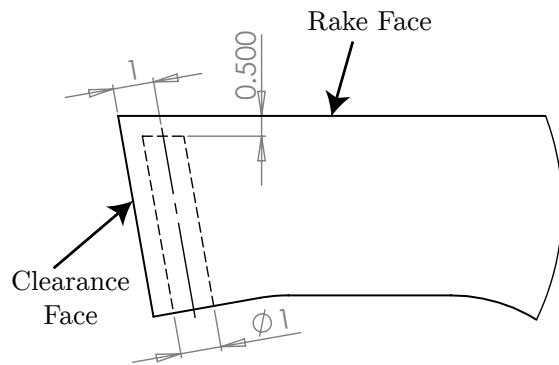
The area of interest for extraction is highlighted in figure 3.3a. A 500 point average of the steady state cutting force, corresponding to 0.31 s , was extracted in this area for each axis. An average of 500 points was used as in some conditions the duration of the machining operation was $< 1\text{ s}$, and thus it was decided to average over the same number of points, with 500 being found to allow the extraction of steady state cutting forces for the shorter machining operations.

3.5 Temperature measurement

Temperature was measured using a K type thermocouple embedded within the tool. Sample temperature data is shown in figure 3.4a, while the positioning of the thermocouple is shown in figure 3.4b. It is evident from the sample temperature data that significant thermal inertia is present in this system.



(a) Sample temperature data



(b) Tool dimensions in mm, showing thermocouple hole

Figure 3.4: Sample temperature data, and dimensions of thermocouple hole in tools.

3.6 Surface roughness measurement

Surface roughness measurements were made using a Mitutoyo SurfTest SJ400 portable surface roughness tester. In chapter 5 these measurements were made perpendicular to the direction of cutting using the built in drive unit and software to give a R_a result. In chapter 6 the surface profile parallel to the direction of machining was also measured. This was achieved by disabling the profilometer drive unit via software, and by mounting the workpiece in a modified 4th axis from a small milling machine. This 4th axis setup consisting of a Röhms ZG $\varnothing 74$ three jaw chuck mounted on a spindle, driven via a toothed belt using a 2:1 gear ratio by an Animatics SmartMotor SM23165D servo motor. This setup is shown in figure 3.5. The workpiece was rotated at a 1 mm/s surface speed, controlled by sending commands to the motor using MATLAB. The acquisition of the profilometer data was via proprietary Mitutoyo software. The controller in the servo motor was tuned using Animatics tuning software to ensure smooth motion of the entire motor - belt - spindle - chuck system.

After acquisition this workpiece profile data was processed in MATLAB by using a 0.05 Hz 10th order Butterworth highpass filter to remove chuck/workpiece runout. A window of relevant data was selected from each profile for further analysis, to allow the removal of unusual peaks or areas. After adjusting each data set to have a mean of zero the RMS of the signal was calculated, and used as a response in Analysis of Variance (ANOVA) in Minitab 16. In addition, chips were collected after each machining operation, and in the case of continuous chips the cut chip thickness was measured five times for each chip, using a micrometer.

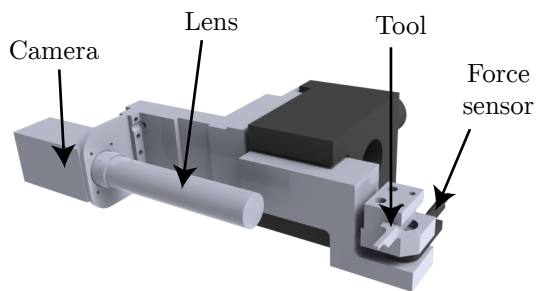


Figure 3.5: Profilometer and spindle setup for measuring surface roughness on round parts. Not shown: Laptop used for control and data acquisition.

EXPERIMENTAL SETUP

3.7 Chip formation analysis

Chip formation was analysed using a PixeLINK PL-A782, mounted to the side of the toolholder, as shown in figure 3.6. A Fostec fiber optic light source was used to ensure sufficient light was available for the low exposure time required. The complete experimental setup is shown in figure 3.7.



- Camera: PixeLINK PL-A782, capable of 180 fps
- Force sensor: Kistler type 9602
- Tool material: High Speed Steel

Figure 3.6: Toolholder with force sensor and camera mounted.

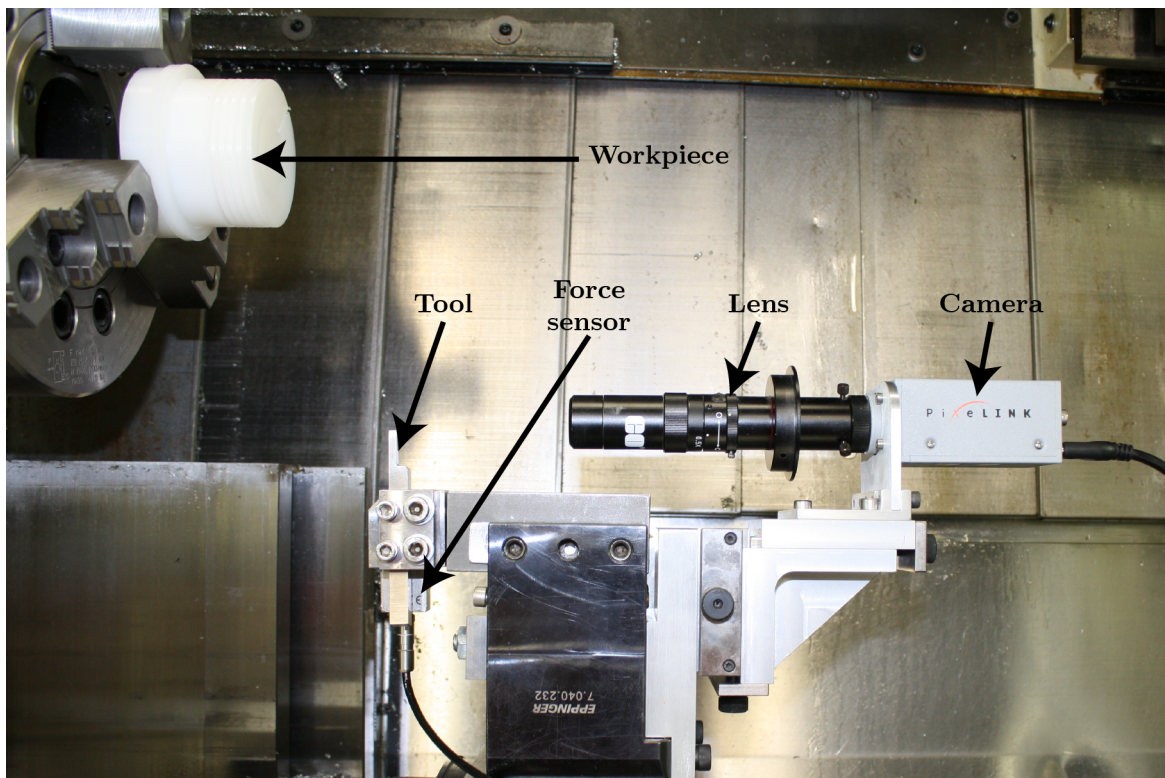


Figure 3.7: Experimental setup. Not shown: Light source, thermocouple.

3.8 Surface integrity analysis

Visual inspections of tools and machined surfaces were made using a toolmakers microscope. Where further magnification was required a Scanning Electron Microscope was used. In order to image non-conductive materials such as polyethylene in a SEM it is necessary to plate the samples with a conductive material. For this work gold plating was used.

3.9 Design of experiments

3.9.1 Design of experiments applied to orthogonal cutting investigations

The factors used in the design of experiments for chapter 5 are detailed in table 3.3. The edge radii corresponding to each sharpness are shown in table 3.4, along with the maximum values of the ratio between edge radius and depth of cut for each sharpness level. The resulting values of the effective rake angle, as described in section 2.3.1, are shown in table 3.5. A full factorial experimental design was used. The rake angle, cutting speed, and depth of cut levels were chosen to allow comparison to the work of Kobayashi [101], while the levels for edge radius were chosen to give an appreciation of the influence of the size effect during machining.

Table 3.3: Factors used in design of experiments for chapter 5.

| Factor | Number of levels | Levels |
|---------------|------------------|---|
| Material | 3 | See section 3.2 |
| Rake angle | 4 | -20° , 0° , 20° , 40° |
| Edge radius | 3 | Sharp, worn, highly worn - See table 3.4 |
| Cutting speed | 2 | 155, 300 <i>m/min</i> |
| Depth of cut | 2 | 0.06, 0.19 <i>mm/rev</i> |

Table 3.4: Sharpness levels.

| Level | Edge radius (μm) | Maximum $\frac{r}{DOC}$ |
|-------------|-------------------------|-------------------------|
| Sharp | 10–15 | 0.25 |
| Worn | 40–60 | 1 |
| Highly worn | 80–120 | 2 |

Table 3.5: Effective rake angles for depths of cut and tool sharpness levels used. Values calculated using equation 2.3.

| Sharpness level | Sharp | | Worn | | Highly worn | |
|--------------------|-------------|-------------|-------------|-------------|-------------|--------------|
| | 0.06 | 0.19 | 0.06 | 0.19 | 0.06 | 0.19 |
| Nominal rake angle | | | | | | |
| -20° | -20° | -20° | -20° | -20° | -30° | -20° |
| 0° | 0° | 0° | 0° | 0° | -30° | 0° |
| 20° | 20° | 20° | 0° | 20° | -30° | 20° |
| 40° | 40° | 40° | 0° | 40° | -30° | 35.7° |

3.9.2 Design of experiments applied to cryogenic cutting investigations

The factors used in the design of experiments for chapter 6 are detailed in table 3.6. The edge radii corresponding to each sharpness and corresponding values for effective rake angle are as were described in section 3.9.1, for chapter 5. A full factorial experimental design was used.

Table 3.6: Factors used in design of experiments for chapter 6.

| Factor | Number of levels | Levels |
|-------------------------------|------------------|---|
| Rake angle | 4 | -20° , 0° , 20° , 40° |
| Initial workpiece temperature | 2 | Cold (100 - 150 K), Room (295 - 300 K) |
| Edge radius | 3 | Sharp, worn, highly worn - See table 3.4 |
| Cutting speed | 2 | 155, 300 <i>m/min</i> |
| Depth of cut | 2 | 0.06, 0.19 <i>mm/rev</i> |

3.9.3 Design of experiments applied to workpiece relaxation investigations

For chapter 7 testing was conducted in two phases:

1. Static loading to simulate clamping forces
2. Machining operations using sharp tools

Each test was replicated three times, with the sample being measured using an Insize[®] digital micrometer, with $\pm 1 \mu m$ accuracy. Five measurements were carried out on each sample to reduce measurement error. Samples were measured at 10, 20, 50, 100, 200, 500, 1000, 2000 and 5000 minutes after unloading, as the response was expected to be logarithmic in nature [75].

3.9.3.1 Static loading

For these tests UHMWPE samples of dimensions $20 \times 10 \times 8.8 \text{ mm}$ were compressed under two loading schemes: constant stress and constant strain. Samples were loaded to 2, 4 and 8 *MPa* for the constant stress tests, as detailed in table 3.7, and 2.5%, 5% and 10% strain for the constant strain tests, as detailed in table 3.8. The duration of loading was 100 seconds for all tests, with unloaded samples measured and stored with those which had been loaded to provide a baseline. These tests were carried out

EXPERIMENTAL SETUP

using samples which had been cooled with liquid nitrogen, as well as samples at room temperature.

Table 3.7: Factors used in design of experiments for section 7.2.1.

| Factor | Number of levels | Levels |
|----------------------------|------------------|--|
| Stress | 4 | 0, 2, 4, 8 <i>MPa</i> |
| Initial sample temperature | 2 | Cold (100 - 150 K), Room (295 - 300 K) |

Table 3.8: Factors used in design of experiments for section 7.2.2.

| Factor | Number of levels | Levels |
|----------------------------|------------------|--|
| Strain | 4 | 0, 2.5, 5, 10 % |
| Initial sample temperature | 2 | Cold (100 - 150 K), Room (295 - 300 K) |

3.9.3.2 Machining operations

Machining operations were carried out on workpieces as described in section 3.3, using a cutting speed of 155 *m/min* and a range of depths of cut from 0.05 to 0.25 *mm/rev*, using sharp tools with 20° and 40° rake angles, as detailed in table 3.9.

Table 3.9: Factors used in design of experiments for section 7.3.

| Factor | Number of levels | Levels |
|--------------|------------------|--|
| Rake angle | 2 | 20°, 40° |
| Depth of cut | 5 | 0.05, 0.10, 0.15, 0.20, 0.25 <i>mm/rev</i> |

In order to have similar loading conditions for each machining operation it was necessary to machine to different diameters, with an aim of maintaining constant machining time, which corresponds to constant cutting length due to the constant surface speed used. The final diameters used for each depth of cut are shown in table 3.10.

These values were calculated by assuming that the chip produced would be of uniform thickness h (corresponding to the depth of cut), with a reduction in diameter from D_1 to D_0 , with the number of “layers” of thickness h being calculated using equation 3.1, and the total length of the chip L being calculated using equation 3.2. From examination of force data the resulting cutting times were approximately 3.5 ± 0.4 s.

Table 3.10: Nominal final diameters used to maintain constant machining times for varying depth of cut.

| Depth of cut <i>mm/rev</i> | Nominal final diameter <i>mm</i> |
|--------------------------------------|--|
| 0.25 | 48 |
| 0.20 | 52.116 |
| 0.15 | 55.921 |
| 0.10 | 59.477 |
| 0.05 | 62.826 |

$$N = \frac{D_1 - D_0}{2h} \quad (3.1)$$

$$\begin{aligned}
 L &= \pi D_0 + \pi(D_0 + 2h) + \pi(D_0 + 4h) + \cdots + \pi(D_0 + 2(N-1)h) \\
 &= \pi(ND_0 + 2h(1 + 2 + \cdots + (N-1))) \\
 &= \pi(ND_0 + hN(N-1)) \quad (\text{Gauss's formula}) \\
 &= \pi N(D_0 + h(N-1))
 \end{aligned} \quad (3.2)$$

3.10 Data processing

Data acquisition was carried out using a National Instruments CompactDAQ 9178 carrier, using NI LabVIEW SignalExpress software to record the data. A flowchart of the DAQ system is shown in figure 3.8. Statistical analysis was carried out using Minitab 16.

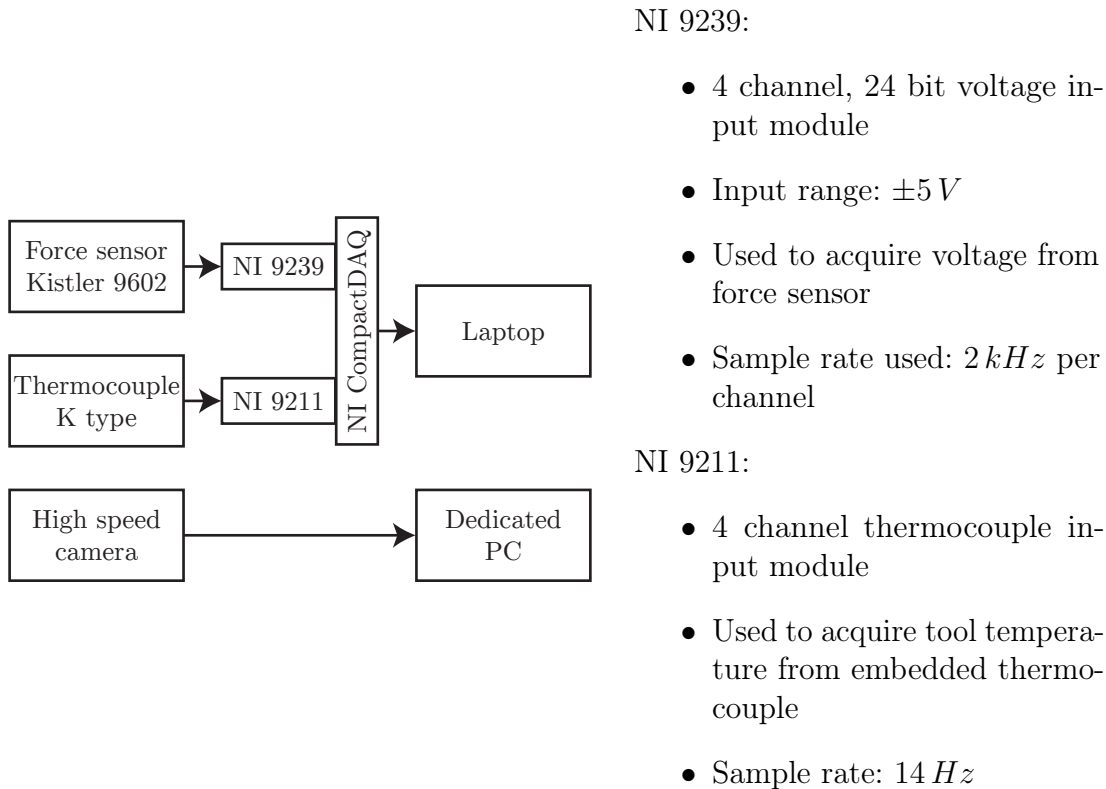


Figure 3.8: Data acquisition flowchart.

The following responses were used for statistical analysis:

1. Cutting force, F_c
2. Thrust force, F_t
3. Peak temperature
4. Surface roughness, R_a
5. Cut chip thickness
6. RMS of profilometer output for surface profile parallel to direction of cut (Chapter 6 only)

In addition, visual data from the high speed camera and SEM were examined on a qualitative basis.

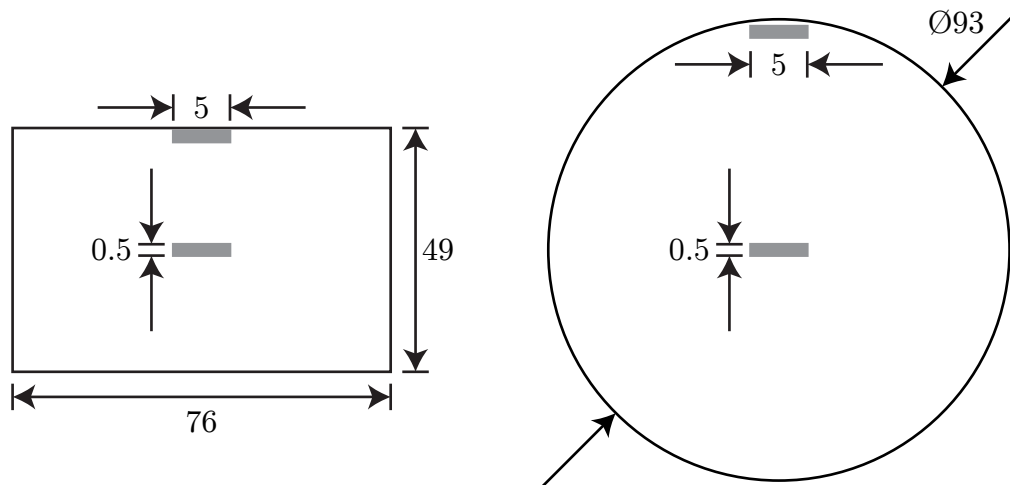
Chapter 4

Material analysis

This chapter establishes the viscoelastic nature of three varieties of UHMWPE through specialised polymer testing techniques, with the aim of establishing the likely effects of viscoelasticity on machining operations. The three varieties used are as follows:

1. Plain UHMWPE (UHMWPE)
2. UHMWPE with antioxidant material added (AOX)
3. UHMWPE which has been crosslinked (XLK)

UHMWPE and AOX were provided in bar form, with XLK coming in rod form. Samples of each were taken from the core (indicated by the suffix -C) and surface (indicated by the suffix -S) of the bar/rod form in which the material was supplied, as shown in figure 4.1.



(a) Locations for UHMWPE and AOX bars

(b) Locations for XLK rod

Figure 4.1: Locations of samples machined from raw bar/rod stock for material analysis, shown on cross section of bar/rod. Sample length was 20mm. (Not to scale.)

4.1 Shore hardness testing

All varieties of UHMWPE used were found to have Shore Type D hardness values of 68-70, with variation within this range caused by the method and speed of the application of the hardness tester to the material. Samples of each material were measured five times, with the results of these tests shown in table 4.1.

Table 4.1: Shore hardness values for each material, measured immediately after loading.

| Material | Measurement | Average |
|-----------------|--------------------|----------------|
| UHMWPE | 68, 68, 68, 69, 68 | 68.2 |
| AOX | 69, 69, 69, 70, 68 | 69 |
| XLK | 69, 68, 70, 68, 68 | 68.6 |

These results show that there is little variation in hardness between or within materials, with all materials showing relatively high levels of hardness. The measured values of 68 - 70 are higher than those typically found for LDPE (40 - 50), and are at the upper bound of those typically found for HDPE (60 - 70) [12]. These results are also higher than the 60 - 63 specified by the manufacturer [177], though those values are for 15 s after loading, and Shore D hardness values typically decrease with increasing time under loading, due to viscoelastic stress relaxation.

4.2 Fourier Transform Infrared Spectroscopy

FTIR results for UHMWPE, AOX and XLK are shown in figures 4.2, 4.3 and 4.4 respectively.

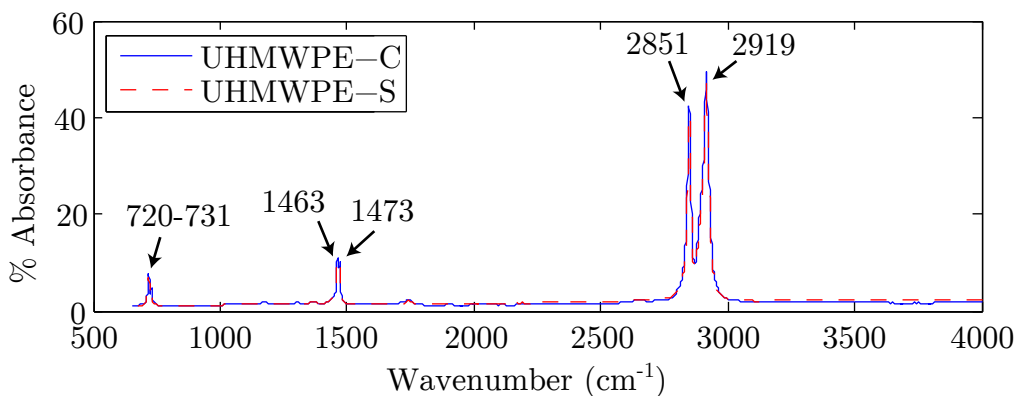


Figure 4.2: FTIR results for UHMWPE.

The magnitude of the variations between materials are less than that seen in past work on identifying the differences between other commercially available grades of polyethylene [48], leading to the conclusion that those variations observed are due to crosslinking and antioxidant additives. The peaks seen for all six samples correspond to the strong intensities detailed in the literature review. Of note is that the peaks at 1473, 1463 and 731-720 are of much lower magnitude than that seen for LLDPE, LDPE and HDPE in the work of Gulmine *et al.* [48]. These peaks correspond to bending and rocking deformation modes, and may be lower in magnitude as a result of the higher molecular weight of UHMWPE causing increased stiffness.

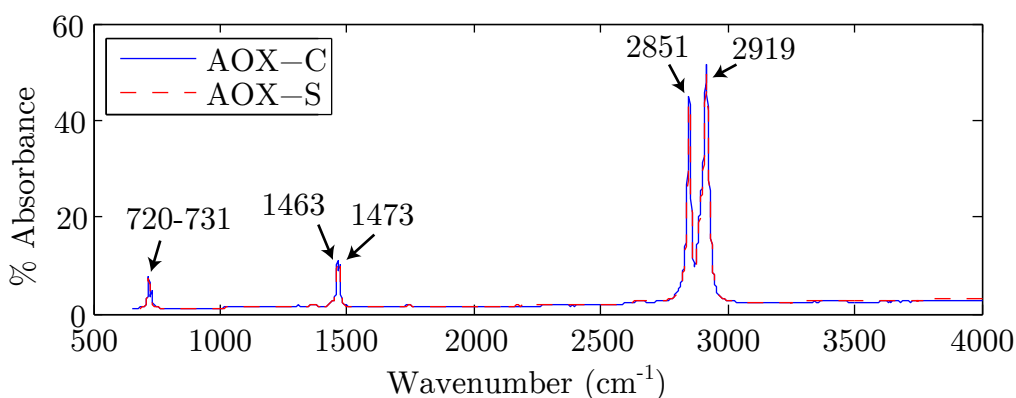


Figure 4.3: FTIR results for AOX.

While there are variations between materials due to changes in crystallinity, crosslinking and additives, there is no variation evident between samples from the same materials,

other than for XLK, as shown in figure 4.4. The surface sample for XLK has peaks which are consistently lower than those of the core sample, while the baseline levels of absorbance remain approximately constant. This is likely a result of poor contact between the sample and the Attenuated Total Reflection crystal used to analyse the samples.

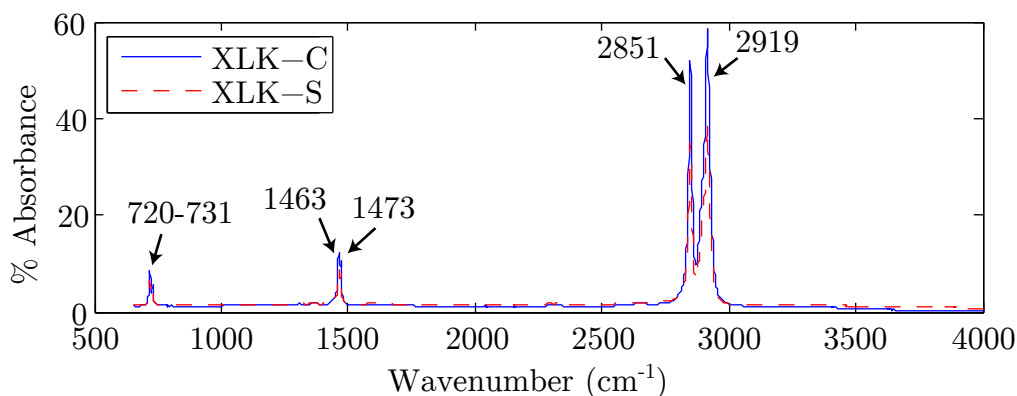


Figure 4.4: FTIR results for XLK.

FTIR results show no major changes in chemical structure between materials beyond that which would be expected as a result of crosslinking and the presence of antioxidant, or within samples as a result of the location in the raw material from which the sample was taken. The peaks observed matched those seen in past work, though the magnitudes of some peaks were lower, possibly as a result of increased molecular weight causing increased material stiffness.

4.3 Dynamic Mechanical Analysis

4.3.1 Varying material

Results from the DMA tests to evaluate changes both between and within the materials under investigation are shown in figures 4.5, 4.6 and 4.7. All samples show a melting temperature of approximately 135°C . These tests were not performed to a sufficiently low temperature to assess the glass transition temperature, due to issues with samples slipping when cooled below -100°C .

It can be seen in figure 4.5 that storage modulus decreases as temperature increases, indicating a softening of the material with increasing temperature, as would be expected for a polymer with temperature dependent elastic properties. While there is variation in the magnitude of the elastic component of the response, the shape of the curves is similar, and thus the variation is likely a result of errors in the measurement of the cross sectional area of the samples being used.

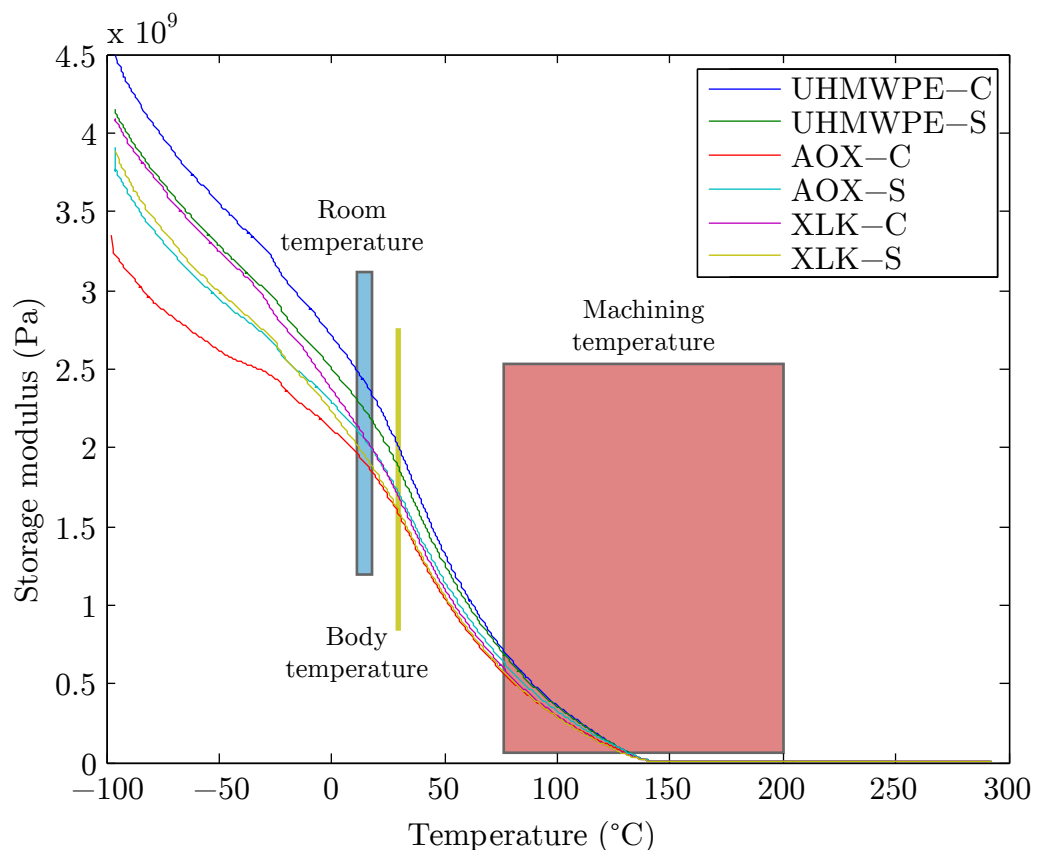


Figure 4.5: Storage modulus for all samples.

In figure 4.6 it can be seen that loss modulus has a peak at 55°C . This peak is of a lower magnitude for the XLK samples, indicating a reduction in the viscous component of the viscoelastic response when the material is crosslinked. It can also be seen that the AOX core sample appears to have higher values of loss modulus at temperatures below approximately 5°C . Above the peak at 55°C the loss modulus decreases for all samples, until it reaches the melting temperature at approximately 135°C , where the loss modulus levels out close to zero.

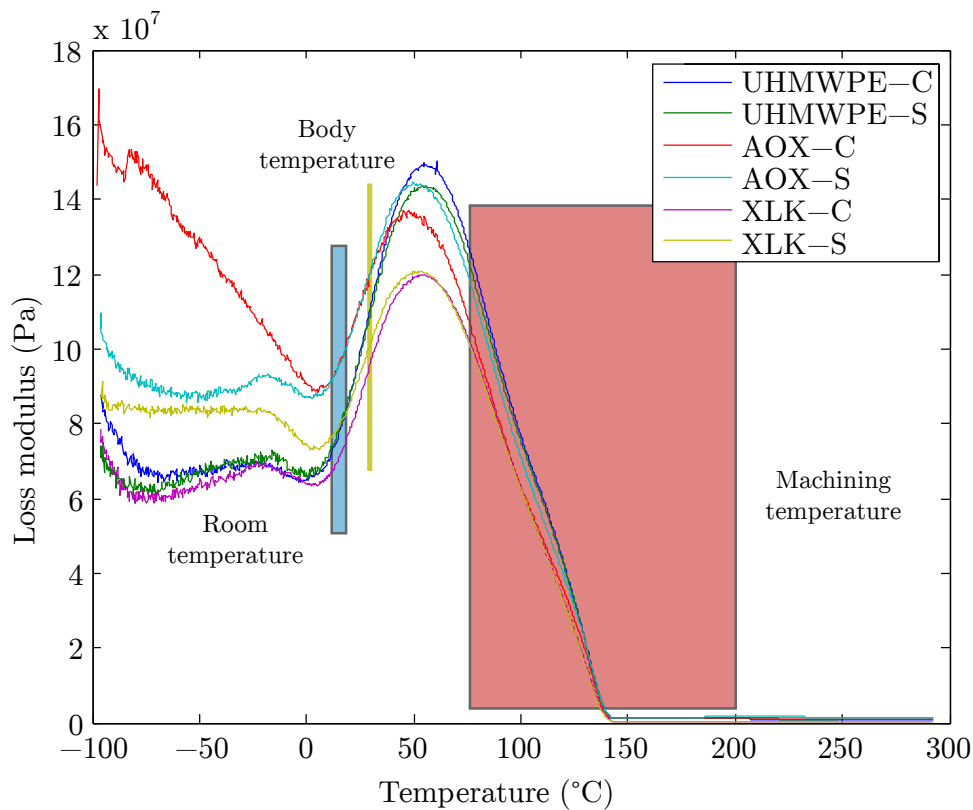


Figure 4.6: Loss modulus for all samples.

Tan Delta results are shown in figure 4.7. The higher loss modulus below 5°C for AOX-C also leads to a higher value of Tan Delta, implying more viscous behaviour for this material at low temperatures. All other samples show very consistent Tan Delta curves across all temperatures, indicating that the differences in storage and loss modulus values are a result of errors in measurement of the sample cross section. Tan Delta results show a sharp decrease from a peak at the melting temperature of 135°C for all samples, though the behaviour above the melting temperature shows variation between but not within materials. The AOX samples show higher values of Tan Delta, while XLK samples show very low values. This indicates more elastic behaviour for the crosslinked material above the melting temperature, as would be expected due to the crosslinking.

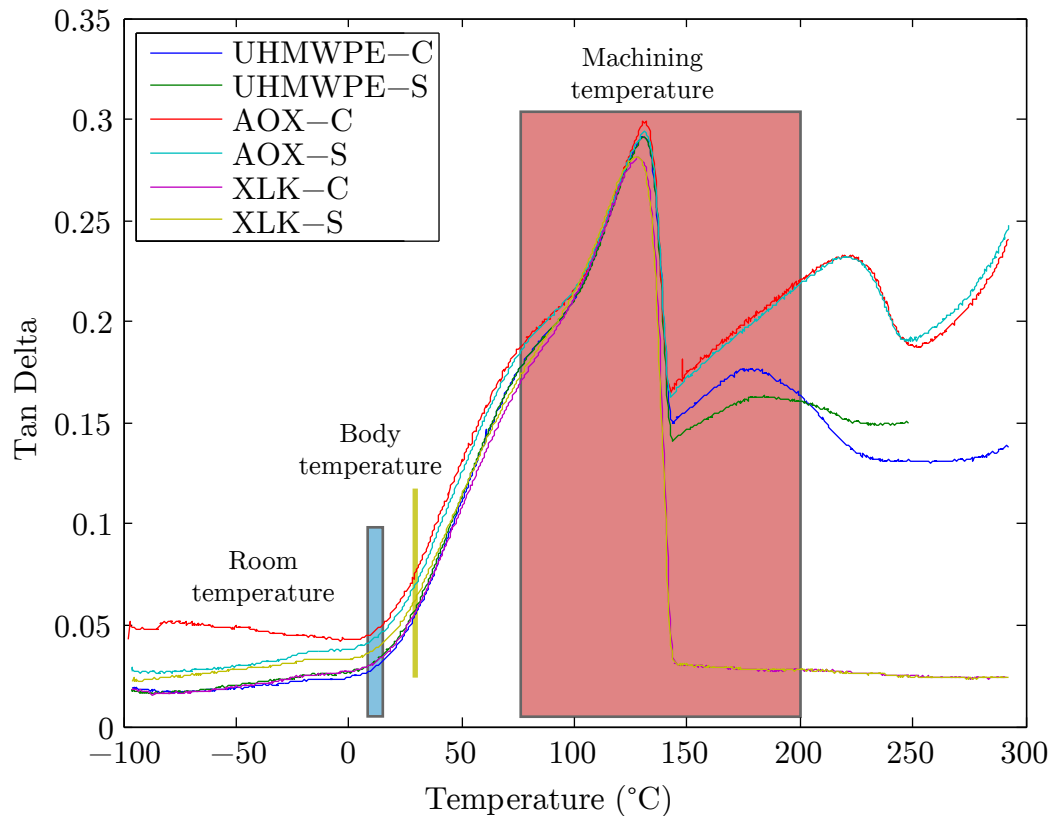


Figure 4.7: Tan Delta for all samples.

When analysing the behaviour of samples from different locations in the raw material, UHMWPE shows consistent behaviour in both samples, with the exception of a small deviation in Tan Delta above the melt temperature which could be influenced by the orientation of the sample, due to the high levels of crystallinity in UHMWPE. AOX shows a large difference in storage and loss modulus below 5°C , with a corresponding effect on the value of Tan Delta. This may be a result of the antioxidant additive concentration varying across samples, and having a freezing point below 5°C , causing variation in the viscoelastic response. This would be unlikely to cause variation at room temperature and above, as seen from the consistency of response displayed by the Tan Delta results for AOX.

It can be seen from all three graphs that while the material behaviour is largely elastic at room and body temperatures. Viscoelastic effects are small below 0°C , whereas at machining temperatures viscoelasticity is a concern, with the peak of the Tan Delta graph occurring at a temperature which will likely be exceeded when machining with certain cutting conditions.

4.3.2 Varying frequency of loading

The effect of varying the frequency of the cyclic loading on storage modulus in UHMWPE is shown in figure 4.8, with examples of the effect of temperature and strain rate in conventional tensile testing shown in appendix B. It can be seen that increased loading frequencies have higher storage modulus values across the entire temperature range, up to the melting temperature, thus indicating higher stiffness at higher strain rates.

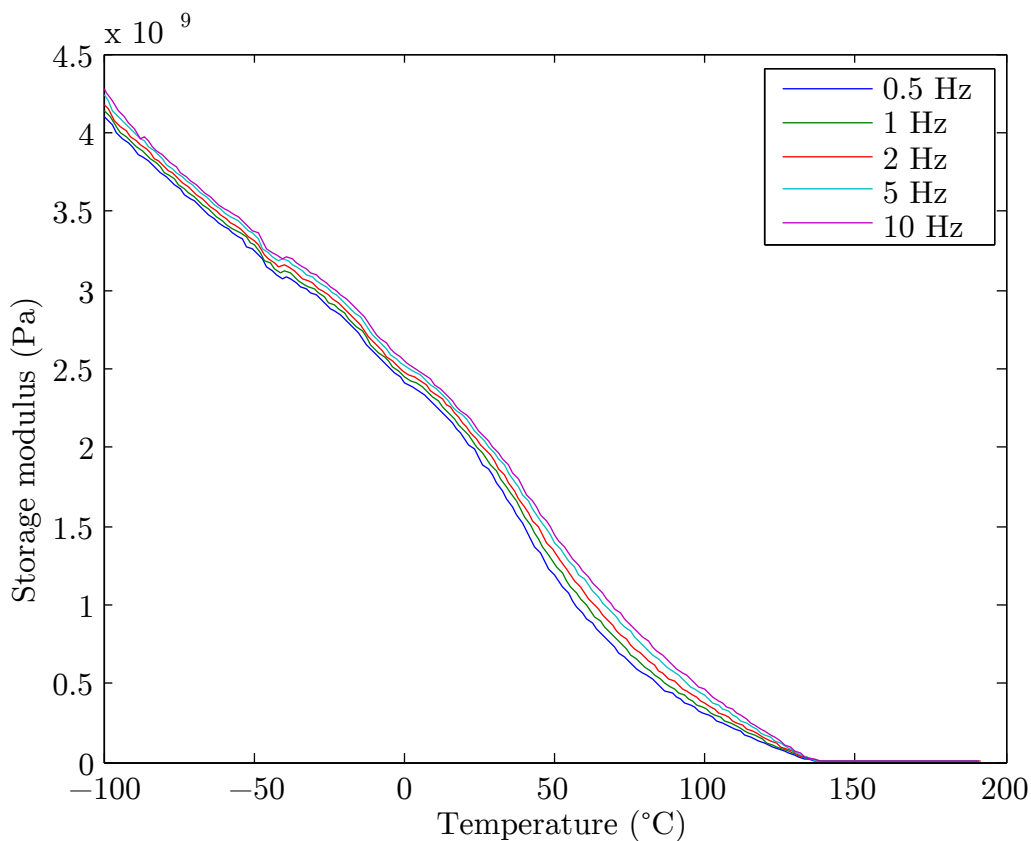


Figure 4.8: Storage modulus for varying strain rate.

The loss modulus results, shown in figure 4.9, show that the loss modulus increases significantly for lower frequencies, and that the peak value of loss modulus occurs at a lower temperature for lower frequencies. Also of interest is that above approximately 100°C the loss modulus shows little variation due to loading frequency, though the trend seen would suggest that for loading frequencies above 10Hz there will be variation in loss modulus above 100°C .

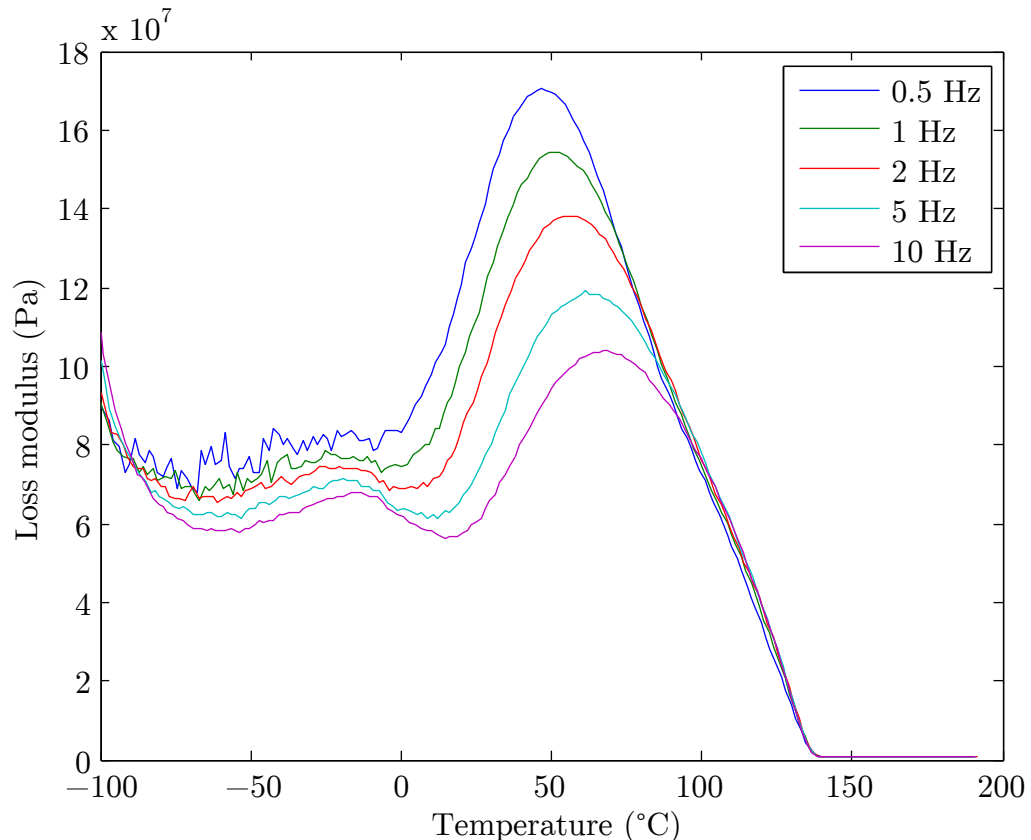


Figure 4.9: Loss modulus for varying strain rate.

Tan Delta results for varying loading frequency are shown in figure 4.10. Similar trends hold as were observed for loss modulus, due to loading frequency causing increases in the storage modulus and decreases in the loss modulus for increased frequency. The melting temperature peak remains constant at approximately 135°C , while lower loading frequencies show increased peaks in Tan Delta. The temperature at which Tan Delta begins to increase from the baseline level shifts to lower temperatures at lower frequencies, from approximately 20°C for 10Hz loading to -10°C for 0.5Hz loading. This indicates that higher strain rates will cause more elastic behaviour at all temperatures, and will also increase the temperature at which the onset of viscous behaviour is observed.

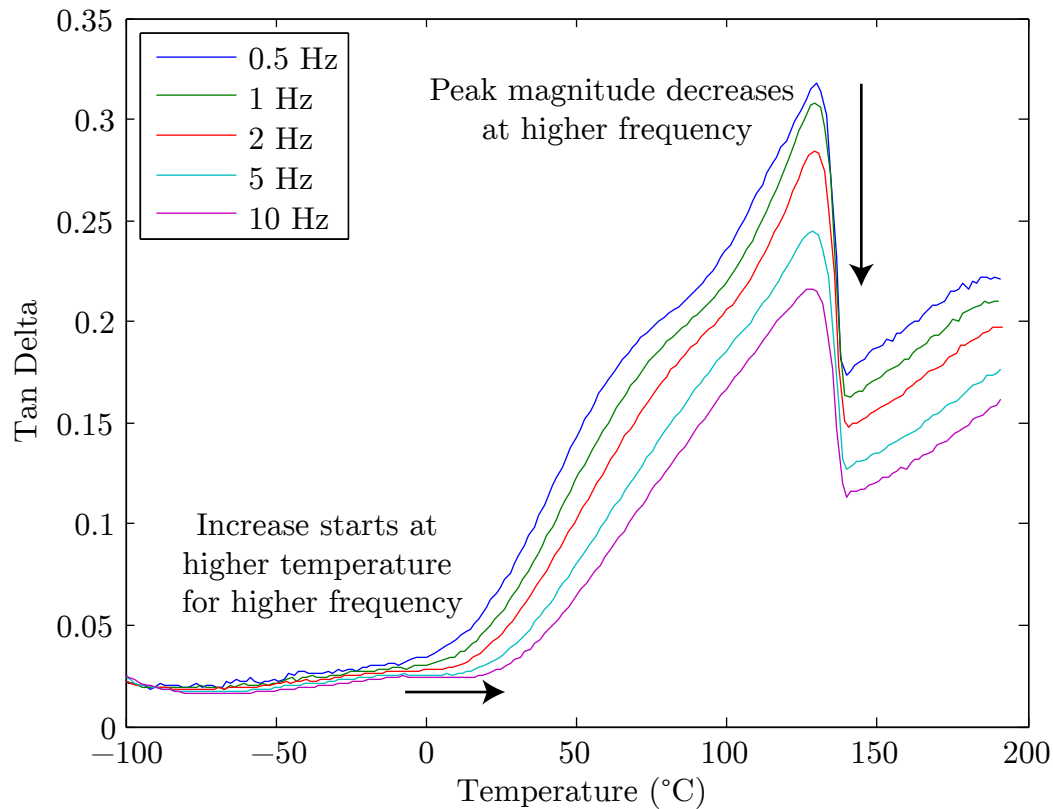


Figure 4.10: Tan Delta for varying strain rate.

DMA has shown that viscoelastic responses of the materials under study display some variation between materials, but that behaviour is relatively consistent when considering samples from the same material. Similar analysis across a range of loading frequencies has shown that the viscous component of the viscoelastic response is highly sensitive to changes in strain rate, while there is a small effect on the elastic component. This is in line with typical viscoelastic material behaviour, as explained in general by Menard [43] in his book on DMA, and as detailed for UHMWPE by Fouad [44]. The melting temperature of each material was measured as approximately 135°C , regardless of material type, material location, or strain rate.

In terms of the machining of these materials, care will be required to avoid workpiece heating above the melting temperature. Material cooling will cause the material to respond in a more elastic manner, while also preventing heating to the melting temperature. Strain rate results show that higher cutting speeds should lead to a more elastic material response.

4.4 Differential Scanning Calorimetry

The results from the DSC testing are shown in figure 4.11. There does not appear to be any significant differences in heat capacity between or within materials. The melting temperature result of approximately 135°C from the DMA results is confirmed by this data. Despite testing to -140°C it was not possible to accurately identify a glass transition temperature, though the small peak at approximately -125°C could be interpreted as a thermal transition, though it is not defined enough to be conclusive. It can be seen that while the thermal properties of the material remain relatively constant at room temperature and body temperature, it varies dramatically as typical machining temperatures are encountered. This may affect heat distribution during machining as the temperature in the material approaches the melting temperature. A full report on the DSC results is included in appendix A.

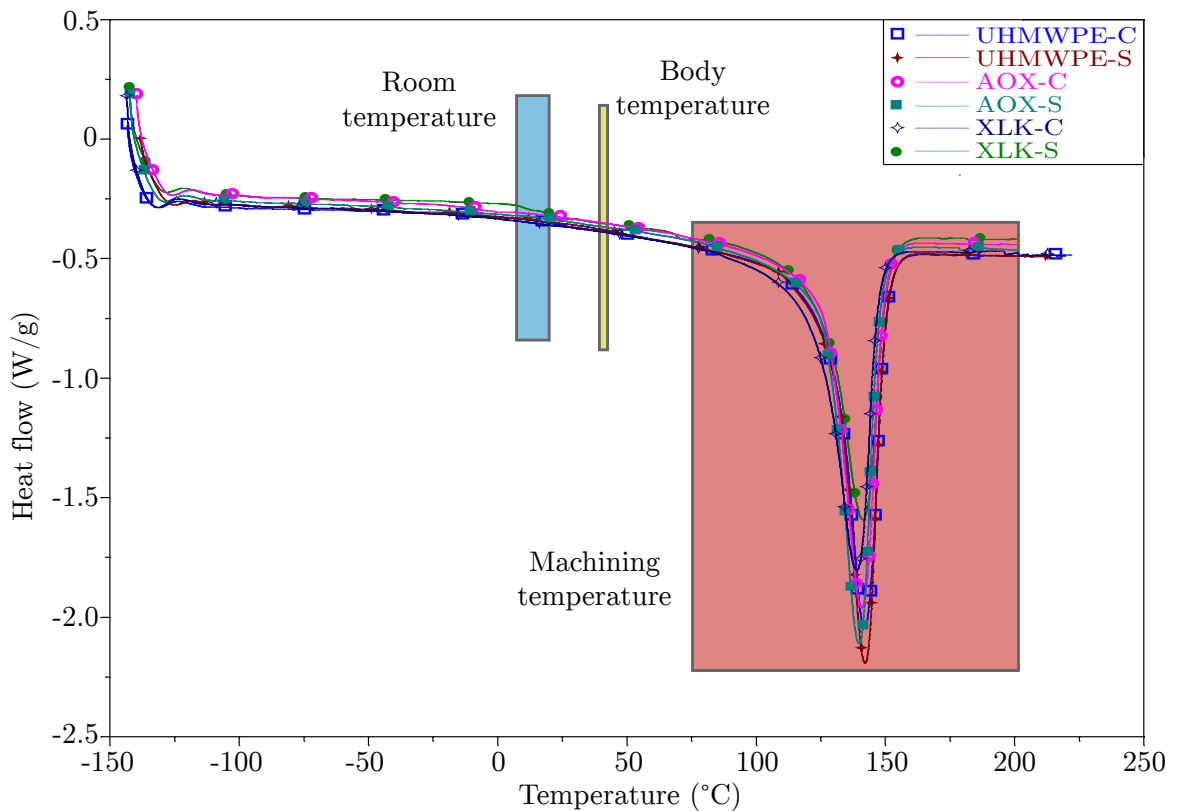


Figure 4.11: DSC results for all samples, from -150 to 250°C .

The melting temperature result shown here confirms the result seen from DMA, and agrees with the findings of Brown *et al.* [78], who measured a melting temperature of 133°C , and Fouad [44], who measured a melting temperature of 132.84°C for non-aged and 136.3°C for aged specimens of UHMWPE. The work of Greco and Maffezzoli [45] showed that the measurement of the melting temperature of recycled HDPE from DSC

MATERIAL ANALYSIS

results is sensitive to the DSC scanning rate, with melting temperatures of 130.15°C to 136.35°C measured using scanning rates from 10 to $50\text{ K}/\text{min}$. The lack of any change in melting temperature for the crosslinked material indicates a relatively low level of crosslinking in the material, as the work of Göschel and Ulrich [46] showed that the level of crosslinking increases the melting temperature of the material.

4.5 Discussion

This chapter established the viscoelastic behaviour of UHMWPE through specialised polymer testing techniques. Shore hardness testing showed no major variations between materials, while DMA, FTIR and DSC analyses show no variations in chemical or thermal properties, and only minor variations in mechanical properties of the materials at low temperatures. DMA analysis showed that strain rate can have major effects on the viscoelastic response of the material to applied mechanical loads. It was not possible to measure a glass transition temperature for any of the samples used, though an upper bound of -140°C was identified, thus meaning that all machining operations at room temperature will be well within the viscous region of mechanical properties. DMA and DSC analyses both showed a melting temperature of approximately 135°C , though this is likely to be sensitive to heating rate, with higher heating rates causing a slight increase in melting temperature.

At the temperatures expected in typical non-cryogenic machining there appears to be no variation in properties as a result of the original position of the material in an extruded bar or rod. At temperatures below 0°C the mechanical response characterised in the DMA results shows that the material behaves in an elastic-dominated manner, with the viscous component of the response being smaller. However, while the temperature dependent viscoelastic properties of all three materials are reasonably constant at room and body temperatures, they vary in typical machining temperature regions, and thus the materials cannot be assumed to be equivalent for machining purposes. It can be concluded that cooling of the workpiece would help in minimising the effects of viscoelasticity during machining.

MATERIAL ANALYSIS

Chapter 5

Fundamental investigation into orthogonal cutting of UHMWPE

5.1 Background and methodology for characterisation of orthogonal cutting of UHMWPE

The objective of this chapter is to gain knowledge of the machinability and surface quality achievable in the orthogonal cutting of three varieties of UHMWPE at room temperature, in light of the material behaviour and characteristics detailed in chapter 4. This is achieved by gathering data using a monitoring and data acquisition system, as detailed in chapter 3 and shown in figure 5.1. Machining forces and temperatures during machining are monitored using this system, along with acquisition of high speed camera images of the cutting zone. These data will be complimented with information gathered post-process, in the form of analysis of chip thickness and form, and profilometer and SEM inspection of the machined surface.

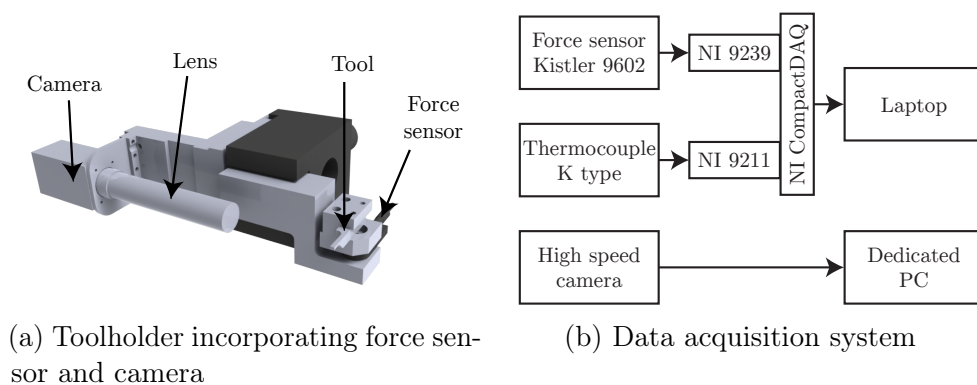


Figure 5.1: Toolholder and data acquisition system.

FUNDAMENTAL INVESTIGATION INTO ORTHOGONAL CUTTING OF UHMWPE

The factors which will be varied include material type, tooling parameters and machining parameters. Rake angle and cutting edge radius will be varied on the tooling, along with the machining parameters of cutting speed and depth of cut. Three varieties of UHMWPE will be machined as part of these experiments. The varieties are:

1. Plain UHMWPE
2. UHMWPE which has had an antioxidant added to reduce material degradation from oxidation in service (AOX)
3. UHMWPE which has been crosslinked to improve mechanical properties and wear behaviour (XLK)

The effect of these factors will be analysed using a full factorial Design Of Experiments (DOE), as detailed in table 5.1.

Table 5.1: Factors used in design of experiments for fundamental investigation into orthogonal cutting of UHMWPE (Repeat of table 3.3).

| Factor | Number of levels | Levels |
|---------------|-------------------------|---|
| Material | 3 | UHMWPE, AOX, XLK |
| Rake angle | 4 | -20° , 0° , 20° , 40° |
| Edge radius | 3 | Sharp, worn, highly worn - See table 3.4 |
| Cutting speed | 2 | 155, 300 <i>m/min</i> |
| Depth of cut | 2 | 0.06, 0.19 <i>mm/rev</i> |

5.2 Machining forces

5.2.1 Cutting force

The main effects plot for cutting force is shown in figure 5.2. Cutting force increases with depth of cut and tool wear, as expected, and decreases with rake angle, indicating easier cutting at higher rake angles. Workpiece material has a small effect, with plain UHMWPE showing higher forces than AOX or XLK. This may indicate that the addition of antioxidant, or the crosslinking of the material, has an adverse effect on the mechanical properties of the material. The variation for AOX workpieces may indicate that the antioxidant additive is acting as a plasticiser. It is possible that the relatively small effect of cutting speed is a result of the effects of increased strain rate and softening of material due to frictional heating offsetting each other at the levels used. Further testing at a wider range of cutting speeds would provide further insight into the true effect of cutting speed.

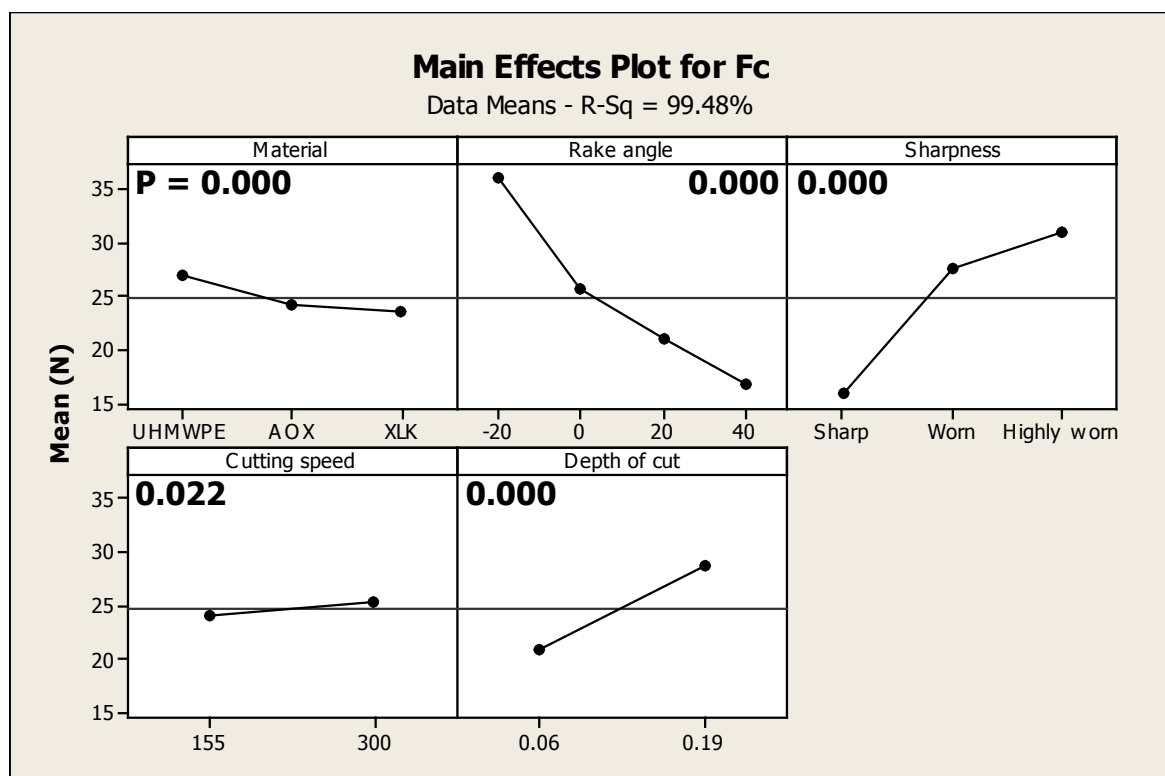


Figure 5.2: Main effects plot for cutting force. Numbers shown within each box are P values from ANOVA, with P values for statistically significant main effects shown in bold.

The two way interactions plot for cutting force is shown in figure 5.3. A full ANOVA table for this analysis is shown in appendix D. 6 of the 10 two way interactions appear

significant, with the material - depth of cut interaction being marginally significant ($P = 0.05$). The interactions of rake angle with sharpness, depth of cut and material may indicate a change in chip formation mechanism. These interactions may also indicate the influence of the size effect on the transition from cutting to material deformation, which occurs at low effective rake angle and/or large edge radius, as discussed in section 2.3.1.

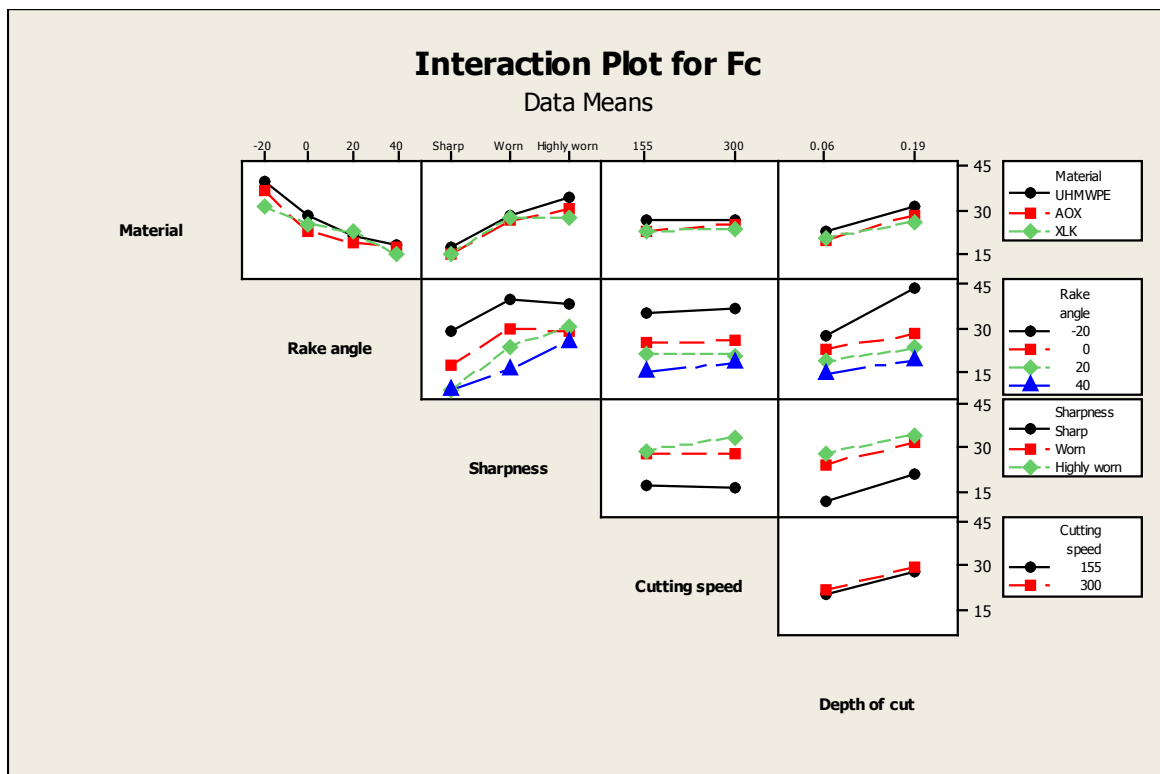


Figure 5.3: Interactions plot for cutting force.

In addition, the three way interactions of material - rake angle - sharpness and rake angle - sharpness - depth of cut were significant, as was the four way interaction of rake angle - sharpness - cutting speed - depth of cut. This complex dependency of cutting force on the cutting parameters further indicates that transitions in chip formation mechanism are occurring within the parameter levels studied. It is interesting to note that cutting speed has the highest P value of the main effects. Cutting speed is significant in only a single two way interaction and no three way interactions, but is significant in the four way interaction. This indicates a relatively weak overall effect from cutting speed compared to the other factors.

It was not possible to study the five way interaction response for cutting force or thrust force, due to the lack of replication.

5.2.2 Thrust force

The main effects plot for thrust force is shown in figure 5.4. The same overall trends hold as for cutting force - with the exception of depth of cut - with thrust force decreasing with increasing depth of cut. This is consistent with the analysis shown in section 2.3.1, as for the large depth of cut the ratio of edge radius to depth of cut remained small for all cutting operations.

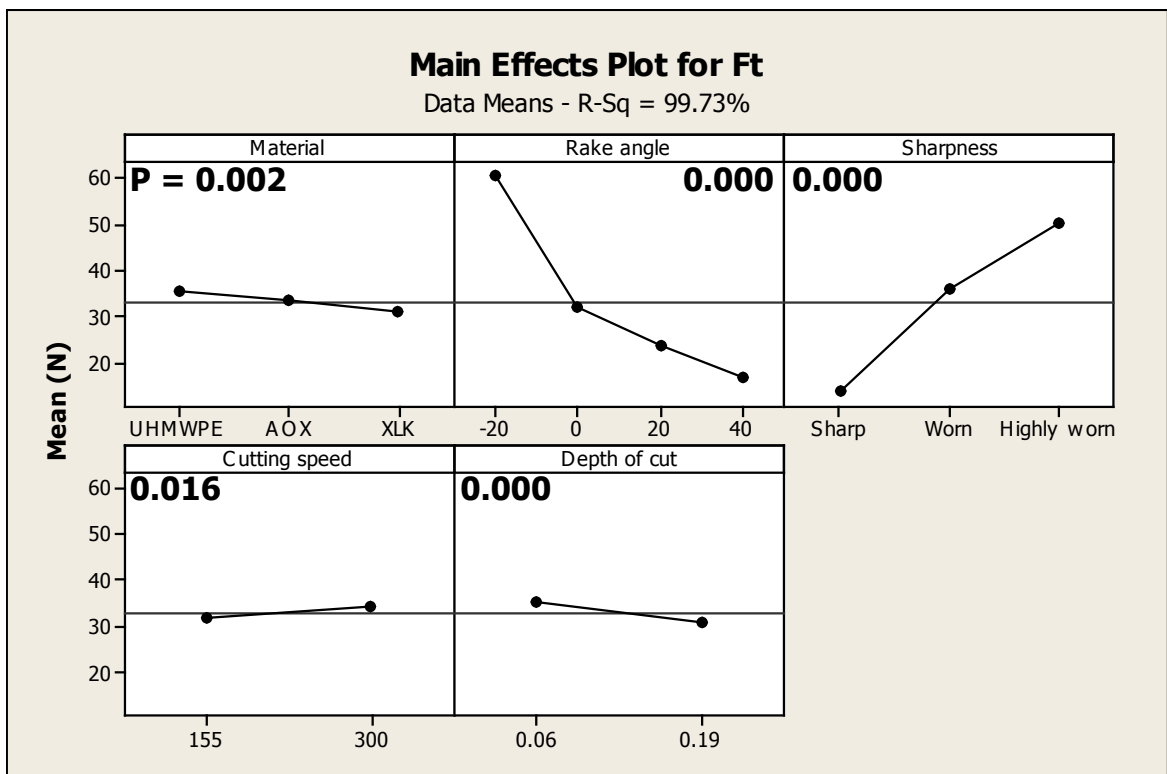


Figure 5.4: Main effects plot for thrust force.

The two way interactions plot for thrust force is shown in figure 5.5. A full ANOVA table for this analysis is shown in appendix D. 7 of the 10 two way interactions appear significant, with the material - cutting speed interaction being marginally significant ($P = 0.04$), as the material - depth of cut interaction was for cutting force. Compared to the two way interactions for cutting force, the interaction between sharpness and depth of cut is highly significant, indicating the effect of the ratio of edge radius and depth of cut, as defined in equation 2.1. This ratio remains small for large depths of cut, but exceeds 1 for small depths of cut, leading to increased thrust force, and thus the interaction between sharpness and depth of cut.

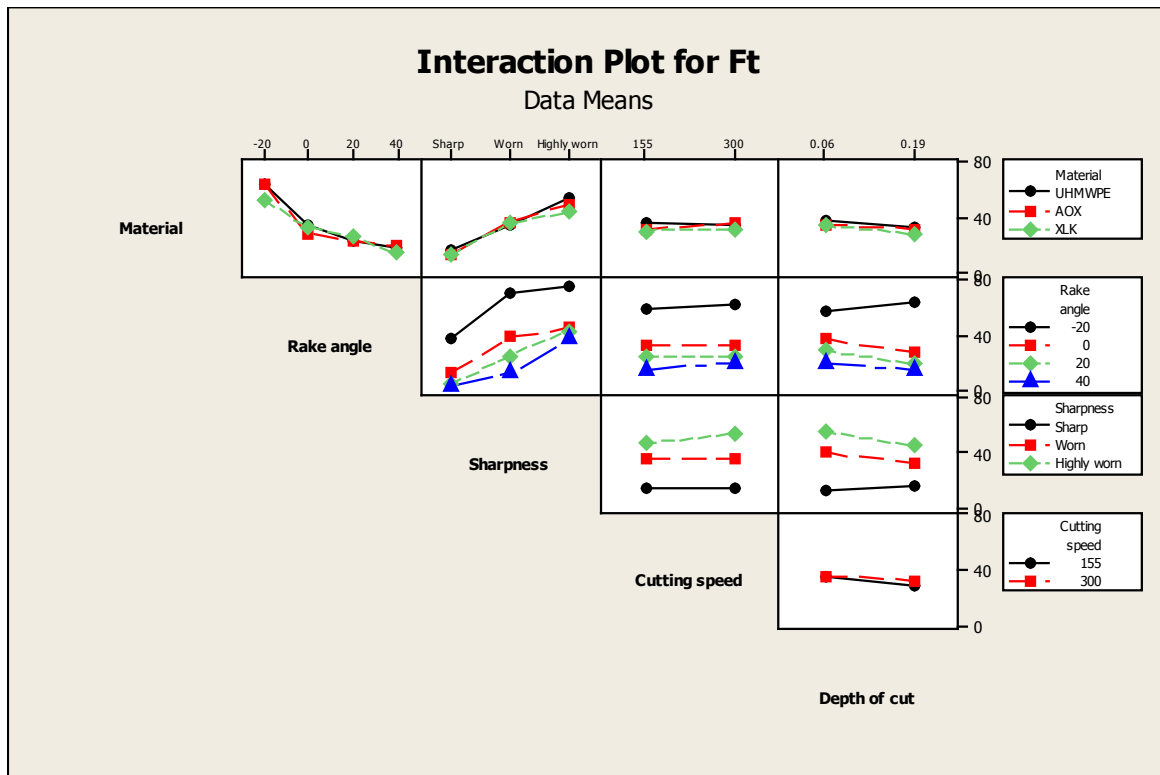


Figure 5.5: Interactions plot for thrust force.

The three and four way interactions for thrust force show the same pattern as for cutting force. The high R^2 values for cutting force and thrust force (99.5% and 99.73%, respectively) show that the model contains little unexplained variation, and thus can be considered accurate for analysis purposes.

5.3 Tool temperature

The full statistical analysis of peak temperature is of limited utility, due to the thermal inertia of the tool-thermocouple system. This thermal inertia causes a large dependence of the tool temperature on the duration of the cut, which is a function of cutting speed and depth of cut. Appendix C contains details of the full statistical analysis. However, the response of peak temperature may still provide useful information for factors which do not directly influence the duration of the cut. Figure 5.6 shows sample temperature data for the range of sharpnesses, with other factors held constant. It can be seen that the duration of the cut is constant between operations, with the size of the peak being a result of transmission of larger amounts of heat to the tool from the cutting zone. Simulations of tool temperature in orthogonal metal cutting such as those carried out by Dogu *et al.* [146] have shown that the surface of the rake face of the tool will have the highest temperature, with subsurface temperatures being lower. It is reasonable to say, therefore, that in a machining operation the subsurface tool temperature in a location such as that of the thermocouple in the current experimental setup can be taken as a lower bound of the temperature at the cutting zone.

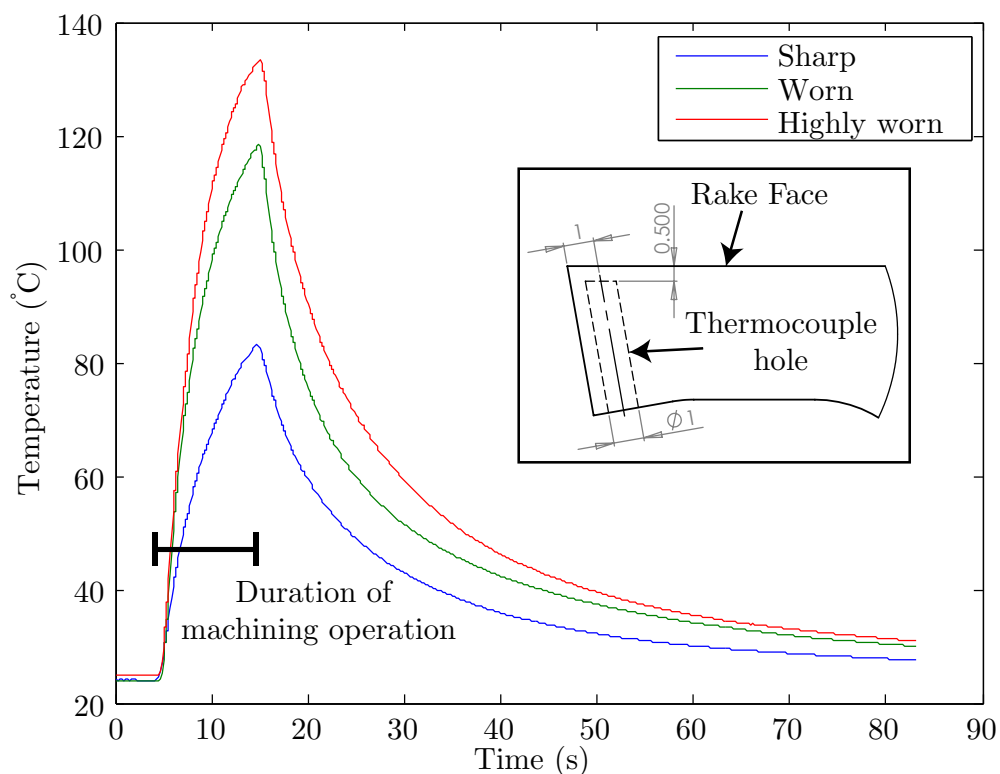


Figure 5.6: Graph showing effect of tool sharpness on tool temperature during machining. Machining operations carried out using UHWMPE workpiece, 0° rake angle, low cutting speed, low depth of cut. Inset: Thermocouple location within cutting tool.

FUNDAMENTAL INVESTIGATION INTO ORTHOGONAL CUTTING OF UHMWPE

The main effects plot for tool temperature is shown in figure 5.7. AOX and XLK have lower average temperatures than UHMWPE, possibly indicating that crosslinking and adding an antioxidant improve the heat capacity of the material, or have lower coefficients of friction. Rake angle shows a strong effect on peak temperature, reducing from 108°C at -20° rake angle to 60°C at 40° rake angle. This could be related to the lower cutting and thrust forces at higher rake angles, indicating that there is a correlation between temperature and cutting forces. The effect of sharpness shows a counterintuitive effect, with worn tools having a higher peak temperature than highly worn tools. This may be a result of machining with highly worn tools causing deformation or smearing of the material rather than cutting, leading to a smaller contact area, as shown in the literature review in section 2.3.1. The highest single temperature measured was 186°C (XLK, 0° rake angle, highly worn tool, 300 m/min , 155 mm/rev), which far exceeds the melting temperature established in chapter 4. The thermal inertia of the tool and distance from the cutting edge means that the peak temperature was likely far higher, and that melting of the material is likely occurring.

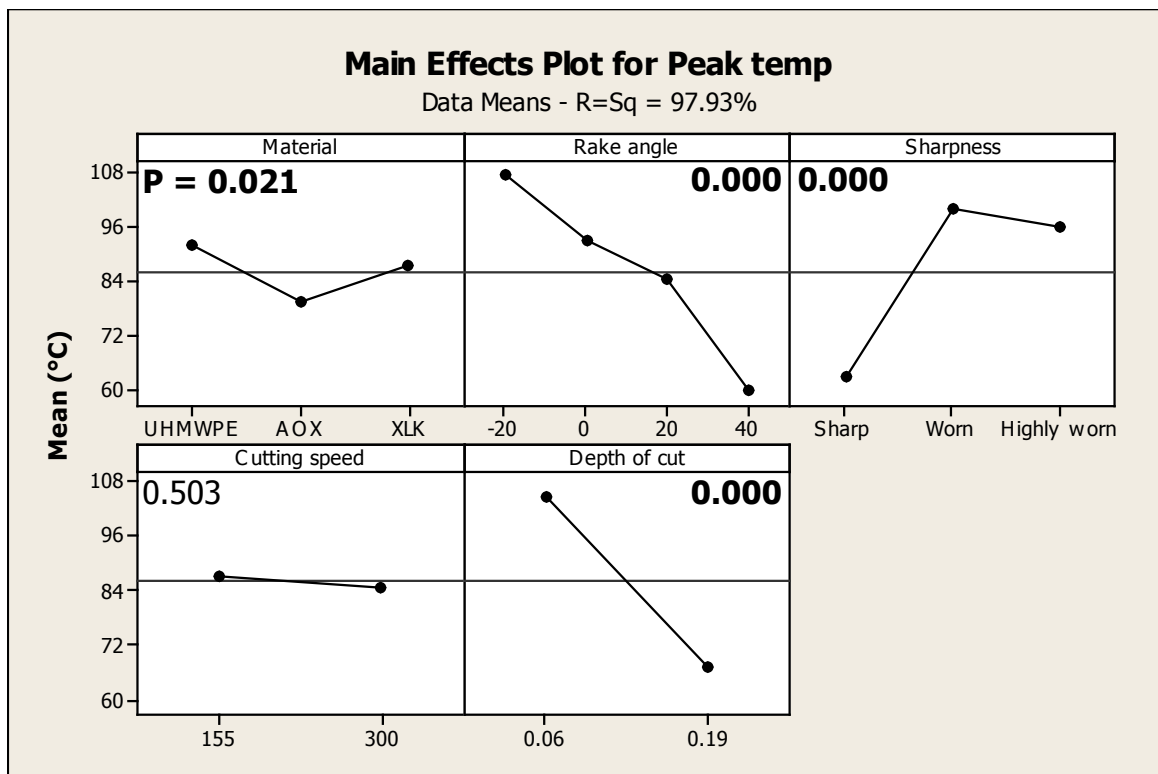


Figure 5.7: Main effects plot for temperature.

5.3. TOOL TEMPERATURE

Due to the unusual relationship with sharpness, and the possibility that highly worn results could be skewing the main effects, a main effects plot for peak tool temperature excluding highly worn results, is shown in figure 5.8. It can be seen that the material effect is far more uniform than before, indicating that this variation occurs only at the highly worn level of sharpness. The rake angle data shows similar behaviour to before, but with 0° and 20° rake angles having lower means. As before, the cutting speed and depth of cut results are aliased with the duration of the cut, and thus cannot be relied upon as main effects.

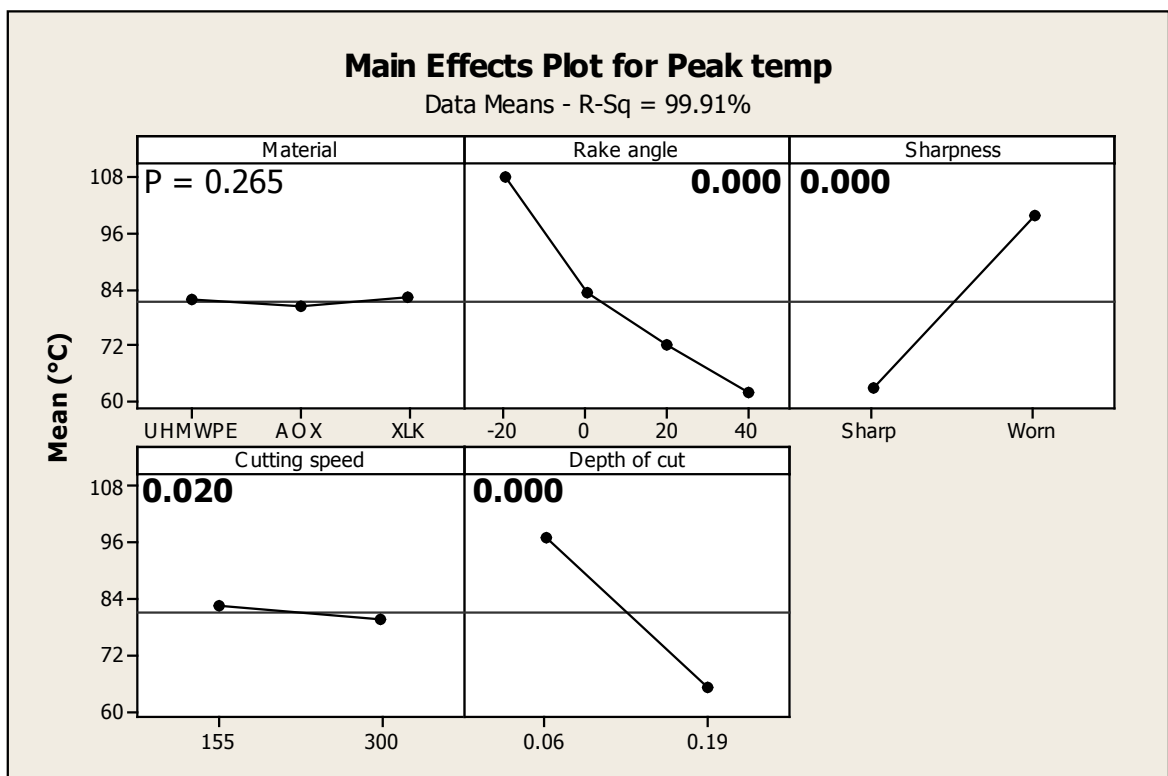


Figure 5.8: Main effects plot for temperature, excluding highly worn tools.

5.4 Surface roughness

The main effects plot for surface roughness is shown in figure 5.9. Due to the extremely rough nature of the machined surfaces for some highly worn tools, as will be shown in section 5.6.1, it was decided to restrict analysis to sharp and worn tools. It is clear that the change in sharpness from sharp to worn has a large effect on surface roughness. A higher depth of cut or smaller edge radius gives a better surface roughness. This dependence may indicate that surface roughness is sensitive to the size effect, as discussed in section 2.3.1. Material and cutting speed do not appear statistically significant.

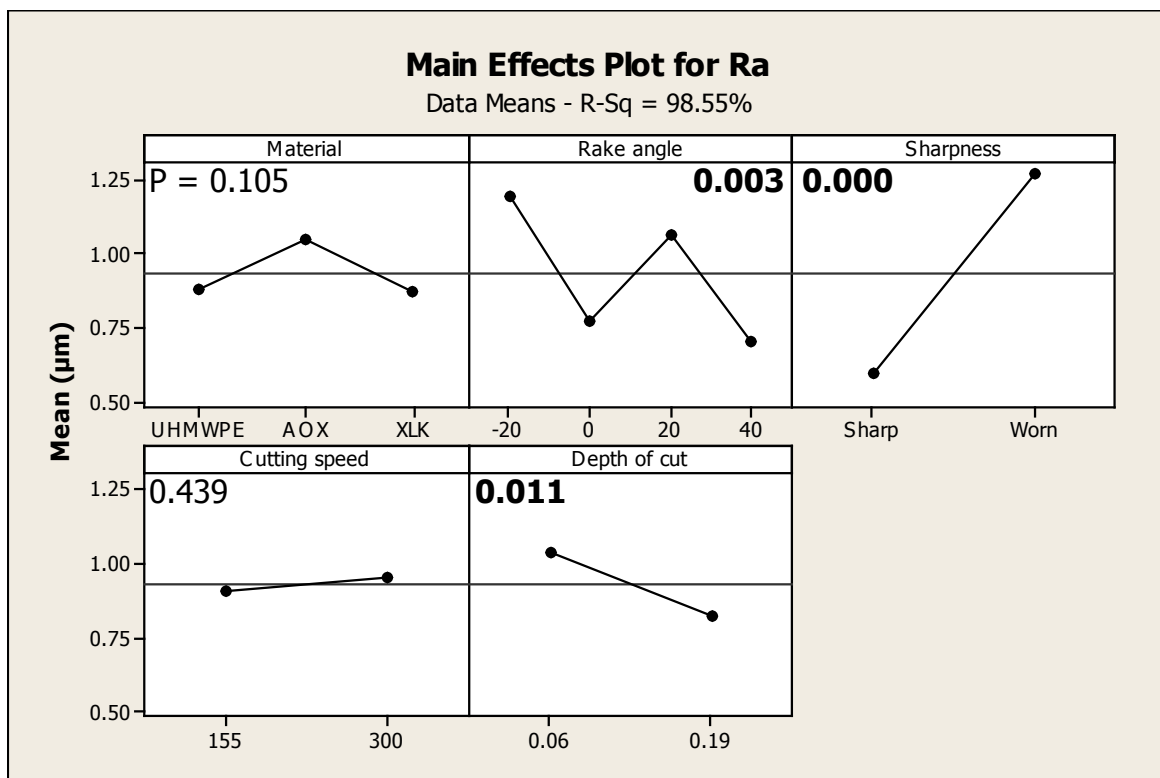


Figure 5.9: Main effects plot for surface roughness.

5.4. SURFACE ROUGHNESS

The two way interactions plot for surface roughness is shown in figure 5.10. The ANOVA table for the analysis is shown in appendix D. The P values from the ANOVA indicate that rake angle-sharpness and sharpness-depth of cut are the only statistically significant interactions. The interaction between sharpness and depth of cut is due to the size effect, as the maximum $\frac{r}{DOC}$ for worn tools was 1, which would cause poor cutting at low depths of cut with worn tools, thus giving poor surface finish. In addition, rake angle appears to be exhibiting complex behaviour, with a strong interaction between rake angle and sharpness. For both sharp and worn tools the surface roughness reading at a rake angle of 20° is greater than that of 0° and 40°. Similar increases at rake angles between 5° and 10° have been reported in the past [106], as has complex behaviour of surface roughness with varying machining parameters [96]. This could be an effect associated with the critical rake angle. For the cutting conditions used in this case the critical rake angle would be in the region of 5° to 20°, as detailed in the literature review, in section 2.3.6.

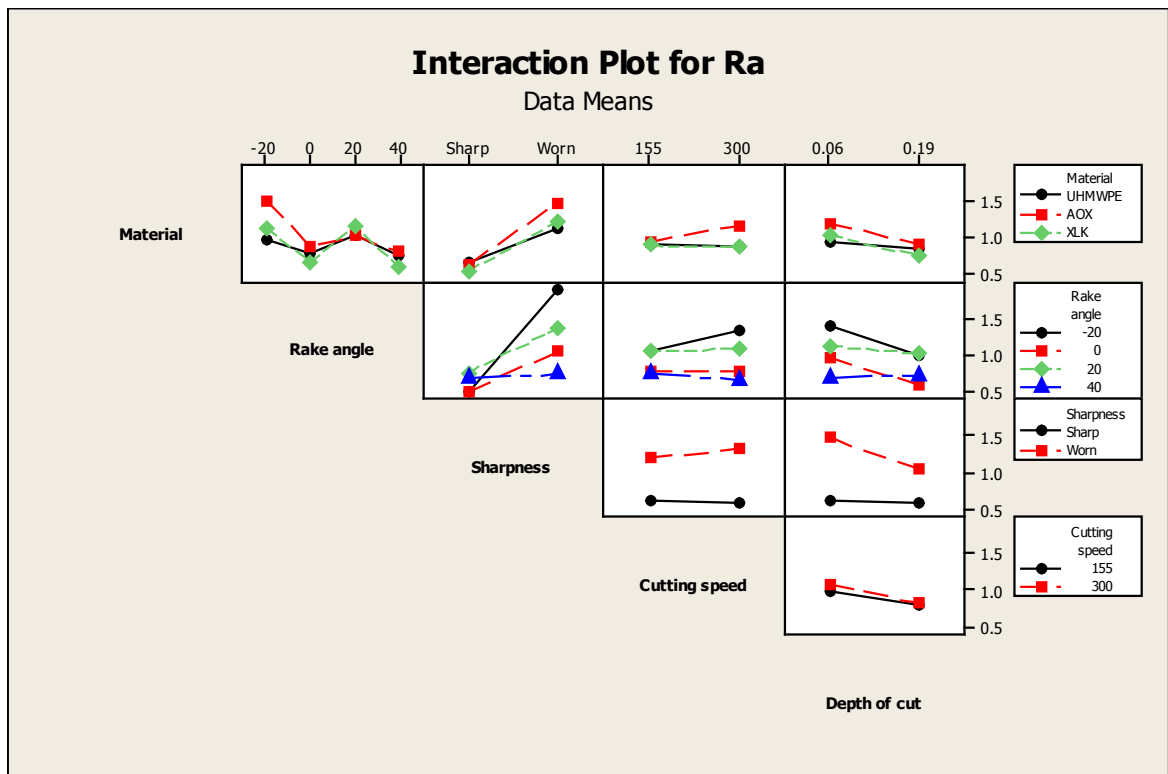
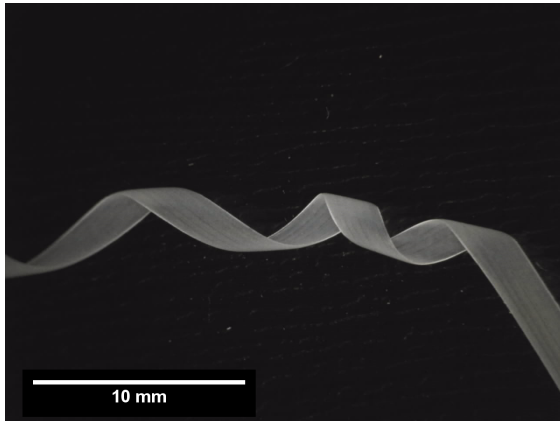


Figure 5.10: Interactions plot for surface roughness.

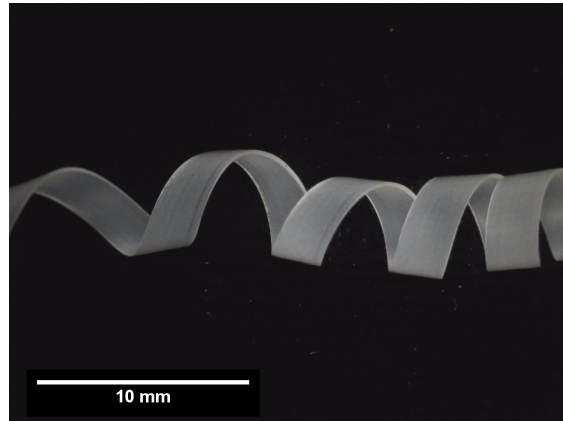
5.5 Chip formation

5.5.1 Chip examination

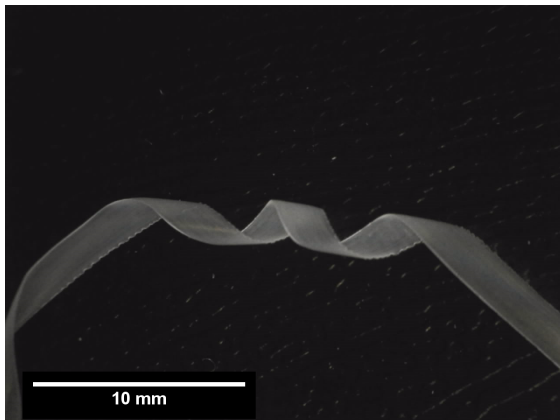
The effect of cutting speed and depth of cut on chip appearance is shown in figure 5.11. It is clear that the radius of curvature is a function of the depth of cut, with a low depth of cut delivering a smaller radius of curvature.



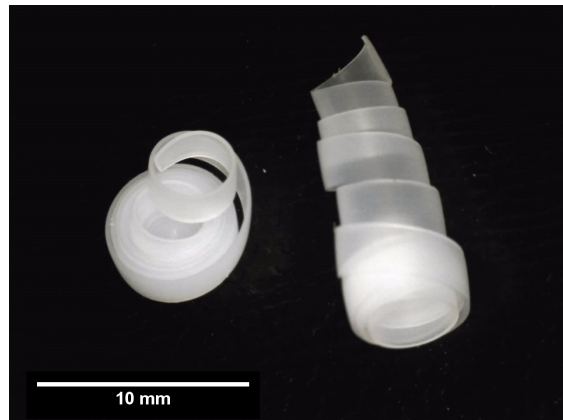
(a) Low cutting speed, low depth of cut



(b) Low cutting speed, high depth of cut



(c) High cutting speed, low depth of cut



(d) High cutting speed, high depth of cut

Figure 5.11: Sample of chips collected after machining operations.

5.5.2 Chip thickness

The main effects plot for the difference between cut and uncut chip thicknesses is shown in figure 5.12. Worn and highly worn tools did not produce a continuous chip in all machining conditions, so the analysis was performed on data from experiments performed with sharp tools. The low correlation between depth of cut and chip thickness is expected, as the variation due to depth of cut has been removed. It is clear that the -20° rake angle produces on average a chip which is significantly thicker than the uncut chip thickness. This indicates that negative rake angle cutting is of the continuous - shear type, as detailed in table 2.6. Cutting at neutral and positive rake angles produces a difference close to zero, indicating that the cut is of the continuous - flow* type. The ANOVA indicates that cutting speed is not statistically significant for chip thickness ($P = 0.172$).

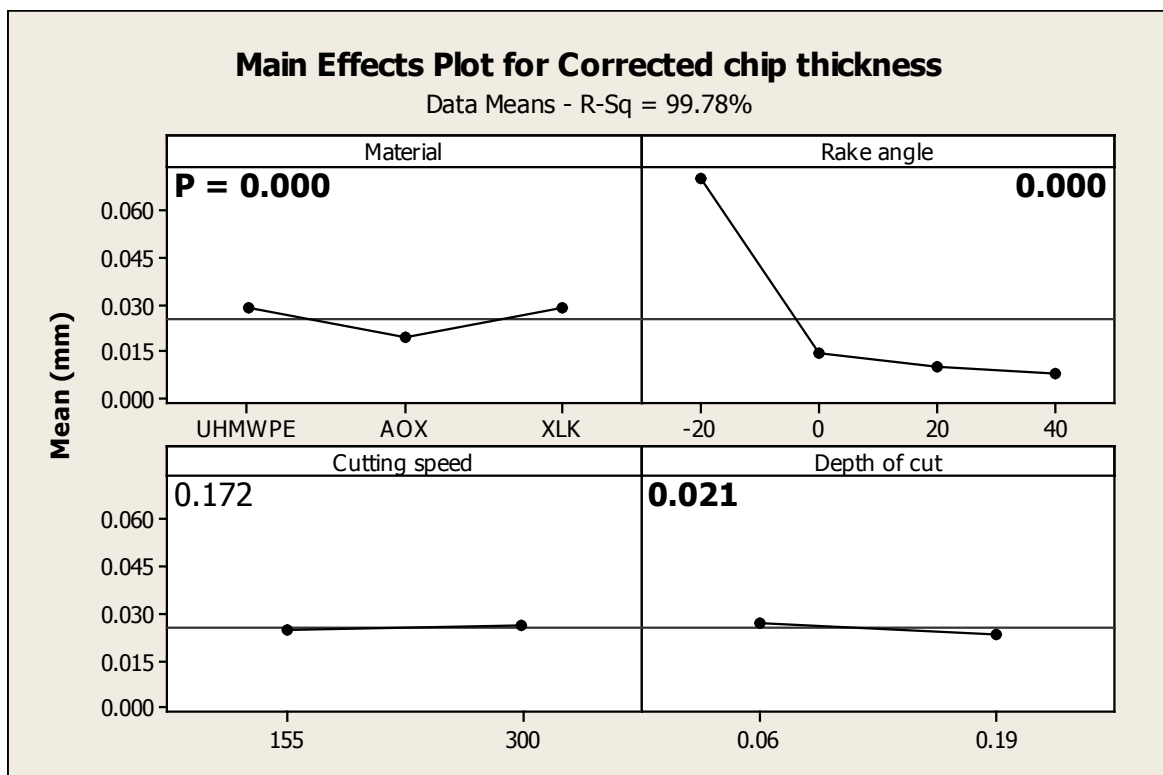


Figure 5.12: Main effects plot for chip thickness.

The two way interactions plot for chip thickness is shown in figure 5.13. The interactions involving cutting speed are all statistically insignificant ($P > 0.131$ in all cases), while all other two way interactions are significant ($P < 0.021$ in all cases), with the rake angle - depth of cut interaction having the most striking effect. It is clear from the interactions that for all materials, cutting speeds, and depths of cut, machining operations carried out using a tool with a negative rake angle produces much

higher chip thickness than at neutral or positive rake angles. The plain UHMWPE and crosslinked material (XLK) display similar behaviour, while the material with added antioxidant (AOX) has a consistently lower chip thickness at all rake angles. This indicates that the addition of antioxidant changes the chip formation mechanism slightly. This is consistent with the surface roughness result, providing further evidence to the plasticiser hypothesis.

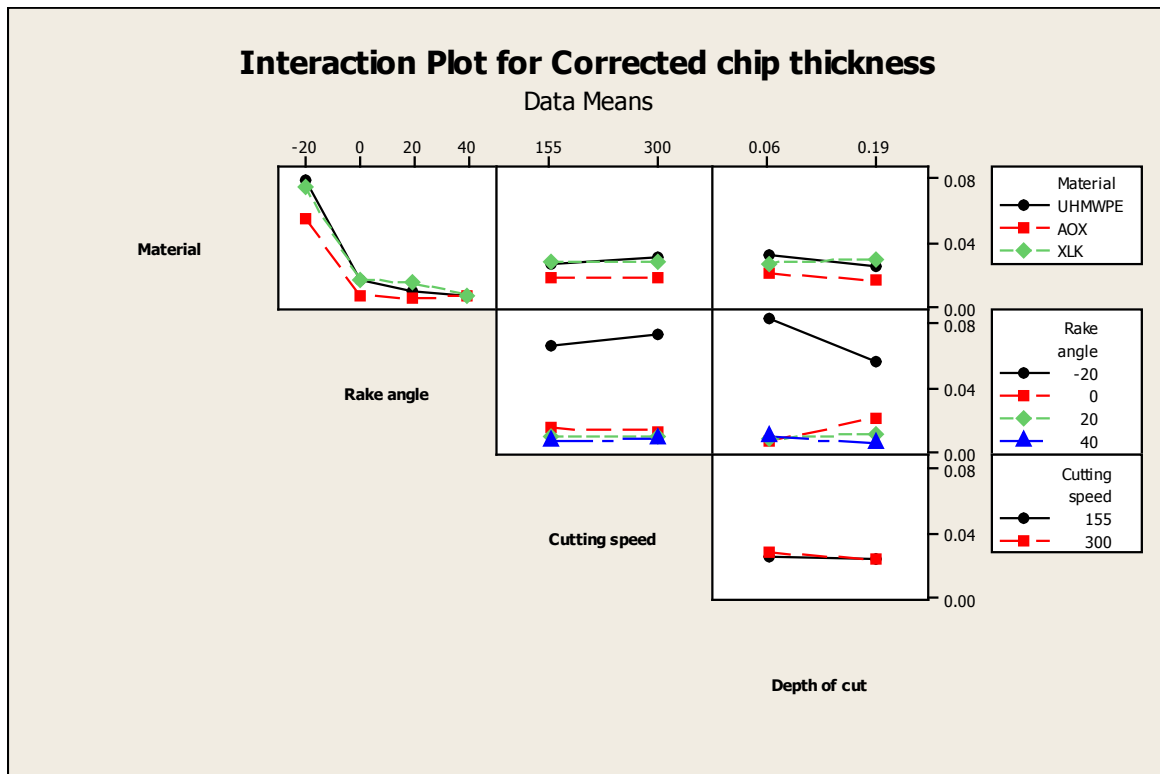


Figure 5.13: Interactions plot for chip thickness.

One three way interaction is significant for chip thickness, the material - cutting speed - depth of cut interaction. It is possible that this indicates that the plasticising effect of the additive is sensitive to machining conditions. This is the only level at which cutting speed appears significant for chip thickness, indicating an extremely weak effect overall. It was not possible to study the four way interaction due to the lack of replication.

5.5.3 Video of chip formation

5.5.3.1 Varying tool sharpness

High speed video of chip formation for varying tool edge radius at low depths of cut is shown in figure 5.14. An example of favourable cutting conditions is shown in figure 5.14a. There is a single cutting edge evident, with no contact on the clearance face and little contact between the chip and the rake face. A smooth continuous chip is being formed. The chip formation for a worn tool (shown in figure 5.14b) shows some workpiece deformation around the cutting edge, and contact between the workpiece and the clearance face of the tool, but there is still a continuous chip being formed.

This is in contrast to the highly worn situation (as shown in figure 5.14c) where there is very large deformation of the workpiece occurring before the cutting point of the tool, and contact between the workpiece and the clearance face of the tool. This is an example of machining with a tool edge radius exceeding the depth of cut, as detailed in section 2.3.1. The expansion of the workpiece after the tool has passed is also evident.

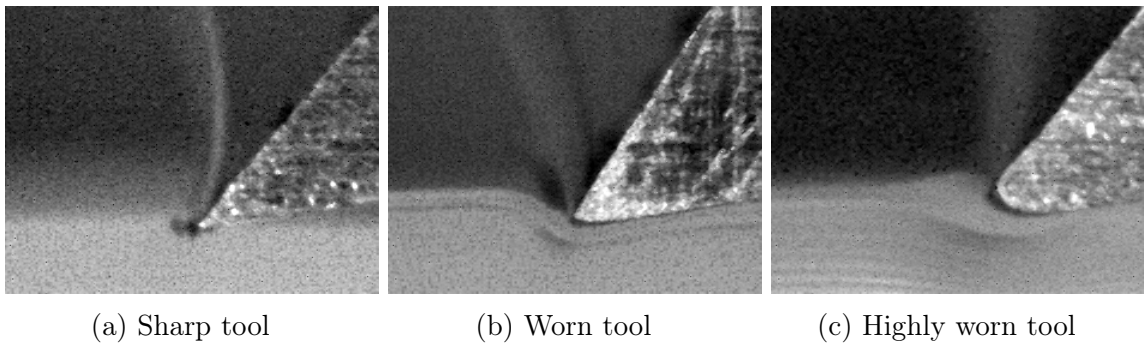


Figure 5.14: High speed camera images showing effect of varying tool sharpness at low depth of cut. (Workpiece moving left to right relative to the tool.)

5.5.3.2 Varying tool rake angle

High speed video of chip formation for varying tool rake angle at low and high depths of cut is shown in figure 5.15. All four rake angles studied show continuous chip formation at both low and high depths of cut, with some workpiece deformation evident at the negative rake angle. The negative rake angle shows that the chip is deflected at a large angle from the rake face, while the positive rake angles show the chip clearing the cutting zone at a smaller angle. The neutral rake angle, however, shows a variation in chip clearance angle, with figure 5.15b showing a large clearance angle while figure 5.15f shows a smaller clearance angle. This may indicate a small change in chip formation mechanism as a function of depth of cut at the neutral rake angle, though the chip thickness results did not indicate a change from continuous-flow* to continuous-shear, and continuous chips were formed in both situations.

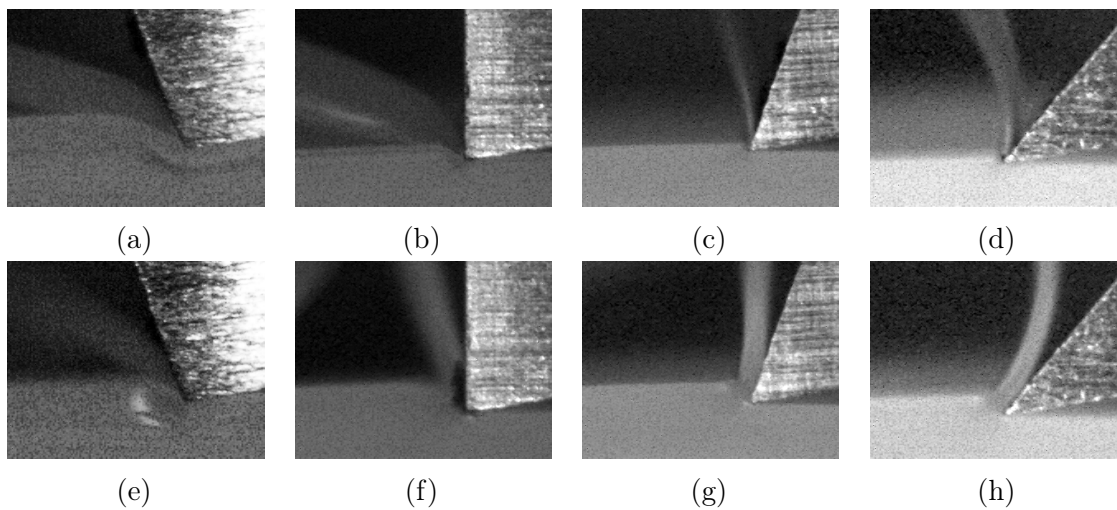


Figure 5.15: High speed camera images showing effect of varying tool rake angle. Low depth of cut shown in a - d, high depth of cut shown in e - h. (Workpiece moving left to right relative to the tool.)

5.5.4 Analysis of chip formation mechanisms

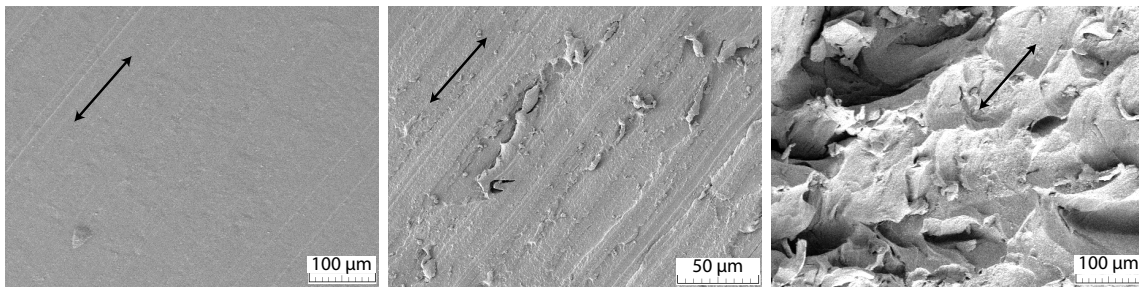
It is clear from the chip thickness main effects plot shown in figure 5.12 that the -20° rake angle produces a chip which is significantly thicker than the uncut chip thickness. This indicates that negative rake angle cutting is of the continuous - shear type, as detailed in table 2.6. Cutting at neutral and positive rake angles produces a difference close to zero, indicating that the cut is of the continuous - flow* type.

The chip formation for a worn tool (shown in figure 5.14b) shows some workpiece deformation around the cutting edge, and contact between the workpiece and the clearance face of the tool, but there is still a continuous chip being formed, indicating that the continuous - flow* chip formation mechanism is still occurring. The chip formation for highly worn tools is shown in figure 5.14c. There is a discontinuous chip of either the discontinuous - simple shear type, or the discontinuous - crack type, being formed.

5.6 Analysis of machined surface

5.6.1 Varying tool sharpness

The effect of varying tool sharpness on the surface finish is shown in figure 5.16. The sharp tool (shown in figure 5.16a) delivers a smooth cut, with undulations on the surface a result of the profile of the tool. The worn tool (shown in figure 5.16b) displays some features associated with smearing rather than cutting, with the largest being on the scale of $80\ \mu\text{m}$. It is clear that there is a slight degradation in surface quality when the tool is worn. This is supported by the surface roughness results. However, transition to the highly worn state causes a marked decrease in the quality of the machined surface. The surface shown in figure 5.16c displays an undulating machined surface indicative of large amounts of smearing and surface deformation, unlikely to be of use in any engineering application. It was not possible to measure R_a in a repeatable manner on this surface due to the undulating surface. Though SEM imaging does not provide any indication of the depth of the surface features shown, the gold coated surface of this sample appears frosted to the naked eye, while samples where it was possible to measure surface roughness showed R_z values of up to $20\ \mu\text{m}$, indicating an extremely rough surface. This deformation is potentially a result of the workpiece being heated to above the melting temperature, as detailed in section 5.3, along with high cutting forces. This combination of high temperature and high forces is likely to lead to smearing of the surface rather than cutting.



(a) Sharp. $R_a = 0.68\ \mu\text{m}$. (b) Worn. $R_a = 0.804\ \mu\text{m}$. (c) Highly worn. R_a unmeasurable.

Figure 5.16: SEM images showing effect of varying tool sharpness. Arrows show direction of cut.

5.6.2 Varying tool rake angle

SEM images of machined surfaces for each rake angle, using sharp tooling, are shown in figure 5.17. For all four rake angles studied the SEM images for sharp tools show a surface which appears free of major defects. It can be seen that the profile of the neutral and positive rake angles reflects the profile of the cutting edge of the tool used in machining. The variations in the edge are a result of the grinding process used to manufacture these tools. The negative rake angle does not appear to have the same sharpness of lines in the direction of cut, which is likely a feature of the continuous - shear chip formation mechanism occurring for this cut, whereas for the other rake angles the chip formation mechanism was continuous - flow*. The surface roughness results for these surfaces do not show a clear trend, with all four having $R_a < 1 \mu m$. It appears likely that for smooth cuts where the continuous - flow* chip formation mechanism is occurring that the R_a value measured perpendicular to the direction of cut is a function of the profile of the tool rather than the machining parameters.

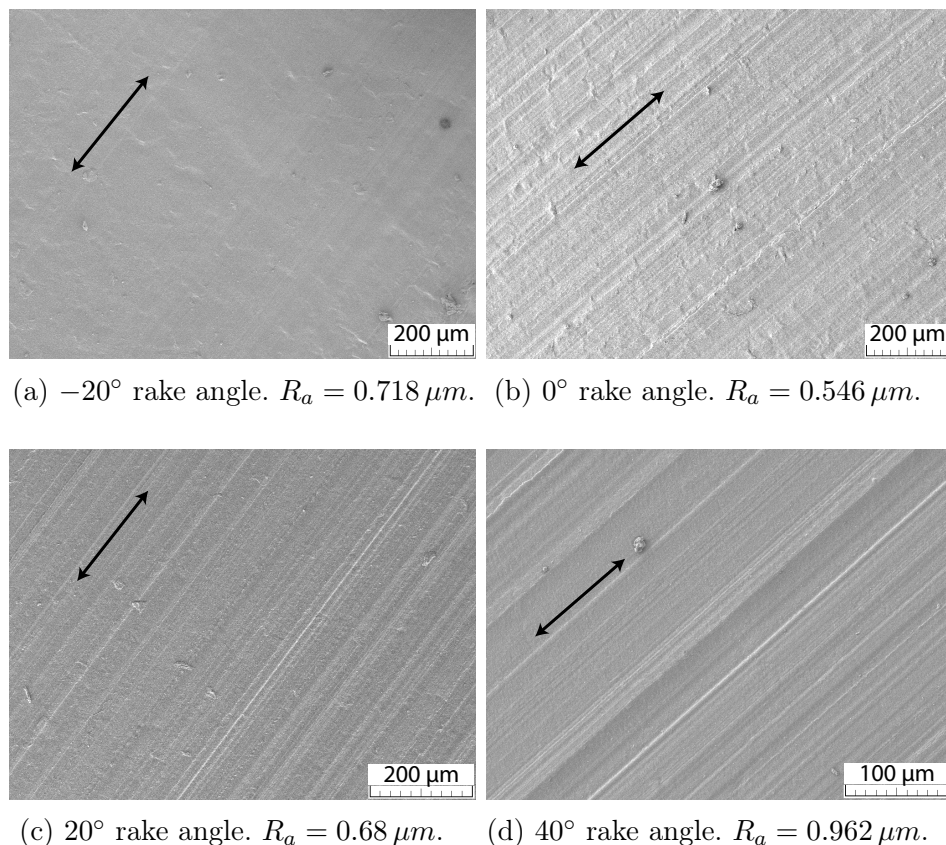


Figure 5.17: SEM images showing effect of varying tool rake angle. Arrows show direction of cut.

5.7 Discussion

In this chapter an investigation into the effect of tool sharpness, rake angle and machining parameters on the machining of three varieties of UHMWPE was carried out. A statistical analysis was then performed on the results. It was found that at low depths of cut with worn tools the area of engagement between the tool and workpiece will present a negative effective rake angle to the workpiece, as discussed in section 2.3.1. Negative rake angles deliver higher forces, temperature, surface roughness and chip thickness than neutral or positive rake angles. The chip thickness result for negative rake angle tools indicates that chip formation is of the continuous - shear type, while the continuous - flow* chip formation mechanism occurs at positive rake angles. This change in chip formation mechanism may account for the increased forces, temperature and surface roughness, since the material is undergoing different yield behaviour. Cutting speed was found to be the least significant factor for all responses, out of the five factors examined. This leads to the hypothesis that the stiffening effect of a higher strain rate and the softening effect of higher frictional heating may offset each other, within the parameters used. Further investigation is warranted to ascertain the effect of cutting speed. The models for cutting force, thrust force, surface roughness and chip thickness displayed high R^2 values, indicating that almost all of the variation in the responses is explained by the factors used in the analysis.

The high thermal inertia displayed by the thermocouple-tool system does not allow accurate measurement of cutting temperature outside of a steady-state cutting condition, which is difficult to maintain. Despite these limitations, the temperature results detailed in this chapter do provide a useful lower bound on cutting temperature, and have demonstrated that in some extreme cutting situations the tool temperature exceeds the melting temperature of UHMWPE.

With regard to surface roughness, there is a large two way interaction between tool rake angle and edge radius. This can be important for tool life analyses, as a larger rake angle will deliver acceptable surface roughness for longer. Conversely, using a negative rake angle and/or allowing the tool to blunt excessively will lead to very poor surface finish. This poor surface finish is a result of the effective rake angle of the part being less than the nominal rake angle as edge radius increases. Inspection of machined surfaces showed that highly worn tools produced very poor surface quality. The surface quality achieved in favourable cutting conditions was comparable to that observed in past work on HDPE [107, 162], while worn tools showed some smearing. This is evident from the surface roughness results.

Workpiece deformation around the cutting edge increases dramatically as edge

radius increases. This causes an increase in force on the tool, particularly the thrust force. This increase in thrust force indicates that the tool is compressing the workpiece as it cuts, which for a viscoelastic material such as polyethylene may lead to issues with workpiece relaxation. This can cause problems with dimensional accuracy in a manufacturing environment. Further work is required to completely characterise the effect of compressive cutting forces on polymer relaxation.

FUNDAMENTAL INVESTIGATION INTO ORTHOGONAL CUTTING OF UHMWPE

Chapter 6

Cryogenic cooling of UHMWPE for machining operations

6.1 Background and methodology for characterisation of cryogenic cooling of UHMWPE for machining operations

This chapter investigates the effect of cooling the workpiece prior to machining using liquid nitrogen (known as workpiece pre-cooling) on the machining of UHMWPE. It was established in chapter 4 that lower temperatures will cause the material to appear stiffer and less viscous, while chapter 5 has shown that it is possible to achieve good machining at room temperature for certain tool and machining parameter combinations. Therefore it should be possible to achieve improvements in machinability from those seen at room temperature, through the pre-cooling of the workpiece. Plain UHMWPE workpieces are to be cooled through submersion in liquid nitrogen before machining, with the same experimental setup as used in chapter 5 used otherwise. The Design of Experiments parameters to be used are shown in table 6.1.

Table 6.1: Factors used in design of experiments.

| Factor | Number of levels | Levels |
|-------------------------------|-------------------------|---|
| Rake angle | 4 | -20° , 0° , 20° , 40° |
| Initial workpiece temperature | 2 | Cold (100 - 150 K), Room (295 - 300 K) |
| Edge radius | 3 | Sharp, worn, highly worn |
| Cutting speed | 2 | 155, 300 <i>m/min</i> |
| Depth of cut | 2 | 0.06, 0.19 <i>mm/rev</i> |

6.2 Machining forces

6.2.1 Cutting force

The main effects plot for cutting force is shown in figure 6.1. All main effects for other than cutting speed appear to be statistically significant, with similar trends seen for rake angle, sharpness, cutting speed and depth of cut as those observed in chapter 5. The lower level of workpiece temperature is shown to deliver higher cutting forces, indicating that the material is stiffer when cooled.

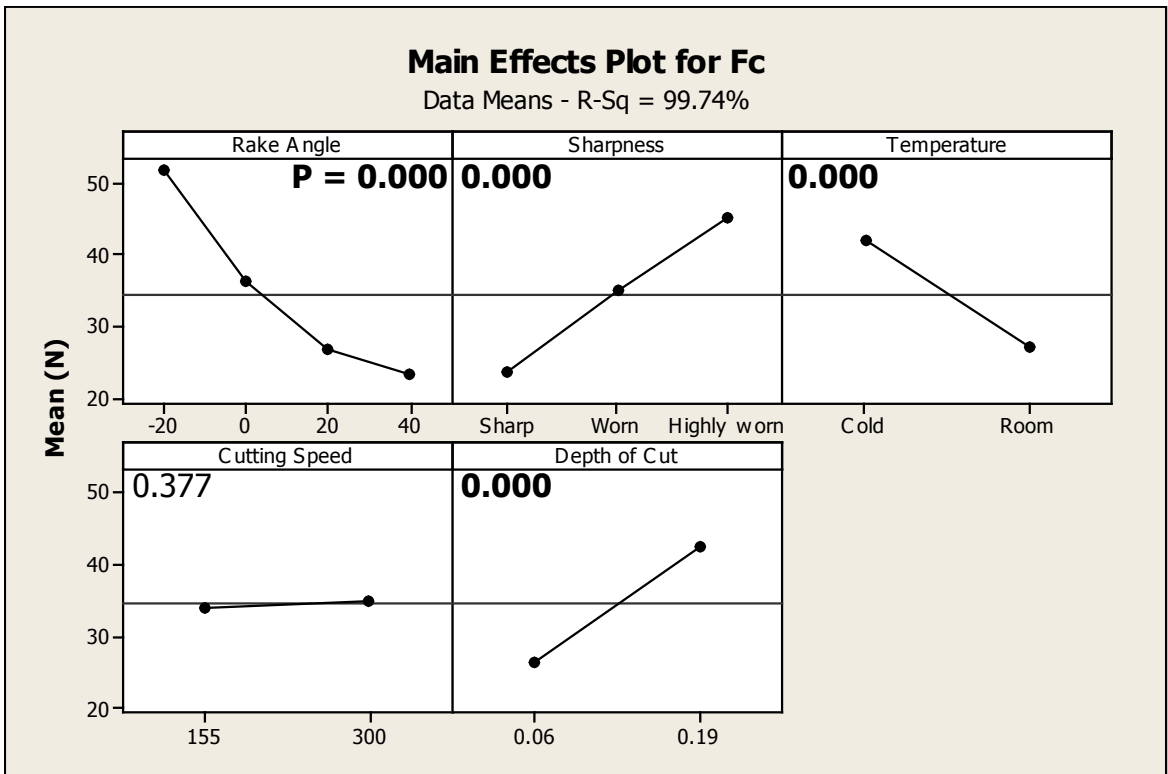


Figure 6.1: Main effects plot for cutting force for plain UHMWPE, including cryogenically cooled workpieces. Numbers shown within each box are P values from ANOVA, with P values for statistically significant main effects shown in bold.

The interactions plot for cutting force is shown in figure 6.2. Of the two way interactions, those between rake angle - sharpness, rake angle - temperature, rake angle - depth of cut, sharpness - temperature and temperature - depth of cut appear statistically significant. The rake angle - sharpness and rake angle - depth of cut interactions were also observed for room temperature machining, in chapter 5, and are a result of the size effect. The interactions involving temperature consistently show higher cutting force at the lower workpiece temperature, again showing increased stiffness at low temperatures.

No two way or higher order interactions involving cutting speed appear significant, which points to cutting speed having an overall weak effect on cutting force. This is

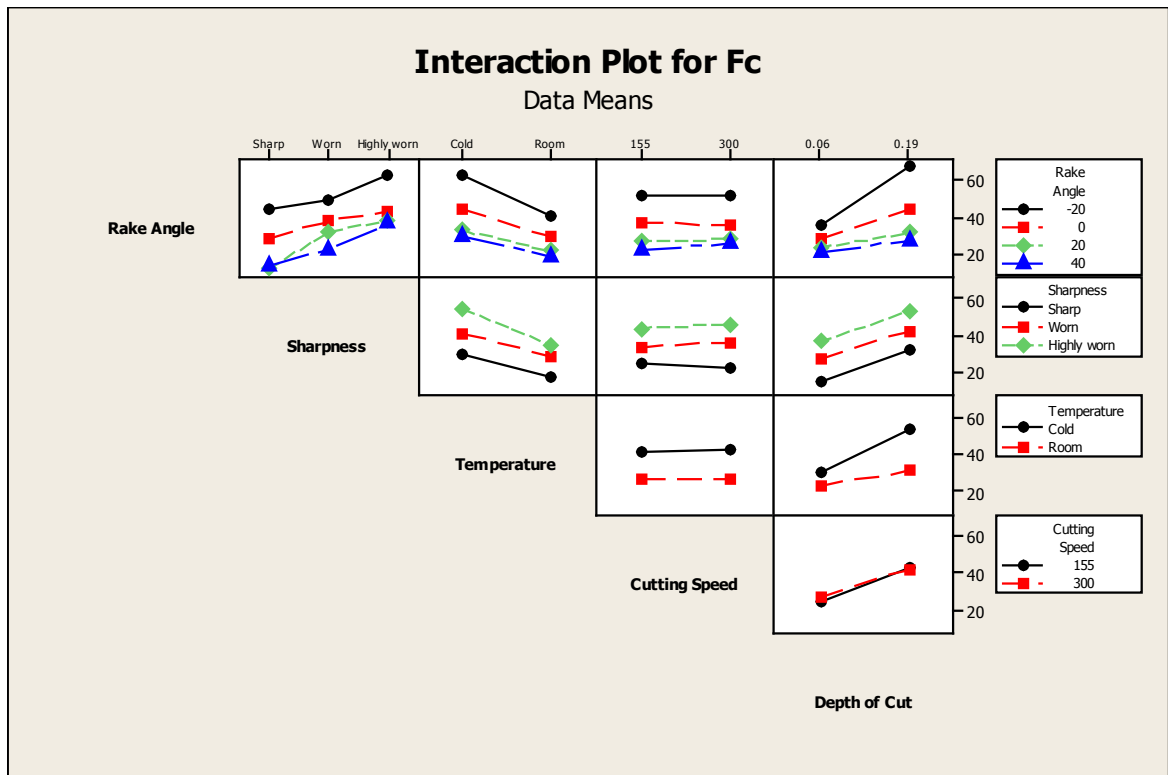


Figure 6.2: Interactions plot for cutting force for plain UHMWPE, including cryogenically cooled workpieces.

consistent with the results shown in chapter 5. Amongst higher order interactions, only rake angle - temperature - depth of cut appears significant ($P = 0.017$), showing that the influence of the size effect upon cutting force is also dependent upon the workpiece temperature.

6.2.2 Thrust force

The main effects plot for thrust force is shown in figure 6.3. Rake angle, sharpness and temperature appear statistically significant, whereas cutting speed and depth of cut do not. This is in contrast to the results at room temperature only, where cutting speed and depth of cut were statistically significant. The trends for rake angle and sharpness show similar trends to those observed in chapter 5.

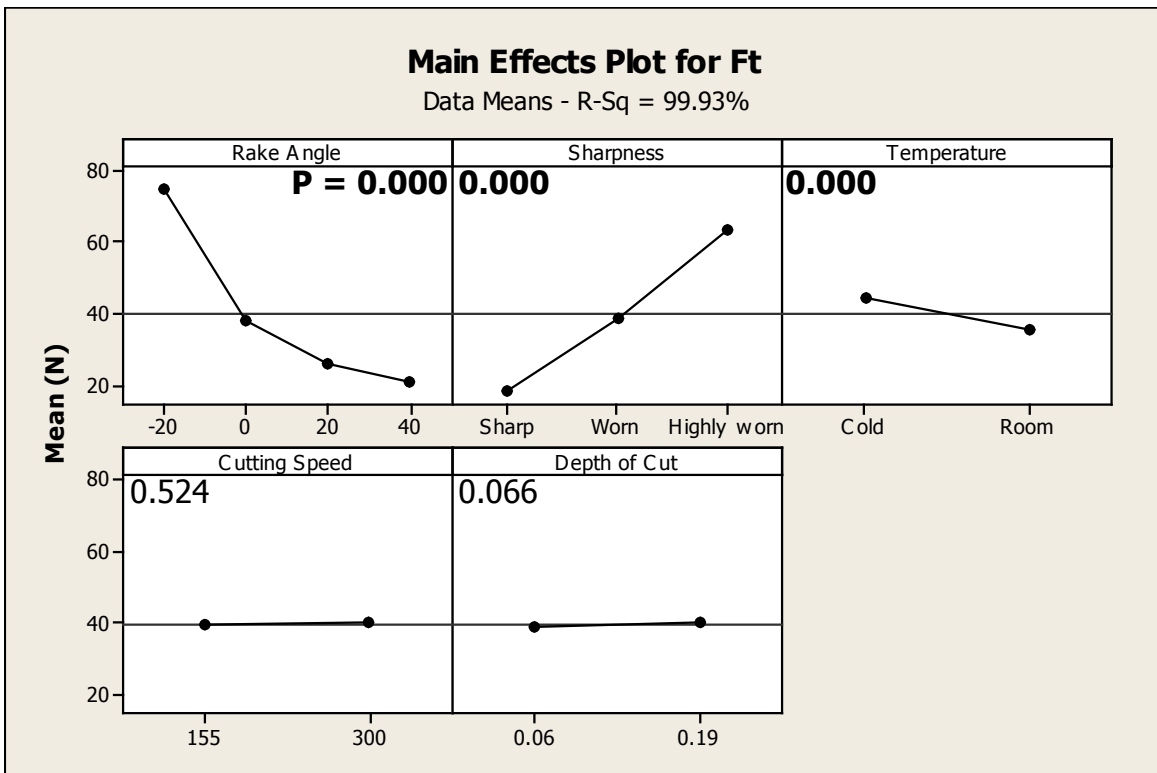


Figure 6.3: Main effects plot for thrust force for plain UHMWPE, including cryogenically cooled workpieces.

The interactions plot for thrust force is shown in figure 6.4. Of the two way interactions, rake angle - sharpness, rake angle - temperature, rake angle - depth of cut, sharpness - temperature, sharpness - cutting speed, sharpness - depth of cut and temperature - depth of cut appear statistically significant. Of the higher order interactions, rake angle - sharpness - temperature, rake angle - sharpness - cutting speed, rake angle - sharpness - depth of cut, rake angle - temperature - depth of cut and sharpness - temperature - cutting speed appear significant, while the four way interaction of rake angle - sharpness - temperature - cutting speed is close to the threshold for significance ($P = 0.052$).

All of the significant two way interactions which do not include workpiece temperature were also significant in the same analysis in chapter 5. The interactions of

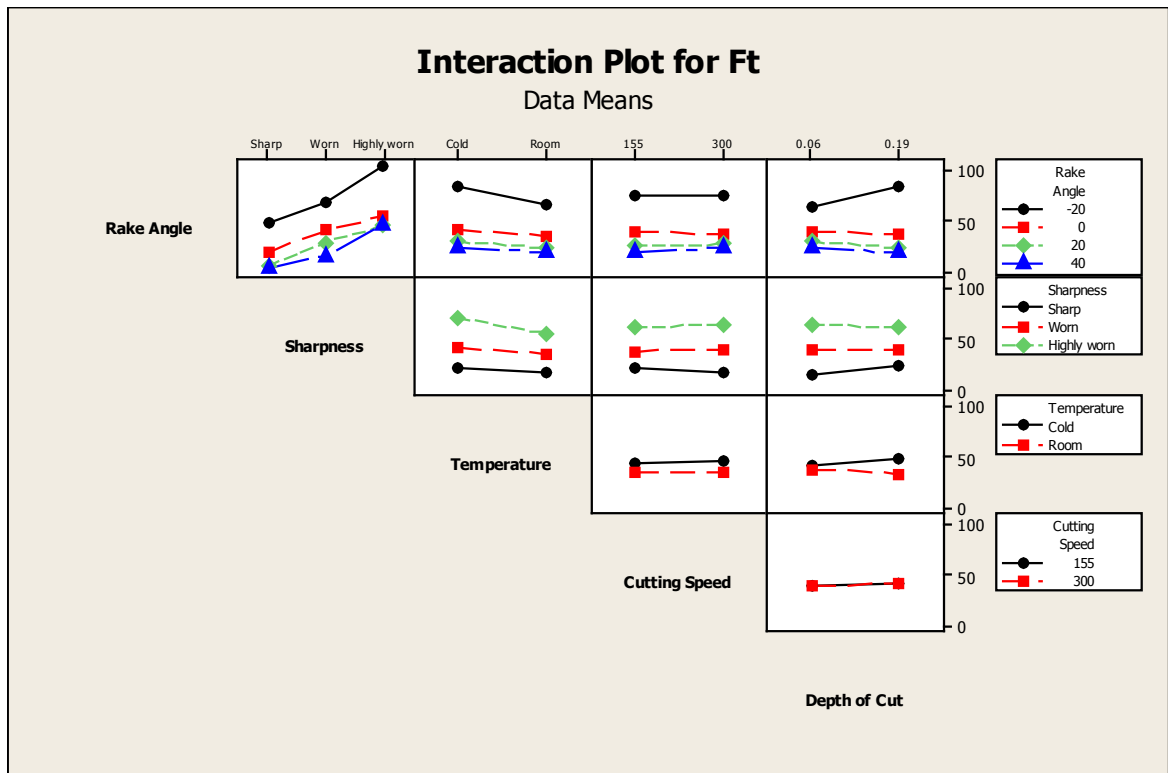


Figure 6.4: Interactions plot for thrust force for plain UHMWPE, including cryogenically cooled workpieces.

temperature with rake angle, sharpness and depth of cut can be seen in figure 6.4, where it is evident that cryogenically pre-cooled workpieces have higher levels of thrust force for negative rake angles and highly worn tools, while the temperature - depth of cut interaction shows that at the higher depth of cut the lower value of workpiece temperature will deliver slightly higher forces, in contrast to the room temperature level where lower forces will occur. These offsetting trends are the likely cause of the lack of significance of the cutting speed and depth of cut main effects, despite many of the significant interactions including these terms.

6.3 Tool temperature

The main effects plot for tool temperature is shown in figure 6.5. As before, due to the thermal inertia of the tool-thermocouple system, there is a large dependence of the tool temperature on the duration of the cut. The duration of the cut is a function of cutting speed and depth of cut. Additionally, shorter duration cuts were taken for cryogenically pre-cooled workpieces to minimise heating from machining. Therefore, the full statistical analysis of peak temperature is of limited utility. Full details of the statistical analysis can be found in appendix C. Despite this, the main effects plot can provide useful information on factors which do not directly influence the duration of the cut, in this case the tool rake angle and sharpness. It can be seen that tool temperature decreases with increasing rake angle, and increases with tool sharpness. The drop in temperature at highly worn compared to worn that was seen in chapter 5 is not seen here, potentially indicating that AOX and XLK may have different behaviour when using highly worn tools than UHMWPE.

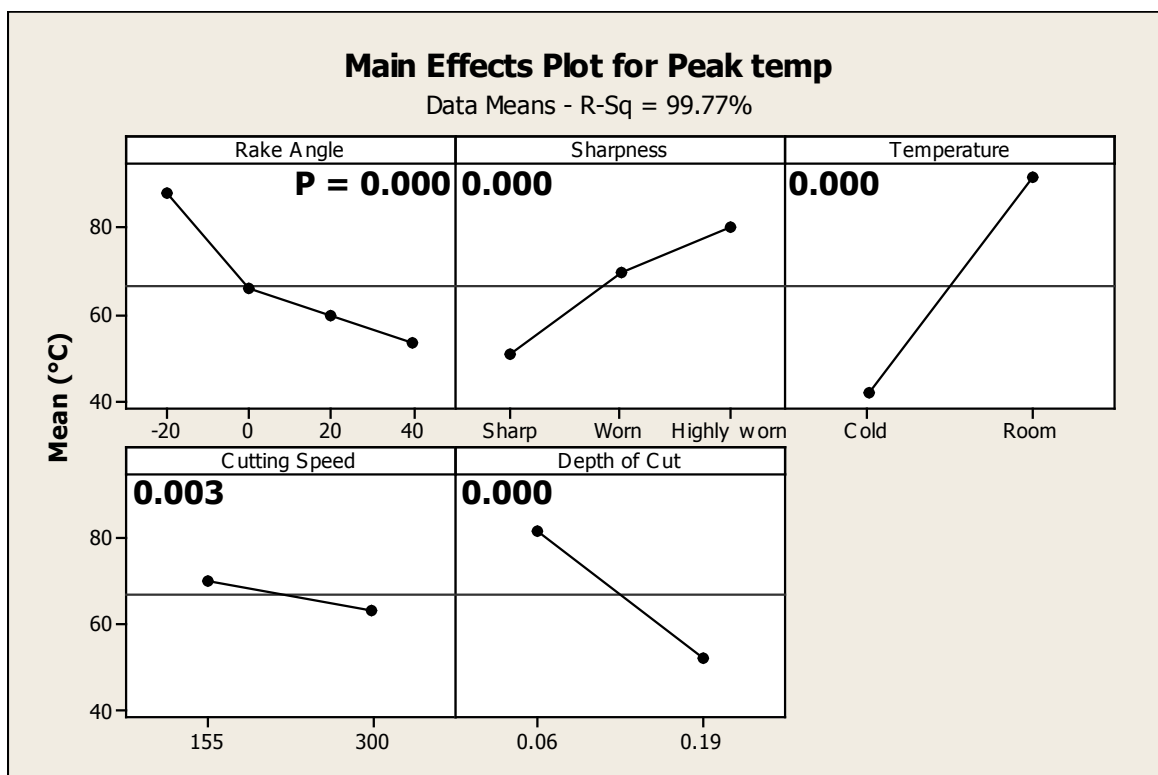


Figure 6.5: Main effects plot for peak temperature for plain UHMWPE, including cryogenically cooled workpieces.

In order to ascertain the effect of workpiece temperature it is necessary to compare experimental data directly. Sample temperature data for room temperature and cryogenically pre-cooled workpieces for the same cutting and tooling parameters are

shown in figure 6.6. Approximately one second of lag due to thermal inertia is evident in both signals, with the onset of machining being evaluated from force data recorded using common timestamping. The longer duration of the room temperature cut causes a higher peak temperature, but it is evident from the slope of the curve for the cryogenically pre-cooled sample that for similar cut durations the cryogenically pre-cooled sample would have reached a higher peak temperature. This is likely a result of the increased material stiffness when cooled, as was observed from DMA results in chapter 4. As will be shown in section 6.4.6, the same chip formation mechanism was observed for both workpiece temperatures, so the difference in heat flux is purely a result of changes in material properties due to temperature. Also of interest in this plot is the slight dip in tool temperature for the cryogenically pre-cooled workpiece at the onset of machining, caused by the tool being in proximity with the cooled workpiece, which was cooling the surrounding air through natural convection, and thus cooling the tool. The subsequent rise in tool temperature as machining occurs shows that heat generation due to machining causes a thermal barrier which prevents any further cooling of the tool by the workpiece.

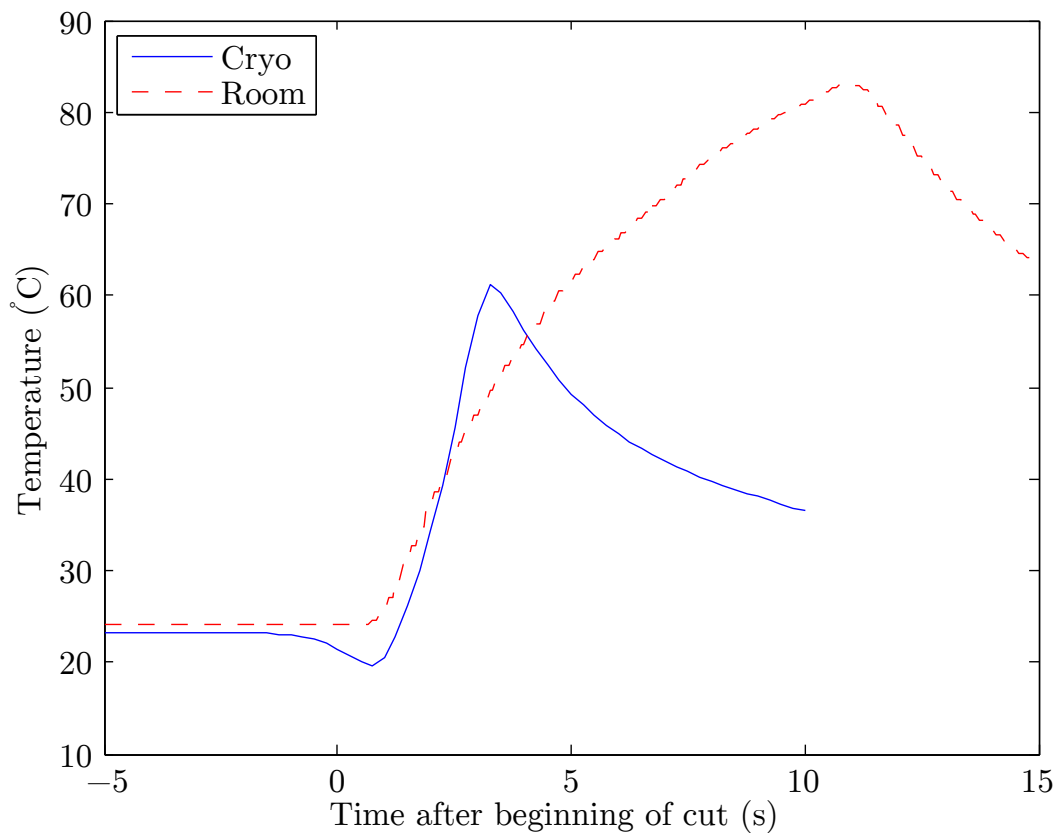
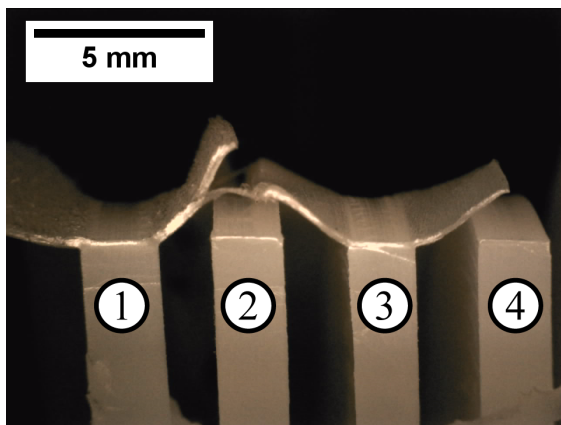


Figure 6.6: Difference in tool temperature data for machining of cryogenically pre-cooled workpieces. Samples machined using 0° rake angle, sharp tool, low cutting speed, low depth of cut. Cut commenced at 0 seconds for both data sets.

6.4 Machined surface analysis

6.4.1 Microscopy

It was found that in many cases where a discontinuous chip was formed that the material had flowed axially, to either side of the tool, forming “wings” on either side of the machined surface. As the tool width exceeded the width of the discs being machined (3.6 mm and 2.2 mm respectively) this phenomenon is a result of workpiece deformation to the sides of the tool. This deformation is seen in cases where large thrust forces have compressed the workpiece during the cut. Figure 6.7 shows a sectioned view of a workpiece where this occurred. The operations in which this was observed are marked by asterisked entries in table 6.2 on page 107.



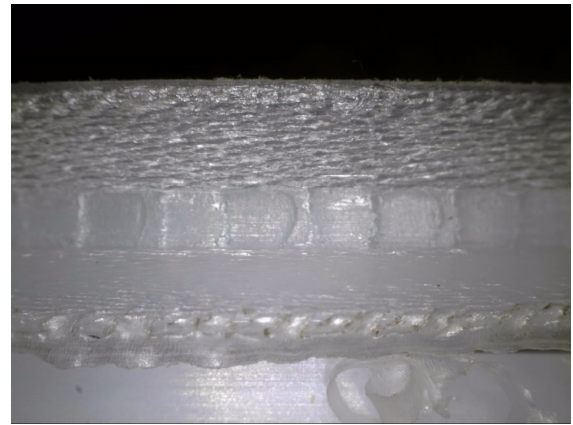
| | Cutting Speed | Depth of cut |
|---|---------------|--------------|
| 1 | Low | Low |
| 2 | Low | High |
| 3 | High | Low |
| 4 | High | High |

Figure 6.7: Sectioned view of workpiece, showing material flow at low depths of cut due to high thrust force. Tests performed with a cooled workpiece, 0° rake angle, worn tool. Each disc is of width 2.2 mm, with the remaining material on 1 being approximately 0.45mm thickness, and on 3 being approximately 0.25 mm thickness.

Optical microscope images of two machined samples are shown in figure 6.8, with the sharp tool showing good surface quality and no workpiece deformation from cutting being evident. This is in contrast to the sharp tool, where a large amount of deformation is evident in the form of “wings” which flowed to either side of the tool during machining, indicating large levels of workpiece deformation. The sides of these deformed strips of material show a textured surface, while the machined surface shows a regular pattern of ridges or steps perpendicular to the direction of the cut. Due to the direction of these features is it unlikely that a conventional surface roughness test carried out perpendicular to the direction of cutting would detect their presence.



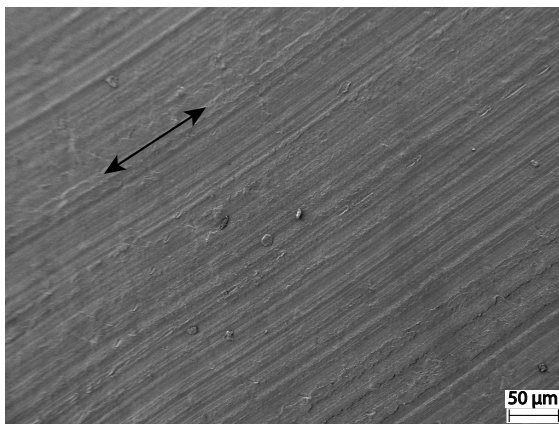
(a) Sharp tool, showing smooth surface and no deformation



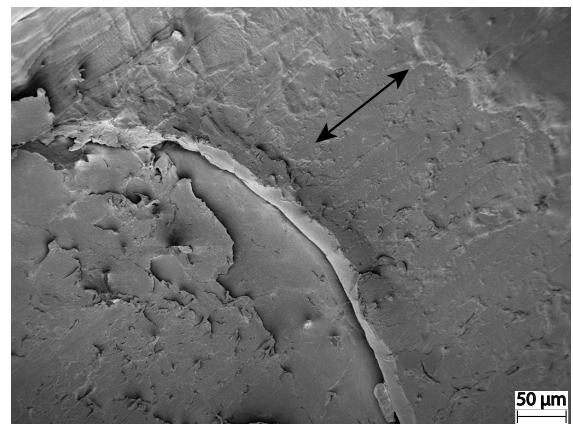
(b) Highly worn tool, showing “wings” on either side of the machined surface

Figure 6.8: Optical microscope images of machined surface, showing variation in the appearance of the machined surface. Samples shown were machined using a 0° rake angle tool, cooled workpiece, low cutting speed and low depth of cut. The direction of cut is from right to left.

Scanning electron microscope images of the same surfaces are shown in figure 6.9. Figure 6.9a shows a smooth surface, with the only major feature being the lines in the direction of cut, reflecting the profile of the tool used to machine the surface. These features are not present in figure 6.9b, which shows a major feature in the form of a large ridge, on both sides of which there is significant smearing of the material. As before, the surface machined with a highly worn tool has features which would not be detected by a surface roughness profile measured perpendicular to the direction of the cut.



(a) Sharp tool



(b) Highly worn tool

Figure 6.9: Scanning electron microscope images of machined surface, showing variation in surface morphology. Samples shown correspond to those illustrated in figure 6.8. Arrows show direction of cut.

Profilometer data measured parallel to the direction of the cut are shown in figure 6.10. It can be seen that the ridges visible in figure 6.8b and shown in more detail in figure 6.9b are reflected in the profilometer data shown in figure 6.10b, with a profilometer RMS value of $35.6 \mu m$. In contrast, the smooth surface seen in figure 6.9a only shows a small amount of runout in figure 6.10a, with a peak to peak runout value of approximately $10 \mu m$, and a corresponding RMS value of approximately $1.6 \mu m$. It is clear that profilometer data measured parallel to the direction of the cut is capable of showing some surface features which would be otherwise difficult to detect. Machined surface profiles which display this regular pattern of cracking, similar to figure 6.10b, will be referred to as displaying “crack-type” features.

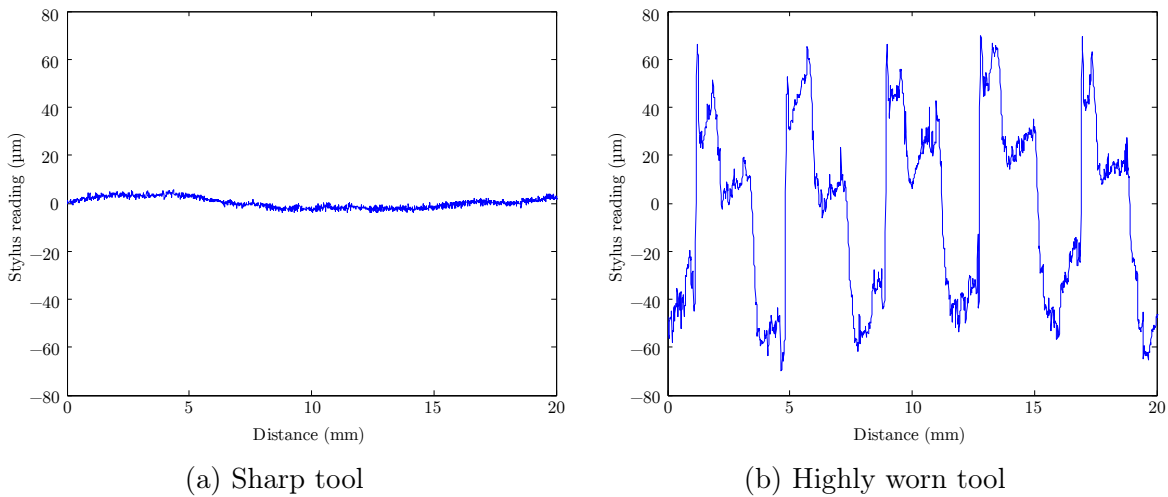


Figure 6.10: Surface profile of machined surfaces, showing peaks and valleys in highly worn example. Samples shown correspond to those illustrated in figure 6.8. Cutting direction is left to right.

6.4.2 Chip thickness

The main effects plot for chip thickness is shown in figure 6.11. The effect of rake angle is similar to that seen in chapter 5, with the negative rake angle having a far higher value of chip thickness than the neutral and positive rake angles. In chapter 5 it was seen that this difference in chip thickness pointed to a change in chip formation mechanism at the negative rake angle. Cutting speed and depth of cut do not appear statistically significant, as was the case for room temperature workpieces. Temperature has a large effect, with pre-cooled workpieces showing a mean close to zero, potentially indicating that the change in chip formation mechanism observed in room temperature workpieces with negative rake angles may not occur for cryogenically pre-cooled workpieces.

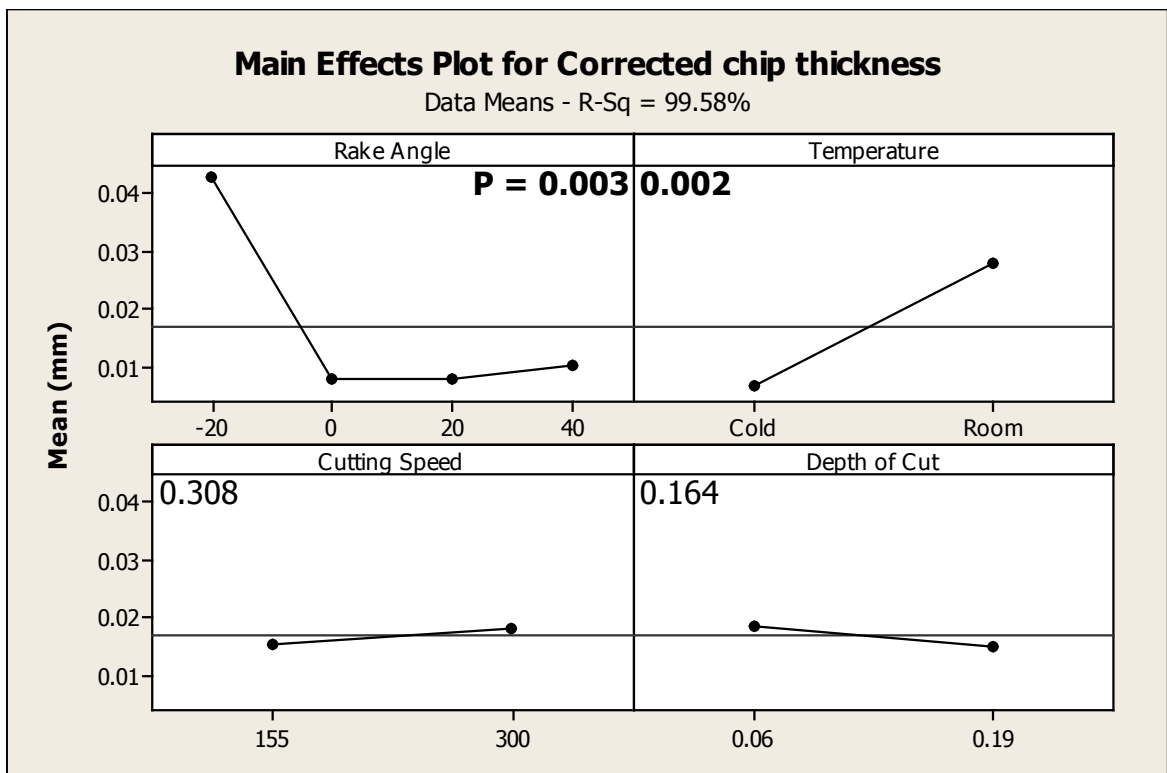


Figure 6.11: Main effects plot for cut chip thickness for plain UHMWPE, including cryogenically cooled workpieces.

The interactions plot for chip thickness is shown in figure 6.12. Only rake angle - temperature appears statistically significant, with rake angle - depth of cut ($P = 0.067$) and temperature - depth of cut ($P = 0.055$) being close to the threshold for statistical significance. Inspection of the interaction plot for these factors shows that for pre-cooled workpieces all rake angles show results close to zero, which is distinct from the room temperature results seen previously, where the negative rake angle showed a larger chip thickness value than the uncut chip thickness, which was caused by a change in chip formation mechanism. Thus it can be concluded that the increase in cut chip thickness seen for negative rake angles observed with room temperature workpieces, corresponding to a change in continuous chip formation mechanism, does not occur when using cryogenically pre-cooled workpieces.

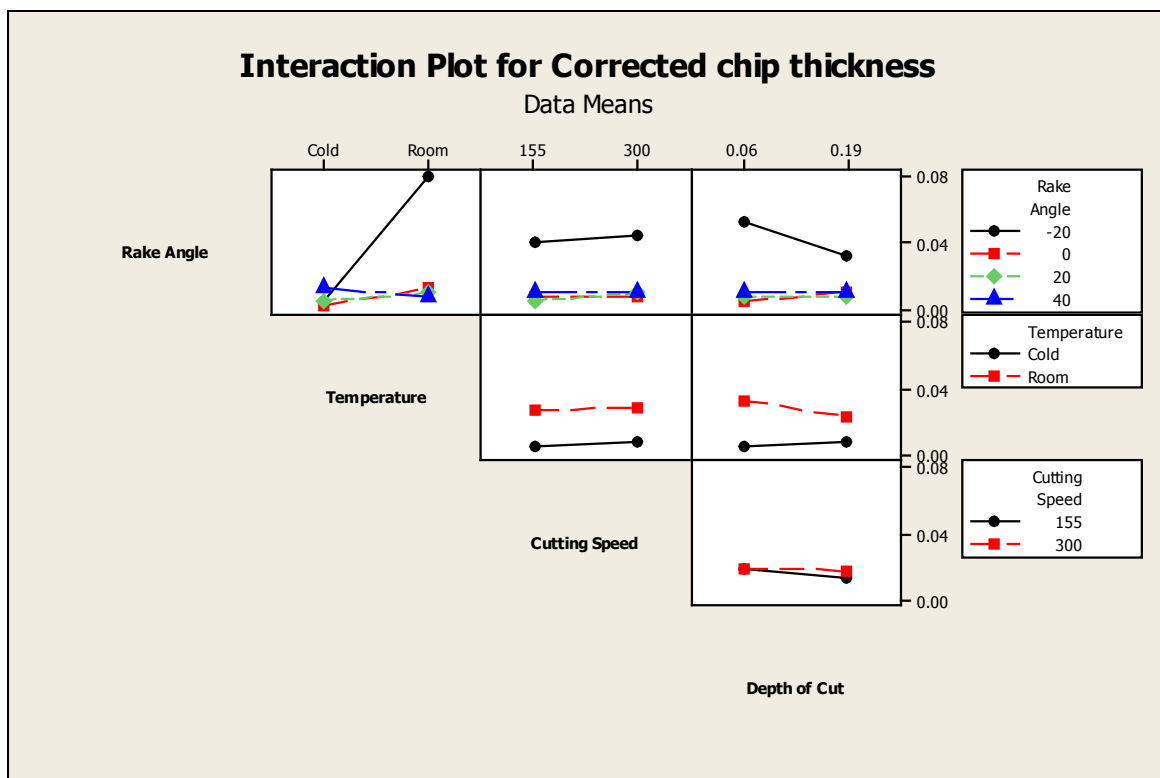


Figure 6.12: Interactions plot for cut chip thickness for plain UHMWPE, including cryogenically cooled workpieces.

6.4.3 Surface roughness

The main effects plot for surface roughness is shown in figure 6.13. As was previously observed for room temperature samples in chapter 5, rake angle, sharpness and depth of cut appear statistically significant, while cutting speed does not. Temperature appears significant, with cryogenically pre-cooled workpieces showing lower readings for surface roughness, pointing to an improvement in surface quality. The complex behaviour of surface roughness with varying rake angle that was observed for room temperature workpieces appears to also occur here.

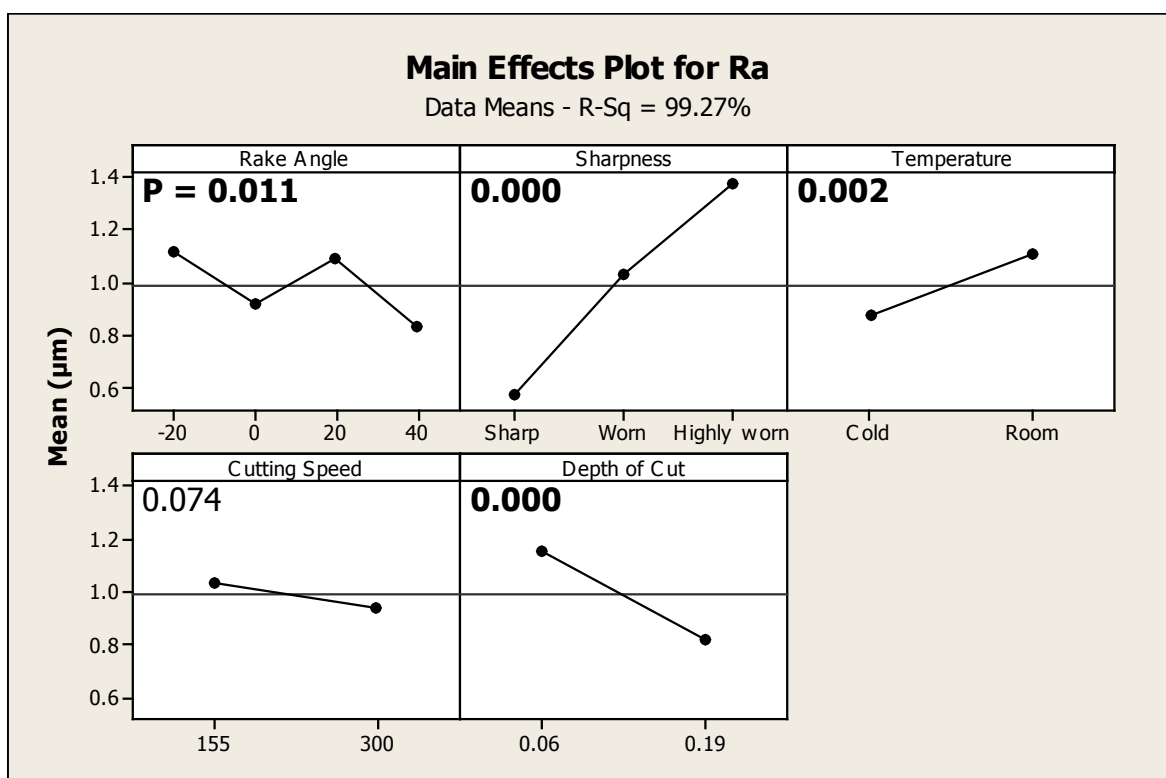


Figure 6.13: Main effects plot for surface roughness for plain UHMWPE, including cryogenically cooled workpieces.

CRYOGENIC COOLING OF UHMWPE FOR MACHINING OPERATIONS

The interactions plot for surface roughness is shown in figure 6.14. Of the two way interactions, rake angle - sharpness and sharpness - depth of cut remain statistically significant, with 5 of the 10 two way interactions, 6 of the 10 three way interactions and 2 of the 5 four way interactions appearing statistically significant. The majority of these interactions involve rake angle, which shows similar behaviour to that seen for room temperature workpieces in chapter 5. Outside of the interactions involving rake angle, temperature also has statistically significant two way interactions with cutting speed and depth of cut, and statistically significant three way interactions with sharpness - depth of cut and cutting speed - depth of cut. While sharpness - temperature - depth of cut may be a manifestation of changes in chip formation mechanism at different workpiece temperatures, the other interactions with cutting speed and depth of cut are unusual, particularly as none of them appeared significant for room temperature workpieces only.

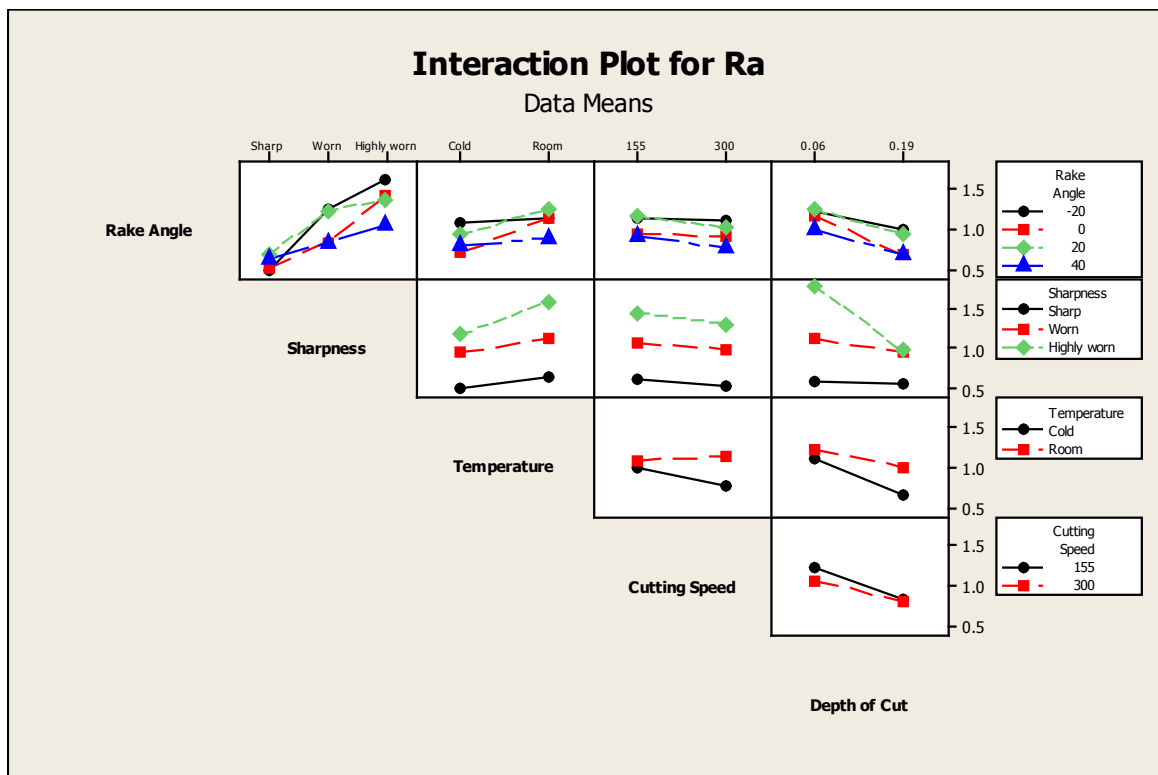


Figure 6.14: Interactions plot for surface roughness for plain UHMWPE, including cryogenically cooled workpieces.

A boxplot of surface roughness, in the form of R_a value, as a function of effective rake angle is shown in figure 6.15. It can be seen that effective rake angle appears to have an inverse relationship with surface roughness. While the median for 20° effective rake is slightly higher than that for 0° , the behaviour seen in the main effects plot is not present. Other metrics of surface quality may be required to ascertain the effects of tooling and workpiece parameters on surface finish.

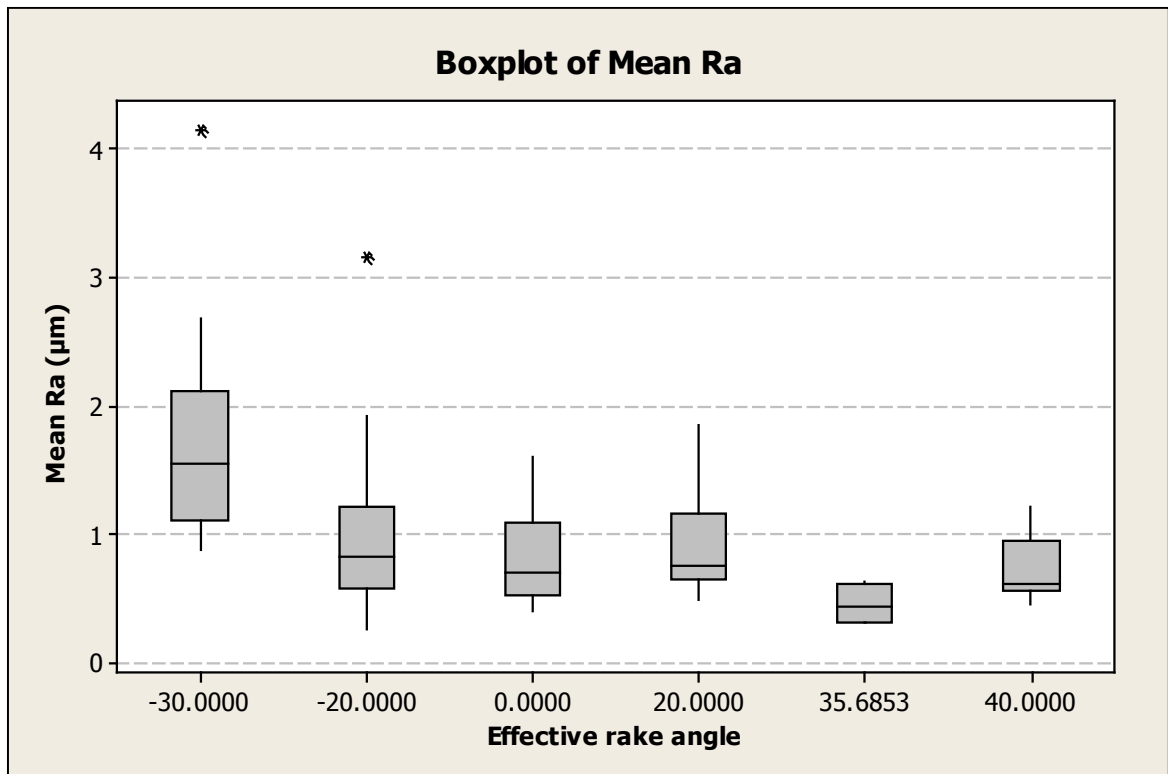


Figure 6.15: Boxplot of mean values of R_a as a function of effective rake angle.

6.4.4 Quantification of surface profile variation

In order to analyse the magnitude of the variation in surface profile in the direction of the cut it is necessary to extract a qualitative feature from the profile data collected. The RMS of the profile data, after filtering to remove runout, will be used for analysis, rather than R_a . This is preferable due to the length of the profile in some cases, and to minimise the level of filtering of the raw signal. A summary of chip type classification and the RMS values from profilometer data is shown in table 6.2 on page 107.

A boxplot of RMS as a function of chip type and observation of cracking on RMS data is shown in figure 6.16. It can be seen that cases where cracking is observed during chip formation have large RMS values, further validating that RMS is an adequate metric for measuring the extent of cracking without conflation of other factors. In cases where cracking is not observed the RMS values are small, regardless of chip type. Where cracking is observed it can be seen that continuous chip types have the lowest mean value of RMS. Situations where only dust is formed have the highest mean value, while discontinuous chip formation mechanisms have more variation, with a maximum of nearly $70 \mu m$. This shows that there is a link between chip type and the magnitude of RMS.

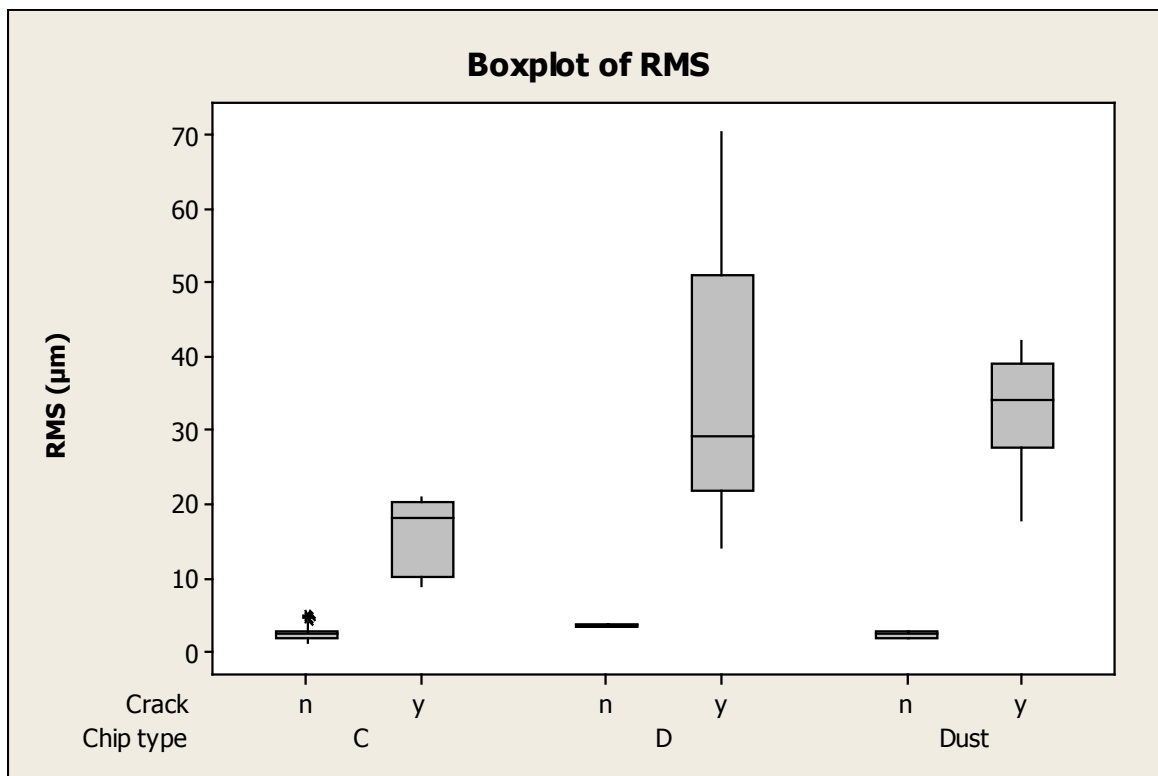


Figure 6.16: Boxplot of RMS as a function of chip type and observation of crack-type chip formation in profilometer output.

Table 6.2: Chip types (left) and associated RMS values for profilometer data (right). Entries in bold highlight differences in chip formation mechanism, workpiece deformation, or surface profile type when transitioning from cold to room temperature workpieces. CS: Cutting Speed. DOC: Depth Of Cut.

| | | CS | 155 | | 300 | | 155 | | 300 | |
|------------|-------------|-------|------------|-----------|------------|-----------|-------------|------|-------------|-------------|
| | | DOC | 0.06 | 0.19 | 0.06 | 0.19 | 0.06 | 0.19 | 0.06 | 0.19 |
| Rake Angle | Sharpness | Temp. | Chip type | | | | RMS value | | | |
| -20 | Sharp | Cold | C* | C | C* | C | <u>19.3</u> | 1.1 | <u>20.9</u> | 1.3 |
| | | Room | C* | C* | C* | C* | <u>20</u> | 2.3 | 1.3 | 1.3 |
| | Worn | Cold | Du* | C* | Du* | C* | 17.7 | 2.7 | 19 | 2.7 |
| | | Room | Du* | C* | D* | C* | 2.7 | 2.7 | 3.4 | 2.7 |
| | Highly worn | Cold | Du* | C* | Du* | C* | 38.5 | 3.3 | 36.9 | 2.7 |
| | | Room | Du* | D* | Du* | D* | 1.8 | 3.7 | 2.4 | 70.3 |
| 0 | Sharp | Cold | C | C | C | C | 1.6 | 1.8 | 1.2 | 1.1 |
| | | Room | C | C | C | C | 2.1 | 2.3 | 1.7 | 1.7 |
| | Worn | Cold | C* | C | C* | C | <u>16.7</u> | 2.1 | 2.3 | 2 |
| | | Room | Du* | C | C* | C | <u>30.5</u> | 4.5 | 3.6 | 1.9 |
| | Highly worn | Cold | Du* | C* | D* | C* | <u>35.6</u> | 2.7 | <u>21.4</u> | 1.6 |
| | | Room | Du* | C* | Du* | C* | <u>31.6</u> | 3 | <u>40.9</u> | 2.4 |
| 20 | Sharp | Cold | C | C | C | C | 2.8 | 1.6 | 1.4 | 1 |
| | | Room | C | C | C | C | 2.7 | 1.9 | 2.2 | 2.1 |
| | Worn | Cold | C | C | C | C | 4 | 2 | 1.9 | 1.1 |
| | | Room | C | C | C | C | 10.6 | 2.9 | 9 | 1.9 |
| | Highly worn | Cold | D* | C | D* | C | <u>31</u> | 1.6 | <u>14</u> | 2.5 |
| | | Room | Du* | C* | Du* | C* | <u>42</u> | 3.3 | <u>32.7</u> | 2.5 |
| 40 | Sharp | Cold | C | C | C | C | 1.9 | 1.9 | 2.4 | 2.3 |
| | | Room | C | C | C | C | 2.7 | 2.6 | 3.3 | 2.7 |
| | Worn | Cold | C | C | C | C | 4.9 | 2.4 | 1.4 | 2.3 |
| | | Room | C | C | C | C | 2.7 | 3 | 3.9 | 3.8 |
| | Highly worn | Cold | D* | C* | D* | C* | <u>27.2</u> | 2.5 | <u>22.9</u> | 2 |
| | | Room | D* | C* | D* | C* | <u>55.7</u> | 2.8 | <u>37</u> | 1.9 |

Chip types

| | |
|----|--|
| C | Continuous chip formed |
| D | Discontinuous chip formed |
| Du | Dust formed |
| * | Workpiece deformation evident during cutting |
| — | Crack-type chip formation evident |

A boxplot illustrating the data presented in table 6.2 is shown in figure 6.17. It can be seen that for rake angles of 0° and above there is an intuitive relationship between sharpness and RMS, with larger edge radii producing larger RMS values, while the sharp level ($r < 15 \mu m$) delivers consistently low RMS values. The effect of temperature is also evident, with cold workpieces having lower values of RMS. It can also be seen that the worn tools at 20° and 40° produce lower values of RMS than 0°, indicating that higher rake angles are more accommodating of increases in tool edge radius, which is in line with previous observations from chapter 5 on the interaction between edge radius and rake angle for surface roughness measured perpendicular to the cutting direction, and indicates that RMS is sensitive to the effective rake angle.

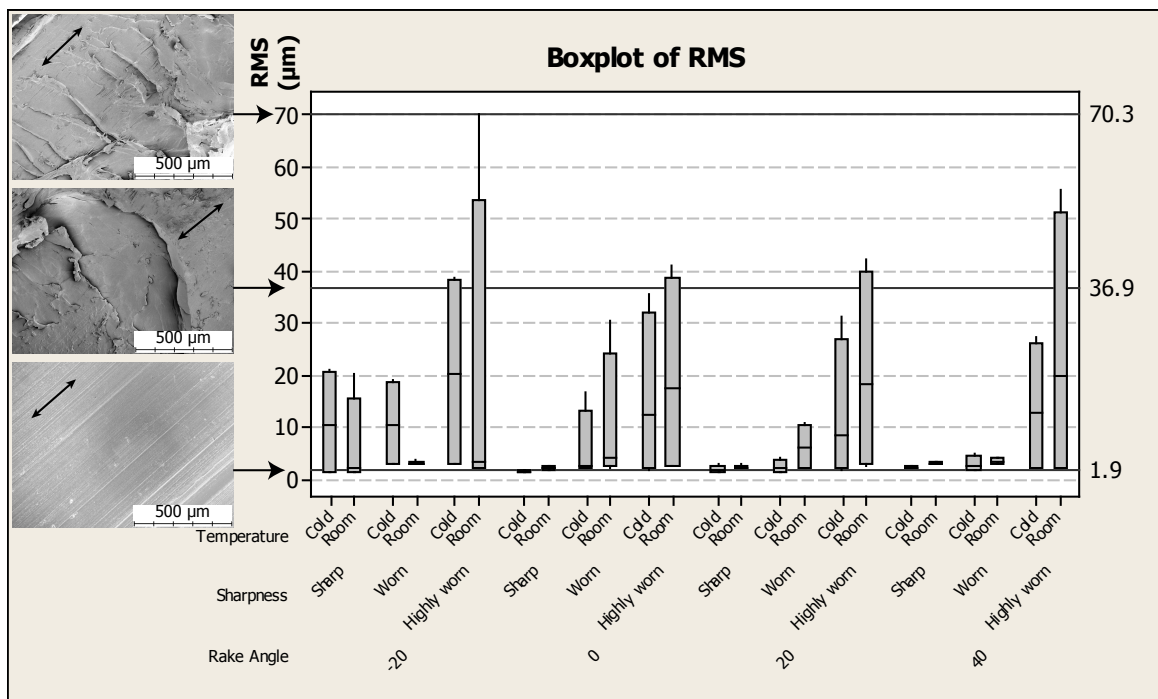


Figure 6.17: Boxplot of RMS as a function of rake angle, sharpness and temperature. SEM images of typical surface topologies and associated RMS values shown at left.

Figure 6.18 displays this relationship. It can be seen that for positive effective rake angles the maximum value of RMS observed is approximately $6 \mu m$, while an effective rake angle of 0° shows a low mean but several outliers of up to $40 \mu m$, while the negative effective rake angles show large increases in RMS, with the -30° effective rake angle having a mean value of over $30 \mu m$.

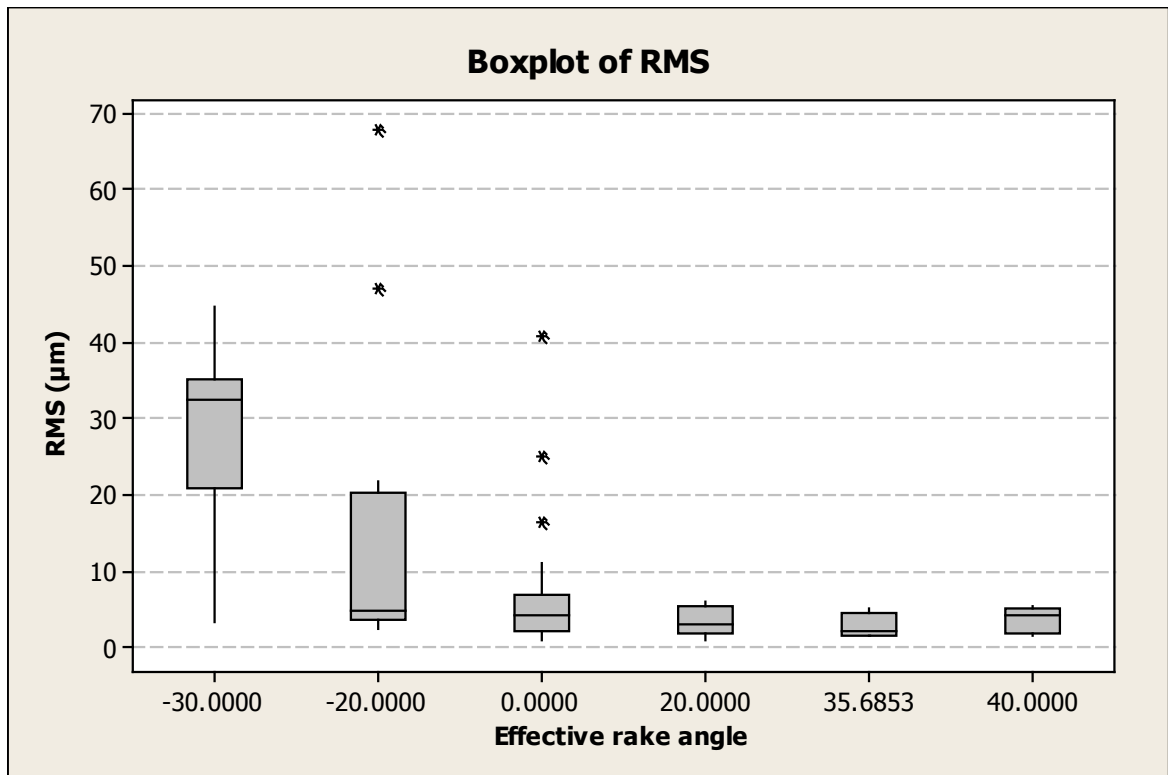


Figure 6.18: Boxplot of RMS plotted as a function of effective rake angle.

While the results for neutral and positive rake angles display clear trends, the results for the -20° rake angle show distinctly different behaviour, with cold workpieces having higher RMS mean values than room temperature workpieces, and sharp tools having similar means to worn tools. Performing Analysis of Variance (ANOVA) on this data set shows eight unusual observations - data points which lie sufficiently far from the predicted value to call the accuracy of the statistical model into question - with all eight occurring for highly worn tools with -20° rake angle. Inspection of table 6.2 shows that there is a RMS value of $70.3 \mu\text{m}$ for highly worn, room temperature, 300 m/min cutting speed and 0.19 mm/rev depth of cut. This is the single highest value of RMS and is an extreme outlier. This point is also the only observed example of crack-type chip formation occurring at the higher depth of cut.

SEM and profilometer data for this outlier point are shown in figure 6.19. It can be seen that the profilometer data does not show a regular pattern, while the SEM image shows what appears to be folding or smearing of the material. It appears that instead of material cutting and associated chip formation the material has been smeared or deformed to the point of spalling. This may be a result of the combination of aggressive cutting conditions and a highly worn tool with negative rake angle, which is an extreme combination of parameters which is unlikely to be considered for use in production.

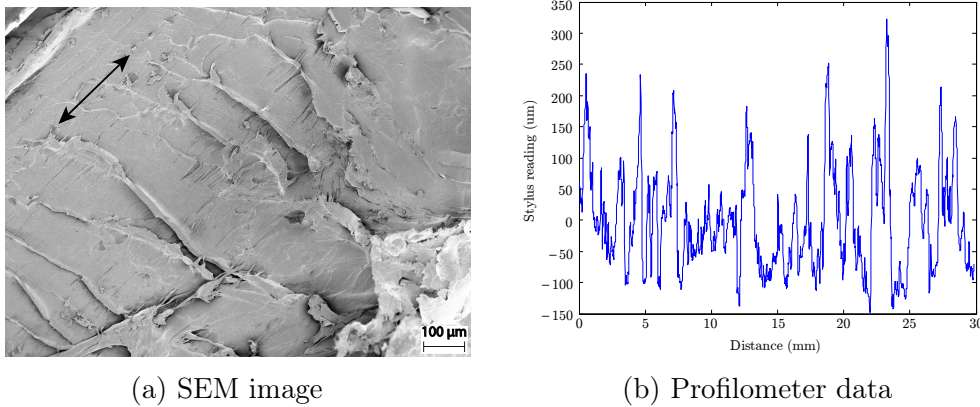


Figure 6.19: Surface topography and profilometer data, for outlier point. Machined using -20° rake angle, highly worn tool, room temperature, high cutting speed, high depth of cut.

The effect of modifying this outlier to bring it into line with the trends shown in the data, and of subsetting the dataset to assess the effect of this outlier on variation within an ANOVA model, are shown in table 6.3.

Table 6.3: Summary of ANOVA tables for RMS, showing effect of subsetting data on model R-Sq, and P values for the main effects. Values highlighted in bold are statistically significant at a 5% significance level.

| | All | No outlier | No negative rake | No highly worn | No negative rake or highly worn |
|-----------------------------|--------------|--------------|------------------|----------------|---------------------------------|
| R-Sq | 98.03% | 99.23% | 99.2% | 98.89% | 99.43% |
| Unusual observations | 8 | 0 | 0 | 0 | 0 |
| P values: | | | | | |
| Rake angle | 0.325 | 0.564 | 0.56 | 0.051 | 0.136 |
| Sharpness | 0.001 | 0 | 0.001 | 0.086 | 0.027 |
| Temperature | 0.319 | 0.715 | 0.029 | 0.799 | 0.075 |
| Cutting speed | 0.44 | 0.022 | 0.05 | 0.058 | 0.048 |
| Depth of cut | 0 | 0 | 0 | 0.007 | 0.034 |

It can be seen that modification of this outlier removes all unusual observations, and causes cutting speed to become statistically significant. In addition, the P value for rake angle increases, showing that the outlier point was causing rake angle to appear more significant than it truly is. The only situation where rake angle comes close to statistical significance ($P = 0.051$) is when highly worn results are omitted, but it has been seen that negative rake angle data trends do not match those seen for neutral and positive rake angles, and thus models which omit negative rake angle are more likely to display the true sources of variation. This is supported by sharpness becoming statistically significant when the negative rake angle data are removed from the model, as from the earlier boxplot it is clear that the variation in RMS is a function of sharpness. Temperature appears to be significant only when negative rake angle data are omitted, while cutting speed is significant or close to significance for all situations where the outlier point is removed or modified. Depth of cut is significant for all models. All five models display R-Sq values greater than 98%. The significance of four out of five factors in the model with no negative rake (compared to two for the original model) and increase in R-Sq is a clear indicator that the negative rake angle data follow different trends to that of neutral and positive rake angles.

with greater frequency at the worn and highly worn levels. Also of interest is the P-value of 1 for cutting speed-deformation, which indicates that deformation is completely independent of the level of cutting speed, which can be verified by inspection of table 6.2.

It was not possible to perform Chi-square analysis on effective rake angle and chip formation mechanism, either as a function of the other or of other factors. This was due to low expected counts for chip formation mechanism and effective rake angle, as the Chi-square distribution is not valid for expected counts below five in each cell [173].

6.4.6 Determination of chip formation mechanism

It has been shown in sections 5.5.2 and 6.4.2 that for continuous chips the chip form may be classified as continuous - flow* or continuous - shear based on chip thickness, with a chip thickness greater than the uncut chip thickness/depth of cut indicating that the chip formation mechanism is continuous - shear. A link between profilometer RMS and cracking as a feature of the chip formation mechanism has been shown, identifying discontinuous chip formation mechanisms where cracking occurs as discontinuous - complex (shear with crack).

For the five cases where discontinuous chips are formed but there is no cracking, further inspection of the machined surface is required, an example of which is shown in figure 6.20. Here it can be seen that there are lines or chevron marks approximately $50\ \mu\text{m}$ apart at 45° to the direction of the cut, which would indicate a shearing action, and identify the chip formation mechanism as discontinuous - shear. Finally, the outlier discussed earlier is labelled as having occurred due to smearing, rather than cutting. The full table of chip formation mechanisms is shown in table 6.6.

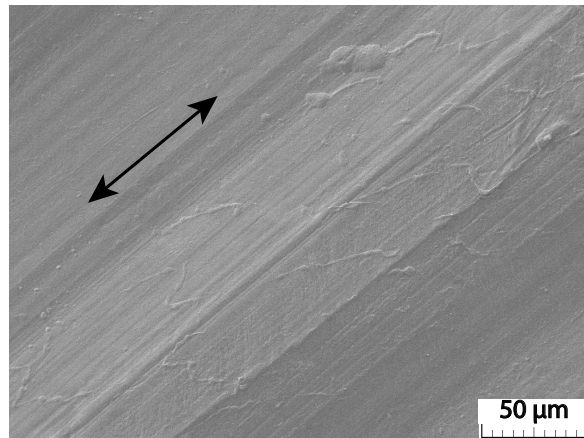


Figure 6.20: Example of surface profile where discontinuous chip was formed without evident cracking. Machined from a room temperature workpiece using a tool with -20° rake angle, highly worn tool, $155\ \text{m}/\text{min}$ cutting speed, $0.06\ \text{mm}/\text{rev}$ depth of cut.

Continuous - flow* type chips are the most common chip formation mechanism, and the most desirable for surface quality [101]. This chip type is typically formed when machining with sharp and worn tools for neutral and positive rake angles, and for highly worn tools at the higher depth of cut, both with cooled and room temperature workpieces. It also occurs for the negative rake angle, but only for sharp tools with cooled workpieces. The continuous - shear chip formation mechanism is observed for all other negative rake angle situations where a continuous chip is formed. This points to the size effect being a major factor in achieving a continuous chip formation mechanism,

Table 6.6: Chip formation mechanisms identified from experimental data. Entries in bold indicate situations where continuous chip formation occurred despite the presence of a pattern in the profilometer data which would be consistent with crack-type chip formation.

| Rake Angle | Sharpness | CS | 155 | | 300 | |
|------------|-------------|-------|--------------------------|------|-------------|----------|
| | | DOC | 0.06 | 0.19 | 0.06 | 0.19 |
| | | Temp. | Chip formation mechanism | | | |
| -20 | Sharp | Cold | C-F* | C-F* | C-F* | C-F* |
| | | Room | C-S | C-S | C-S | C-S |
| | Worn | Cold | D-C(s&c) | C-S | D-C(s&c) | C-S |
| | | Room | D-S | C-S | D-S | C-S |
| | Highly worn | Cold | D-C(s&c) | C-S | D-C(s&c) | C-S |
| | | Room | D-S | D-S | D-S | Smearing |
| 0 | Sharp | Cold | C-F* | C-F* | C-F* | C-F* |
| | | Room | C-F* | C-F* | C-F* | C-F* |
| | Worn | Cold | C-F* | C-F* | C-F* | C-F* |
| | | Room | D-C(s&c) | C-F* | C-F* | C-F* |
| | Highly worn | Cold | D-C(s&c) | C-F* | D-C(s&c) | C-F* |
| | | Room | D-C(s&c) | C-F* | D-C(s&c) | C-F* |
| 20 | Sharp | Cold | C-F* | C-F* | C-F* | C-F* |
| | | Room | C-F* | C-F* | C-F* | C-F* |
| | Worn | Cold | C-F* | C-F* | C-F* | C-F* |
| | | Room | C-F* | C-F* | C-F* | C-F* |
| | Highly worn | Cold | D-C(s&c) | C-F* | D-C(s&c) | C-F* |
| | | Room | D-C(s&c) | C-F* | D-C(s&c) | C-F* |
| 40 | Sharp | Cold | C-F* | C-F* | C-F* | C-F* |
| | | Room | C-F* | C-F* | C-F* | C-F* |
| | Worn | Cold | C-F* | C-F* | C-F* | C-F* |
| | | Room | C-F* | C-F* | C-F* | C-F* |
| | Highly worn | Cold | D-C(s&c) | C-F* | D-C(s&c) | C-F* |
| | | Room | D-C(s&c) | C-F* | D-C(s&c) | C-F* |

Chip formation mechanisms

| | |
|----------|--|
| C-F* | Continuous - Flow* |
| C-S | Continuous - Shear |
| D-S | Discontinuous - Shear |
| D-C(s&c) | Discontinuous - Complex (Shear with Crack) |

as at a high depth of cut a continuous chip was formed for all cases other than when machining with highly worn tools, and room temperature workpieces.

As with the continuous - shear mechanism, the discontinuous - shear chip formation mechanism is also only observed at the negative rake angle, at room temperature using worn tools with the low value of depth of cut, or with highly worn tools. These correspond to machining parameters which cause a negative effective rake angle. At high material removal rates this chip formation mechanism appears to transition into spalling. The continuous - shear and discontinuous - shear type chip formation mechanisms were observed only at the negative rake angle, for cuts where the machined surface displayed low RMS values. This explains the differing trends in RMS data at the negative rake angle compared to neutral and positive rake angles.

The discontinuous - complex (shear with crack) chip formation mechanism occurs only at low depths of cut. For negative rake angles it occurs for cooled workpieces with worn and highly worn tools, while for neutral and positive rake angles it occurs for highly worn tools, and also occurs for worn tools with 0° rake angle with room temperature workpieces.

There are six situations where a continuous chip was formed, but the profilometer RMS data showed apparent crack-type chip formation. These cases all occur at the low depth of cut, in situations where an increase in workpiece temperature or tool edge radius would cause a transition to a discontinuous chip formation mechanism. Slight variations in machining parameters in these transitional cases could cause a change in chip formation mechanism, and potentially a deterioration in surface quality.

6.5 Discussion

An investigation into the effect of workpiece pre-cooling on cutting forces, chip formation and surface quality in the machining of UHMWPE was carried out. It was found that workpiece pre-cooling to cryogenic temperatures (100 - 150 K) leads to increased cutting forces and heat generation, and improves surface quality in the machining of UHMWPE. These improvements in surface quality were not of a magnitude which exceeds that of the other factors studied, unlike in materials such as neoprene where the material is not machinable without cryogenic cooling [135]. Thus, the choice of rake angle, tool edge radius and cutting parameters remain important factors if a transition is made from machining at room temperature (300 K) to cryogenic temperatures (100 - 150 K). Tool temperature results showed increased heat generation for cryogenically pre-cooled workpieces compared to those machined at room temperature. It was identified that the heat generated during machining caused a hot zone between the tool and workpiece. This hot zone acted as a thermal barrier, thus preventing the tool from being cooled by the workpiece, despite the large temperature differential.

Variations in surface topology and quality were assessed optically and quantified using profilometer data, with the use of RMS of profilometer data measured parallel to the cutting direction as a measure of surface quality found to provide information on the surface profile and thus the chip formation mechanism. Analysis of the RMS of profilometer data measured parallel to the direction of cut for a range of machining parameters shows that tool edge radius, cutting speed and depth of cut were statistically significant, with use of a higher level of depth of cut providing superior surface quality in the majority of cases. The data collected was used to identify the chip formation mechanism for each combination of machining parameters. All but one situation was identified as one of the chip formation mechanisms defined by Kobayashi [101]. It was identified that the variation in surface quality due to machining and tool parameters for negative rake angles does not follow the same trends as for neutral and positive rake angles. This can be attributed to differing chip formation mechanisms at negative rake angles, where shear-type chip formation was observed. Additionally, an outlier was identified where aggressive cutting parameters in conjunction with a highly worn tool with a negative rake angle caused a smeared surface topography. It was also observed that situations where the nominal rake angle was positive, but a large cutting edge radius and low depth of cut led to a negative effective rake angle had chip formation mechanisms similar to those observed at negative rake angles.

While initial workpiece temperature did not appear to be statistically significant, it was observed that transitioning from room temperature to cryogenically pre-cooled

CRYOGENIC COOLING OF UHMWPE FOR MACHINING OPERATIONS

workpieces can modify the chip formation mechanism, though these transitions are typically only seen in already unfavourable tooling conditions such as highly worn tools and/or negative rake angles. Favourable machining conditions are typically found when the continuous-flow* chip formation mechanism is occurring, which can be consistently achieved by using positive rake angles, and by ensuring that the edge radius of the tool exceeds the depth of cut.

Chapter 7

Viscoelastic relaxation of UHMWPE following machining operations

7.1 Background and methodology for characterisation of viscoelastic relaxation of UHMWPE following machining operations

Thus far the viscoelastic nature of the response of UHMWPE to applied loads has been seen in the form of the DMA results shown in chapter 4, and in the observation of material deformation during machining and smeared machined surfaces in chapters 5 and 6. Variations in machining forces have also been observed as a result of tooling and machining parameters, and as a result of workpiece cooling. There is potential for workpiece deformation during machining operations, from both the machining forces, and from the clamping forces used to hold the workpiece. Thus, for this chapter, testing was conducted in two phases:

1. Static loading to simulate clamping forces, and establish if viscoelastic stress relaxation is a measurable phenomenon in UHMWPE.
2. Machining operations using sharp tools.

7.1.1 Static loading methodology

7.1.1.1 Sample design

Static loading operations were carried out on UHMWPE samples of dimensions $20 \times 10 \times 8.8 \text{ mm}$, with the loading being in the direction of the 8.8 mm dimension. The samples were compressed under two loading schemes: constant stress and constant strain.

7.1.1.2 Loading apparatus

Constant stress loading was carried out using an Instron 8801 compressive testing machine with manual load control. The duration of loading was 100 s for all tests. The

cross sectional area of each sample was measured and used to calculate the appropriate force for the stress level required. Samples were loaded to 2, 4 and 8 *MPa*, with unloaded samples used as a reference, as detailed in table 7.1. These loads were chosen to allow comparison with past work [75] and as an approximation of the stresses during machining. These stresses were assumed to be due to a force of 0 – 5 *N* over an area 2.2 *mm* wide and 0.19 *mm* high. These parameters are similar to the cutting forces observed previously, the width of the discs being machined, and the higher level (0.19 *mm*) of the depth of cut.

Table 7.1: Factors used in design of experiments for constant stress loading.

| Factor | Number of levels | Levels |
|----------------------------|------------------|--|
| Stress | 4 | 0, 2, 4, 8 <i>MPa</i> |
| Initial sample temperature | 2 | Cold (100 - 150 <i>K</i>), Room (295 - 300 <i>K</i>) |

Constant strain loading was carried out using an Instron 5589 compressive testing machine. As before, the duration of loading was 100 *s* for all tests. The thickness of each sample was measured using a digital micrometer. These measurements were then used to calculate the required displacement for the appropriate strain level. The levels used were 2.5%, 5% and 10% strain, as detailed in table 7.2.

Table 7.2: Factors used in design of experiments for constant strain loading.

| Factor | Number of levels | Levels |
|----------------------------|------------------|--|
| Strain | 4 | 0, 2.5, 5, 10 % |
| Initial sample temperature | 2 | Cold (100 - 150 <i>K</i>), Room (295 - 300 <i>K</i>) |

7.1.1.3 Measurements carried out during loading and after unloading

To achieve constant stress loading, it was necessary to use manual load control via the control panel of the Instron 8801. This was due to the relatively low forces required. Maintaining a low force setpoint was not achievable when controlled by the associated PC due to the tuning of the controller, which tended to overcorrect for setpoint errors. This overcorrection meant that the machine was unable to maintain the desired loads. As a consequence of using manual load control, it was not possible to measure the change in sample thickness while loading. The constant strain tests were carried out using

7.1. BACKGROUND AND METHODOLOGY FOR CHARACTERISATION OF VISCOELASTIC RELAXATION OF UHMWPE FOLLOWING MACHINING OPERATIONS

constant displacement, and thus it was possible to measure force data as a function of displacement and time, and to convert this force and displacement data to stress and strain, respectively. The thickness of the samples, which was originally 8.8 mm , was measured at given intervals after unloading, for both loading schemes. This thickness data was used for a regression analysis to ascertain if the material was relaxing after unloading. Measurements were made at 10, 20, 50, 100, 200, 500, 1000, 2000 and 5000 minutes after unloading.

7.1.2 Machining operations methodology

Machining operations were carried out on workpieces of the same design as those used in chapters 5 and 6, using a cutting speed of 155 m/min and a range of depths of cut from 0.05 to 0.25 mm/rev . Sharp tools with 20° and 40° rake angles were used, as detailed in table 7.3. The diameter of the machined samples, at given intervals after unloading, was used in a regression analysis to ascertain if the material was relaxing after machining. Measurements were made at 10, 20, 50, 100, 200, 500, 1000, 2000 and 5000 minutes after unloading. In order to have similar loading conditions for each machining operation, it was necessary to machine to different diameters, with the aim of maintaining constant machining time. This corresponds to constant cutting length, due to the use of the constant surface speed capability of the lathe. The resulting cutting times were approximately $3.5 \pm 0.4\text{ s}$.

Table 7.3: Factors used in design of experiments for machining operations.

| Factor | Number of levels | Levels |
|--------------|------------------|--|
| Rake angle | 2 | 20° , 40° |
| Depth of cut | 5 | 0.05 , 0.10 , 0.15 , 0.20 , 0.25 mm/rev |

7.2 Relaxation of test samples after static loading

7.2.1 Constant stress

Sample thickness data for 8 MPa load from 10 to 2000 minutes is shown in figure 7.1. Replicates A, B and C are those which were cryogenically cooled, while D, E and F were maintained at room temperature. It is clear that each replicate is showing logarithmic decay towards a steady state value. It can be seen that each replicate is decaying toward a slightly different steady state value, as a result of variations in the heights of the original samples. It is also evident that thickness stabilises at a steady state value approximately 200 minutes after unloading. This is a similar time to that observed by Fouad [44] in creep/recovery tests. The regression analysis was carried out using data from times of 10 to 200 minutes.

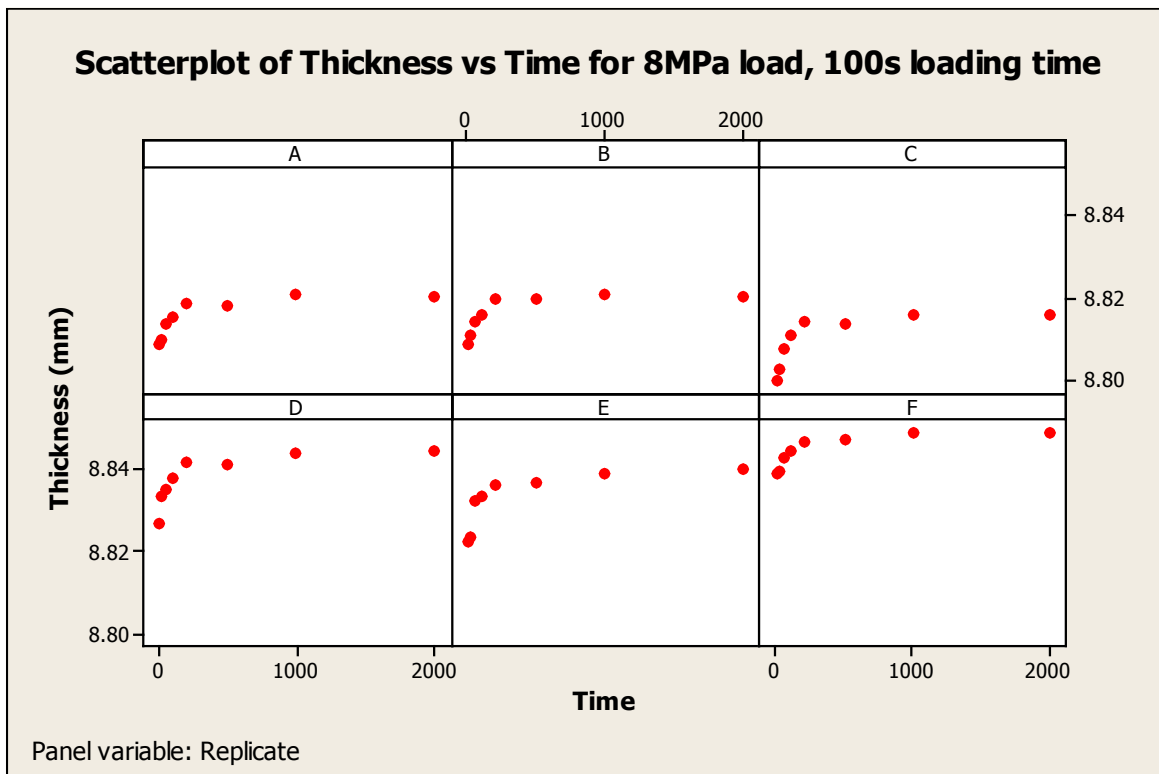


Figure 7.1: Scatterplot of thickness as a function of time for 8 MPa stress, 100 s loading time.

7.2. RELAXATION OF TEST SAMPLES AFTER STATIC LOADING

Data from 10 to 200 minutes after unloading are presented with a logarithmic x-axis in figure 7.2, with separate regression lines shown. It is clear that thickness from 10 to 200 minutes is a suitable response for linear regression against LogTime.

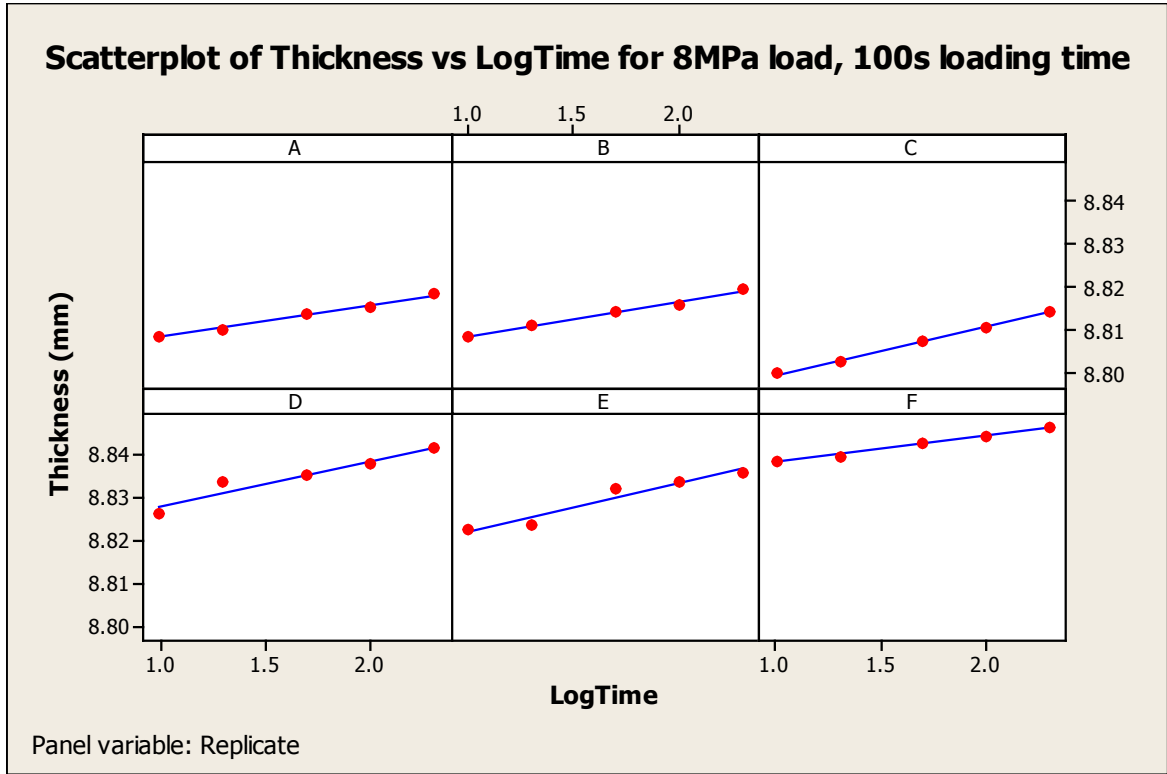


Figure 7.2: Scatterplot of thickness as a function of $\log_{10}(\text{time})$ for 8 MPa stress, 100 s loading time, from 10 to 200 minutes after loading.

In order to assess the effect of varying load and sample temperature prior to loading, a multiple linear regression model was used, with thickness as the response. The predictors chosen were LogTime (continuous), Replicate (categorical), Cryo, Load2, Load4 and Load8 (all indicator variables). Indicator variables were used to analyse the variation due to changes in load and temperature.

Figure 7.3 shows the variations which are captured in regression lines due to the inclusion of indicator variables. Figure 7.3a shows the variation which can be captured when using an indicator variable to assess the effect of a change in intercept - it is assumed that the slope remains constant regardless of the value of the indicator variable. The associated ANOVA table shows an analysis of the statistical significance of the difference in intercepts, using the null hypothesis that the difference is zero, and that there is no change in intercept. The regression coefficient associated with the indicator variable is equal to the change in intercept, $i_1 - i_0$.

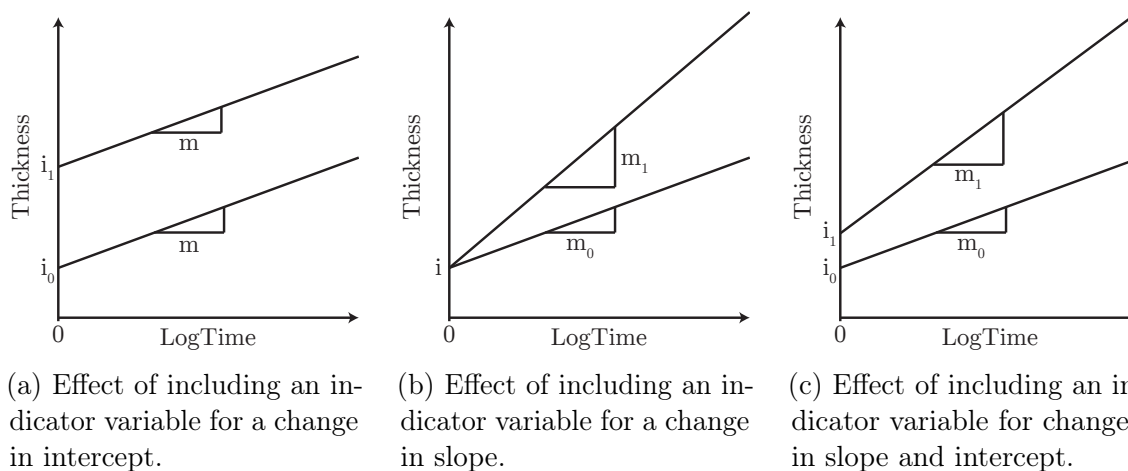


Figure 7.3: Effects of including indicator variables on slopes and intercepts of regression models.

Figure 7.3b shows the effect of using an indicator variable to measure changes in slope, with the intercept assumed not to change with the indicator variable. The ANOVA table shows an analysis of the statistical significance of the change in slope, with the regression coefficient for the indicator variable showing the change in slope, $m_1 - m_0$. Figure 7.3c shows the effect of using indicator variables to capture changes in both slope and intercept. The regression model includes coefficients for the changes in slope and intercept, along with statistical tests on the significance of these changes. This is the type of analysis which was used to evaluate the effect of load level and cryogenic pre-cooling on the relaxation of UHMWPE.

A single indicator variable was used to represent the change in slope due to cryogenic cooling, while the replicate code was used to capture changes in intercept due to variation in sample size. Information on the nature of each predictor and the interactions used in the model is given in table 7.4.

7.2. RELAXATION OF TEST SAMPLES AFTER STATIC LOADING

Table 7.4: Regression model information for constant stress loading, for 100 s loading time. The response for the model is Thickness.

| Predictors | |
|-------------------|------------------------------|
| Continuous | LogTime |
| Categorical | Replicate |
| Indicator | Cryo, Load 2, Load 4, Load 8 |

| Model structure | |
|------------------------|---|
| Slope | LogTime LogTime-Load 2 LogTime-Load 4 LogTime-Load 8 LogTime-Cryo LogTime-Cryo-Load 2 LogTime-Cryo-Load 4 LogTime-Cryo-Load 8 |
| Intercept | Load 2 Load 4 Load 8 Replicate Replicate-Load 2 Replicate-Load 4 Replicate-Load 8 |

A summary of the relative and absolute slope and intercept coefficients¹ and associated P values are shown in tables 7.5 and 7.6, respectively. In table 7.5 it can be seen that none of the slope coefficients including the cryogenic cooling term appear statistically significant, indicating that cryogenic cooling does not appear to change the slope in a statistically significant manner, while there is a baseline slope of 0.00392, indicating a baseline level of growth in the unloaded samples. The effect of increasing load causes an increase in the slope, of a statistically significant scale for all load levels. This load-slope relationship appears non-linear.

Table 7.5: Slope coefficients and P values for constant stress loading, for 100 s loading time.

| Term | Coefficient | | P value |
|---------------------|--------------------|-----------------|----------------|
| | Relative | Absolute | |
| LogTime | 0.00392 | 0.00392 | 0 |
| LogTime-Load 2 | 0.00173 | 0.00565 | 0.036 |
| LogTime-Load 4 | 0.00185 | 0.00577 | 0.025 |
| LogTime-Load 8 | 0.00544 | 0.00936 | 0 |
| LogTime-Cryo | 0.00118 | 0.00510 | 0.15 |
| LogTime-Cryo-Load 2 | -0.00207 | 0.00476 | 0.074 |
| LogTime-Cryo-Load 4 | -0.00072 | 0.00623 | 0.533 |
| LogTime-Cryo-Load 8 | -0.00152 | 0.00902 | 0.188 |

In table 7.6 it can be seen that the changes in coefficient due to increasing load

¹Absolute slope coefficients are calculated for each situation by calculating a sum of the relative coefficients which apply to the situation in question. For room temperature, with no load applied, this is simply the LogTime coefficient, while room temperature for load 2 is the sum of the LogTime and LogTime-Load 2 coefficients, and for cryo, load 2 the absolute coefficient is the sum of LogTime, LogTime-Load 2, LogTime-Cryo and LogTime-Cryo-Load 2.

VISCOELASTIC RELAXATION OF UHMWPE FOLLOWING MACHINING OPERATIONS

are all statistically significant, with some of the interactions between replicate and load level not appearing statistically significant. This is due to a combination of the changes in sample sizes due to loading, and the variation in thickness of the original samples from the nominal value of 8.8 mm. The unloaded samples show intercepts from 8.80666 mm to 8.8383 mm.

Table 7.6: Intercept coefficients and P values for constant stress loading, for 100 seconds loading time.

| | Term | Coefficient | | P value |
|-------------|----------|-------------|----------|---------|
| | | Relative | Absolute | |
| | Constant | 8.82096 | - | 0 |
| | Load 2 | -0.01185 | - | 0 |
| | Load 4 | -0.00492 | - | 0 |
| | Load 8 | -0.01266 | - | 0 |
| Replicate | A | -0.00826 | 8.8127 | 0 |
| | B | -0.0093 | 8.81166 | 0 |
| | C | -0.00574 | 8.81522 | 0 |
| | D | -0.0143 | 8.80666 | 0 |
| | E | 0.01734 | 8.8383 | 0 |
| | F | - | 8.82096 | - |
| Rep.-Load 2 | A | 0.00137 | 8.81048 | 0.225 |
| | B | 0.00449 | 8.8136 | 0 |
| | C | -0.00003 | 8.80908 | 0.982 |
| | D | 0.01937 | 8.82848 | 0 |
| | E | -0.01115 | 8.79796 | 0 |
| | F | - | 8.80911 | - |
| Rep.-Load 4 | A | -0.00668 | 8.80936 | 0 |
| | B | -0.00492 | 8.81112 | 0 |
| | C | -0.01004 | 8.806 | 0 |
| | D | 0.03093 | 8.84697 | 0 |
| | E | -0.00671 | 8.80933 | 0 |
| | F | - | 8.81604 | - |
| Rep.-Load 8 | A | -0.0018 | 8.8065 | 0.113 |
| | B | -0.00008 | 8.80822 | 0.942 |
| | C | -0.01056 | 8.79774 | 0 |
| | D | 0.02551 | 8.83381 | 0 |
| | E | -0.01145 | 8.79685 | 0 |
| | F | - | 8.8083 | - |

7.2. RELAXATION OF TEST SAMPLES AFTER STATIC LOADING

In order to analyse the lack of significance of cryogenic cooling it is necessary to examine the time scale over which the material warms from cryogenic temperature to room temperature when left to warm in air. Temperature data from an embedded thermocouple in a UHMWPE sample sized $8.8 \times 10 \times 20 \text{ mm}$ after removal from liquid nitrogen are shown in figure 7.4. The placement of the thermocouple within the sample shown in inset (a) of this figure.

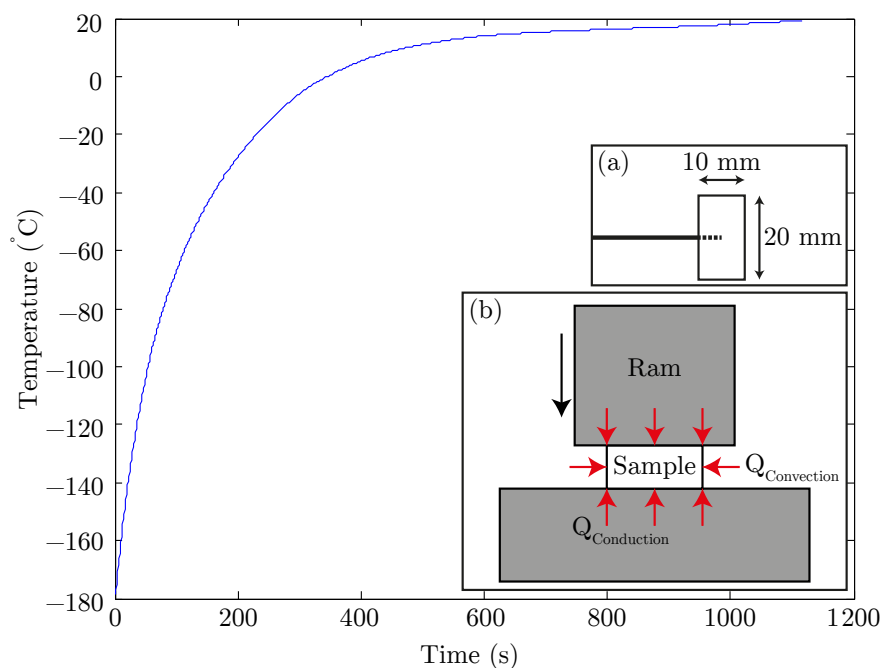


Figure 7.4: Temperature at core of $8.8 \times 10 \times 20 \text{ mm}$ UHMWPE sample after removal from liquid nitrogen, while warming in air. Inset figure (a) shows thermocouple placement within the sample. Inset figure (b) shows the avenues of heat ingress to samples while loading.

The sample core temperature becomes positive approximately 346 seconds after removal from liquid nitrogen. At 700 seconds - the earliest point at which the first thickness measurement can be made after 100 seconds of loading - the core temperature is 15.4°C , for a temperature differential of $< 10 \text{ K}$. For a coefficient of linear thermal expansion of $150 \times 10^{-6} \text{ K}^{-1}$ [177] and $\Delta T = 10 \text{ K}$, this equates to a strain due to heating of 0.15%, or approximately $13.2 \mu\text{m}$ for an 8.8 mm nominal thickness, which is of a similar magnitude to the variation observed between replicates. The process of handling and loading the samples between metal platens will accelerate the heating process, as illustrated in inset (b) in figure 7.4. Due to this added conductive heat source, 10 minutes after unloading the temperature of the sample will be approaching room temperature, as the loading process causes conductive heat transfer from the metal surfaces of the compressive testing machine to the sample.

7.2.2 Constant strain

7.2.2.1 Material behaviour during loading

The loading conditions used during these tests are shown in figure 7.5. Due to each level of strain being applied in 10 seconds in all cases, differing strain rates are experienced by the material, ranging from $2.5 \times 10^{-3} \text{ s}^{-1}$ to $10 \times 10^{-3} \text{ s}^{-1}$.

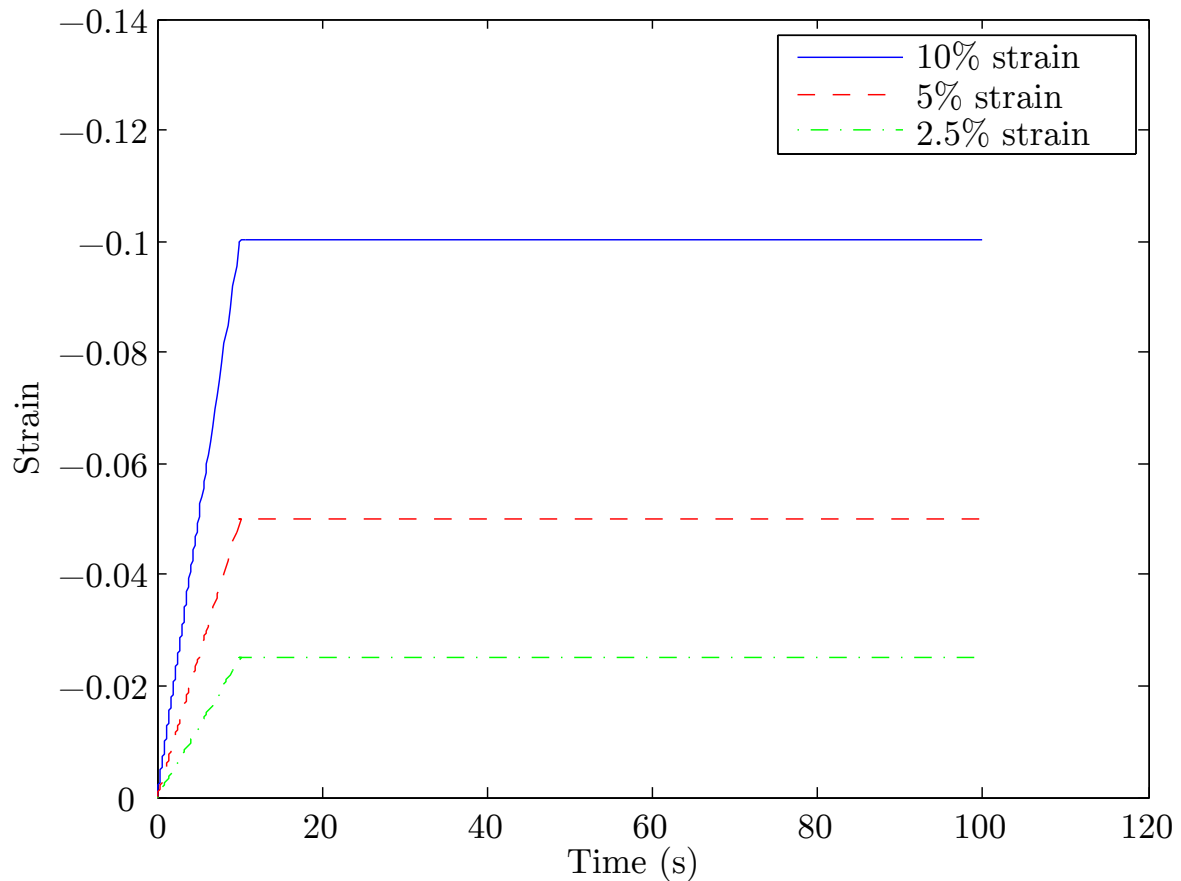


Figure 7.5: Strain as a function of time for constant strain loading.

7.2. RELAXATION OF TEST SAMPLES AFTER STATIC LOADING

Figure 7.6 shows stress as a function of time for cryogenically pre-cooled and room temperature samples. The decrease in stress after the peak strain is reached is a clear indication of stress relaxation.

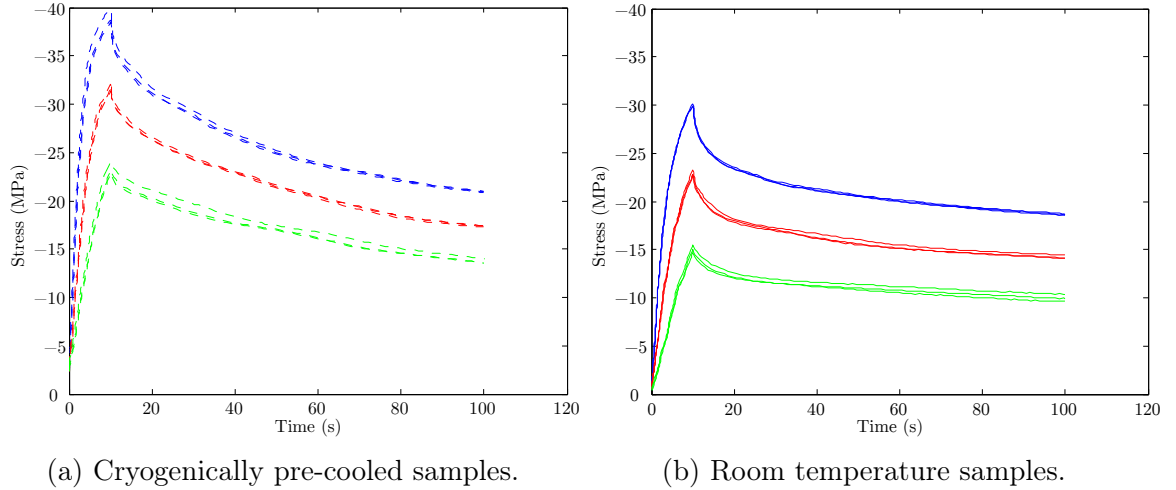


Figure 7.6: Stress as a function of time for constant strain loading.

The extent of this stress relaxation is summarised in table 7.7, where it can be seen that cryogenically cooled samples decreased in stress between 41.45% and 46.27% while room temperature samples decreased in stress between 33.77% and 37.99%. The increase for cryogenically cooled samples may be another indicator that the sample temperature is changing during loading, causing thermal expansion of the sample and increased stress as a result. It is clear that cryogenically cooled samples have increased stiffness compared to room temperature samples, and that their stress relaxation behaviour under constant strain is of a larger magnitude.

Table 7.7: Decrease in stress due to viscoelastic stress relaxation under constant strain. The stress values are calculated as the mean value of peaks and final values of stress data for each stress and temperature combination.

| Strain | Temperature | Stress [<i>MPa</i>] | | Percentage decrease |
|--------|-------------|-----------------------|---------|---------------------|
| | | Peak | Final | |
| 2.5% | Cryo | -23.408 | -13.704 | 41.454 |
| | Room | -15.065 | -9.978 | 33.767 |
| 5% | Cryo | -31.635 | -17.361 | 45.121 |
| | Room | -22.901 | -14.227 | 37.879 |
| 10% | Cryo | -38.975 | -20.94 | 46.272 |
| | Room | -29.995 | -18.599 | 37.994 |

The stress - strain behaviour for all samples is shown in figure 7.7. The effect of sample temperature is clear, with the decreases in each data set at the final strains of 2.5%, 5% and 10% are a result of stress relaxation after the final strain has been reached, 10 seconds after loading commences. It can be seen that room temperature results show very little spread over these 10 seconds of loading, while cryogenically pre-cooled samples show more scatter, possibly as a result of slight variations in sample temperature. It is also observed that the lower strain rates experienced by the 5% and 2.5% strain samples result in a slight decrease in slope as strain increases, indicating a strain-rate effect. These curves also predict that for 8 MPa the corresponding strains are approximately 0.6% for cryogenically cooled samples, and 1.1% for room temperature samples.

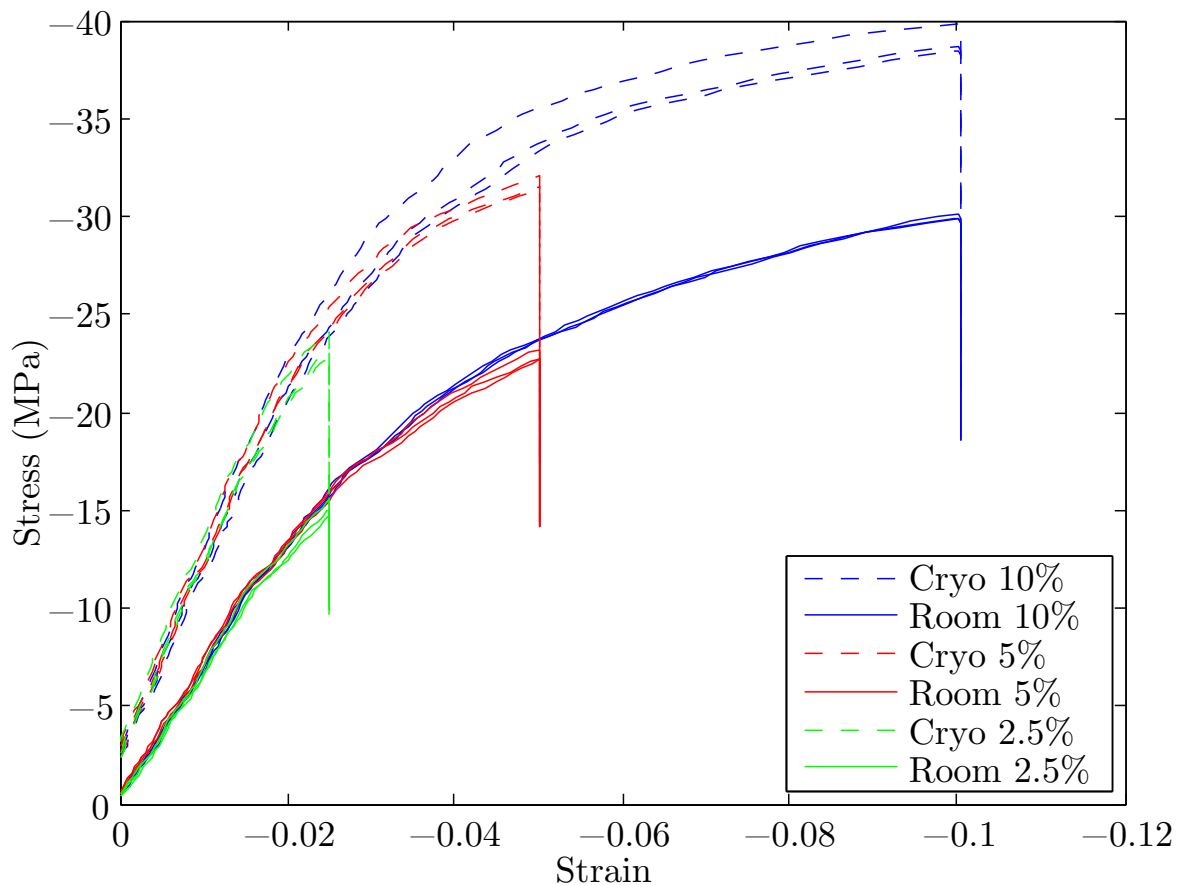


Figure 7.7: Stress as a function of strain for constant strain loading. Room temperature samples are shown with solid lines. Cryogenically pre-cooled samples are shown with dashed lines.

7.2.2.2 Relaxation after unloading

It is observed that thickness data reached a steady state value between 1000 and 2000 minutes after unloading, leading to 1000 minutes being used as a cutoff. Data for thickness as a function of LogTime is shown in figure 7.8.

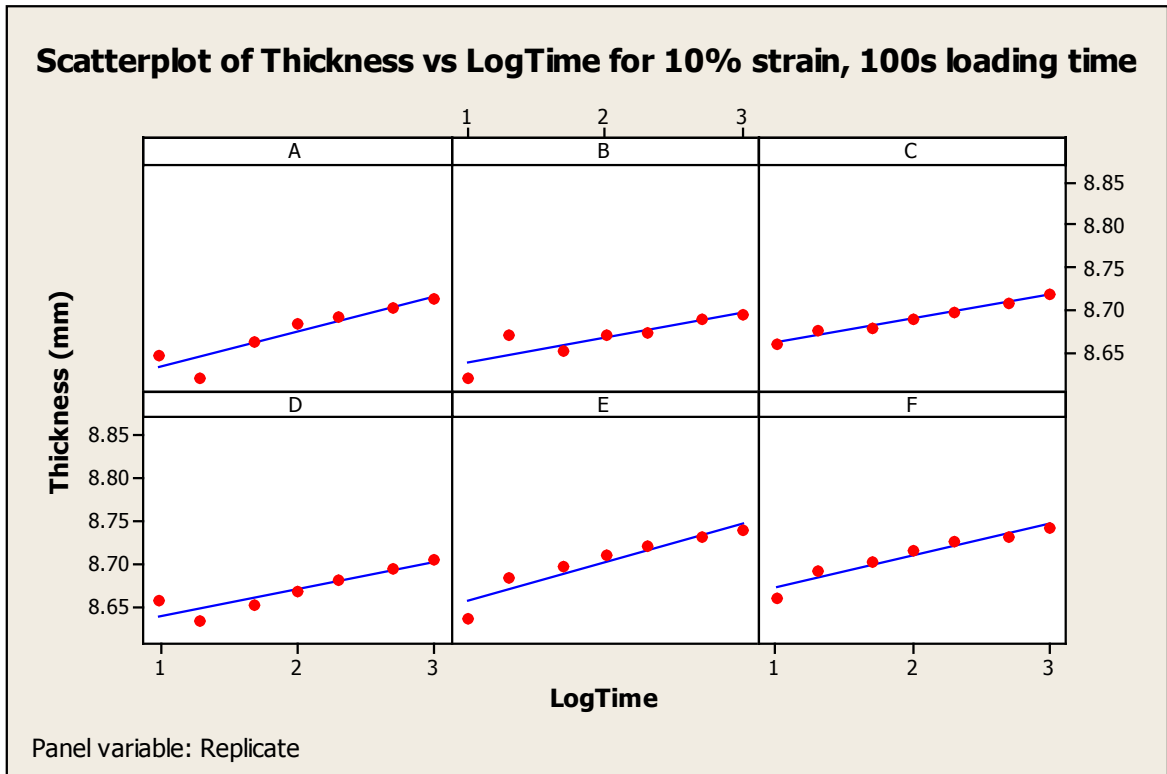


Figure 7.8: Scatterplot of thickness as a function of $\log_{10}(\text{time})$ for 10% strain, 100 s loading time, from 10 to 1000 minutes after loading.

It can be seen that some data points at 10 and 20 minutes display unusual behaviour, which was only observed for 10% strain. These data caused excess variation in the regression model. More detail provided in appendix F. This issue was potentially related to exposure of the micrometer used to extremes of temperature, causing inaccurate thickness readings.

VISCOELASTIC RELAXATION OF UHMWPE FOLLOWING MACHINING OPERATIONS

Due to the effect of these points on the model it was decided to omit them and use times from 50 to 1000 minutes for the regression analysis, with sample data shown in figure 7.9, and information on the regression model used shown in table 7.8.

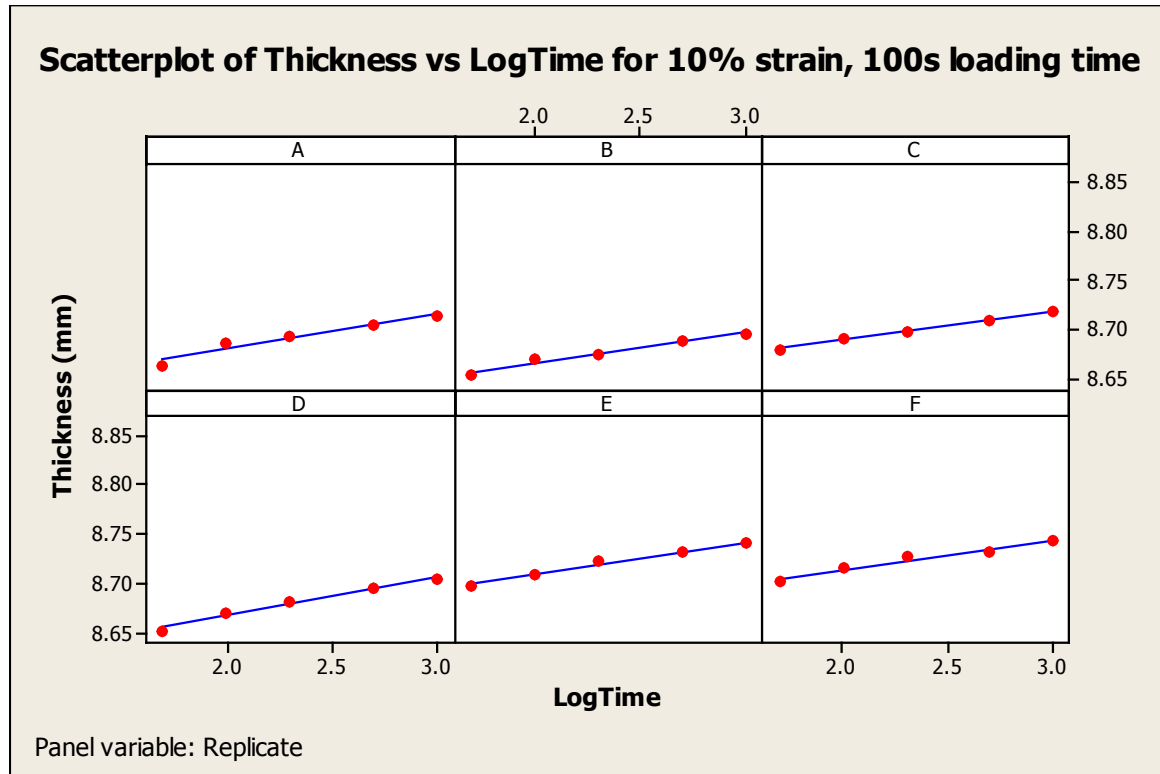


Figure 7.9: Scatterplot of thickness as a function of $\log_{10}(\text{time})$ for 10% strain, 100 s loading time, from 50 to 1000 minutes after loading.

Table 7.8: Regression model information for constant strain loading, for 100 seconds loading time. The response for the model is Thickness.

| Predictors | |
|-------------|---------------------------------|
| Continuous | LogTime |
| Categorical | Replicate |
| Indicator | Cryo, Load 2.5, Load 5, Load 10 |

| Model structure | |
|-----------------|---|
| Slope | LogTime LogTime-Load 2.5 LogTime-Load 5 LogTime-Load 10 LogTime-Cryo LogTime-Cryo-Load 2.5 LogTime-Cryo-Load 5 LogTime-Cryo-Load 10 |
| Intercept | Load 2.5 Load 5 Load 10 Replicate Replicate-Load 2.5 Replicate-Load 5 Replicate-Load 10 |

7.2. RELAXATION OF TEST SAMPLES AFTER STATIC LOADING

A summary of the relative and absolute slope and intercept coefficients and associated P values are shown in tables 7.9 and 7.10 (on page 134) respectively. Table 7.9 shows that the unloaded case continues to show a baseline level of growth, with a slope of 0.00550 *mm* per order of magnitude increase, which is an increase from the slope seen in the constant stress analysis. Increasing strain causes a statistically significant increase in the slope of the Thickness-LogTime regression line for the 5% and 10% strains, while the 2.5% strain shows an increase, but not one which is statistically significant (P = 0.208). As before, there is a non-linear relationship between the increase in slope and the magnitude of the applied strain. Cryogenic cooling does not show a statistically significant change in slope regardless of strain level, as was also observed in the constant stress loading.

Table 7.9: Slope coefficients and P values for constant strain loading, for 100 seconds loading time.

| Term | Coefficient | | P value |
|-----------------------|-------------|----------|---------|
| | Relative | Absolute | |
| LogTime | 0.00550 | 0.00550 | 0 |
| LogTime-Load 2.5 | 0.00229 | 0.00779 | 0.208 |
| LogTime-Load 5 | 0.01007 | 0.01557 | 0 |
| LogTime-Load 10 | 0.02851 | 0.03401 | 0 |
| LogTime-Cryo | -0.00005 | 0.00545 | 0.978 |
| LogTime-Cryo-Load 2.5 | -0.00078 | 0.00696 | 0.76 |
| LogTime-Cryo-Load 5 | -0.00098 | 0.01454 | 0.7 |
| LogTime-Cryo-Load 10 | -0.00198 | 0.03198 | 0.438 |

Table 7.10 shows that the change in intercept due to load is more pronounced at high strains, with 10% strain producing an intercept which is on average 200 μm smaller than an unloaded sample. This also gives an insight into the division of the response of the material into elastic and viscous components, as the 10% strain samples were originally compressed to 90% of their original thickness, or approximately 7.92 *mm*. This indicates that after unloading approximately 77% of the deformation was instantaneous, elastic deformation, with approximately 23% occurring over time as a result of viscoelasticity.

VISCOELASTIC RELAXATION OF UHMWPE FOLLOWING MACHINING OPERATIONS

Table 7.10: Intercept coefficients and P values for constant strain loading, for 100 seconds loading time.

| | Term | Coefficient | | P value |
|---------------|----------|-------------|----------|---------|
| | | Relative | Absolute | |
| | Constant | 8.82058 | - | 0 |
| | Load 2.5 | -0.02132 | - | 0 |
| | Load 5 | -0.06288 | - | 0 |
| | Load 10 | -0.19953 | - | 0 |
| Replicate | A | -0.00881 | 8.81177 | 0 |
| | B | -0.00901 | 8.81157 | 0 |
| | C | -0.00513 | 8.81545 | 0.029 |
| | D | -0.01392 | 8.80666 | 0 |
| | E | 0.01752 | 8.8381 | 0 |
| | F | - | 8.82058 | - |
| Rep.-Load 2.5 | A | 0.00171 | 8.80097 | 0.601 |
| | B | 0.00851 | 8.80777 | 0.011 |
| | C | -0.01081 | 8.78845 | 0.001 |
| | D | 0.02093 | 8.82019 | 0 |
| | E | -0.01691 | 8.78235 | 0 |
| | F | - | 8.79926 | - |
| Rep.-Load 5 | A | -0.01678 | 8.74092 | 0 |
| | B | 0.00034 | 8.75804 | 0.916 |
| | C | -0.0037 | 8.754 | 0.26 |
| | D | 0.03496 | 8.79266 | 0 |
| | E | 0.00348 | 8.76118 | 0.289 |
| | F | - | 8.7577 | - |
| Rep.-Load 10 | A | 0.00435 | 8.6254 | 0.186 |
| | B | -0.01069 | 8.61036 | 0.001 |
| | C | 0.00795 | 8.629 | 0.017 |
| | D | -0.00653 | 8.61452 | 0.048 |
| | E | 0.00159 | 8.62264 | 0.628 |
| | F | - | 8.62105 | - |

7.3 Relaxation of test samples after machining operations

7.3.1 Machining forces

The machining forces recorded during the machining operations are shown in figure 7.10. It can be seen that thrust force does not exceed 7 N for 20° rake angle, and does not exceed 5 N for 40° rake angle. This indicates that the force levels assumed for the constant stress levels in section 7.1.1.2 are of the same order of magnitude as those seen in machining.

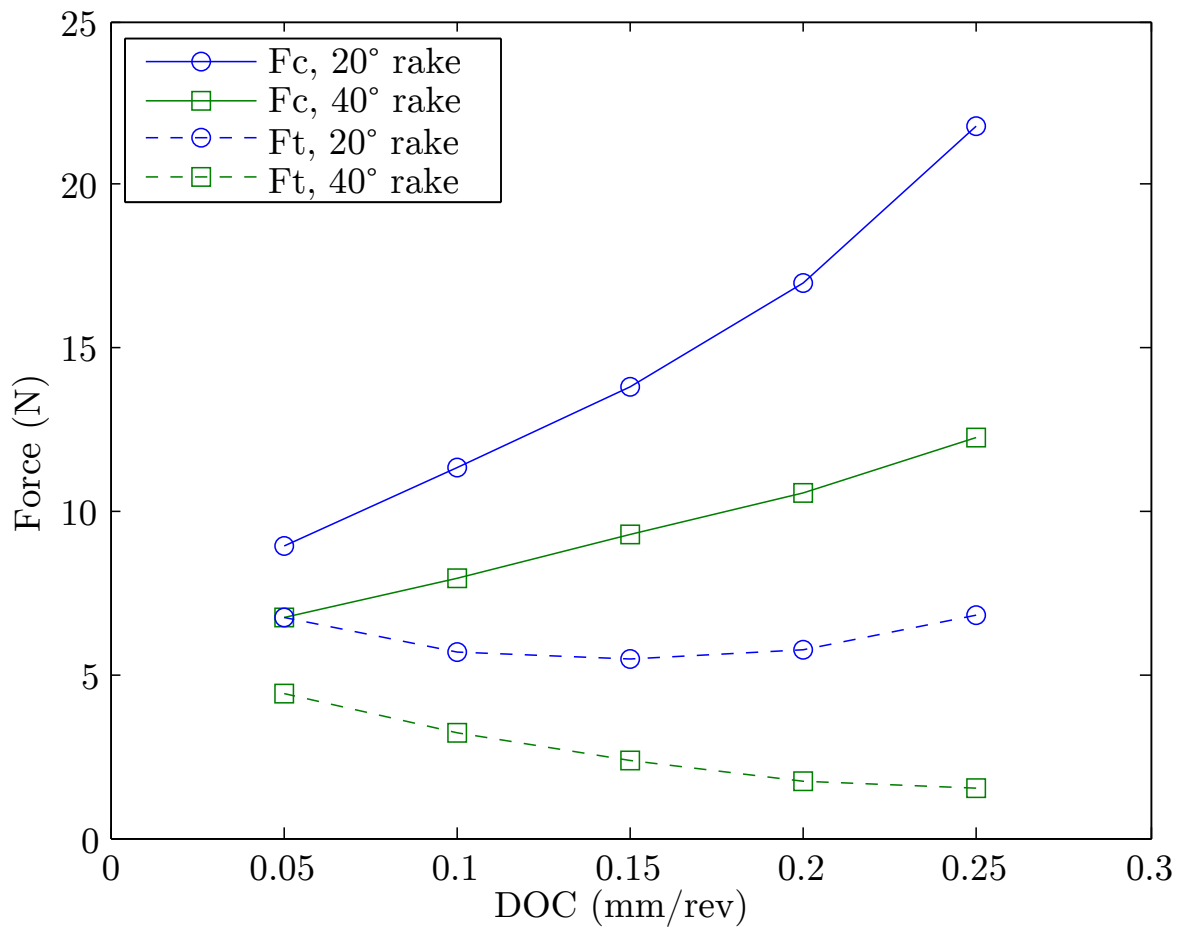


Figure 7.10: Machining forces recorded during cutting operations. Solid lines show cutting force, while dashed lines show thrust force. 20° rake angle forces are shown with a circle marker, while 40° rake angle forces are shown with a square marker.

7.3.2 Change in dimensions

The diameter of the machined samples for the 20° rake angle from 10 to 2000 minutes after machining is shown in figure 7.11. It is clear that there is little variation as a function of time. Information on the regression analysis used is provided in table 7.11.

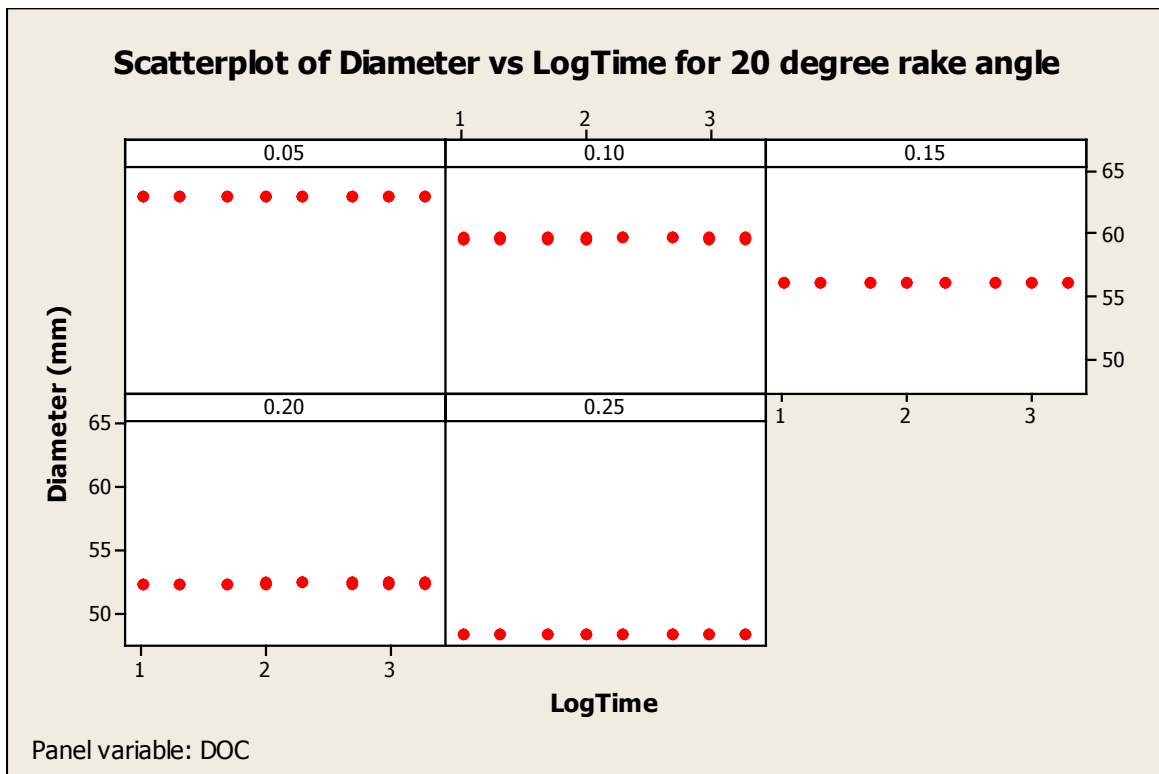


Figure 7.11: Change in diameter of machined samples as a function of time.

Table 7.11: Regression model information for machining operations. The response for the model is Diameter.

| Predictors | |
|-------------|---|
| Continuous | LogTime |
| Categorical | Replicate |
| Indicator | Rake 40, DOC 0.10, DOC 0.15, DOC 0.20, DOC 0.25 |

| Model structure | |
|-----------------|---|
| Slope | LogTime LogTime-Rake 40 |
| Intercept | DOC 0.10, DOC 0.15, DOC 0.20, DOC 0.25, Replicate |

7.3. RELAXATION OF TEST SAMPLES AFTER MACHINING OPERATIONS

The intercept and slope coefficients shown in table 7.12 were determined by regression analysis on data from samples machined using 20° and 40° tools. The statistical significance of the DOC indicator variables is due to the differences in diameter due to maintaining cutting time as constant for differing depths of cut, while the Replicate categorical variable shows variation due to differences in diameter between replicates, with the 20° rake (A-C) showing slightly smaller sizes on average. The slope coefficients are not statistically significant, showing that there is no change in the diameter of the samples as a function of LogTime, and thus that there is no detectable stress relaxation occurring in the samples.

Table 7.12: Coefficients and P values for machining operations.

| Term | Coefficient | | P value |
|------------------|-------------|----------|---------|
| | Relative | Absolute | |
| Intercept | | | |
| Constant | 62.9178 | 62.9178 | 0 |
| DOC 0.10 | -3.2603 | 59.6575 | 0 |
| DOC 0.15 | -6.754 | 56.1638 | 0 |
| DOC 0.20 | -10.4379 | 52.4799 | 0 |
| DOC 0.25 | -14.4622 | 48.4556 | 0 |
| Replicate | | | |
| A | -0.1087 | 62.8091 | 0 |
| B | -0.1078 | 62.81 | 0 |
| C | -0.1088 | 62.809 | 0 |
| D | 0.1056 | 63.0234 | 0 |
| E | 0.1037 | 63.0215 | 0 |
| F | 0 | 62.9178 | - |
| Slope | | | |
| LogTime | 0.0051 | 0.0051 | 0.287 |
| LogTime-Rake 40 | -0.008 | -0.0029 | 0.237 |

7.4 Discussion

In this chapter it has been demonstrated that viscoelastic relaxation after unloading can be observed in UHMWPE. The nature of the relaxation is a feature of the magnitude of the load and the length of time for which the load is applied. This is in agreement with the results obtained by Popelar *et al.* [118] using HDPE. Constant stress loading up to 8 MPa for 100 seconds produced relaxation which reached a steady state value approximately 200 minutes after unloading. Constant strain loading up to 10% strain produced relaxation which did not reach a steady state until over 1000 minutes after unloading. The stress-strain and stress-time data collected during the constant strain loading showed significant stress relaxation of up to 45% of the peak value over 90 seconds of constant strain. Shorter loading times would produce less relaxation, while longer loading times would produce more, up to a maximum value, after which the stress relaxation would reach a steady state. While cryogenic pre-cooling of the sample showed increased stiffness and changes in stress relaxation behaviour, it did not appear to have a statistically significant effect on the logarithmic slope of the increase in sample size. This is a result of the workpiece would have reached room temperature shortly after the first measurement. As the measurements were carried out after reaching room temperature, the change due to thermal expansion will be minimal. This can be taken to show that the loading being applied to a cooled workpiece will not change the relaxation behaviour if the workpiece is subsequently brought to room temperature while relaxation is occurring.

In contrast, the machining operations appeared to produce no detectable level of material relaxation. This is a result of the small magnitude and short duration of the loading. Thus it can be concluded that, when favourable machining conditions are used, material relaxation is not of concern. Workpiece fixturing and holding should be carried out with care, as it may distort or deform the workpiece, causing relaxation over a long timescale after unclamping.

Chapter 8

Conclusions and further work

8.1 Conclusions

8.1.1 Fundamental investigation into machining of UHMWPE

In chapter 5, a fundamental investigation into the machining of UHMWPE was carried out using a data acquisition system, and a full factorial design of experiments. This investigation quantified the effects of variations in workpiece material, tooling parameters and machining parameters on cutting forces, tool temperature, and surface quality of the machined surface. Statistical analysis was carried out on the data collected to quantify the factors which were causing variation in each response. The objective of this chapter was to address research questions 1 and 2, as detailed in section 1.2. From the work conducted in this chapter it can be concluded that:

- The main influence on machining forces and surface quality is the ratio of the edge radius to the depth of cut, also known as the size effect. Machining operations where the depth of cut exceeded the edge radius of the tool showed high forces ($F_c > 50 N$, $F_t > 100 N$ in the most extreme cases), high tool temperatures ($T > 150^\circ C$ in the most extreme cases), and poor surface finish (R_a unmeasurable in the most extreme cases).
- The lowest machining forces ($F_c = 5$ to $20 N$, $F_t = 0$ to $5 N$) and best surface quality ($R_a < 0.8 \mu m$) were observed in situations where the continuous - flow* chip formation mechanism was occurring, with positive rake angles ($\alpha = 20^\circ$ or 40°), sharp tools ($r < 15 \mu m$) and large depths of cut ($DOC = 0.19 mm$) providing the best results at the levels studied.
- For sharp tools ($r < 15 \mu m$), it was identified that at negative rake angles ($\alpha = -20^\circ$) there is a different chip formation mechanism occurring, with the continuous - shear mechanism occurring at the negative rake angle, whereas the continuous - flow* mechanism was observed at neutral and positive rake angles.

CONCLUSIONS AND FURTHER WORK

- Observation of the cutting zone for situations where the depth of cut exceeded the edge radius showed high workpiece deformation both before and after the tool tip, with some extreme examples showing rubbing on the clearance face of the tool.
- No large changes in machinability were observed as a result of the presence of antioxidant additives or crosslinking of the polyethylene.
- Cutting speed in the range of 155 to 300 m/min did not appear to have as large an effect as would be expected for a viscoelastic material, particularly in light of the change in the nature of the viscoelastic behaviour of the material with varying strain rate, as observed from Dynamic Mechanical Analysis results.

8.1.2 Cryogenic pre-cooling of UHMWPE for machining operations

In chapter 6, the effect of cryogenic pre-cooling of workpieces using liquid nitrogen on machining was investigated. This work was carried out in light of the findings of chapters 4 and 5, with the intention of addressing research question 3. From this work it can be concluded that:

- The increased material stiffness as a result of cooling the workpiece to below 150 K caused higher cutting forces (Typical values: $F_c = 7$ to $10 N$ room, 10 to $20 N$ cryo, $F_t = 0$ to $3 N$ room, -2 to $4 N$ cryo)¹ and increased temperature generation. Improvements in the surface roughness of the machined part were observed ($R_a = 0.6$ to $1.2 \mu m$ room, 0.45 to $0.55 \mu m$ cryo), as a result of the increased stiffness and more elastic behaviour of the material when cooled. The effect of workpiece cooling on surface roughness did not dwarf those of the parameters previously shown to be of importance in machining UHMWPE, such as tool rake angle and sharpness, and depth of cut.
- The cooling of the workpiece was also found to have an effect on the chip formation mechanism for some combinations of cutting and tooling parameters, in particular in situations with negative effective rake angles.
- In favourable cutting situations, with a positive rake angle and depth of cut exceeding the tool edge radius, the continuous - flow* chip formation mechanism was observed for both room temperature and cryogenically pre-cooled workpieces, thus reinforcing the importance of selecting tooling and cutting parameters regardless of the workpiece temperature.

¹Comparison of data from 40° rake angle, sharp tool.

8.1.3 Viscoelastic stress relaxation in machining

In chapter 7, the effect of viscoelastic stress relaxation on machining operations was analysed, in order to address research question 4. Stress relaxation has the potential to cause machined parts to slowly change out of the desired shape over minutes or hours after a machining operation, and can cause part rejection and rework issues in large scale production. The first stage of testing was carried out in controlled conditions, using compressive testing machines. From this work it can be concluded that:

- The time scale over which relaxation will occur is dependent upon the magnitude of the applied load, with smaller loads causing relaxation over a shorter timescale. For loading up to 8 MPa (approximately 0.6% strain for cryogenically cooled samples, and 1.1% for room temperature samples) the samples reached a steady state after 200 minutes, while applying 10% strain (peak stress of approximately 39 MPa for cryogenically cooled samples, and 30 MPa for room temperature samples) caused relaxation which did not reach a steady state until between 1000 and 2000 minutes after unloading.
- Despite an increase in material stiffness at cryogenic temperatures observed in stress-strain plots, the cryogenic pre-cooling of the sample did not cause a statistically significant variation in the relaxation rate after unloading. This may be due to the sample temperature approaching room temperature in less than 10 minutes when exposed to air.
- Workholding and clamping is of great importance when machining UHMWPE, as placing large clamping pressures on the part is likely to cause stress relaxation while loaded and relaxation after unloading.
- The time of application for and large clamping forces should be minimized, to reduce the magnitude of the resulting relaxation.

CONCLUSIONS AND FURTHER WORK

In light of these conclusions, machining operations were carried out to evaluate the magnitude of relaxation during machining operations. While it was clear from machining force results from earlier chapters that it would be possible to apply large compressive forces to the workpiece using combinations of large tool edge radii and low depths of cut to produce negative effective rake angles, such machining operations would produce surfaces which would never be acceptable in a finishing operation during machining. Thus it was decided to concentrate on machining conditions which had been found to produce acceptable surface quality, using positive rake angles and sharp tools, to ascertain if workpiece relaxation would be an issue for machining operations which would be likely to be encountered in production. From this work it can be concluded that:

- Short duration, finish machining operations with sharp tools and positive rake angles will not cause detectable stress relaxation of the finished part after machining in UHMWPE.

8.1.4 Contribution to knowledge

This thesis has made contributions to knowledge in the following ways:

- By contributing to knowledge on the machining parameters of importance in the machining of UHMWPE.
- By demonstrating that the machinability of UHMWPE is not significantly changed by the addition of antioxidants, or the crosslinking of the material.
- By determining the extent of the influence of workpiece pre-cooling using liquid nitrogen on the machinability and surface quality of UHMWPE.
- By quantifying the influence of viscoelastic stress relaxation on the machining of UHMWPE, and the potential for changes in the size of a part to occur after clamping and machining operations.

8.1.5 Concluding remarks

Fundamental knowledge of the machinability of the workpiece material is a necessity for efficient, cost effective manufacturing. Without this knowledge the design of a machining process for a component becomes costly, both in time and money. In a process where this fundamental knowledge is absent, repetitive trial runs must be made to arrive at an acceptable set of tooling and machining parameters which satisfy surface finish, dimensional accuracy and cycle time requirements. This approach is conducted with no real understanding of why the solution arrived at works, or insight into how to streamline the process for future components or materials. This is particularly key in situations where the material choice is dictated by factors other than machinability, as is the case for the use of UHMWPE in total joint replacement, where the key requirements are wear resistance and biocompatibility.

Past work has established the effects of some machining and tooling parameters for polyethylene, while identifying the chip formation mechanisms occurring for sharp tools [101]. Work since then has concentrated mainly on the use of sharp tooling in oblique cutting [152, 162] and drilling [141, 163, 164], but with no information on the effects of tool edge radius, or the implications of viscoelasticity in the machining of polyethylene. This work has provided increased insight into the machining of UHMWPE, putting scientific knowledge and rigour behind the empirical knowledge previously discovered and rediscovered through trial and error by machine operators and manufacturing engineers, while providing fundamental knowledge on the effects of clamping, tooling, machining and workpiece parameters on the quality of the finished part.

8.2 Further work

Areas in which further work could be carried out include:

- Further experimental investigations of machining and tooling parameters. This work could potentially include investigations such as identification of the effect of large variations in cutting speed, depth of cut or tool material on workpiece deformation, relaxation, and surface quality. Other potential avenues of work include investigations into the implications of using large depths of cut during roughing cycles on later stress relaxation of the part, or the effect of progressive tool wear, in the form of cutting edge radius increases, on stress relaxation. The results of such investigations would expand upon this work, and provide increased insight into the machining of UHMWPE.
- Oblique and/or interrupted cutting experiments, to provide machining parameters for milling operations, and to expand upon both this work and the work of Yong-hwan [162]. Oblique cutting operations would provide information of more immediate use to machine operators in the selection of machining parameters, though monitoring of these operations can be challenging. This work would also involve an increased number of tool geometry variables, such as nose radius, which would affect the surface roughness of the machined surface.
- In-process cooling using liquid nitrogen to cool the material in the cutting zone to below the glass transition temperature, as conducted by Dhokia *et al.* for elastomers [135]. This could potentially eliminate the need to soak the workpiece in liquid nitrogen before machining, as only the cutting zone would be cooled. Care would be required to avoid workpiece distortion due to temperature changes, with a control system and temperature monitoring system required to regulate the supply of liquid nitrogen.
- Finite element modelling of UHMWPE. Modelling of the machining of polymers using viscoelastic and viscoplastic material models is almost nonexistent, largely due to the difficulties in developing both an appropriate material model, and in accurately representing the variety of chip formation mechanisms. Challenges include accurately capturing the transition between brittle and ductile failure that for polymers is dependent upon temperature and strain rate, and developing appropriate flow stress equations for UHMWPE, which are accurate at high strain rates. If an accurate FE model were developed and validated it would provide new insight into chip formation mechanisms and temperature generation during

8.2. FURTHER WORK

the machining operation, and facilitate greater understanding of the mechanical and thermal interactions between the tool, workpiece and chip in the machining of polymers.

CONCLUSIONS AND FURTHER WORK

References

- [1] Plastics Europe and The European Association of Plastics Recycling and Recovery Organisations, “Plastics - the Facts 2014/2015,” 2015.
- [2] F. Galiè and C. Trabucchi, “ICIS world polymers outlook,” March 2014.
- [3] Eurostat, “Annual detailed enterprise statistics for industry,” January 2015. Accessed 22/3/2015.
- [4] European Plastics Converters Association and Plastics Europe, “The Plastics Industry: A strategic partner for economic recovery and sustainable growth in Europe,” 2014.
- [5] G. Chakrabarty, M. Vashishtha, and D. Leeder, “Polyethylene in knee arthroplasty: A review,” *Journal of Clinical Orthopaedics and Trauma*, vol. 6, no. 2, pp. 108 – 112, 2015.
- [6] S. M. Kurtz, *UHMWPE Biomaterials Handbook, Second Edition: Ultra High Molecular Weight Polyethylene in Total Joint Replacement and Medical Devices*. Elsevier, 2009.
- [7] E. Brach del Prever, A. Bistolfi, P. Bracco, and L. Costa, “UHMWPE for arthroplasty: past or future?,” *Journal of Orthopaedics and Traumatology*, vol. 10, pp. 1 – 8, 2009.
- [8] M. E. Turell, G. E. Friedlaender, A. Wang, T. S. Thornhill, and A. Bellare, “The effect of counterface roughness on the wear of UHMWPE for rectangular wear paths,” *Wear*, vol. 259, pp. 984 – 991, 2005.
- [9] M. Sobieraj and C. Rimnac, “Ultra high molecular weight polyethylene: Mechanics, morphology, and clinical behavior,” *Journal of the Mechanical Behavior of Biomedical Materials*, vol. 2, no. 5, pp. 433 – 443, 2009.
- [10] F. Renò and M. Cannas, “UHMWPE and vitamin E bioactivity: An emerging perspective,” *Biomaterials*, vol. 27, no. 16, pp. 3039 – 3043, 2006.

REFERENCES

- [11] R. J. Crawford, "1: Structure of plastics," *Progress in Polymer Science*, vol. 7, pp. 7 – 29, 1981.
- [12] M. Kutz, *Handbook of materials selection*. Wiley Online Library, 2002.
- [13] E. Oral, E. S. Greenbaum, A. S. Malhi, W. H. Harris, and O. K. Muratoglu, "Characterization of irradiated blends of α -tocopherol and UHMWPE," *Biomaterials*, vol. 26, no. 33, pp. 6657 – 6663, 2005.
- [14] N. Štrumberger, A. Gospočić, and Čedomir Bartulić, "Polymeric materials in automobiles," *Promet - Traffic - Traffico*, vol. 3, pp. 149 – 160, 2005.
- [15] F. Pardos, "Engineering and high performance plastics: Now and in 2015," in *High Performance Plastics 2005*, Rapra Technology Limited, April 2005.
- [16] M. Kozakiewicz, "Computer-aided orbital wall defects treatment by individual design ultrahigh molecular weight polyethylene implants," *Journal of Cranio-Maxillofacial Surgery*, vol. 42, no. 4, pp. 283 – 289, 2014.
- [17] S. Bastida, J. I. Eguiazábal, M. Gaztelumendi, and J. Nazábal, "On the thickness dependence of the modulus of elasticity of polymers," *Polymer Testing*, vol. 17, no. 2, pp. 139 – 145, 1998.
- [18] A. J. Shih, M. A. Lewis, and J. S. Strenkowski, "End milling of elastomers - fixture design and tool effectiveness for material removal," *Journal of Manufacturing Science and Engineering*, vol. 126, no. 1, pp. 115 – 123, 2004.
- [19] I. M. Ward, "Review: The yield behaviour of polymers," *Journal of Materials Science*, vol. 6, pp. 1397 – 1417, 1971.
- [20] Y. Haddad, *Viscoelasticity of Engineering Materials*. Chapman & Hall, 1995.
- [21] F. Berto, D. Cendon, P. Lazzarin, and M. Elices, "Fracture behaviour of notched round bars made of PMMA subjected to torsion at -60°C ," *Engineering Fracture Mechanics*, vol. 102, pp. 271 – 287, 2013.
- [22] R. J. Crawford, "3: Mechanical properties of plastics (part 2)," *Progress in Polymer Science*, vol. 7, pp. 85 – 143, 1981.
- [23] G. P. Gubbels, F. L. M. Delbressine, L. E. Govaert, and P. H. Schellekens, "Precision cutting of glassy polymers: influence of aging on the cutting process," *Optical Fabrication, Testing, and Metrology*, vol. 5252, no. 1, pp. 111 – 121, 2004.

- [24] A. Kobayashi and N. Ohtani, "Initial slow crack growth behavior followed by rapid brittle fracture in a viscoelastic solid," *Journal of Applied Polymer Science*, vol. 21, no. 5, pp. 1351 – 1358, 1977.
- [25] A. Kobayashi and N. Ohtani, "The effects of initial nonconstant transient cross-head speed on the stress - strain curve of viscoelastic material," *Journal of Applied Polymer Science*, vol. 16, no. 10, pp. 2523 – 2530, 1972.
- [26] A. Kobayashi and N. Ohtani, "Strain rate dependency on stress - strain relations of polypropylene," *Journal of Applied Polymer Science*, vol. 15, no. 4, pp. 975 – 985, 1971.
- [27] A. Kobayashi, N. Ohtani, and S. Ino, "On creep test loading for soft polymers," *Journal of Applied Polymer Science*, vol. 15, no. 12, pp. 3009 – 3013, 1971.
- [28] R. M. Guedes, "A viscoelastic model for a biomedical ultra-high molecular weight polyethylene using the time-temperature superposition principle," *Polymer Testing*, vol. 30, no. 3, pp. 294 – 302, 2011.
- [29] R. J. Crawford, "2: Mechanical properties of plastics (part 1)," *Progress in Polymer Science*, vol. 7, pp. 31 – 83, 1981.
- [30] R. Ghosh, J. A. Knopf, D. J. Gibson, and T. Mebrahtu, "Cryogenic machining of polymeric biomaterials: An intraocular lens case study," in *Medical Device Materials IV: Proceedings of the Materials and Processes for Medical Devices Conference 2007*, 2007.
- [31] S. M. Kurtz, M. L. Villarraga, M. P. Herr, J. S. Bergström, C. M. Rimnac, and A. A. Edidin, "Thermomechanical behavior of virgin and highly crosslinked ultra-high molecular weight polyethylene used in total joint replacements," *Biomaterials*, vol. 23, no. 17, pp. 3681 – 3697, 2002.
- [32] N. A. Fleck, W. J. Stronge, and J. H. Liu, "High strain-rate shear response of polycarbonate and polymethyl methacrylate," *Proceedings of the Royal Society of London. A. Mathematical and Physical Sciences*, vol. 429, no. 1877, pp. 459 – 479, 1990.
- [33] Y. Liu, Y. Hu, T. Liu, J. Ding, and W. Zhong, "Mechanical behavior of high density polyethylene and its carbon nanocomposites under quasi-static and dynamic compressive and tensile loadings," *Polymer Testing*, vol. 41, pp. 106 – 116, 2015.

REFERENCES

- [34] A. Avanzini, "Effect of cyclic strain on the mechanical behavior of virgin ultra-high molecular weight polyethylene," *Journal of the Mechanical Behavior of Biomedical Materials*, vol. 4, no. 7, pp. 1242 – 1256, 2011.
- [35] D. J. Krzypow and C. M. Rimnac, "Cyclic steady state stress – strain behavior of UHMW polyethylene," *Biomaterials*, vol. 21, no. 20, pp. 2081 – 2087, 2000.
- [36] M. Del Nobile, S. Chillo, A. Mentana, and A. Baiano, "Use of the generalized maxwell model for describing the stress relaxation behavior of solid-like foods," *Journal of Food Engineering*, vol. 78, no. 3, pp. 978 – 983, 2007.
- [37] N. Aleksy, G. Kermouche, A. Vautrin, and J.-M. Bergheau, "Mechanical study of polymers in scratch test," *International Journal of Material Forming*, vol. 1, no. 1, pp. 595 – 598, 2008.
- [38] T. Chen, "Determining a prony series for a viscoelastic material from time varying strain data," tech. rep., National Aeronautics and Space Administration, and the U.S. Army Research Laboratory, 2000.
- [39] R. Singh, P. Davies, and A. Bajaj, "Estimation of the dynamical properties of polyurethane foam through use of prony series," *Journal of Sound and Vibration*, vol. 264, no. 5, pp. 1005 – 1043, 2003.
- [40] S. Park and R. Schapery, "Methods of interconversion between linear viscoelastic material functions. Part I: A numerical method based on prony series," *International Journal of Solids and Structures*, vol. 36, no. 11, pp. 1653 – 1675, 1999.
- [41] F. Quadrini, "Machining of plastics: A new approach for modeling," *Polymer Engineering & Science*, vol. 48, no. 3, pp. 434 – 438, 2008.
- [42] A.-G. Denay, S. Castagnet, A. Roy, G. Alise, and N. Thenard, "Compression behavior of glass-fiber-reinforced and pure polyurethane foams at negative temperatures down to cryogenic ones," *Journal of Cellular Plastics*, vol. 49, no. 3, pp. 209 – 222, 2013.
- [43] K. P. Menard, *Dynamic mechanical analysis: a practical introduction*. CRC press, 1999.
- [44] H. Fouad, "Effect of long-term natural aging on the thermal, mechanical, and viscoelastic behavior of biomedical grade of ultra high molecular weight polyethylene," *Journal of Applied Polymer Science*, vol. 118, no. 1, pp. 17 – 24, 2010.

- [45] A. Greco and A. Maffezzoli, "Correction of melting peaks of different PE grades accounting for heat transfer in DSC samples," *Polymer Testing*, vol. 27, no. 1, pp. 61 – 74, 2008.
- [46] U. Göschel and C. Ulrich, "Mechanical relaxation of medical grade UHMWPE of different crosslink density as prepared by electron beam irradiation," *Journal of Applied Polymer Science*, vol. 113, no. 1, pp. 49 – 59, 2009.
- [47] P. Bracco, V. Brunella, M. Luda, M. Zanetti, and L. Costa, "Radiation-induced crosslinking of UHMWPE in the presence of co-agents: chemical and mechanical characterisation," *Polymer*, vol. 46, no. 24, pp. 10648 – 10657, 2005.
- [48] J. Gulmine, P. Janissek, H. Heise, and L. Akcelrud, "Polyethylene characterization by FTIR," *Polymer Testing*, vol. 21, no. 5, pp. 557 – 563, 2002.
- [49] J. Brydson, *Plastics Materials*. Referex Engineering, Butterworth-Heinemann, 1999.
- [50] S. M. Kurtz, O. K. Muratoglu, M. Evans, and A. A. Edidin, "Advances in the processing, sterilization, and crosslinking of ultra-high molecular weight polyethylene for total joint arthroplasty," *Biomaterials*, vol. 20, no. 18, pp. 1659 – 1688, 1999.
- [51] E. Oral, A. L. Neils, C. Lyons, M. Fung, B. Doshi, and O. K. Muratoglu, "Surface cross-linked UHMWPE can enable the use of larger femoral heads in total joints," *Journal of Orthopaedic Research*, vol. 31, pp. 59 – 66, 2012.
- [52] E. Oral, K. K. Wannomae, N. Hawkins, W. H. Harris, and O. K. Muratoglu, " α -tocopherol-doped irradiated UHMWPE for high fatigue resistance and low wear," *Biomaterials*, vol. 25, no. 24, pp. 5515 – 5522, 2004.
- [53] E. Oral, K. K. Wannomae, S. L. Rowell, and O. K. Muratoglu, "Migration stability of alpha-tocopherol in irradiated UHMWPE," *Biomaterials*, vol. 27, no. 11, pp. 2434 – 2439, 2006.
- [54] C. A. Harper and A.-M. Baker, *Modern plastics handbook*. McGraw-Hill New York, 2000.
- [55] Y.-F. Huang, J.-Z. Xu, J.-S. Li, B.-X. He, L. Xu, and Z.-M. Li, "Mechanical properties and biocompatibility of melt processed, self-reinforced ultrahigh molecular weight polyethylene," *Biomaterials*, vol. 35, no. 25, pp. 6687 – 6697, 2014.

REFERENCES

- [56] A. A. Edidin and S. M. Kurtz, "Influence of mechanical behavior on the wear of 4 clinically relevant polymeric biomaterials in a hip simulator," *The Journal of Arthroplasty*, vol. 15, no. 3, pp. 321 – 331, 2000.
- [57] S. M. Kurtz, L. Pruitt, C. W. Jewett, R. P. Crawford, D. J. Crane, and A. A. Edidin, "The yielding, plastic flow, and fracture behavior of ultra-high molecular weight polyethylene used in total joint replacements," *Biomaterials*, vol. 19, no. 21, pp. 1989 – 2003, 1998.
- [58] J. S. Day, D. W. MacDonald, M. Olsen, C. Getz, G. R. Williams, and S. M. Kurtz, "Polyethylene wear in retrieved reverse total shoulder components," *Journal of Shoulder and Elbow Surgery*, vol. 21, no. 5, pp. 667 – 674, 2012.
- [59] E. Oral, S. D. Christensen, A. S. Malhi, K. K. Wannomae, and O. K. Muratoglu, "Wear resistance and mechanical properties of highly cross-linked, ultrahigh-molecular weight polyethylene doped with vitamin E," *The Journal of arthroplasty*, vol. 21, no. 4, pp. 580 – 591, 2006.
- [60] J. H. Dumbleton, M. T. Manley, and A. A. Edidin, "A literature review of the association between wear rate and osteolysis in total hip arthroplasty," *The Journal of Arthroplasty*, vol. 17, no. 5, pp. 649 – 661, 2002.
- [61] A. A. Edidin, L. Pruitt, C. W. Jewett, D. J. Crane, D. Roberts, and S. M. Kurtz, "Plasticity-induced damage layer is a precursor to wear in radiation-cross-linked UHMWPE acetabular components for total hip replacement," *The Journal of Arthroplasty*, vol. 14, no. 5, pp. 616 – 627, 1999.
- [62] S. Kurtz, F. J. Medel, and M. Manley, "Wear in highly crosslinked polyethylenes," *Current Orthopaedics*, vol. 22, no. 6, pp. 392 – 399, 2008.
- [63] J. Zhang, "Surface modification of ultra-high-molecular-weight polyethylene by argon plasma," *Journal of Thermoplastic Composite Materials*, vol. 27, no. 6, pp. 758 – 764, 2014.
- [64] L. A. Pruitt, "Deformation, yielding, fracture and fatigue behavior of conventional and highly cross-linked ultra high molecular weight polyethylene," *Biomaterials*, vol. 26, no. 8, pp. 905 – 915, 2005.
- [65] S. M. Kurtz, L. A. Pruitt, C. W. Jewett, J. R. Foulds, and A. A. Edidin, "Radiation and chemical crosslinking promote strain hardening behavior and molecular alignment in ultra high molecular weight polyethylene during multi-axial loading conditions," *Biomaterials*, vol. 20, no. 16, pp. 1449 – 1462, 1999.

- [66] D. MacDonald, A. Sakona, A. Ianuzzi, C. M. Rimnac, and S. M. Kurtz, “Do first-generation highly crosslinked polyethylenes oxidize in vivo?,” *Clinical Orthopaedics and Related Research*, vol. 469, pp. 2278 – 2285, 2011.
- [67] E. Gomez-Barrena, J.-A. Puertolas, L. Munuera, and Y. T. Konttinen, “Update on UHMWPE research from the bench to the bedside,” *Acta Orthopaedica*, vol. 79, no. 6, pp. 832 – 840, 2008.
- [68] J. Fisher, L. M. Jennings, A. L. Galvin, Z. M. Jin, M. H. Stone, and E. Ingham, “2009 knee society presidential guest lecture: Polyethylene wear in total knees,” *Clinical Orthopaedics and Related Research*, vol. 468, pp. 12 – 18, 2010.
- [69] F. J. Medel, S. M. Kurtz, J. Parvizi, G. R. Klein, M. J. Kraay, and C. M. Rimnac, “In vivo oxidation contributes to delamination but not pitting in polyethylene components for total knee arthroplasty,” *The Journal of Arthroplasty*, vol. 26, no. 5, pp. 802 – 810, 2011.
- [70] F. J. Medel, S. M. Kurtz, P. F. Sharkey, M. S. Austin, G. R. Klein, A. R. Cohen, H. Patel, V. M. Goldberg, M. J. Kraay, and C. M. Rimnac, “Post damage in contemporary posterior-stabilized tibial inserts: Influence of implant design and clinical relevance,” *The Journal of Arthroplasty*, vol. 26, no. 4, pp. 606 – 614, 2011.
- [71] C. A. Jacobs, C. P. Christensen, A. S. Greenwald, and H. McKellop, “Clinical performance of highly cross-linked polyethylenes in total hip arthroplasty,” *The Journal of Bone & Joint Surgery*, vol. 89, no. 12, pp. 2779 – 2786, 2007.
- [72] S. M. Kurtz, J. R. Foulds, C. W. Jewett, S. Srivastav, and A. A. Edidin, “Validation of a small punch testing technique to characterize the mechanical behaviour of ultra-high-molecular-weight polyethylene,” *Biomaterials*, vol. 18, no. 24, pp. 1659 – 1663, 1997.
- [73] A. D. Drozdov and Q. Yuan, “The viscoelastic and viscoplastic behavior of low-density polyethylene,” *International Journal of Solids and Structures*, vol. 40, no. 10, pp. 2321 – 2342, 2003.
- [74] A. D. Drozdov and Q. Yuan, “Effect of annealing on the viscoelastic and viscoplastic responses of low-density polyethylene,” *Journal of Polymer Science Part B: Polymer Physics*, vol. 41, no. 14, pp. 1638 – 1655, 2003.

REFERENCES

- [75] K.-Y. Lee and D. Pienkowski, "Compressive creep characteristics of extruded ultrahigh-molecular-weight polyethylene," *Journal of Biomedical Materials Research*, vol. 39, no. 2, pp. 261 – 265, 1998.
- [76] K.-Y. Lee, D. Pienkowski, and S. Lee, "Dynamic compressive creep of extruded ultra-high molecular weight polyethylene," *KSME International Journal*, vol. 17, no. 9, pp. 1332 – 1338, 2003.
- [77] K.-Y. Lee and D. Pienkowski, "Reduction in the initial wear of ultrahigh molecular weight polyethylene after compressive creep deformation," *Wear*, vol. 203 - 204, pp. 375 – 379, 1997. 11th International Conference on Wear of Materials.
- [78] E. Brown, R. Willms, I. Gray, G.T., P. Rae, C. Cady, K. Vecchio, J. Flowers, and M. Martinez, "Influence of molecular conformation on the constitutive response of polyethylene: A comparison of HDPE, UHMWPE, and PEX," *Experimental Mechanics*, vol. 47, no. 3, pp. 381 – 393, 2007.
- [79] B. D. Beake, G. A. Bell, W. Brostow, and W. Chonkaew, "Nanoindentation creep and glass transition temperatures in polymers," *Polymer International*, vol. 56, no. 6, pp. 773 – 778, 2007.
- [80] B. Beake, "Modelling indentation creep of polymers: a phenomenological approach," *Journal of Physics D: Applied Physics*, vol. 39, no. 20, p. 4478, 2006.
- [81] Y. Hu, T. Liu, J. Ding, and W. Zhong, "Behavior of high density polyethylene and its nanocomposites under static and dynamic compression loadings," *Polymer Composites*, vol. 34, no. 3, pp. 417 – 425, 2013.
- [82] K. K. Wannomae, S. D. Christensen, A. A. Freiberg, S. Bhattacharyya, W. H. Harris, and O. K. Muratoglu, "The effect of real-time aging on the oxidation and wear of highly cross-linked UHMWPE acetabular liners," *Biomaterials*, vol. 27, no. 9, pp. 1980 – 1987, 2006.
- [83] S. M. Kurtz, W. Hozack, M. Marcolongo, J. Turner, C. Rimnac, and A. Edidin, "Degradation of mechanical properties of UHMWPE acetabular liners following long-term implantation," *The Journal of Arthroplasty*, vol. 18, Supplement, pp. 68 – 78, 2003.
- [84] F. Buchanan, B. Sim, and S. Downes, "Influence of packaging conditions on the properties of gamma-irradiated UHMWPE following accelerated ageing and shelf ageing," *Biomaterials*, vol. 20, no. 9, pp. 823 – 837, 1999.

- [85] D. Baker, R. Hastings, and L. Pruitt, "Compression and tension fatigue resistance of medical grade ultra high molecular weight polyethylene: the effect of morphology, sterilization, aging and temperature," *Polymer*, vol. 41, no. 2, pp. 795 – 808, 2000.
- [86] M. Regis, P. Bracco, L. Giorgini, S. Fusi, P. Dalla Pria, L. Costa, and C. Schmid, "Correlation between in vivo stresses and oxidation of UHMWPE in total hip arthroplasty," *Journal of Materials Science: Materials in Medicine*, vol. 25, no. 9, pp. 2185 – 2192, 2014.
- [87] F. Medel, S. Kurtz, D. MacDonald, F. J. Pascual, and J. A. Puértolas, "Does cyclic stress play a role in highly crosslinked polyethylene oxidation?," *Clinical Orthopaedics and Related Research*, vol. 473, no. 3, pp. 1022 – 1029, 2015.
- [88] L. Zhang, Y. Sawae, T. Yamaguchi, T. Murakami, and H. Yang, "Investigation on oxidation of shelf-aged crosslinked ultra-high molecular weight polyethylene (UHMWPE) and its effects on wear characteristics," *Tribology Online*, vol. 10, no. 1, pp. 1 – 10, 2015.
- [89] W. Hasenkamp, N. Thevenaz, J. Villard, A. Bertsch, A. Arami, K. Aminian, A. Terrier, and P. Renaud, "Design and test of a MEMS strain-sensing device for monitoring artificial knee implants," *Biomedical Microdevices*, vol. 15, no. 5, pp. 831 – 839, 2013.
- [90] J. van Dingenen, "High performance Dyneema fibres in composites," *Materials & Design*, vol. 10, no. 2, pp. 101 – 104, 1989.
- [91] C. Ong, C. Boey, R. S. Hixson, and J. O. Sinibaldi, "Advanced layered personnel armor," *International Journal of Impact Engineering*, vol. 38, no. 5, pp. 369 – 383, 2011.
- [92] Z. Zhang, S. Shen, H. Song, and D. Zhang, "Ballistic penetration of Dyneema fiber laminate," *Journal Of Materials Science And Technology - Shenyang*, vol. 14, pp. 265 – 268, 1998.
- [93] R. J. Crawford, "4: Processing of plastics," *Progress in Polymer Science*, vol. 7, pp. 145 – 222, 1981.
- [94] J. Seror, L. Zhu, R. Goldberg, A. J. Day, and J. Klein, "Supramolecular synergy in the boundary lubrication of synovial joints," *Nature communications*, vol. 6, 2015.

REFERENCES

- [95] J. Lankford, C. R. Blanchard, and C. M. Agrawal, "Wear mechanisms and particle generation in ultrahigh molecular weight polyethylene," in *Proceedings of the 1995 Fourteenth Southern Biomedical Engineering Conference*, pp. 270 – 273, April 1995.
- [96] J. Song, "Effects of machining on tribological behavior of ultra high molecular weight polyethylene (UHMWPE) under dry reciprocating sliding," *Wear*, vol. 225 - 229, pp. 716 – 723, 1999.
- [97] M. P. Gispert, A. P. Serro, R. Colaço, E. Pires, and B. Saramago, "The effect of roughness on the tribological behavior of the prosthetic pair uhmwpe/tin-coated stainless steel," *Journal of Biomedical Materials Research Part B: Applied Biomaterials*, vol. 84B, no. 1, pp. 98 – 107, 2008.
- [98] L. C. Benson, J. D. DesJardins, and M. LaBerge, "Effects of in vitro wear of machined and molded UHMWPE tibial inserts on TKR kinematics," *Journal of Biomedical Materials Research*, vol. 58, no. 5, pp. 496 – 504, 2001.
- [99] M. Berins, *Plastics engineering handbook of the society of the plastics industry*. Springer Science & Business Media, 1991.
- [100] A. Kobayashi and K. Saito, "On the cutting mechanism of high polymers," *Journal of Polymer Science*, vol. 58, no. 166, pp. 1377 – 1396, 1962.
- [101] A. Kobayashi, *Machining of plastics*. McGraw-Hill, 1967.
- [102] U. M. Rao, J. D. Cumming, and E. G. Thomsen, "Some observations on the mechanics of orthogonal cutting of Delrin and Zytel plastics," *Journal of Engineering for Industry*, vol. 86, no. 2, pp. 117 – 121, 1964.
- [103] Y. N. Kazanskii, "Machining of polymeric materials by cutting," *Soviet Plastics*, vol. 5, pp. 78 – 85, 1971.
- [104] A. Shokrani, V. Dhokia, and S. T. Newman, "Environmentally conscious machining of difficult-to-machine materials with regard to cutting fluids," *International Journal of Machine Tools and Manufacture*, vol. 57, pp. 83 – 101, 2012.
- [105] C. Rubenstein and R. M. Storie, "The cutting of polymers," *International Journal of Machine Tool Design and Research*, vol. 9, no. 2, pp. 117 – 130, 1969.
- [106] J. W. Carr and C. Feger, "Ultraprecision machining of polymers," *Precision Engineering*, vol. 15, no. 4, pp. 221 – 237, 1993.

REFERENCES

- [107] L. Costa, K. Jacobson, V. Brunella, and P. Bracco, “Effects of microtomy on the material properties of ultra high molecular weight polyethylene,” *Polymer Testing*, vol. 20, no. 6, pp. 649 – 659, 2001.
- [108] D. Wyeth, “An investigation into the mechanics of cutting using data from orthogonally cutting Nylon 66,” *International Journal of Machine Tools and Manufacture*, vol. 48, no. 7 - 8, pp. 896 – 904, 2008.
- [109] D. J. Wyeth and A. G. Atkins, “Mixed mode fracture toughness as a separation parameter when cutting polymers,” *Engineering Fracture Mechanics*, vol. 76, no. 18, pp. 2690 – 2697, 2009.
- [110] S. F. Malak and I. A. Anderson, “Orthogonal cutting of polyurethane foam,” *International Journal of Mechanical Sciences*, vol. 47, no. 6, pp. 867 – 883, 2005.
- [111] E. Oberg, F. D. Jones, H. L. Horton, and H. H. Ryffel, *Machinery’s Handbook (29th Edition) & Guide to Machinery’s Handbook*. Industrial Press, 2012.
- [112] *Quadrant’s Machinist Handbook*. Quadrant Engineering Plastic Products, 2006.
- [113] R. J. Crawford, “6: Fabrication and finishing of plastics,” *Progress in Polymer Science*, vol. 7, pp. 285 – 322, 1981.
- [114] E. A. Reeves, D. C. Barton, D. P. Fitzpatrick, and J. Fisher, “A two-dimensional model of cyclic strain accumulation in ultra-high molecular weight polyethylene knee replacements,” *Proceedings of the Institution of Mechanical Engineers, Part H: Journal of Engineering in Medicine*, vol. 212, no. 3, pp. 189 – 198, 1998.
- [115] A. Kobayashi and N. Ohtani, “Prefatigue hysteresis effects on viscoelastic crack propagation,” *Journal of Applied Polymer Science*, vol. 21, no. 10, pp. 2861 – 2866, 1977.
- [116] J. Yan and J. S. Strenkowski, “A finite element analysis of orthogonal rubber cutting,” *Journal of Materials Processing Technology*, vol. 174, pp. 102 – 108, 2006.
- [117] K. Q. Xiao and L. C. Zhang, “The role of viscous deformation in the machining of polymers,” *International Journal of Mechanical Sciences*, vol. 44, no. 11, pp. 2317 – 2336, 2002.
- [118] C. F. Popelar, C. H. Popelar, and V. H. Kenner, “Viscoelastic material characterization and modeling for polyethylene,” *Polymer Engineering & Science*, vol. 30, no. 10, pp. 577 – 586, 1990.

REFERENCES

- [119] D. Lucca, R. Rhorer, and R. Komanduri, "Energy dissipation in the ultraprecision machining of copper," *CIRP Annals - Manufacturing Technology*, vol. 40, no. 1, pp. 69 – 72, 1991.
- [120] K. S. Woon, M. Rahman, K. S. Neo, and K. Liu, "The effect of tool edge radius on the contact phenomenon of tool-based micromachining," *International Journal of Machine Tools and Manufacture*, vol. 48, no. 12 - 13, pp. 1395 – 1407, 2008.
- [121] D. Dornfeld, S. Min, and Y. Takeuchi, "Recent advances in mechanical micromachining," *CIRP Annals - Manufacturing Technology*, vol. 55, no. 2, pp. 745 – 768, 2006.
- [122] S. Son, H. Lim, and J. Ahn, "The effect of vibration cutting on minimum cutting thickness," *International Journal of Machine Tools and Manufacture*, vol. 46, no. 15, pp. 2066 – 2072, 2006.
- [123] R. Connolly and C. Rubenstein, "The mechanics of continuous chip formation in orthogonal cutting," *International Journal of Machine Tool Design and Research*, vol. 8, no. 3, pp. 159 – 187, 1968.
- [124] M. E. Abdelmoneim and R. Scrutton, "Tool edge roundness and stable build-up formation in finish machining," *Journal of Manufacturing Science and Engineering*, vol. 96, no. 4, pp. 1258 – 1267, 1974.
- [125] D. Taminiau and J. Dautzenberg, "Bluntness of the tool and process forces in high-precision cutting," *CIRP Annals - Manufacturing Technology*, vol. 40, no. 1, pp. 65 – 68, 1991.
- [126] F. Z. Fang and Y. C. Liu, "On minimum exit-burr in micro cutting," *Journal of Micromechanics and Microengineering*, vol. 14, no. 7, p. 984, 2004.
- [127] H. U. Lee, D.-W. Cho, and K. F. Ehmann, "A mechanistic model of cutting forces in micro-end-milling with cutting-condition-independent cutting force coefficients," *Journal of Manufacturing Science and Engineering*, vol. 130, no. 3, pp. 1 – 9, 2008.
- [128] L. Rebaioli, G. Biella, M. Annoni, J. R. Mayor, and Q. Semeraro, "Applicability of an orthogonal cutting slip-line field model for the microscale," *Proceedings of the Institution of Mechanical Engineers, Part B: Journal of Engineering Manufacture*, In Press, 2014.

- [129] X. Lai, H. Li, C. Li, Z. Lin, and J. Ni, "Modelling and analysis of micro scale milling considering size effect, micro cutter edge radius and minimum chip thickness," *International Journal of Machine Tools and Manufacture*, vol. 48, no. 1, pp. 1 – 14, 2008.
- [130] M. Masuko, J. Kumabe, and S. Ammi, "On the tool wear in cutting of plastics," *Bulletin of JSME*, vol. 7, no. 25, pp. 209 – 215, 1964.
- [131] G. P. Gubbels, G. J. F. T. van der Beek, A. L. Hoep, F. L. M. Delbressine, and H. van Halewijn, "Diamond tool wear when cutting amorphous polymers," *CIRP Annals - Manufacturing Technology*, vol. 53, no. 1, pp. 447 – 450, 2004.
- [132] Y. Kakinuma, S. Kidani, and T. Aoyama, "Ultra-precision cryogenic machining of viscoelastic polymers," *CIRP Annals - Manufacturing Technology*, vol. 61, no. 1, pp. 79 – 82, 2012.
- [133] C. R. Friedrich, "Near-cryogenic machining of polymethyl methacrylate for micromilling tool development," *Materials and Manufacturing Processes*, vol. 15, no. 5, pp. 667 – 678, 2000.
- [134] Y. Kakinuma, N. Yasuda, and T. Aoyama, "Micromachining of soft polymer material applying cryogenic cooling," *Journal of Advanced Mechanical Design, Systems, and Manufacturing*, vol. 2, no. 4, pp. 560 – 569, 2008.
- [135] V. G. Dhokia, S. T. Newman, P. Crabtree, and M. P. Ansell, "A process control system for cryogenic CNC elastomer machining," *Robotics and Computer-Integrated Manufacturing*, vol. 27, no. 4, pp. 779 – 784, 2011.
- [136] V. G. Dhokia, S. T. Newman, P. Crabtree, and M. P. Ansell, "A methodology for the determination of foamed polymer contraction rates as a result of cryogenic CNC machining," *Robotics and Computer-Integrated Manufacturing*, vol. 26, no. 6, pp. 665 – 670, 2010.
- [137] P. Crabtree, V. G. Dhokia, S. T. Newman, and M. P. Ansell, "Manufacturing methodology for personalised symptom-specific sports insoles," *Robotics and Computer-Integrated Manufacturing*, vol. 25, no. 6, pp. 972 – 979, 2009.
- [138] V. G. Dhokia, A. Nassehi, S. A. Wolf, and S. T. Newman, "Cryogenic CNC machining of individualised packaging," in *Proceedings of the 37th International MATADOR Conference*, pp. 165 – 168, 2012.

REFERENCES

- [139] V. G. Dhokia, S. T. Newman, P. Crabtree, and M. P. Ansell, "The formation of adiabatic shear bands as a result of cryogenic CNC machining of elastomers," in *Proceedings of the 36th International MATADOR Conference*, pp. 235 – 238, Springer London, 2010.
- [140] V. G. Dhokia, S. T. Newman, P. Crabtree, and M. P. Ansell, "Adiabatic shear band formation as a result of cryogenic CNC machining of elastomers," *Proceedings of the Institution of Mechanical Engineers, Part B: Journal of Engineering Manufacture*, vol. 225, no. 9, pp. 1482 – 1492, 2011.
- [141] J. Brunette, M. Jeu-Hérault, V. Songmene, and J. Masounave, "Understanding and characterizing the drilling of recycled plastics," *Machining Science and Technology*, vol. 8, no. 1, pp. 141 – 170, 2004.
- [142] J. P. Davim, L. R. Silva, A. Festas, and A. Abrão, "Machinability study on precision turning of PA66 polyamide with and without glass fiber reinforcing," *Materials & Design*, vol. 30, no. 2, pp. 228 – 234, 2009.
- [143] N. N. Z. Gindy, "Minimum energy criterion applied to the orthogonal machining of polymers," *International Journal of Production Research*, vol. 26, no. 11, pp. 1769 – 1778, 1988.
- [144] N. N. Z. Gindy, "Critical rake angle and cutting forces prediction in the orthogonal cutting of polymers," *International Journal of Production Research*, vol. 26, no. 9, pp. 1535 – 1545, 1988.
- [145] A. Kobayashi, M. Munemura, N. Ohtani, and H. Suemasu, "Estimation of heat evolution during viscoelastic crack propagation by liquid crystal film technique," *Journal of Applied Polymer Science*, vol. 27, no. 10, pp. 3763 – 3768, 1982.
- [146] Y. Dogu, E. Aslan, and N. Camuscu, "A numerical model to determine temperature distribution in orthogonal metal cutting," *Journal of Materials Processing Technology*, vol. 171, no. 1, pp. 1 – 9, 2006.
- [147] J. Kaminski and B. Alvelid, "Temperature reduction in the cutting zone in water-jet assisted turning," *Journal of Materials Processing Technology*, vol. 106, no. 1 - 3, pp. 68 – 73, 2000.
- [148] S. Bahadur and K. Ludema, "The viscoelastic nature of the sliding friction of polyethylene, polypropylene and copolymers," *Wear*, vol. 18, no. 2, pp. 109 – 128, 1971.

- [149] S. Bahadur, “Dependence of polymer sliding friction on normal load and contact pressure,” *Wear*, vol. 29, no. 3, pp. 323 – 336, 1974.
- [150] S. Wang, L. Pan, and Q. Li, “Tribological behaviors of polytetrafluoroethylene composites under dry sliding and seawater lubrication,” *Journal of Applied Polymer Science*, vol. 130, no. 4, pp. 2523 – 2531, 2013.
- [151] G. P. H. Gubbels, *Diamond turning of glassy polymers*. PhD thesis, Eindhoven University of Technology, 2006.
- [152] J. L. C. Salles and M. T. T. Gonçalves, “Effects of machining parameters on surface quality of the ultra high molecular weight polyethylene (UHMWPE),” *Matéria*, vol. 8, pp. 1 – 10, 2003.
- [153] S. Yilmaz, A. Arici, and E. Feyzullahoglu, “Surface roughness prediction in machining of cast polyamide using neural network,” *Neural Computing and Applications*, vol. 20, pp. 1249 – 1254, 2011.
- [154] V. Dhokia, S. Kumar, P. Vichare, S. Newman, and R. Allen, “Surface roughness prediction model for CNC machining of polypropylene,” *Proceedings of the Institution of Mechanical Engineers, Part B: Journal of Engineering Manufacture*, vol. 222, no. 2, pp. 137 – 157, 2008.
- [155] V. G. Dhokia, S. Kumar, P. Vichare, and S. T. Newman, “An intelligent approach for the prediction of surface roughness in ball-end machining of polypropylene,” *Robotics and Computer-Integrated Manufacturing*, vol. 24, no. 6, pp. 835 – 842, 2008.
- [156] A. Bruzzone, H. Costa, P. Lonardo, and D. Lucca, “Advances in engineered surfaces for functional performance,” *CIRP Annals - Manufacturing Technology*, vol. 57, no. 2, pp. 750 – 769, 2008.
- [157] P. Benardos and G.-C. Vosniakos, “Predicting surface roughness in machining: a review,” *International Journal of Machine Tools and Manufacture*, vol. 43, no. 8, pp. 833 – 844, 2003.
- [158] M. R. Jackson and T. C. Buttery, “Some effects of machine parameters on cutting forces and surface geometry in the rotary planing of wood and polymers,” *Second Joint Polytechnics Symposium on Manufacturing Engineering*, vol. 2, pp. 196 – 201, 1979.

REFERENCES

- [159] M. Alauddin, I. Choudhury, M. E. Baradie, and M. Hashmi, "Plastics and their machining: A review," *Journal of Materials Processing Technology*, vol. 54, pp. 40 – 46, 1995.
- [160] G. Byrne, D. Dornfeld, and B. Denkena, "Advancing cutting technology," *CIRP Annals - Manufacturing Technology*, vol. 52, no. 2, pp. 483 – 507, 2003.
- [161] B. Denkena, J. Köhler, and M. Mengesha, "Influence of the cutting edge rounding on the chip formation process: Part 1. Investigation of material flow, process forces, and cutting temperature," *Production Engineering*, vol. 6, no. 4 - 5, pp. 1 – 10, 2012.
- [162] P. K. Yong-hwan, *Behaviour of polymeric materials in machining*. PhD thesis, University of Warwick, May 1989.
- [163] M. Altan and E. Altan, "Investigation of burr formation and surface roughness in drilling engineering plastics," *Journal of the Brazilian Society of Mechanical Sciences and Engineering*, vol. 36, no. 2, pp. 347 – 354, 2014.
- [164] J. C. Campos Rubio, T. H. Panzera, and F. Scarpa, "Machining behaviour of three high-performance engineering plastics," *Proceedings of the Institution of Mechanical Engineers, Part B: Journal of Engineering Manufacture*, vol. 229, pp. 28 – 37, January 2015.
- [165] F. Caiazzo, F. Curcio, G. Daurelio, and F. C. Minutolo, "Laser cutting of different polymeric plastics (PE, PP and PC) by a CO2 laser beam," *Journal of Materials Processing Technology*, vol. 159, no. 3, pp. 279 – 285, 2005.
- [166] R. Teti, K. Jemielniak, G. E. O'Donnell, and D. Dornfeld, "Advanced monitoring of machining operations," *CIRP Annals - Manufacturing Technology*, vol. 59, no. 2, pp. 717 – 739, 2010.
- [167] P. Ervine, *Fundamental Investigations into the Micromilling of a Biomedical Grade Polymer*. PhD thesis, Trinity College Dublin, December 2012.
- [168] R. Komanduri and Z. B. Hou, "A review of the experimental techniques for the measurement of heat and temperatures generated in some manufacturing processes and tribology," *Tribology International*, vol. 34, no. 10, pp. 653 – 682, 2001.

- [169] K. Kerrigan, *Characterisation of an Integrated Telemetric Temperature Sensor for CFRP Milling Applications*. PhD thesis, Trinity College Dublin, December 2012.
- [170] M. A. Davies, T. Ueda, R. M'Saoubi, B. Mullany, and A. L. Cooke, "On the measurement of temperature in material removal processes," *CIRP Annals - Manufacturing Technology*, vol. 56, no. 2, pp. 581 – 604, 2007.
- [171] A. Basti, T. Obikawa, and J. Shinozuka, "Tools with built-in thin film thermocouple sensors for monitoring cutting temperature," *International Journal of Machine Tools and Manufacture*, vol. 47, no. 5, pp. 793 – 798, 2007.
- [172] R. A. Fisher, "The use of multiple measurements in taxonomic problems," *Annals of Eugenics*, vol. 7, no. 2, pp. 179 – 188, 1936.
- [173] G. E. Box, J. S. Hunter, and W. G. Hunter, *Statistics for experimenters: design, innovation, and discovery*, vol. 2. Wiley Online Library, 2005.
- [174] E. Mullins, *Statistics for the quality control chemistry laboratory*. Royal Society of Chemistry, 2003.
- [175] N. Hope and A. Bellare, "A comparison of the efficacy of various antioxidants on the oxidative stability of irradiated polyethylene," *Clinical Orthopaedics and Related Research*, vol. 473, no. 3, pp. 936 – 941, 2015.
- [176] G. Lewis, "Properties of crosslinked ultra-high-molecular-weight polyethylene," *Biomaterials*, vol. 22, no. 4, pp. 371 – 401, 2001.
- [177] *GUR Ultra-high Molecular Weight Polyethylene (PE-UHMW)*. Ticona GmbH, 2001.

Appendix

Appendix A

DSC Report

In this report references are made to samples 1 - 6. These correspond to the following samples:

Table A.1: Sample numbers for material analysis.

| Number | Corresponding sample |
|--------|----------------------|
| 1 | UHMWPE Core |
| 2 | UHMWPE Surface |
| 3 | AOX Core |
| 4 | AOX Surface |
| 5 | XLK Core |
| 6 | XLK Surface |

Differential scanning calorimetry (DSC)

The samples were tested using a TA 2010 differential scanning calorimeter shown in Figure 1. The samples (15.5 +/- 0.5 mg) were placed and sealed in aluminium pans, and tested within a temperature range of -140 to 220 °C. All DSC tests were carried out under a 30 mL per minute flow of nitrogen to prevent oxidation. Calibration of the instrument was performed using indium as standard (see Figure 2).



Figure 1 A TA 2010 differential scanning calorimeter.

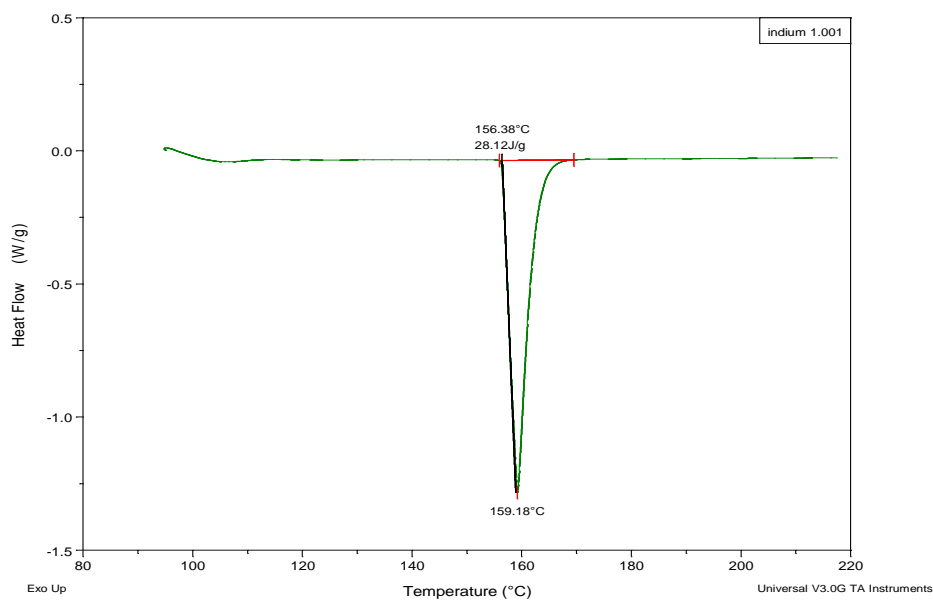


Figure 2 Thermogram of the calibration standard Indium with an onset temperature of 156.38 °C.

The thermal history was removed from each of the samples to get an accurate view of the materials(this is common practice for processed materials). This was achieved by heating the sample above its melt and then cooling, after which the test begins. To illustrate the effect of the removal of the thermal history, there is a difference of 4.36 °C between the first and second run as presented in Figure 3.

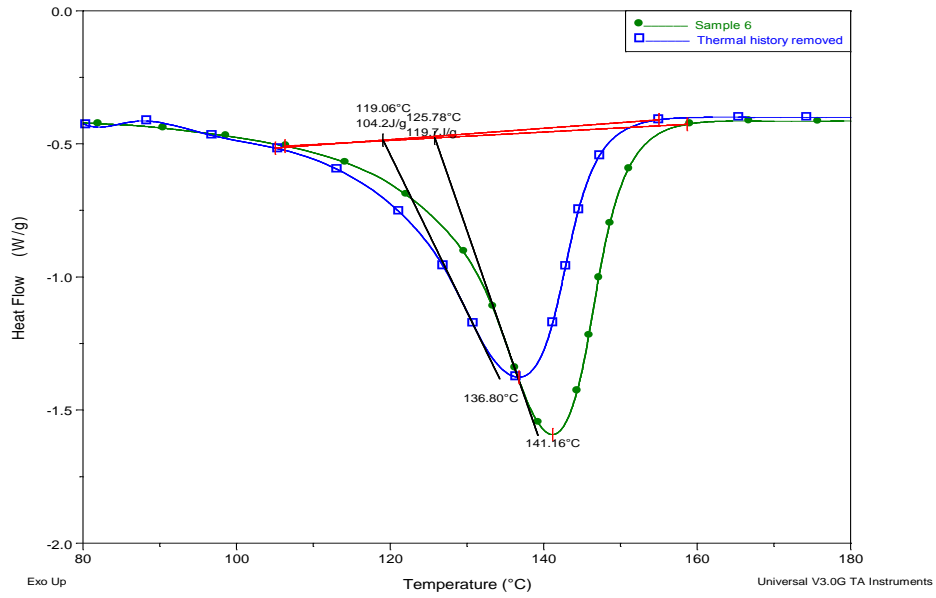


Figure 3 Effects of removing the thermal history.

The combined melts are shown in Figure 4(thermal history removed)

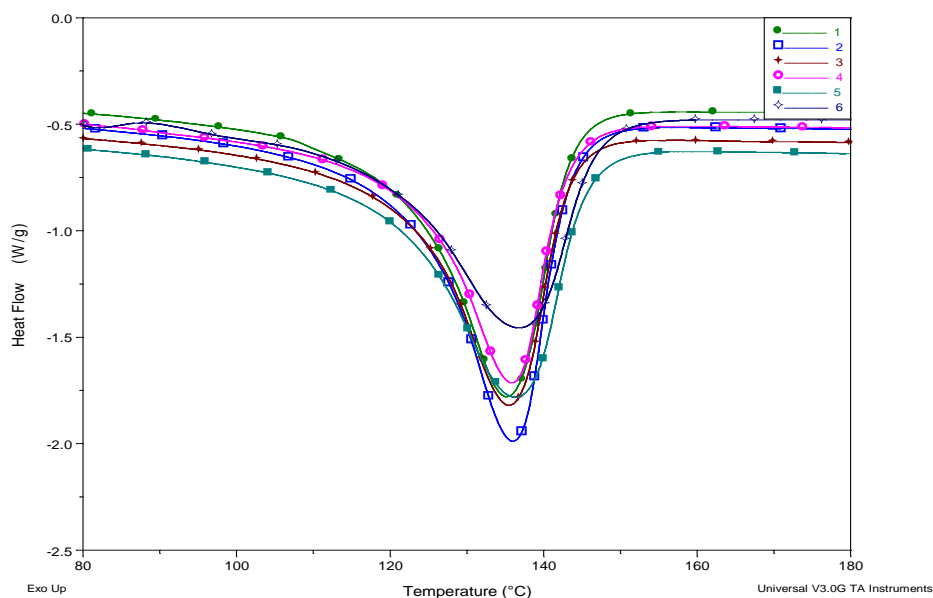


Figure 4 The melt temperatures of all samples.

Due to the nature of the polymer and the highly crystalline structure of the materials, the DSC did not show strong significant data that there was a shift in the base line at sub-ambient temperatures; thus the T_g (glass transition) was difficult to quantify. Regarding the end use of the material, the T_g at that temperature will not affect the properties at body temperature, that is, assuming the material is not significantly altered both chemically or physically. From the Hand book of UHMWPE, the T_g is referenced as -160°C and our system went to -140°C .

(http://books.google.ie/books?id=bkuFjppEdMcC&pg=PA7&lpg=PA7&dq=lg+of+ultra+high+molecular+weight+polyethylene&source=bl&ots=plei4INET7&sig=btWjEjxJTGTp50A_Tx_3PEKXilE&hl=en&ei=IPiXTv6flcS5hAfv9LyKBA&sa=X&oi=book_result&ct=result&resnum=4&ved=0CDcQ6AEwAw#v=onepage&q&f=false).

The following are the thermograms of the study and all of the melts are in line with the referenced value from the Handbook.

Appendix A

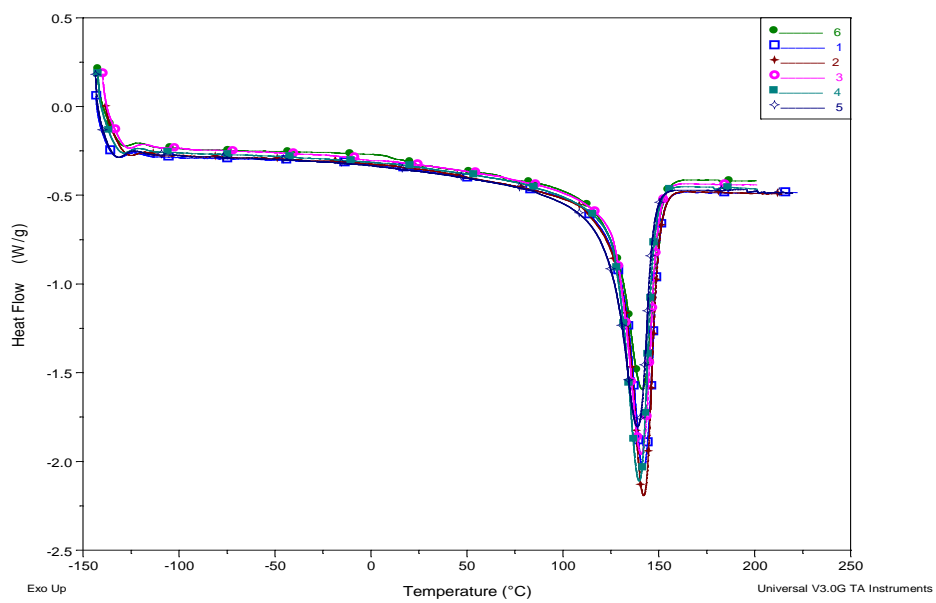


Figure 4 All of thermograms on the first run.

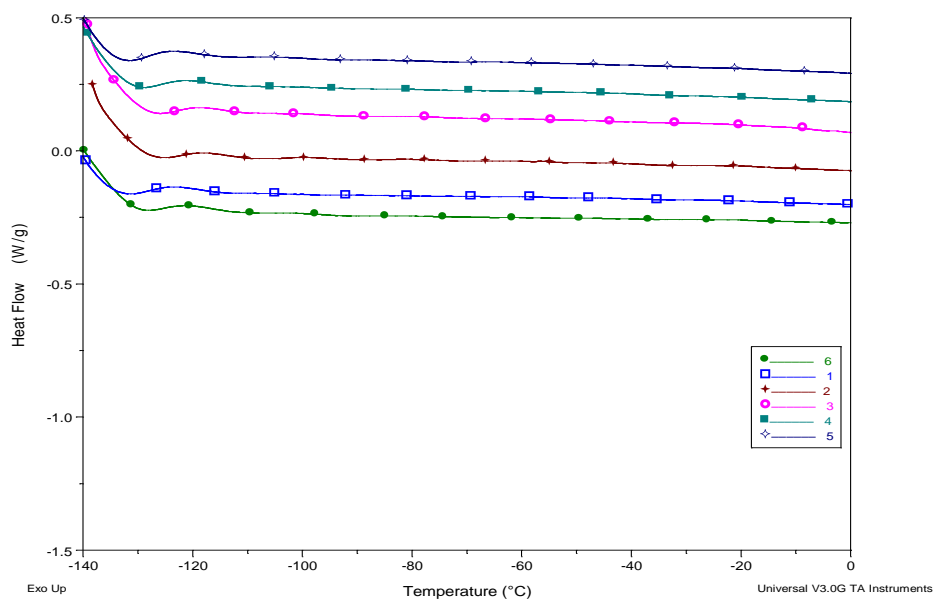


Figure 5 All of thermograms on the first run from -140 to 0 °C.

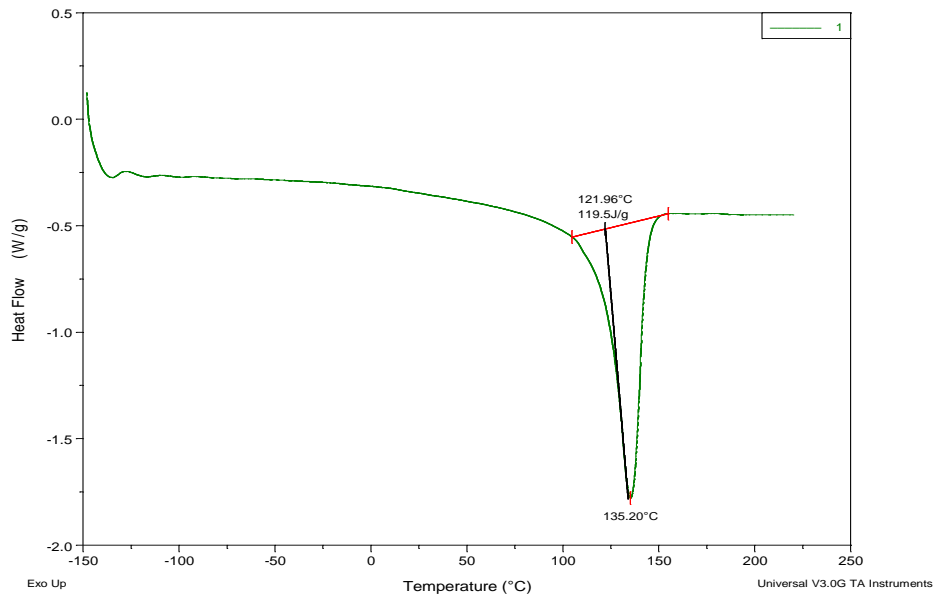


Figure 6 Thermogram of sample 1.

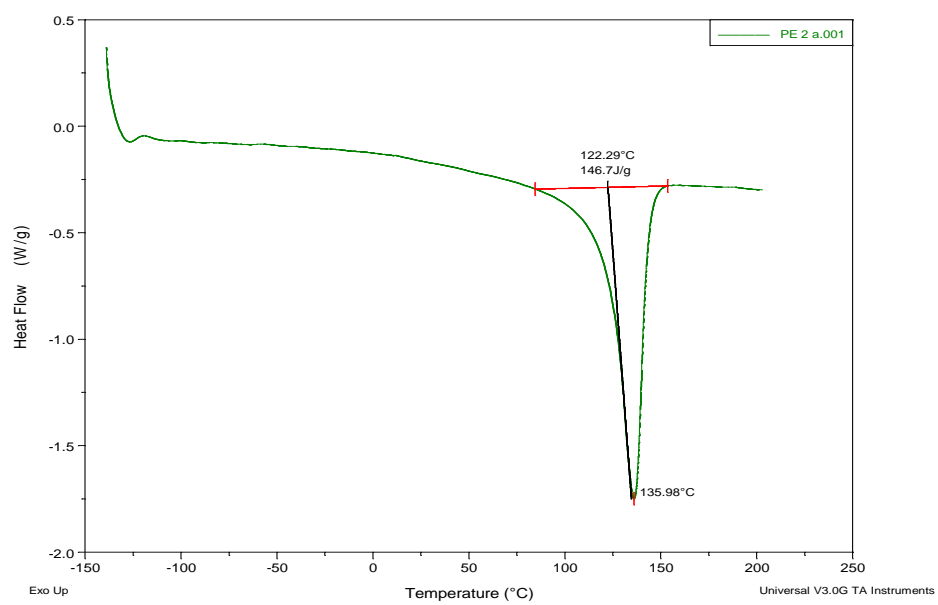


Figure 7 Thermogram of sample 2.

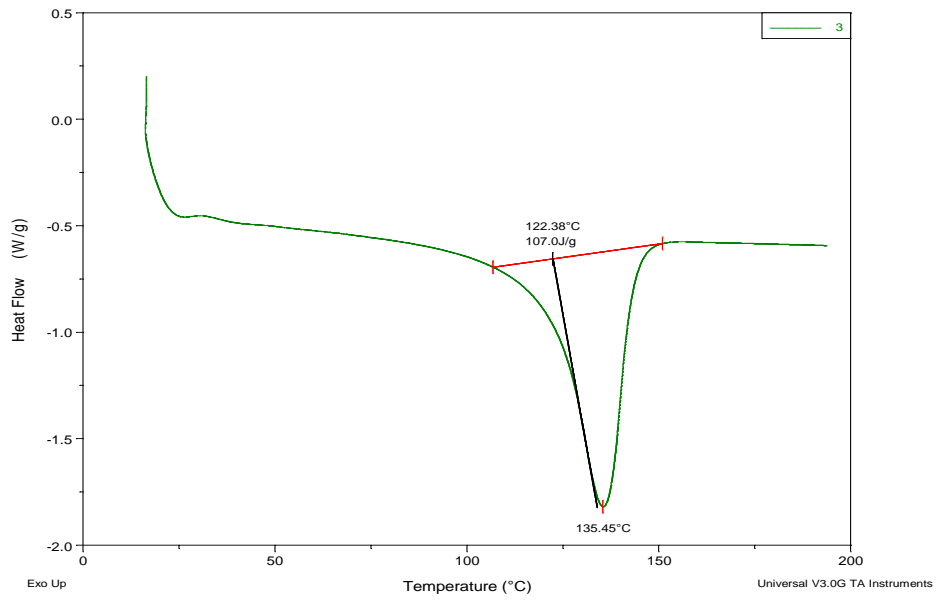


Figure 7 Thermogram of sample 3.

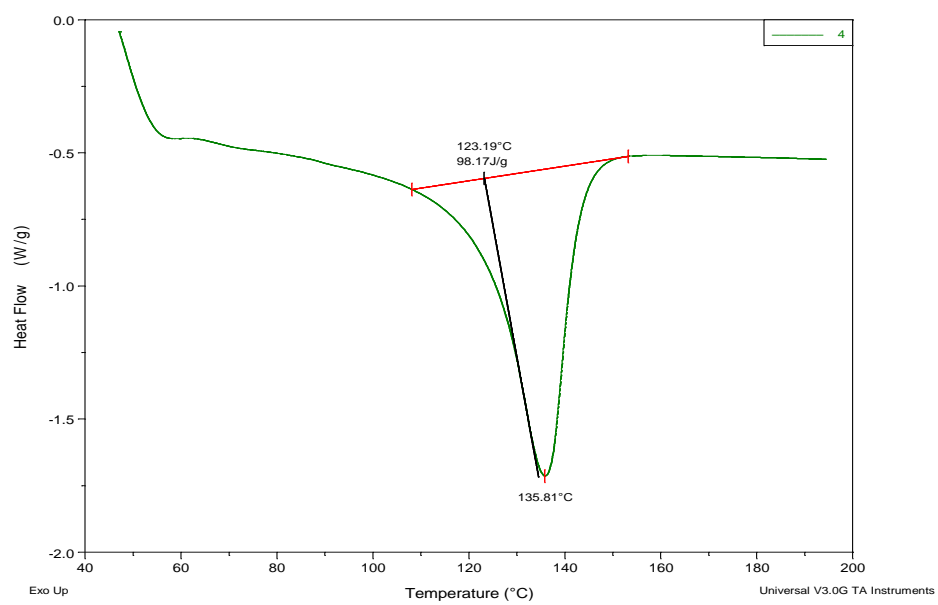


Figure 8 Thermogram of sample 4.

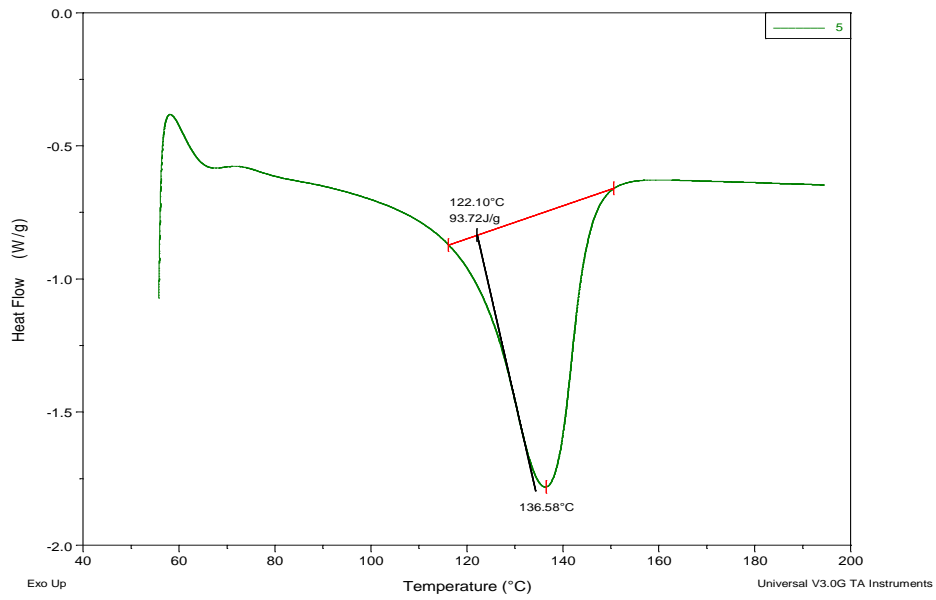


Figure 9 Thermogram of sample 5.

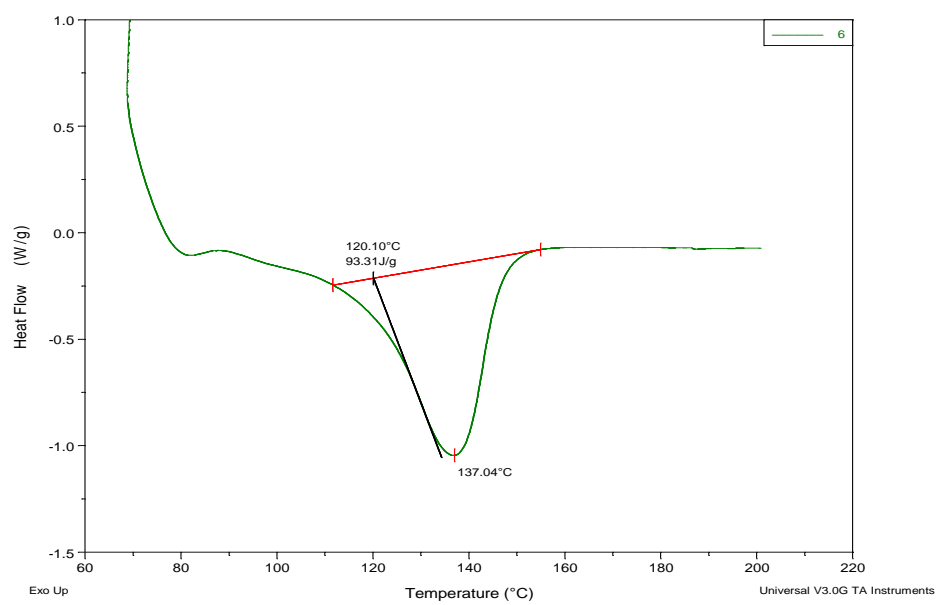


Figure 10 Thermogram of sample 6.

Appendix A

Appendix B

Tensile testing

This appendix contains data from standard tensile tests performed on samples of UHMWPE which were at room temperature, and samples which were cryogenically cooled. This data is intended to illustrate the effects of temperature and strain rate on stiffness and elongation to failure.

Typical stress-strain curves for plain UHMWPE are shown in figure B.1. It can be seen that cryogenically cooled samples have a significantly higher yield stress, which varies slightly with strain rate. For room temperature samples the strain to failure is higher for 100 *mm/min* strain rate than for 1000 *mm/min* strain rate, whereas for cryogenically cooled samples the strain to failure is approximately equal for both strain rates. Significant necking was evident on all samples after failure, as would be expected with such high elongations to failure.

Appendix B

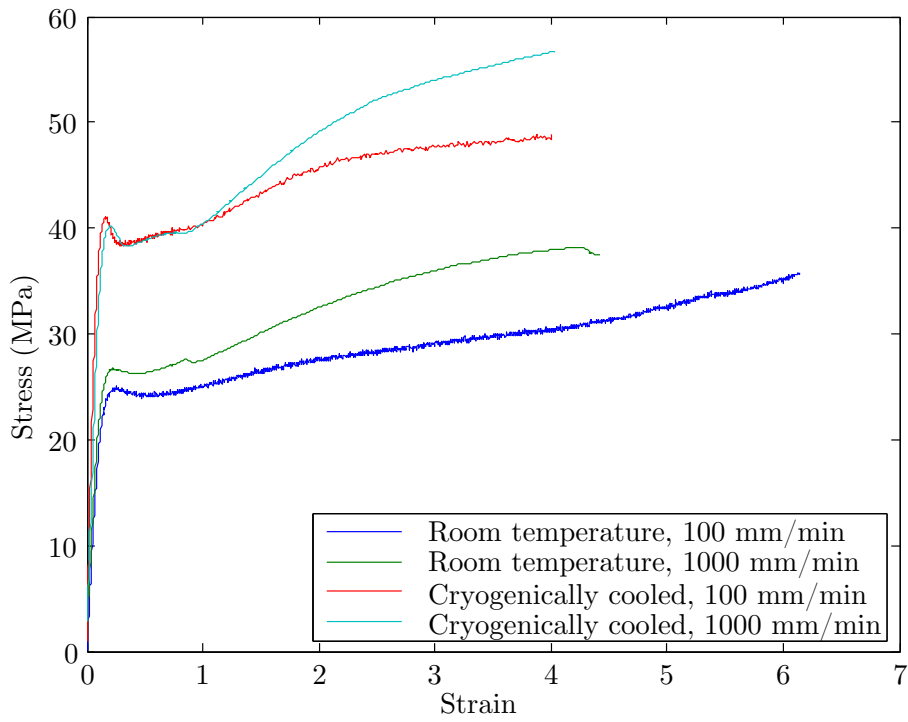


Figure B.1: Tensile testing results for varying sample temperature and strain rate.

Appendix C

Statistical analysis of tool temperature in machining

This appendix contains the statistical analysis of the peak tool temperature response for the results shown in chapters 5 and 6.

C.1 Results corresponding to chapter 5

The main effects for tool temperature are shown in figure C.1. AOX and XLK have lower average temperatures than UHMWPE, possibly indicating that crosslinking and adding an antioxidant improve the heat capacity of the material, or have lower coefficients of friction. Rake angle shows a strong effect on peak temperature, reducing from 108°C at -20° rake angle to 60°C at 40° rake angle. This could be related to the lower cutting and thrust forces at higher rake angles, indicating that there is a correlation between temperature and cutting forces. The effect of sharpness shows a counterintuitive effect, with worn tools having a higher peak temperature than highly worn. This may be a result of machining with highly worn tools causing deformation or smearing of the material rather than cutting, leading to a smaller contact area, as shown in figure 2.12. The highest single temperature measured was 186°C (XLK, 0° rake angle, highly worn tool, 300 m/min , 155 mm/rev), which far exceeds the melting temperature established in chapter 4. The thermal inertia of the tool and distance from the cutting edge means that the peak temperature was likely far higher, and that melting of the material is likely occurring.

The effects of cutting speed and depth of cut are difficult to interpret from this data, as the peak temperature is highly sensitive to the duration of the cut, due to the thermal inertia shown, with the duration of the cut being a function of cutting speed and depth of cut. Higher cutting speeds and higher depths of cut result in a shorter cutting time, as is evident in this data, but further conclusions cannot be made without a detailed heat transfer analysis.

The two way interactions for temperature are shown in figure C.2, with a full ANOVA table shown in table C.1. 3 of the 10 two way interactions appear significant:

Appendix C

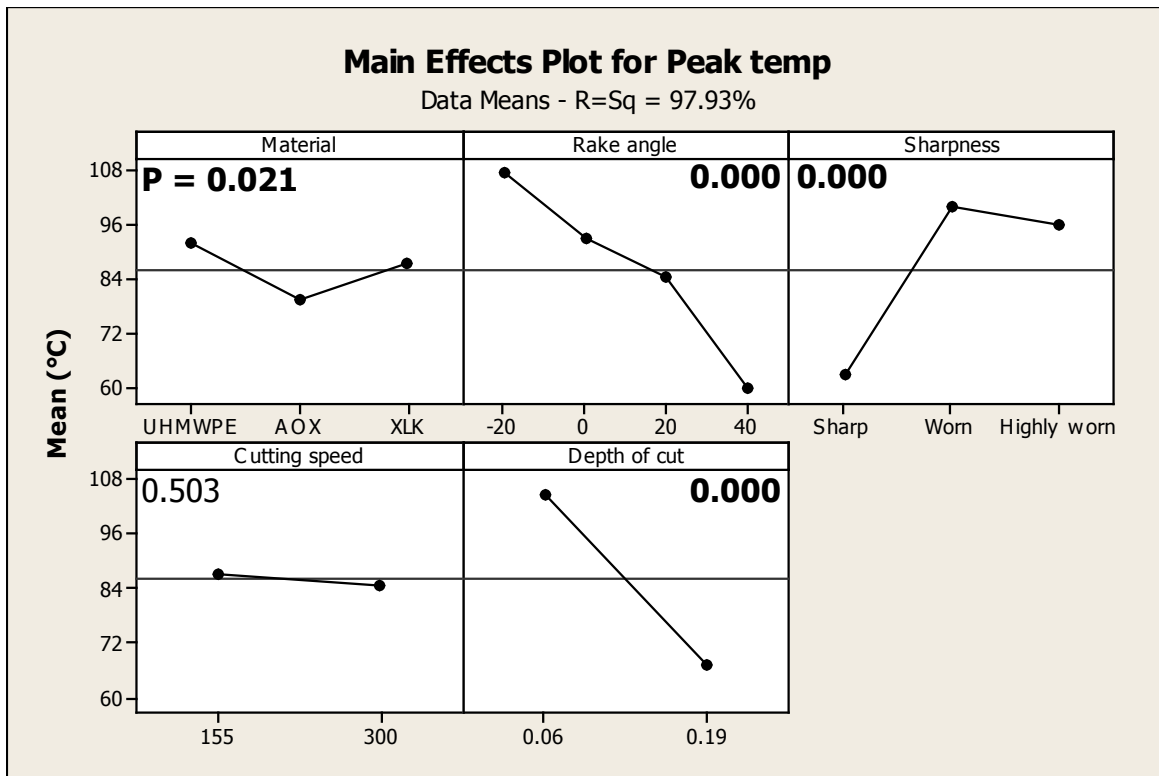


Figure C.1: Main effects plot for temperature.

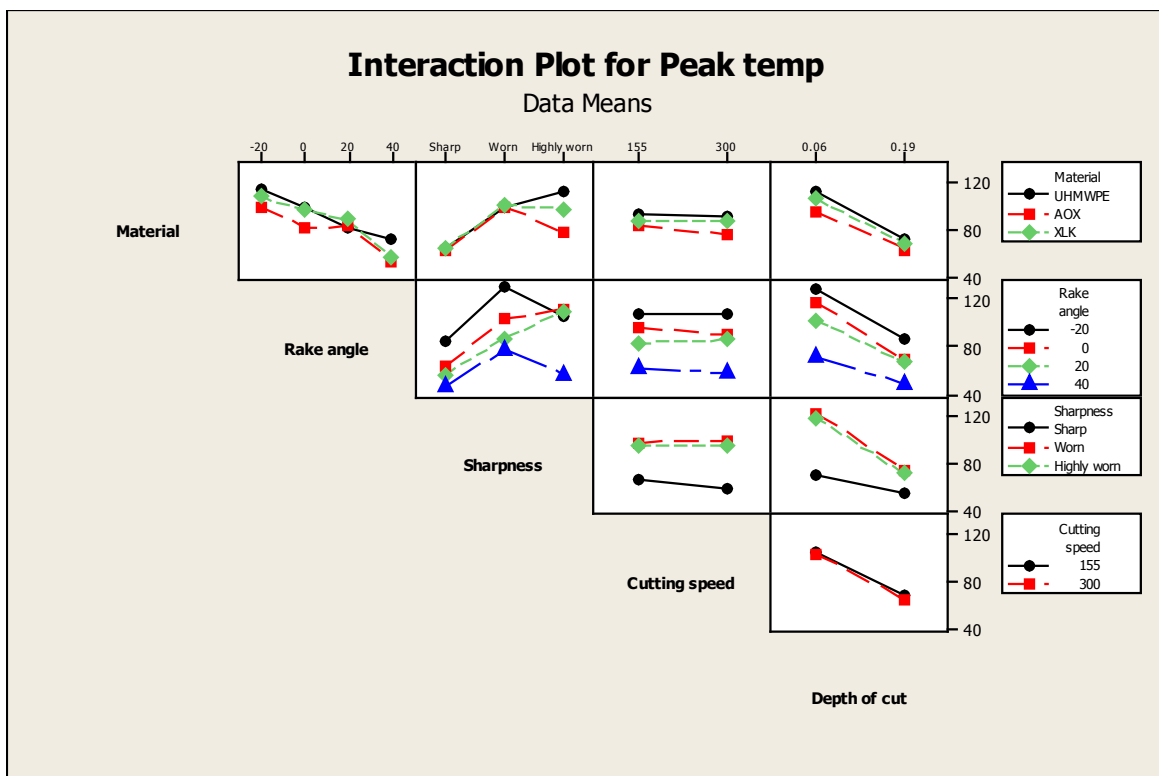


Figure C.2: Interactions plot for temperature.

Material - sharpness, rake angle - sharpness and sharpness - depth of cut. The material - sharpness interaction shows that there is little variation between materials with sharp and worn tools, but large variation with highly worn tools, with AOX having the lowest temperature and UHMWPE having the highest. Rake angle - sharpness shows similar behaviour, with consistent variation between sharp and worn, and much larger variation at the highly worn level.

None of the three and four way interactions for temperature appear significant, quite possibly due to a large proportion of the variation coming from the highly worn data. As a result the ANOVA was repeated with the highly worn data excluded, to assess the effect this data was having on the overall model. The main effects are shown in figure C.3, with the interactions shown in figure C.4 and the full ANOVA table shown in table C.2

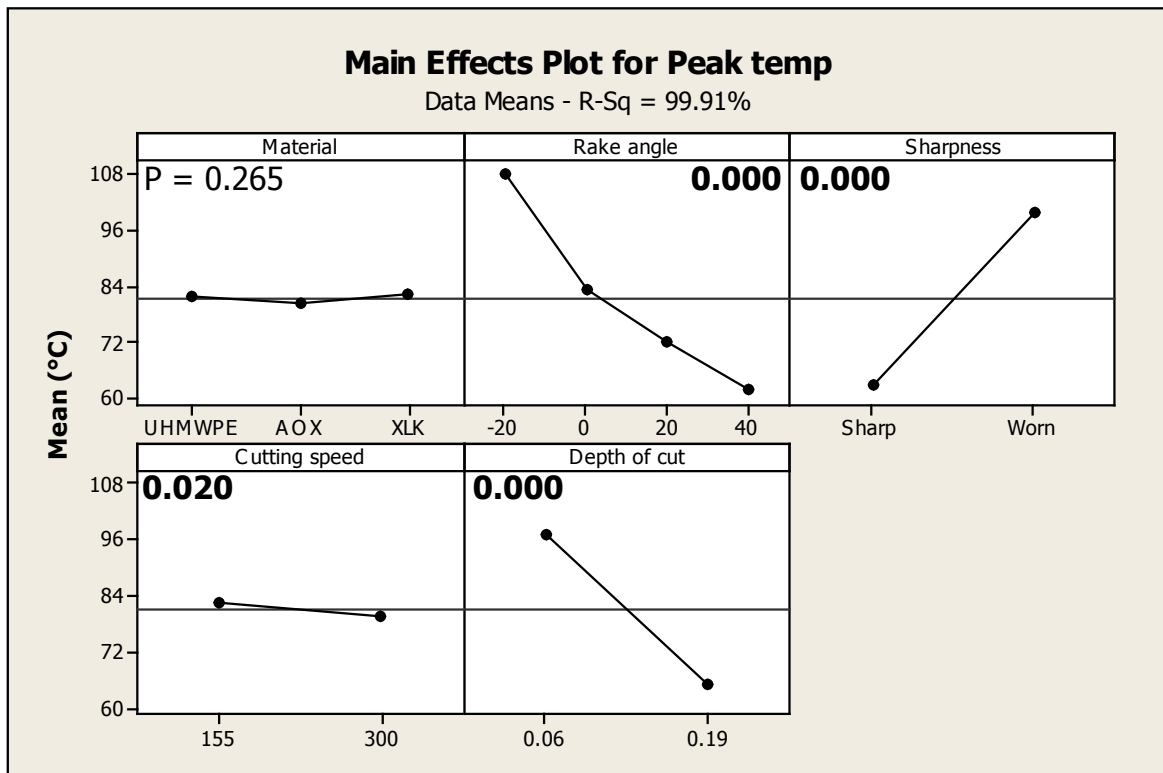


Figure C.3: Main effects plot for temperature, excluding highly worn tools.

The main effects plot shows reduced variation between materials, with the materials factor no longer significant ($P = 0.265$ without highly worn, compared to $P = 0.021$ with), and the cutting speed factor now showing significance ($P = 0.02$ without highly worn, compared to $P = 0.503$ with). This shows that a large amount of the variation in the original model was a result of the highly worn data. This is verified by the change in the Mean Square Error, which reduced from 348.3 to 14.7, and the improvement in

Appendix C

Table C.1: ANOVA table for temperature. $R - Sq = 97.93\%$.

| Source | DF | Seq SS | Adj SS | Adj MS | F | P |
|---------------|-----|----------|---------|---------|--------|-------|
| Material | 2 | 3758.5 | 3758.5 | 1879.2 | 5.4 | 0.021 |
| Rake angle | 3 | 43153.6 | 43153.6 | 14384.5 | 41.3 | 0 |
| Sharpness | 2 | 38956.9 | 38956.9 | 19478.5 | 55.92 | 0 |
| Cutting speed | 1 | 165.9 | 165.9 | 165.9 | 0.48 | 0.503 |
| Depth of cut | 1 | 49334.2 | 49334.2 | 49334.2 | 141.63 | 0 |
| M*R | 6 | 2140.7 | 2140.7 | 356.8 | 1.02 | 0.455 |
| M*S | 4 | 6056.3 | 6056.3 | 1514.1 | 4.35 | 0.021 |
| M*CS | 2 | 360.6 | 360.6 | 180.3 | 0.52 | 0.609 |
| M*DOC | 2 | 348 | 348 | 174 | 0.5 | 0.619 |
| R*S | 6 | 12082 | 12082 | 2013.7 | 5.78 | 0.005 |
| R*CS | 3 | 483.7 | 483.7 | 161.2 | 0.46 | 0.713 |
| R*DOC | 3 | 3155.3 | 3155.3 | 1051.8 | 3.02 | 0.072 |
| S*CS | 2 | 487.5 | 487.5 | 243.7 | 0.7 | 0.516 |
| S*DOC | 2 | 7930.4 | 7930.4 | 3965.2 | 11.38 | 0.002 |
| CS*DOC | 1 | 123.3 | 123.3 | 123.3 | 0.35 | 0.563 |
| M*R*S | 12 | 8244.4 | 8244.4 | 687 | 1.97 | 0.127 |
| M*R*CS | 6 | 1533.5 | 1533.5 | 255.6 | 0.73 | 0.632 |
| M*R*DOC | 6 | 1975.3 | 1975.3 | 329.2 | 0.95 | 0.499 |
| M*S*CS | 4 | 1339.8 | 1339.8 | 334.9 | 0.96 | 0.463 |
| M*S*DOC | 4 | 515.8 | 515.8 | 129 | 0.37 | 0.825 |
| M*CS*DOC | 2 | 583.8 | 583.8 | 291.9 | 0.84 | 0.456 |
| R*S*CS | 6 | 584.6 | 584.6 | 97.4 | 0.28 | 0.936 |
| R*S*DOC | 6 | 4049.9 | 4049.9 | 675 | 1.94 | 0.155 |
| R*CS*DOC | 3 | 586.3 | 586.3 | 195.4 | 0.56 | 0.651 |
| S*CS*DOC | 2 | 266.6 | 266.6 | 133.3 | 0.38 | 0.69 |
| M*R*S*CS | 12 | 2245.8 | 2245.8 | 187.2 | 0.54 | 0.852 |
| M*R*S*DOC | 12 | 2904.6 | 2904.6 | 242 | 0.69 | 0.731 |
| M*R*CS*DOC | 6 | 1998.5 | 1998.5 | 333.1 | 0.96 | 0.493 |
| M*S*CS*DOC | 4 | 1507 | 1507 | 376.8 | 1.08 | 0.408 |
| R*S*CS*DOC | 6 | 1053.7 | 1053.7 | 175.6 | 0.5 | 0.794 |
| Error | 12 | 4179.9 | 4179.9 | 348.3 | - | - |
| Total | 143 | 202106.5 | - | - | - | - |

R-Sq value from 97.93% to 99.91%.

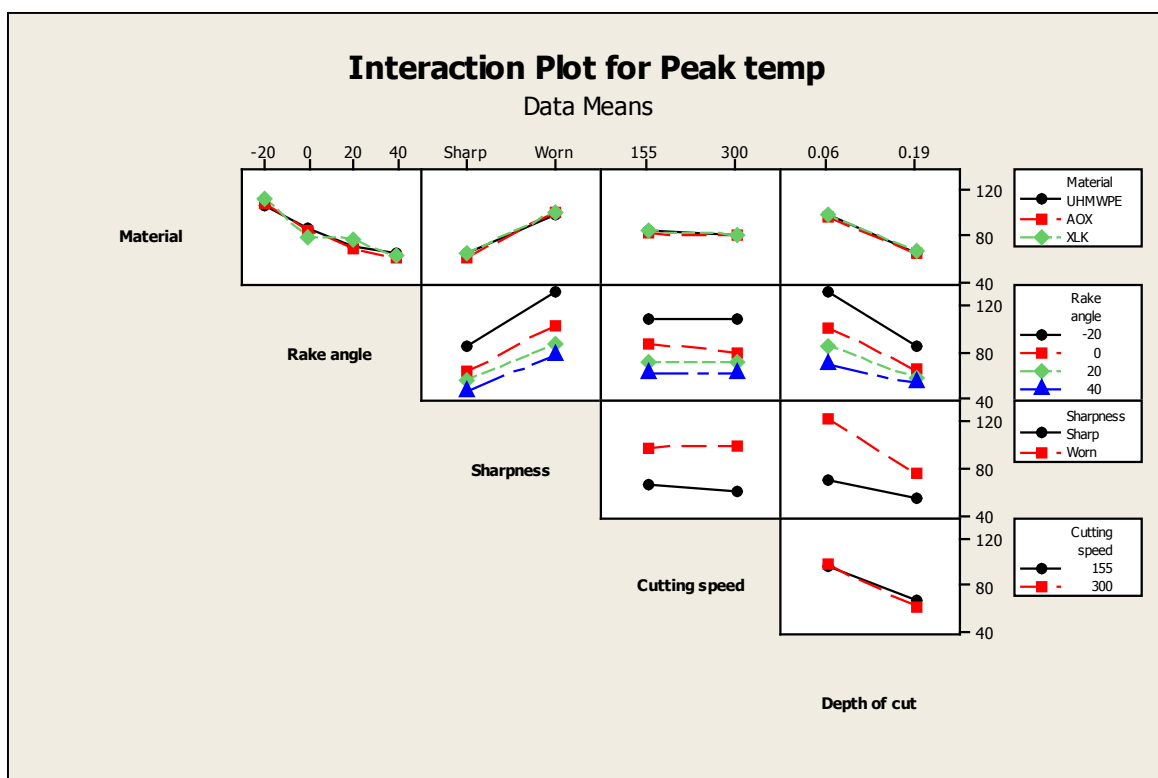


Figure C.4: Interactions plot for temperature, excluding highly worn tools.

This reduction in MSE has allowed the true significance of many of the interactions to be quantified, with 7 of the 10 two way interactions appearing significant, and 4 of the 10 three way interactions appearing significant. Of these two and three way interactions, only 3 do not involve cutting speed or depth of cut, and thus can be analysed without concern of hidden factors. These are material - rake angle, rake angle - sharpness, and material - rake angle - sharpness. All three show increased significance with the reduction in MSE. The significance of interactions involving material is interesting, as when the highly worn data is excluded the material factor does not appear significant. It is clear that further work is required to remove the hidden factor of cutting time, with a more detailed heat transfer analysis required, taking into account the thermal inertia of the tool and the contact areas involved.

C.2 Results corresponding to chapter 6

The main effects and interactions for tool temperature are shown in figures C.5 and C.6, with a full ANOVA table shown in table C.3.

All five factors appear significant, with rake angle, cutting speed and depth of cut showing similar trends as were seen in chapter 5. The sharpness trend differs from

Appendix C

Table C.2: ANOVA table for temperature, excluding highly worn tools. $R-Sq = 99.91\%$.

| Source | DF | Seq SS | Adj SS | Adj MS | F | P |
|---------------|----|----------|---------|---------|---------|-------|
| Material | 2 | 49 | 49 | 24.5 | 1.67 | 0.265 |
| Rake angle | 3 | 28711 | 28711 | 9570.3 | 652.77 | 0 |
| Sharpness | 1 | 32269.9 | 32269.9 | 32269.9 | 2201.07 | 0 |
| Cutting speed | 1 | 145.1 | 145.1 | 145.1 | 9.9 | 0.02 |
| Depth of cut | 1 | 24393 | 24393 | 24393 | 1663.81 | 0 |
| M*R | 6 | 734.4 | 734.4 | 122.4 | 8.35 | 0.01 |
| M*S | 2 | 81.6 | 81.6 | 40.8 | 2.78 | 0.14 |
| M*CS | 2 | 14 | 14 | 7 | 0.48 | 0.642 |
| M*DOC | 2 | 31.3 | 31.3 | 15.6 | 1.07 | 0.402 |
| R*S | 3 | 1002.7 | 1002.7 | 334.2 | 22.8 | 0.001 |
| R*CS | 3 | 227 | 227 | 75.7 | 5.16 | 0.042 |
| R*DOC | 3 | 3243.2 | 3243.2 | 1081.1 | 73.74 | 0 |
| S*CS | 1 | 480.5 | 480.5 | 480.5 | 32.77 | 0.001 |
| S*DOC | 1 | 6029.6 | 6029.6 | 6029.6 | 411.27 | 0 |
| CS*DOC | 1 | 306.6 | 306.6 | 306.6 | 20.91 | 0.004 |
| M*R*S | 6 | 2267.7 | 2267.7 | 378 | 25.78 | 0 |
| M*R*CS | 6 | 467.6 | 467.6 | 77.9 | 5.32 | 0.031 |
| M*R*DOC | 6 | 160.7 | 160.7 | 26.8 | 1.83 | 0.241 |
| M*S*CS | 2 | 257.7 | 257.7 | 128.8 | 8.79 | 0.016 |
| M*S*DOC | 2 | 64.3 | 64.3 | 32.2 | 2.19 | 0.193 |
| M*CS*DOC | 2 | 6 | 6 | 3 | 0.2 | 0.82 |
| R*S*CS | 3 | 131.4 | 131.4 | 43.8 | 2.99 | 0.118 |
| R*S*DOC | 3 | 637.1 | 637.1 | 212.4 | 14.48 | 0.004 |
| R*CS*DOC | 3 | 26.3 | 26.3 | 8.8 | 0.6 | 0.639 |
| S*CS*DOC | 1 | 52.7 | 52.7 | 52.7 | 3.59 | 0.107 |
| M*R*S*CS | 6 | 269.3 | 269.3 | 44.9 | 3.06 | 0.1 |
| M*R*S*DOC | 6 | 366.2 | 366.2 | 61 | 4.16 | 0.053 |
| M*R*CS*DOC | 6 | 183.1 | 183.1 | 30.5 | 2.08 | 0.197 |
| M*S*CS*DOC | 2 | 39.9 | 39.9 | 20 | 1.36 | 0.325 |
| R*S*CS*DOC | 3 | 152.6 | 152.6 | 50.9 | 3.47 | 0.091 |
| Error | 6 | 88 | 88 | 14.7 | - | - |
| Total | 95 | 102889.5 | - | - | - | - |

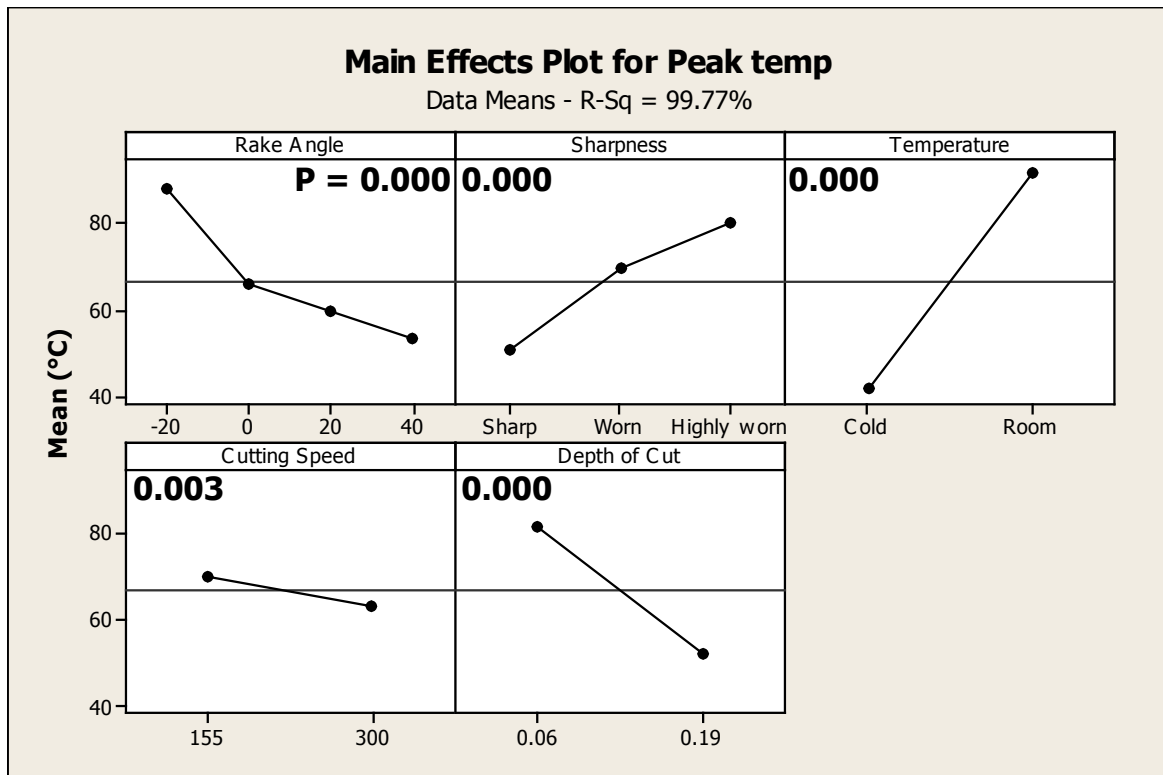


Figure C.5: Main effects plot for peak temperature for plain UHMWPE, including cryogenically cooled workpieces.

that seen previously, but examination of the material - sharpness interaction in figure C.2 shows that plain UHMWPE at room temperature only has a similar effect due to sharpness as that seen here. The scale of the effect of workpiece temperature is evident, however this is as a result of shorter cuts being taken on the cryogenically pre-cooled workpieces. Similarly, the effect of cutting speed and depth of cut is deceptive, as the duration of the cut and thus the heat transferred are a function of these factors. There were no statistically significant interactions which did not involve temperature, cutting speed or depth of cut.

Appendix C

Table C.3: ANOVA table for peak temperature for plain UHMWPE, including cryogenically cooled workpieces. $R - Sq = 99.77\%$.

| Source | DF | Seq SS | Adj SS | Adj MS | F | P |
|---------------|----|----------|---------|---------|---------|-------|
| Rake Angle | 3 | 16552.2 | 16552.2 | 5517.4 | 102.12 | 0 |
| Sharpness | 2 | 14129.6 | 14129.6 | 7064.8 | 130.76 | 0 |
| Temperature | 1 | 60089.3 | 60089.3 | 60089.3 | 1112.16 | 0 |
| Cutting Speed | 1 | 1204.7 | 1204.7 | 1204.7 | 22.3 | 0.003 |
| Depth of Cut | 1 | 20560.5 | 20560.5 | 20560.5 | 380.54 | 0 |
| R*S | 6 | 1052.6 | 1052.6 | 175.4 | 3.25 | 0.089 |
| R*T | 3 | 3338.7 | 3338.7 | 1112.9 | 20.6 | 0.001 |
| R*CS | 3 | 244.2 | 244.2 | 81.4 | 1.51 | 0.306 |
| R*DOC | 3 | 416.5 | 416.5 | 138.8 | 2.57 | 0.15 |
| S*T | 2 | 6174.1 | 6174.1 | 3087.1 | 57.14 | 0 |
| S*CS | 2 | 132.4 | 132.4 | 66.2 | 1.23 | 0.358 |
| S*DOC | 2 | 2543.9 | 2543.9 | 1271.9 | 23.54 | 0.001 |
| T*CS | 1 | 890.9 | 890.9 | 890.9 | 16.49 | 0.007 |
| T*DOC | 1 | 3103 | 3103 | 3103 | 57.43 | 0 |
| CS*DOC | 1 | 59.1 | 59.1 | 59.1 | 1.09 | 0.336 |
| R*S*T | 6 | 3309.7 | 3309.7 | 551.6 | 10.21 | 0.006 |
| R*S*CS | 6 | 950.4 | 950.4 | 158.4 | 2.93 | 0.108 |
| R*S*DOC | 6 | 1621.9 | 1621.9 | 270.3 | 5 | 0.035 |
| R*T*CS | 3 | 376.2 | 376.2 | 125.4 | 2.32 | 0.175 |
| R*T*DOC | 3 | 404.6 | 404.6 | 134.9 | 2.5 | 0.157 |
| R*CS*DOC | 3 | 23 | 23 | 7.7 | 0.14 | 0.931 |
| S*T*CS | 2 | 118.1 | 118.1 | 59 | 1.09 | 0.394 |
| S*T*DOC | 2 | 584.2 | 584.2 | 292.1 | 5.41 | 0.045 |
| S*CS*DOC | 2 | 198 | 198 | 99 | 1.83 | 0.239 |
| T*CS*DOC | 1 | 847.3 | 847.3 | 847.3 | 15.68 | 0.007 |
| R*S*T*CS | 6 | 462.4 | 462.4 | 77.1 | 1.43 | 0.339 |
| R*S*T*DOC | 6 | 816.4 | 816.4 | 136.1 | 2.52 | 0.143 |
| R*S*CS*DOC | 6 | 162.9 | 162.9 | 27.2 | 0.5 | 0.788 |
| R*T*CS*DOC | 3 | 300.5 | 300.5 | 100.2 | 1.85 | 0.238 |
| S*T*CS*DOC | 2 | 107.2 | 107.2 | 53.6 | 0.99 | 0.424 |
| Error | 6 | 324.2 | 324.2 | 54 | - | - |
| Total | 95 | 141098.7 | - | - | - | - |

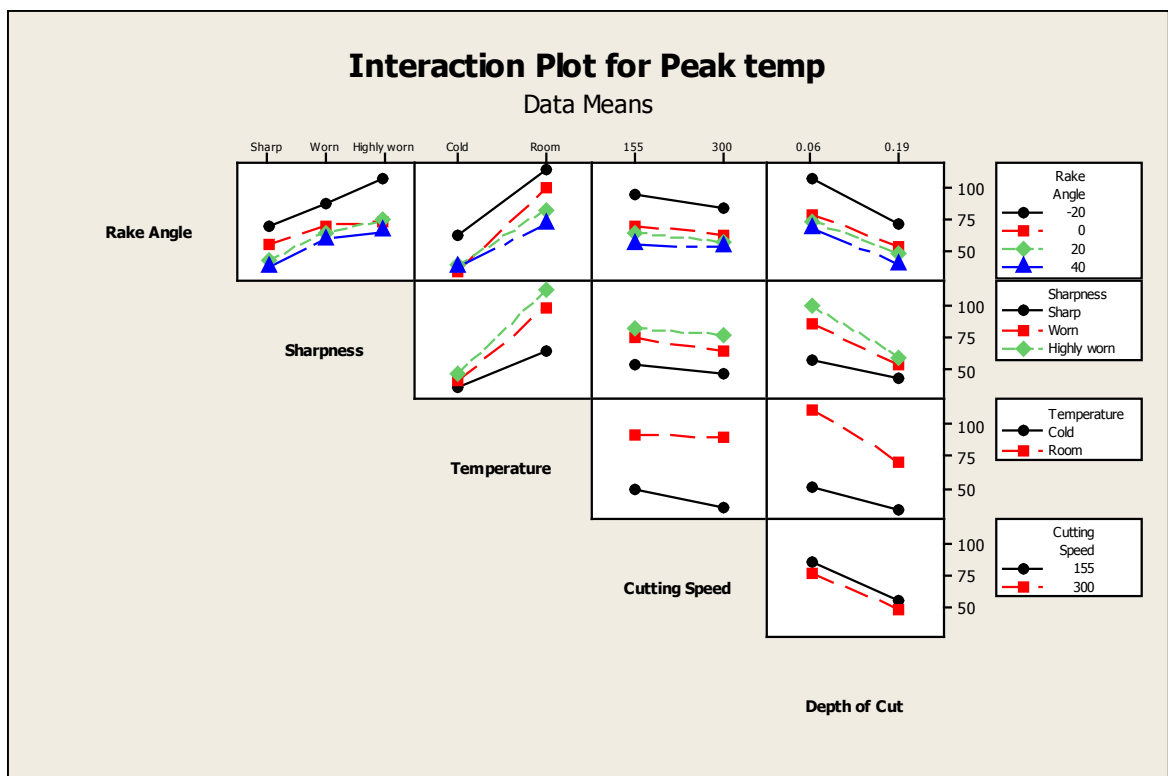


Figure C.6: Interactions plot for peak temperature for plain UHMWPE, including cryogenically cooled workpieces.

Appendix C

Appendix D

ANOVA tables for chapter 5

This appendix contains the analysis of variance tables for the analysis shown in chapter 5. The factors and levels used were as follows:

Table D.1: Factors used in design of experiments for chapter 5. (Repeat of table 3.3.)

| Factor | Number of levels | Levels |
|---------------|-------------------------|---|
| Material | 3 | UHMWPE, AOX, XLK |
| Rake angle | 4 | -20° , 0° , 20° , 40° |
| Edge radius | 3 | Sharp, worn, highly worn - See table 3.4 |
| Cutting speed | 2 | 155, 300 <i>m/min</i> |
| Depth of cut | 2 | 0.06, 0.19 <i>mm/rev</i> |

The analysis for chip thickness used results from sharp tools only, removing sharpness as a factor from that analysis. All analyses used a single replicate at each level.

Appendix D

Table D.2: ANOVA table for cutting force. $R - Sq = 99.5\%$.

| Source | DF | Seq SS | Adj SS | Adj MS | F | P |
|---------------|-----|----------|---------|---------|--------|-------|
| Material | 2 | 309.56 | 309.56 | 154.78 | 18.29 | 0 |
| Rake angle | 3 | 7384.08 | 7384.08 | 2461.36 | 290.86 | 0 |
| Sharpness | 2 | 5837.7 | 5837.7 | 2918.85 | 344.92 | 0 |
| Cutting speed | 1 | 69.18 | 69.18 | 69.18 | 8.17 | 0.014 |
| Depth of cut | 1 | 2124.59 | 2124.59 | 2124.59 | 251.06 | 0 |
| M*R | 6 | 489.45 | 489.45 | 81.58 | 9.64 | 0.001 |
| M*S | 4 | 236.55 | 236.55 | 59.14 | 6.99 | 0.004 |
| M*CS | 2 | 54.53 | 54.53 | 27.26 | 3.22 | 0.076 |
| M*DOC | 2 | 65.82 | 65.82 | 32.91 | 3.89 | 0.05 |
| R*S | 6 | 818.04 | 818.04 | 136.34 | 16.11 | 0 |
| R*CS | 3 | 32.64 | 32.64 | 10.88 | 1.29 | 0.324 |
| R*DOC | 3 | 957.75 | 957.75 | 319.25 | 37.73 | 0 |
| S*CS | 2 | 176.26 | 176.26 | 88.13 | 10.41 | 0.002 |
| S*DOC | 2 | 49.86 | 49.86 | 24.93 | 2.95 | 0.091 |
| CS*DOC | 1 | 1.86 | 1.86 | 1.86 | 0.22 | 0.647 |
| M*R*S | 12 | 605.3 | 605.3 | 50.44 | 5.96 | 0.002 |
| M*R*CS | 6 | 44.54 | 44.54 | 7.42 | 0.88 | 0.539 |
| M*R*DOC | 6 | 135.78 | 135.78 | 22.63 | 2.67 | 0.069 |
| M*S*CS | 4 | 42.96 | 42.96 | 10.74 | 1.27 | 0.335 |
| M*S*DOC | 4 | 16.72 | 16.72 | 4.18 | 0.49 | 0.741 |
| M*CS*DOC | 2 | 5.46 | 5.46 | 2.73 | 0.32 | 0.73 |
| R*S*CS | 6 | 55.47 | 55.47 | 9.24 | 1.09 | 0.42 |
| R*S*DOC | 6 | 201.56 | 201.56 | 33.59 | 3.97 | 0.02 |
| R*CS*DOC | 3 | 31.27 | 31.27 | 10.42 | 1.23 | 0.341 |
| S*CS*DOC | 2 | 21.15 | 21.15 | 10.58 | 1.25 | 0.321 |
| M*R*S*CS | 12 | 64.35 | 64.35 | 5.36 | 0.63 | 0.78 |
| M*R*S*DOC | 12 | 118 | 118 | 9.83 | 1.16 | 0.4 |
| M*R*CS*DOC | 6 | 60.24 | 60.24 | 10.04 | 1.19 | 0.376 |
| M*S*CS*DOC | 4 | 10.82 | 10.82 | 2.7 | 0.32 | 0.86 |
| R*S*CS*DOC | 6 | 205.59 | 205.59 | 34.27 | 4.05 | 0.019 |
| Error | 12 | 101.55 | 101.55 | 8.46 | - | - |
| Total | 143 | 20328.64 | - | - | - | - |

Table D.3: ANOVA table for thrust force. $R - Sq = 99.73\%$.

| Source | DF | Seq SS | Adj SS | Adj MS | F | P |
|---------------|-----|----------|----------|----------|--------|-------|
| Material | 2 | 425.88 | 425.88 | 212.94 | 10.95 | 0.002 |
| Rake angle | 3 | 40308.24 | 40308.24 | 13436.08 | 690.84 | 0 |
| Sharpness | 2 | 31985 | 31985 | 15992.5 | 822.28 | 0 |
| Cutting speed | 1 | 162.26 | 162.26 | 162.26 | 8.34 | 0.014 |
| Depth of cut | 1 | 760.34 | 760.34 | 760.34 | 39.09 | 0 |
| M*R | 6 | 1329.32 | 1329.32 | 221.55 | 11.39 | 0 |
| M*S | 4 | 638.82 | 638.82 | 159.71 | 8.21 | 0.002 |
| M*CS | 2 | 165.35 | 165.35 | 82.68 | 4.25 | 0.04 |
| M*DOC | 2 | 72.29 | 72.29 | 36.14 | 1.86 | 0.198 |
| R*S | 6 | 2141.85 | 2141.85 | 356.97 | 18.35 | 0 |
| R*CS | 3 | 156.83 | 156.83 | 52.28 | 2.69 | 0.093 |
| R*DOC | 3 | 1659.11 | 1659.11 | 553.04 | 28.44 | 0 |
| S*CS | 2 | 492.48 | 492.48 | 246.24 | 12.66 | 0.001 |
| S*DOC | 2 | 1178.31 | 1178.31 | 589.16 | 30.29 | 0 |
| CS*DOC | 1 | 12.52 | 12.52 | 12.52 | 0.64 | 0.438 |
| M*R*S | 12 | 2093.58 | 2093.58 | 174.47 | 8.97 | 0 |
| M*R*CS | 6 | 201.94 | 201.94 | 33.66 | 1.73 | 0.197 |
| M*R*DOC | 6 | 249.63 | 249.63 | 41.6 | 2.14 | 0.124 |
| M*S*CS | 4 | 107.08 | 107.08 | 26.77 | 1.38 | 0.3 |
| M*S*DOC | 4 | 45.82 | 45.82 | 11.45 | 0.59 | 0.677 |
| M*CS*DOC | 2 | 13.91 | 13.91 | 6.96 | 0.36 | 0.707 |
| R*S*CS | 6 | 214.09 | 214.09 | 35.68 | 1.83 | 0.175 |
| R*S*DOC | 6 | 659.89 | 659.89 | 109.98 | 5.65 | 0.005 |
| R*CS*DOC | 3 | 170.27 | 170.27 | 56.76 | 2.92 | 0.078 |
| S*CS*DOC | 2 | 21.97 | 21.97 | 10.98 | 0.56 | 0.583 |
| M*R*S*CS | 12 | 230 | 230 | 19.17 | 0.99 | 0.51 |
| M*R*S*DOC | 12 | 345.09 | 345.09 | 28.76 | 1.48 | 0.254 |
| M*R*CS*DOC | 6 | 161.99 | 161.99 | 27 | 1.39 | 0.295 |
| M*S*CS*DOC | 4 | 23.02 | 23.02 | 5.75 | 0.3 | 0.875 |
| R*S*CS*DOC | 6 | 519.53 | 519.53 | 86.59 | 4.45 | 0.013 |
| Error | 12 | 233.39 | 233.39 | 19.45 | - | - |
| Total | 143 | 86779.81 | - | - | - | - |

Appendix D

Table D.4: ANOVA table for surface roughness. $R - Sq = 98.55\%$.

| Source | DF | Seq SS | Adj SS | Adj MS | F | P |
|---------------|----|----------|----------|----------|--------|-------|
| Material | 2 | 0.60099 | 0.60099 | 0.3005 | 3.37 | 0.105 |
| Rake angle | 3 | 4.03183 | 4.03183 | 1.34394 | 15.06 | 0.003 |
| Sharpness | 1 | 10.81652 | 10.81652 | 10.81652 | 121.17 | 0 |
| Cutting speed | 1 | 0.06121 | 0.06121 | 0.06121 | 0.69 | 0.439 |
| Depth of cut | 1 | 1.15545 | 1.15545 | 1.15545 | 12.94 | 0.011 |
| M*R | 6 | 1.04968 | 1.04968 | 0.17495 | 1.96 | 0.217 |
| M*S | 2 | 0.60952 | 0.60952 | 0.30476 | 3.41 | 0.102 |
| M*CS | 2 | 0.29315 | 0.29315 | 0.14658 | 1.64 | 0.27 |
| M*DOC | 2 | 0.21274 | 0.21274 | 0.10637 | 1.19 | 0.367 |
| R*S | 3 | 5.67718 | 5.67718 | 1.89239 | 21.2 | 0.001 |
| R*CS | 3 | 0.39751 | 0.39751 | 0.1325 | 1.48 | 0.311 |
| R*DOC | 3 | 0.76744 | 0.76744 | 0.25581 | 2.87 | 0.126 |
| S*CS | 1 | 0.10989 | 0.10989 | 0.10989 | 1.23 | 0.31 |
| S*DOC | 1 | 0.98334 | 0.98334 | 0.98334 | 11.02 | 0.016 |
| CS*DOC | 1 | 0.04386 | 0.04386 | 0.04386 | 0.49 | 0.51 |
| M*R*S | 6 | 1.50089 | 1.50089 | 0.25015 | 2.8 | 0.118 |
| M*R*CS | 6 | 1.30526 | 1.30526 | 0.21754 | 2.44 | 0.151 |
| M*R*DOC | 6 | 0.4088 | 0.4088 | 0.06813 | 0.76 | 0.624 |
| M*S*CS | 2 | 0.30826 | 0.30826 | 0.15413 | 1.73 | 0.256 |
| M*S*DOC | 2 | 0.28949 | 0.28949 | 0.14474 | 1.62 | 0.274 |
| M*CS*DOC | 2 | 0.52215 | 0.52215 | 0.26108 | 2.92 | 0.13 |
| R*S*CS | 3 | 0.28439 | 0.28439 | 0.0948 | 1.06 | 0.432 |
| R*S*DOC | 3 | 1.08677 | 1.08677 | 0.36226 | 4.06 | 0.068 |
| R*CS*DOC | 3 | 0.18419 | 0.18419 | 0.0614 | 0.69 | 0.592 |
| S*CS*DOC | 1 | 0.01612 | 0.01612 | 0.01612 | 0.18 | 0.686 |
| M*R*S*CS | 6 | 1.4792 | 1.4792 | 0.24653 | 2.76 | 0.121 |
| M*R*S*DOC | 6 | 0.50225 | 0.50225 | 0.08371 | 0.94 | 0.53 |
| M*R*CS*DOC | 6 | 0.9956 | 0.9956 | 0.16593 | 1.86 | 0.235 |
| M*S*CS*DOC | 2 | 0.52726 | 0.52726 | 0.26363 | 2.95 | 0.128 |
| R*S*CS*DOC | 3 | 0.223 | 0.223 | 0.07433 | 0.83 | 0.523 |
| Error | 6 | 0.53561 | 0.53561 | 0.08927 | - | - |
| Total | 95 | 36.97957 | - | - | - | - |

Table D.5: ANOVA table for chip thickness. $R - Sq = 99.78\%$.

| Source | DF | Seq SS | Adj SS | Adj MS | F | P |
|---------------|----|-----------|-----------|-----------|-------|-------|
| Material | 2 | 0.0010667 | 0.0010667 | 0.0005333 | 38.4 | 0 |
| Rake angle | 3 | 0.032075 | 0.032075 | 0.0106917 | 769.8 | 0 |
| Cutting speed | 1 | 0.0000333 | 0.0000333 | 0.0000333 | 2.4 | 0.172 |
| Depth of cut | 1 | 0.0001333 | 0.0001333 | 0.0001333 | 9.6 | 0.021 |
| M*R | 6 | 0.0008 | 0.0008 | 0.0001333 | 9.6 | 0.007 |
| M*CS | 2 | 0.0000667 | 0.0000667 | 0.0000333 | 2.4 | 0.171 |
| M*DOC | 2 | 0.0002167 | 0.0002167 | 0.0001083 | 7.8 | 0.021 |
| R*CS | 3 | 0.0001167 | 0.0001167 | 0.0000389 | 2.8 | 0.131 |
| R*DOC | 3 | 0.0027833 | 0.0027833 | 0.0009278 | 66.8 | 0 |
| CS*DOC | 1 | 0.0000083 | 0.0000083 | 0.0000083 | 0.6 | 0.468 |
| M*R*CS | 6 | 0.0001333 | 0.0001333 | 0.0000222 | 1.6 | 0.291 |
| M*R*DOC | 6 | 0.0003167 | 0.0003167 | 0.0000528 | 3.8 | 0.065 |
| M*CS*DOC | 2 | 0.0003167 | 0.0003167 | 0.0001583 | 11.4 | 0.009 |
| R*CS*DOC | 3 | 0.0000417 | 0.0000417 | 0.0000139 | 1 | 0.455 |
| Error | 6 | 0.0000833 | 0.0000833 | 0.0000139 | - | - |
| Total | 47 | 0.0381917 | - | - | - | - |

Appendix D

Appendix E

ANOVA tables for chapter 6

This appendix contains the analysis of variance tables for the analysis shown in chapter 6. The factors and levels used were as follows:

Table E.1: Factors used in design of experiments for chapter 6. (Repeat of table 3.6.)

| Factor | Number of levels | Levels |
|-------------------------------|-------------------------|--|
| Rake angle | 4 | $-20^\circ, 0^\circ, 20^\circ, 40^\circ$ |
| Initial workpiece temperature | 2 | Cold (100 - 150 K), Room (295 - 300 K) |
| Edge radius | 3 | Sharp, worn, highly worn - See table 3.4 |
| Cutting speed | 2 | 155, 300 <i>m/min</i> |
| Depth of cut | 2 | 0.06, 0.19 <i>mm/rev</i> |

The analysis for chip thickness used results from sharp tools only, removing sharpness as a factor from that analysis. All analyses used a single replicate at each level.

Appendix E

Table E.2: ANOVA table for cutting force for plain UHMWPE, including cryogenically cooled workpieces. $R - Sq = 99.74\%$.

| Source | DF | Seq SS | Adj SS | Adj MS | F | P |
|---------------|----|----------|----------|---------|--------|-------|
| Rake Angle | 3 | 11472.32 | 11472.32 | 3824.11 | 231.62 | 0 |
| Sharpness | 2 | 7275.7 | 7275.7 | 3637.85 | 220.34 | 0 |
| Temperature | 1 | 5436.71 | 5436.71 | 5436.71 | 329.3 | 0 |
| Cutting Speed | 1 | 15.04 | 15.04 | 15.04 | 0.91 | 0.377 |
| Depth of Cut | 1 | 6440.38 | 6440.38 | 6440.38 | 390.09 | 0 |
| R*S | 6 | 681.88 | 681.88 | 113.65 | 6.88 | 0.017 |
| R*T | 3 | 612.15 | 612.15 | 204.05 | 12.36 | 0.006 |
| R*CS | 3 | 64.51 | 64.51 | 21.5 | 1.3 | 0.357 |
| R*DOC | 3 | 2582.83 | 2582.83 | 860.94 | 52.15 | 0 |
| S*T | 2 | 245.43 | 245.43 | 122.72 | 7.43 | 0.024 |
| S*CS | 2 | 167.53 | 167.53 | 83.76 | 5.07 | 0.051 |
| S*DOC | 2 | 8.24 | 8.24 | 4.12 | 0.25 | 0.787 |
| T*CS | 1 | 10.96 | 10.96 | 10.96 | 0.66 | 0.446 |
| T*DOC | 1 | 1430.82 | 1430.82 | 1430.82 | 86.66 | 0 |
| CS*DOC | 1 | 31.45 | 31.45 | 31.45 | 1.9 | 0.217 |
| R*S*T | 6 | 285.65 | 285.65 | 47.61 | 2.88 | 0.112 |
| R*S*CS | 6 | 162.38 | 162.38 | 27.06 | 1.64 | 0.282 |
| R*S*DOC | 6 | 189.57 | 189.57 | 31.6 | 1.91 | 0.225 |
| R*T*CS | 3 | 41.48 | 41.48 | 13.83 | 0.84 | 0.521 |
| R*T*DOC | 3 | 387.33 | 387.33 | 129.11 | 7.82 | 0.017 |
| R*CS*DOC | 3 | 30.41 | 30.41 | 10.14 | 0.61 | 0.631 |
| S*T*CS | 2 | 111.52 | 111.52 | 55.76 | 3.38 | 0.104 |
| S*T*DOC | 2 | 16.53 | 16.53 | 8.27 | 0.5 | 0.629 |
| S*CS*DOC | 2 | 48.55 | 48.55 | 24.28 | 1.47 | 0.302 |
| T*CS*DOC | 1 | 16.43 | 16.43 | 16.43 | 1 | 0.357 |
| R*S*T*CS | 6 | 117.31 | 117.31 | 19.55 | 1.18 | 0.421 |
| R*S*T*DOC | 6 | 132.14 | 132.14 | 22.02 | 1.33 | 0.368 |
| R*S*CS*DOC | 6 | 85.96 | 85.96 | 14.33 | 0.87 | 0.566 |
| R*T*CS*DOC | 3 | 10.15 | 10.15 | 3.38 | 0.2 | 0.889 |
| S*T*CS*DOC | 2 | 66.71 | 66.71 | 33.35 | 2.02 | 0.213 |
| Error | 6 | 99.06 | 99.06 | 16.51 | - | - |
| Total | 95 | 38277.13 | - | - | - | - |

Table E.3: ANOVA table for thrust force for plain UHMWPE, including cryogenically cooled workpieces. $R - Sq = 99.93\%$.

| Source | DF | Seq SS | Adj SS | Adj MS | F | P |
|---------------|----|----------|----------|----------|---------|-------|
| Rake Angle | 3 | 42959.1 | 42959.1 | 14319.7 | 1428.02 | 0 |
| Sharpness | 2 | 32280.24 | 32280.24 | 16140.12 | 1609.56 | 0 |
| Temperature | 1 | 2018.43 | 2018.43 | 2018.43 | 201.29 | 0 |
| Cutting Speed | 1 | 4.59 | 4.59 | 4.59 | 0.46 | 0.524 |
| Depth of Cut | 1 | 50.41 | 50.41 | 50.41 | 5.03 | 0.066 |
| R*S | 6 | 1751.39 | 1751.39 | 291.9 | 29.11 | 0 |
| R*T | 3 | 729.73 | 729.73 | 243.24 | 24.26 | 0.001 |
| R*CS | 3 | 123.92 | 123.92 | 41.31 | 4.12 | 0.066 |
| R*DOC | 3 | 3202.35 | 3202.35 | 1067.45 | 106.45 | 0 |
| S*T | 2 | 464.38 | 464.38 | 232.19 | 23.15 | 0.002 |
| S*CS | 2 | 132.25 | 132.25 | 66.13 | 6.59 | 0.031 |
| S*DOC | 2 | 539.5 | 539.5 | 269.75 | 26.9 | 0.001 |
| T*CS | 1 | 10.48 | 10.48 | 10.48 | 1.04 | 0.346 |
| T*DOC | 1 | 784.73 | 784.73 | 784.73 | 78.26 | 0 |
| CS*DOC | 1 | 15.28 | 15.28 | 15.28 | 1.52 | 0.263 |
| R*S*T | 6 | 377.72 | 377.72 | 62.95 | 6.28 | 0.021 |
| R*S*CS | 6 | 289.4 | 289.4 | 48.23 | 4.81 | 0.039 |
| R*S*DOC | 6 | 309.53 | 309.53 | 51.59 | 5.14 | 0.033 |
| R*T*CS | 3 | 51.79 | 51.79 | 17.26 | 1.72 | 0.261 |
| R*T*DOC | 3 | 417.97 | 417.97 | 139.32 | 13.89 | 0.004 |
| R*CS*DOC | 3 | 90.92 | 90.92 | 30.31 | 3.02 | 0.116 |
| S*T*CS | 2 | 122.85 | 122.85 | 61.42 | 6.13 | 0.036 |
| S*T*DOC | 2 | 75.12 | 75.12 | 37.56 | 3.75 | 0.088 |
| S*CS*DOC | 2 | 30.87 | 30.87 | 15.43 | 1.54 | 0.289 |
| T*CS*DOC | 1 | 15.14 | 15.14 | 15.14 | 1.51 | 0.265 |
| R*S*T*CS | 6 | 253.56 | 253.56 | 42.26 | 4.21 | 0.052 |
| R*S*T*DOC | 6 | 48.91 | 48.91 | 8.15 | 0.81 | 0.596 |
| R*S*CS*DOC | 6 | 89.42 | 89.42 | 14.9 | 1.49 | 0.321 |
| R*T*CS*DOC | 3 | 32.25 | 32.25 | 10.75 | 1.07 | 0.429 |
| S*T*CS*DOC | 2 | 24.11 | 24.11 | 12.05 | 1.2 | 0.364 |
| Error | 6 | 60.17 | 60.17 | 10.03 | - | - |
| Total | 95 | 87356.52 | - | - | - | - |

Appendix E

Table E.4: ANOVA table for cut chip thickness for plain UHMWPE, including cryogenically cooled workpieces. $R - Sq = 99.52\%$.

| Source | DF | Seq SS | Adj SS | Adj MS | F | P |
|---------------|----|-----------|-----------|-----------|--------|-------|
| Rake Angle | 3 | 0.0070375 | 0.0070375 | 0.0023458 | 70.38 | 0.003 |
| Temperature | 1 | 0.0036125 | 0.0036125 | 0.0036125 | 108.38 | 0.002 |
| Cutting Speed | 1 | 0.00005 | 0.00005 | 0.00005 | 1.5 | 0.308 |
| Depth of Cut | 1 | 0.0001125 | 0.0001125 | 0.0001125 | 3.38 | 0.164 |
| R*T | 3 | 0.0079375 | 0.0079375 | 0.0026458 | 79.38 | 0.002 |
| R*CS | 3 | 0.00005 | 0.00005 | 0.0000167 | 0.5 | 0.708 |
| R*DOC | 3 | 0.0007375 | 0.0007375 | 0.0002458 | 7.38 | 0.067 |
| T*CS | 1 | 0 | 0 | 0 | 0 | 1 |
| T*DOC | 1 | 0.0003125 | 0.0003125 | 0.0003125 | 9.38 | 0.055 |
| CS*DOC | 1 | 0.00005 | 0.00005 | 0.00005 | 1.5 | 0.308 |
| R*T*CS | 3 | 0.0002 | 0.0002 | 0.0000667 | 2 | 0.292 |
| R*T*DOC | 3 | 0.0005375 | 0.0005375 | 0.0001792 | 5.38 | 0.1 |
| R*CS*DOC | 3 | 0.00015 | 0.00015 | 0.00005 | 1.5 | 0.374 |
| T*CS*DOC | 1 | 0 | 0 | 0 | 0 | 1 |
| Error | 3 | 0.0001 | 0.0001 | 0.0000333 | - | - |
| Total | 31 | 0.0208875 | - | - | - | - |

Table E.5: ANOVA table for surface roughness for plain UHMWPE, including cryogenically cooled workpieces. $R - Sq = 99.27\%$.

| Source | DF | Seq SS | Adj SS | Adj MS | F | P |
|---------------|----|----------|----------|---------|--------|-------|
| Rake Angle | 3 | 1.30387 | 1.30387 | 0.43462 | 9.25 | 0.011 |
| Sharpness | 2 | 10.30665 | 10.30665 | 5.15332 | 109.65 | 0 |
| Temperature | 1 | 1.35565 | 1.35565 | 1.35565 | 28.85 | 0.002 |
| Cutting Speed | 1 | 0.2185 | 0.2185 | 0.2185 | 4.65 | 0.074 |
| Depth of Cut | 1 | 2.74862 | 2.74862 | 2.74862 | 58.49 | 0 |
| R*S | 6 | 1.53832 | 1.53832 | 0.25639 | 5.46 | 0.029 |
| R*T | 3 | 0.61163 | 0.61163 | 0.20388 | 4.34 | 0.06 |
| R*CS | 3 | 0.08027 | 0.08027 | 0.02676 | 0.57 | 0.655 |
| R*DOC | 3 | 0.25803 | 0.25803 | 0.08601 | 1.83 | 0.242 |
| S*T | 2 | 0.31878 | 0.31878 | 0.15939 | 3.39 | 0.103 |
| S*CS | 2 | 0.02456 | 0.02456 | 0.01228 | 0.26 | 0.778 |
| S*DOC | 2 | 2.65747 | 2.65747 | 1.32874 | 28.27 | 0.001 |
| T*CS | 1 | 0.47208 | 0.47208 | 0.47208 | 10.05 | 0.019 |
| T*DOC | 1 | 0.32248 | 0.32248 | 0.32248 | 6.86 | 0.04 |
| CS*DOC | 1 | 0.11043 | 0.11043 | 0.11043 | 2.35 | 0.176 |
| R*S*T | 6 | 1.55636 | 1.55636 | 0.25939 | 5.52 | 0.028 |
| R*S*CS | 6 | 0.08649 | 0.08649 | 0.01441 | 0.31 | 0.912 |
| R*S*DOC | 6 | 1.24793 | 1.24793 | 0.20799 | 4.43 | 0.047 |
| R*T*CS | 3 | 1.63282 | 1.63282 | 0.54427 | 11.58 | 0.007 |
| R*T*DOC | 3 | 1.98932 | 1.98932 | 0.66311 | 14.11 | 0.004 |
| R*CS*DOC | 3 | 0.60137 | 0.60137 | 0.20046 | 4.27 | 0.062 |
| S*T*CS | 2 | 0.5457 | 0.5457 | 0.27285 | 5.81 | 0.04 |
| S*T*DOC | 2 | 0.44625 | 0.44625 | 0.22312 | 4.75 | 0.058 |
| S*CS*DOC | 2 | 0.40051 | 0.40051 | 0.20025 | 4.26 | 0.071 |
| T*CS*DOC | 1 | 0.34849 | 0.34849 | 0.34849 | 7.42 | 0.035 |
| R*S*T*CS | 6 | 2.0383 | 2.0383 | 0.33972 | 7.23 | 0.015 |
| R*S*T*DOC | 6 | 2.11608 | 2.11608 | 0.35268 | 7.5 | 0.014 |
| R*S*CS*DOC | 6 | 2.48527 | 2.48527 | 0.41421 | 8.81 | 0.009 |
| R*T*CS*DOC | 3 | 0.05048 | 0.05048 | 0.01683 | 0.36 | 0.786 |
| S*T*CS*DOC | 2 | 0.29667 | 0.29667 | 0.14834 | 3.16 | 0.116 |
| Error | 6 | 0.28198 | 0.28198 | 0.047 | - | - |
| Total | 95 | 38.45134 | - | - | - | - |

Appendix E

Table E.6: ANOVA table for RMS of profilometer output, with high RMS outlier removed. $R - Sq = 99.23\%$.

| Source | DF | Seq SS | Adj SS | Adj MS | F | P |
|---------------|----|----------|---------|---------|--------|-------|
| Rake Angle | 3 | 39.98 | 39.98 | 13.33 | 0.74 | 0.564 |
| Sharpness | 2 | 2895.77 | 2895.77 | 1447.89 | 80.72 | 0 |
| Temperature | 1 | 2.63 | 2.63 | 2.63 | 0.15 | 0.715 |
| Cutting Speed | 1 | 168.32 | 168.32 | 168.32 | 9.38 | 0.022 |
| Depth of Cut | 1 | 3505.57 | 3505.57 | 3505.57 | 195.44 | 0 |
| R*S | 6 | 560.03 | 560.03 | 93.34 | 5.2 | 0.032 |
| R*T | 3 | 812.93 | 812.93 | 270.98 | 15.11 | 0.003 |
| R*CS | 3 | 30.2 | 30.2 | 10.07 | 0.56 | 0.66 |
| R*DOC | 3 | 27.41 | 27.41 | 9.14 | 0.51 | 0.69 |
| S*T | 2 | 17.24 | 17.24 | 8.62 | 0.48 | 0.64 |
| S*CS | 2 | 23.06 | 23.06 | 11.53 | 0.64 | 0.559 |
| S*DOC | 2 | 2603.66 | 2603.66 | 1301.83 | 72.58 | 0 |
| T*CS | 1 | 1.15 | 1.15 | 1.15 | 0.06 | 0.809 |
| T*DOC | 1 | 3.07 | 3.07 | 3.07 | 0.17 | 0.694 |
| CS*DOC | 1 | 128.21 | 128.21 | 128.21 | 7.15 | 0.037 |
| R*S*T | 6 | 366.15 | 366.15 | 61.03 | 3.4 | 0.081 |
| R*S*CS | 6 | 230.11 | 230.11 | 38.35 | 2.14 | 0.189 |
| R*S*DOC | 6 | 700.15 | 700.15 | 116.69 | 6.51 | 0.019 |
| R*T*CS | 3 | 21.75 | 21.75 | 7.25 | 0.4 | 0.756 |
| R*T*DOC | 3 | 808.13 | 808.13 | 269.38 | 15.02 | 0.003 |
| R*CS*DOC | 3 | 14.61 | 14.61 | 4.87 | 0.27 | 0.844 |
| S*T*CS | 2 | 25.16 | 25.16 | 12.58 | 0.7 | 0.532 |
| S*T*DOC | 2 | 15.34 | 15.34 | 7.67 | 0.43 | 0.67 |
| S*CS*DOC | 2 | 21.13 | 21.13 | 10.56 | 0.59 | 0.584 |
| T*CS*DOC | 1 | 0.46 | 0.46 | 0.46 | 0.03 | 0.878 |
| R*S*T*CS | 6 | 147.34 | 147.34 | 24.56 | 1.37 | 0.356 |
| R*S*T*DOC | 6 | 407.4 | 407.4 | 67.9 | 3.79 | 0.065 |
| R*S*CS*DOC | 6 | 205.23 | 205.23 | 34.21 | 1.91 | 0.226 |
| R*T*CS*DOC | 3 | 30.94 | 30.94 | 10.31 | 0.58 | 0.652 |
| S*T*CS*DOC | 2 | 22.59 | 22.59 | 11.29 | 0.63 | 0.565 |
| Error | 6 | 107.62 | 107.62 | 17.94 | - | - |
| Total | 95 | 13943.36 | - | - | - | - |

Appendix F

ANOVA tables for chapter 7

This appendix contains the analysis of variance tables and residuals plots for the analysis shown in chapter 7. The factors and levels used were as follows:

Table F.1: Factors used in design of experiments for constant stress loading. (Repeat of table 7.1.)

| Factor | Number of levels | Levels |
|----------------------------|-------------------------|--|
| Stress | 4 | 0, 2, 4, 8 <i>MPa</i> |
| Initial sample temperature | 2 | Cold (100 - 150 <i>K</i>), Room (295 - 300 <i>K</i>) |

Table F.2: Factors used in design of experiments for constant strain loading. (Repeat of table 7.2.)

| Factor | Number of levels | Levels |
|----------------------------|-------------------------|--|
| Strain | 4 | 0, 2.5, 5, 10% |
| Initial sample temperature | 2 | Cold (100 - 150 <i>K</i>), Room (295 - 300 <i>K</i>) |

Table F.3: Factors used in design of experiments for machining operations. (Repeat of table 7.3.)

| Factor | Number of levels | Levels |
|---------------|-------------------------|--|
| Rake angle | 2 | 20°, 40° |
| Depth of cut | 5 | 0.05, 0.10, 0.15, 0.20, 0.25 <i>mm/rev</i> |

Appendix F

Table F.4: ANOVA table for regression model of thickness of samples with constant stress applied for 100 seconds, measured from 10 to 200 minutes after unloading. $R - Sq = 99.55\%$.

| Source | DF | Seq SS | Adj SS | Adj MS | F | P |
|---------------------|-----|------------------|--------|--------|---------|-------|
| | | $\times 10^{-3}$ | | | | |
| Regression | 31 | 20.948 | 20.948 | 0.676 | 626.687 | 0 |
| LogTime | 1 | 1.015 | 0.05 | 0.05 | 46.643 | 0 |
| Load 2 | 1 | 1.53 | 0.155 | 0.155 | 143.425 | 0 |
| Load 4 | 1 | 0 | 0.027 | 0.027 | 24.733 | 0 |
| Load 8 | 1 | 0.359 | 0.177 | 0.177 | 163.811 | 0 |
| LogTime-Load 2 | 1 | 0.009 | 0.005 | 0.005 | 4.558 | 0.036 |
| LogTime-Load 4 | 1 | 0.003 | 0.006 | 0.006 | 5.193 | 0.025 |
| LogTime-Load 8 | 1 | 0.072 | 0.049 | 0.049 | 44.994 | 0 |
| LogTime-Cryo | 1 | 11.182 | 0.002 | 0.002 | 2.104 | 0.15 |
| LogTime-Cryo-Load 2 | 1 | 0.431 | 0.004 | 0.004 | 3.266 | 0.074 |
| LogTime-Cryo-Load 4 | 1 | 0.481 | 0 | 0 | 0.391 | 0.533 |
| LogTime-Cryo-Load 8 | 1 | 0.423 | 0.002 | 0.002 | 1.764 | 0.188 |
| Replicate | 5 | 2.143 | 3.84 | 0.768 | 712.185 | 0 |
| Replicate-Load 2 | 5 | 0.399 | 1.746 | 0.349 | 323.876 | 0 |
| Replicate-Load 4 | 5 | 0.892 | 2.222 | 0.444 | 412.183 | 0 |
| Replicate-Load 8 | 5 | 2.009 | 2.009 | 0.402 | 372.607 | 0 |
| Error | 88 | 0.095 | 0.095 | 0.001 | - | - |
| Total | 119 | 21.043 | - | - | - | - |

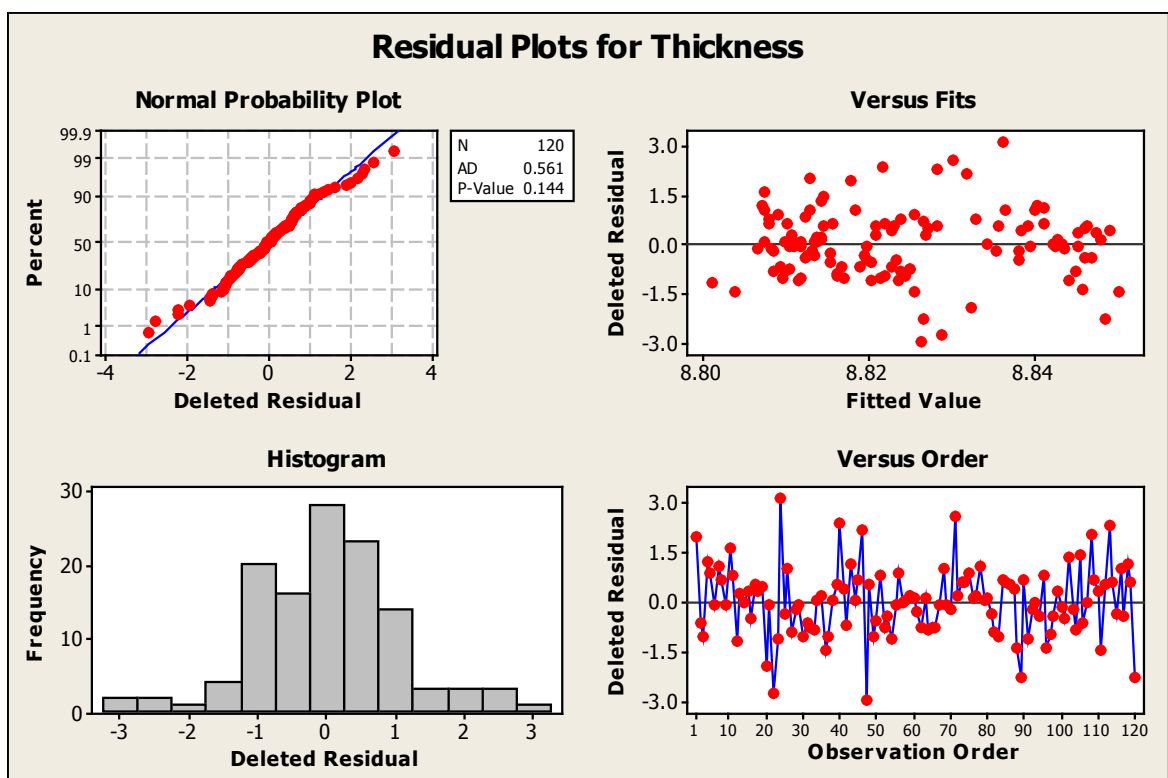


Figure F.1: Residuals plot for regression model of thickness of samples with constant stress applied for 100 seconds.

Appendix F

Table F.5: ANOVA table for regression model of thickness of samples with constant strain applied for 100 seconds. $R - Sq = 99.21\%$.

| Source | DF | Seq SS | Adj SS | Adj MS | F | P |
|-----------------------|-----|------------------|---------|--------|---------|-------|
| | | $\times 10^{-3}$ | | | | |
| Regression | 31 | 602.935 | 602.935 | 19.45 | 548.64 | 0 |
| LogTime | 1 | 18.613 | 0.269 | 0.269 | 7.58 | 0.007 |
| Load 2.5 | 1 | 65.545 | 1.074 | 1.074 | 30.29 | 0 |
| Load 5 | 1 | 23.194 | 9.05 | 9.05 | 255.29 | 0 |
| Load 10 | 1 | 447.344 | 91.339 | 91.339 | 2576.53 | 0 |
| LogTime-Load 2.5 | 1 | 1.832 | 0.014 | 0.014 | 0.39 | 0.532 |
| LogTime-Load 5 | 1 | 0.29 | 0.552 | 0.552 | 15.58 | 0 |
| LogTime-Load 10 | 1 | 8.87 | 5.009 | 5.009 | 141.29 | 0 |
| LogTime-Cryo | 1 | 15.782 | 0.005 | 0.005 | 0.14 | 0.706 |
| LogTime-Cryo-Load 2.5 | 1 | 0.087 | 0.004 | 0.004 | 0.11 | 0.744 |
| LogTime-Cryo-Load 5 | 1 | 1.281 | 0.001 | 0.001 | 0.02 | 0.88 |
| LogTime-Cryo-Load 10 | 1 | 0.04 | 0.035 | 0.035 | 0.98 | 0.323 |
| Replicate | 5 | 5.979 | 5.33 | 1.066 | 30.07 | 0 |
| Replicate-Load 2.5 | 5 | 4.23 | 3.486 | 0.697 | 19.67 | 0 |
| Replicate-Load 5 | 5 | 9.187 | 6.121 | 1.224 | 34.53 | 0 |
| Replicate-Load 10 | 5 | 0.66 | 0.66 | 0.132 | 3.72 | 0.003 |
| Error | 136 | 4.821 | 4.821 | 0.036 | - | - |
| Total | 167 | 607.756 | - | - | - | - |

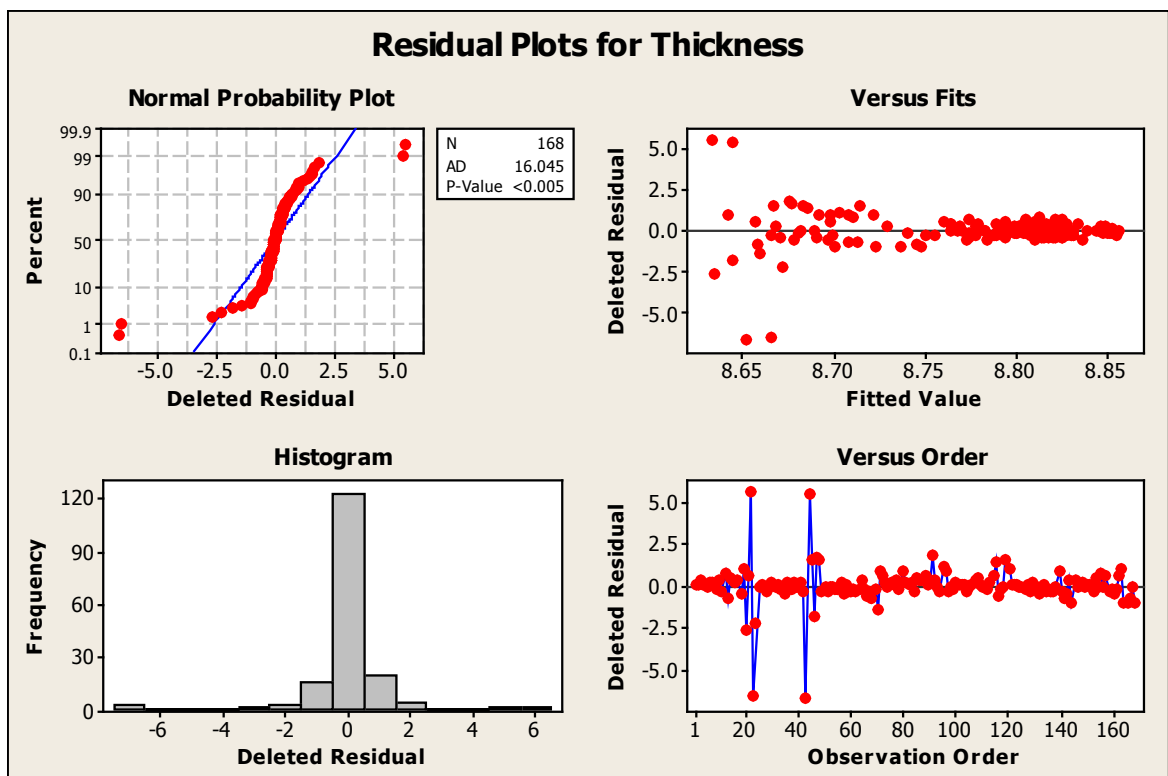


Figure F.2: Residuals plot for regression model of thickness of samples with constant strain applied for 100 seconds.

Appendix F

Table F.6: ANOVA table for regression model of thickness of samples with constant strain applied for 100 seconds, from 50 to 1000 minutes after unloading. $R - Sq = 99.87\%$.

| Source | DF | Seq SS | Adj SS | Adj MS | F | P |
|-----------------------|-----|------------------|---------|--------|---------|-------|
| | | $\times 10^{-3}$ | | | | |
| Regression | 31 | 365.043 | 365.043 | 11.776 | 2217.25 | 0 |
| LogTime | 1 | 6.073 | 0.099 | 0.099 | 18.64 | 0 |
| Load 2.5 | 1 | 39.05 | 0.262 | 0.262 | 49.25 | 0 |
| Load 5 | 1 | 14.688 | 2.276 | 2.276 | 428.61 | 0 |
| Load 10 | 1 | 273.969 | 22.919 | 22.919 | 4315.55 | 0 |
| LogTime-Load 2.5 | 1 | 0.539 | 0.009 | 0.009 | 1.61 | 0.208 |
| LogTime-Load 5 | 1 | 0.076 | 0.166 | 0.166 | 31.28 | 0 |
| LogTime-Load 10 | 1 | 2.482 | 1.332 | 1.332 | 250.77 | 0 |
| LogTime-Cryo | 1 | 12.58 | 0 | 0 | 0 | 0.978 |
| LogTime-Cryo-Load 2.5 | 1 | 0.097 | 0 | 0.001 | 0.09 | 0.76 |
| LogTime-Cryo-Load 5 | 1 | 0.933 | 0.001 | 0.001 | 0.15 | 0.7 |
| LogTime-Cryo-Load 10 | 1 | 0.051 | 0.003 | 0.003 | 0.61 | 0.438 |
| Replicate | 5 | 4.135 | 3.614 | 0.723 | 136.1 | 0 |
| Replicate-Load 2.5 | 5 | 2.949 | 2.319 | 0.464 | 87.34 | 0 |
| Replicate-Load 5 | 5 | 6.793 | 4.014 | 0.803 | 151.15 | 0 |
| Replicate-Load 10 | 5 | 0.628 | 0.628 | 0.126 | 23.64 | 0 |
| Error | 88 | 0.467 | 0.467 | 0.005 | - | - |
| Total | 119 | 365.51 | - | - | - | - |

Table F.7: ANOVA table for diameter of machined samples. $R - Sq = 99.99\%$.

| Source | DF | Seq SS | Adj SS | Adj MS | F | P |
|-----------------|-----|---------|---------|---------|---------|-------|
| Source | DF | Seq SS | Adj SS | Adj MS | F | P |
| Regression | 11 | 6268.69 | 6268.69 | 569.88 | 362337 | 0 |
| LogTime | 1 | 0 | 0 | 0 | 1 | 0.287 |
| LogTime-Rake 40 | 1 | 2.08 | 0 | 0 | 1 | 0.237 |
| DOC 0.10 | 1 | 831.45 | 255.11 | 255.11 | 162204 | 0 |
| DOC 0.15 | 1 | 86.05 | 1094.78 | 1094.78 | 696076 | 0 |
| DOC 0.20 | 1 | 329.08 | 2614.81 | 2614.81 | 1662526 | 0 |
| DOC 0.25 | 1 | 5019.71 | 5019.71 | 5019.71 | 3191596 | 0 |
| Replicate | 5 | 0.31 | 0.31 | 0.06 | 40 | 0 |
| Error | 228 | 0.36 | 0.36 | 0 | 0 | 0 |
| Total | 239 | 6269.05 | 0 | 0 | 0 | 0 |

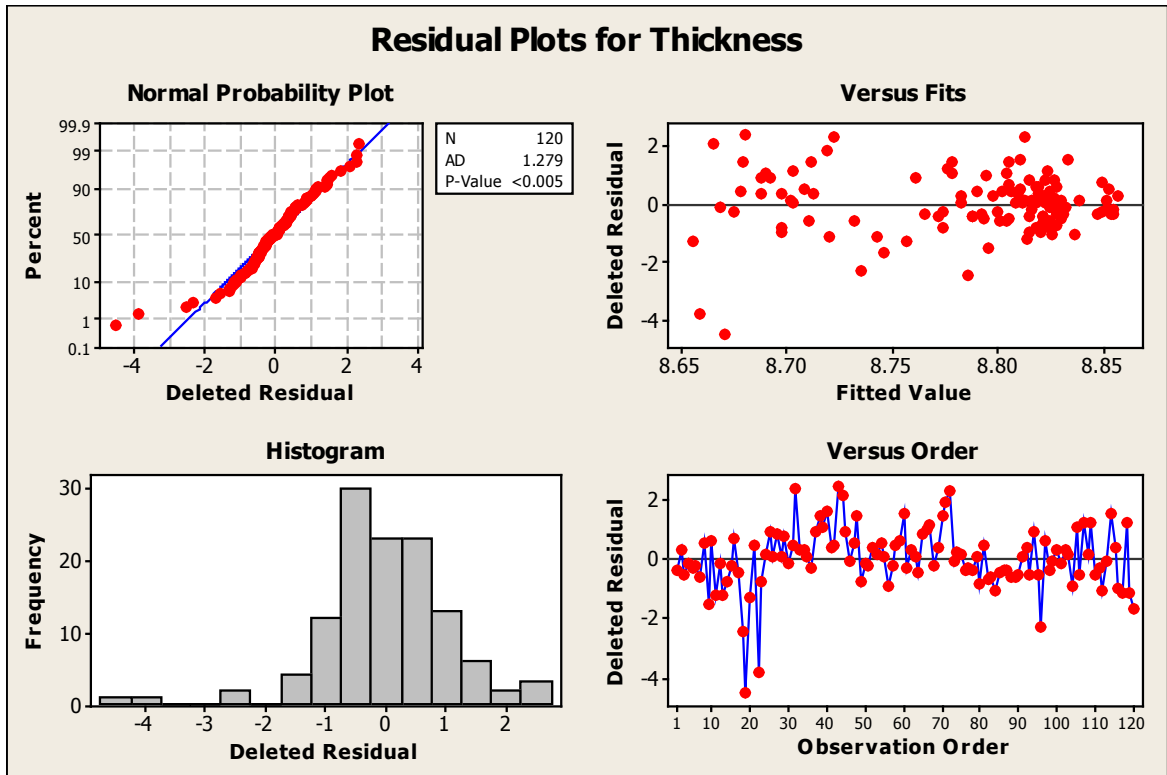


Figure F.3: Residuals plot for regression model of thickness of samples with constant strain applied for 100 seconds, from 50 to 1000 minutes after unloading.

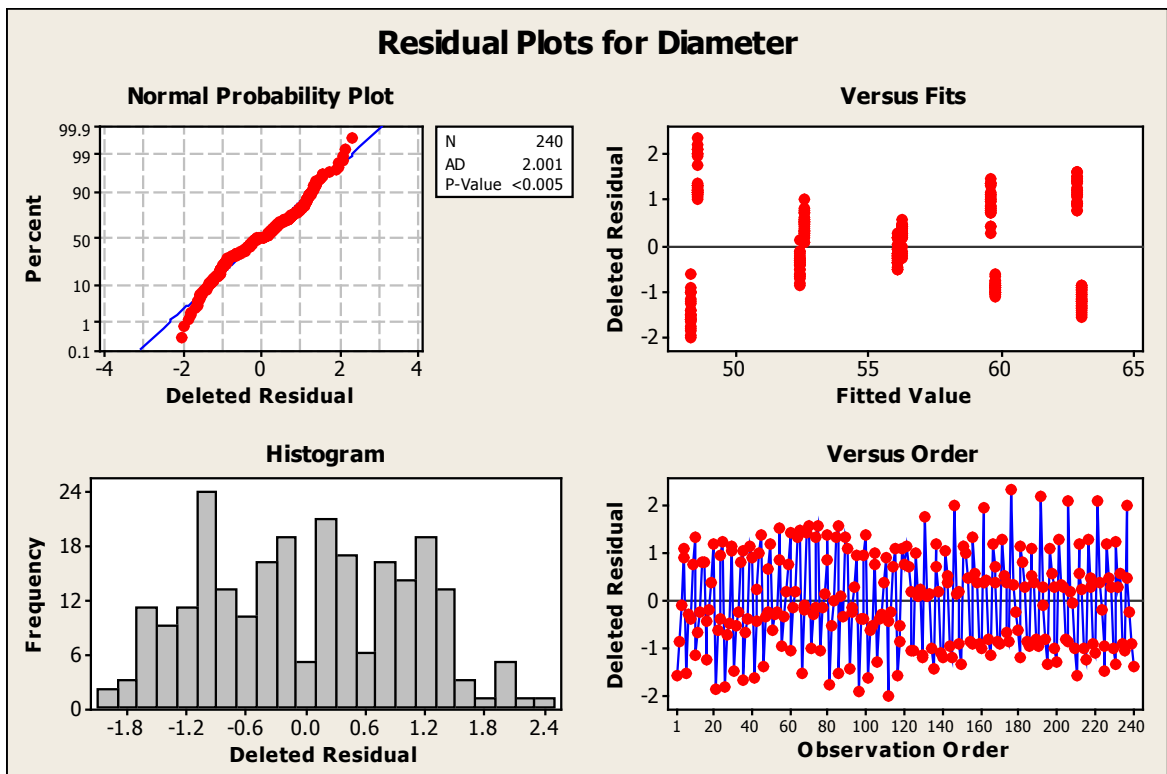


Figure F.4: Residuals plot for diameter of machined samples.